"NEUTRON DIFFUSION AND MULTIPLICATION IN REACTOR LATTICES"

A Thesis Submitted to the
University of London for the
Degree of Ph.D. in the Faculty of Science

by

MUHAMMAD RAFIQ HAROON
B.Sc., M.Sc., D.I.C., Graduate I.E.E.,
Member BNES

Department of Mechanical Engineering
Nuclear Power Group
Imperial College of Science and Technology
London, S.W.7.

September 1966

ABSTRACT

The systematic variation of neutron flux distribution and buckling measurements as a function of fuel loading in a sub-critical assembly (natural uranium, graphite moderated) have been investigated in a symmetrical square configuration at the centre. Some control rod effectiveness studies have been carried out on the same pattern.

The results have been correlated on the basis of Diffusion Theory. For full assembly cases lattice parameters were calculated, and compared with Syrett's model for graphite moderated reactors and are in good agreement. The correlation of partially filled assembly cases (clean core and vacancy) was based on the concept of reflector savings calculated by both One- and Two-group theory formulation in an infinite plane slab system and on Two-group heterogeneous theory (source-sink) for finite systems. The results confirm that the homogenised concept of reactor lattices (Wigner-Sietz) holds well down to 36 fuel elements. For fewer numbers of fuel elements, serious deviations become apparent compared with heterogeneous theory which predicts results correctly down to 16 - 9 fuel elements. Curves of K_∞ and B_m^2 vs. number of fuel elements and reflector savings vs. reflector thickness have been drawn and show the physical breakdown of the first theory. The flux distributions by heterogeneous theory are also much better than the

homogenised theory for small numbers of fuel elements.

All these results (clean core) were also analysed by numerical methods and compared.

The analysis of the control rod (mild steel, transparent to fast neutrons) effects has been based on (a) super-cell calculations and (b) the heterogeneous theory. The experimental predictions have wide variations in comparison to the super-cell calculations and are in good agreement with heterogeneous theory if diffusion area of the fueled lattice is used to calculate the controlled reactivity.

ACKNOWLEDGEMENTS

The present project would have been incomplete but for the constant encouragement and guidance cheerfully given by my supervisor, Dr. P.J.Grant, and the author takes this opportunity to thank him gratefully. Thanks are also due to members of the Imperial College staff, especially Dr. N. Solntseff. I am very grateful to the technician staff, namely Mr. G.Slater, Mr. N.D.Keates and Mr. M.Smith, especially Mr.Keates for his help in the technical details of the experiments.

I am grateful to Mr.G.Näslund and Dr.A.Jonsson of the Swedish AB-Atomenergi for providing the "Hetero" programme and their continued interest in its use. Thanks are also due to the computing staff of Imperial College, specially Mr.J.Cox, and the London University Computer staff for the facilities provided.

This work has been done during the tenure of a Colombo Plan Scholarship and I am very grateful to the Pakistan Atomic Energy Commission for providing the opportunity, and to the Colombo Plan Authorities and the British Council for financial assistance and admirable co-operation. Finally I wish to express my gratitude to Miss Margaret Hudgell for "patiently" typing this thesis.

CONTENTS

CHAPTER 3

HOMOGENEOUS REACTOR THEORY (UNIT CELL METHOD), DERIVATION OF CHARACTERISTIC PARAMETERS AND EXPERIMENTAL RESULTS

CHAPTER 4

CALCULATION OF FLUX, K-INFINITY AND THE REFLECTOR SAVINGS FOR PARTIALLY FILLED (CORE) SUB-CRITICAL ASSEMBLY ON THE BASIS OF "ONE-GROUP THEORY"

CHAPTER 5

CALCULATION OF FLUX, K-INFINITY AND THE REFLECTOR SAVINGS FOR PARTIALLY FILLED (CORE) SUB-CRITICAL ASSEMBLY ON THE BASIS OF "TWO-GROUP THEORY"

CHAPTER 6

ANALYSIS OF THE HETEROGENEOUS REFLECTED REACTOR SYSTEMS ON THE BASIS OF TWO-GROUP HETEROGENEOUS THEORY

CHAPTER 1

HETEROGENEOUS REACTOR SYSTEMS AND METHODS OF ANALYSIS

1.1 INTRODUCTION

The importance of detailed knowledge of the neutron flux distribution and the related parameters in a reactor cannot be over-emphasised in the present-day world. For large reactors the problem is simple and can be analysed fairly easily. But then the reactor is not just a heterogeneous or homogeneous mixture of fissile materials with coolant and/or moderator. The situation is more theoretically complex and experimentally difficult as well as hazardous to study. Recourse, therefore, is taken to small sub-critical assemblies, which are excited by a source and are always in a steady rather than critical state. More complicated details will be considered in the succeeding sections and chapters; here it will suffice to say that a sub-critical assembly is a powerful tool in the hands of a reactor analyst and it seems it would remain so for some time to come.

The following experimental investigations have been carried out with the sub-critical assembly (Chapter 2) available at the College.

1) Four natural uranium fueled graphite moderated lattices with varying diameter of the coolant channels have been studied experimentally. Five more cases of fully fueled assembly (Chapter 3) with varying degrees of homogenization were investigated.

2) Research was carried out for twenty-five partially filled assembly cases and a few partially filled assembly cases with vacancies were also considered.

3) Experiments to calculate the control rod effectiveness for mild steel were carried out.

The diffusion theory has been assumed to hold in all analyses. The experimental results have been correlated on the basis of

a) Unit-cell model of Wigner-Sietz and

b) Heterogeneous method of Feinberg-Galanin.

In the first case both one-group and two-group theory calculations were carried out, while in the latter case only two-group theory calculations were employed. The full and partially filled assembly cases were also analysed by solving two-group theory diffusion equations by finite difference methods. The results have been compared and correlated. The control rod calculations

were based on two-group theory in both cases.

The measured relaxation lengths in combination with the measured extrapolation lengths were used to predict the measured value of the material buckling and K_∞ for the system. The theoretical and experimental flux distributions have been compared and the relationship of all the related parameters discussed.

1.2 HETEROGENEOUS REACTOR SYSTEMS

The heterogeneous reactors are characterised by the geometric separation of fuel and moderator materials. The fuel in such a system may appear in the form of rods or metal plates which are distributed throughout the moderator according to some prescribed lattice configurations. In the early days of Reactor technology heterogeneity was the basis for the maintenance of chain-reaction with the available fuel enrichments (natural uranium) and moderating materials (graphite with water). With the exception of heavy water, a homogeneous mixture of fuel (natural uranium) and moderator materials (C, H_2O) could not be made critical.

Besides the physical separation of fuel and moderator, the most important feature of such systems is the fact that they are practically thermal, i.e. most of the fissions are caused by thermal neutrons. Physically this means that the ratio of moderator atoms to fuel (uranium atom or any other fissile material) is sufficiently large that relatively few neutrons are captured during slowing down from fission energies to thermal energies. Thus to put crudely the localizing of the fuel concentration produces the following changes relative to the characteristics of a homogenized system,

in thermal reactors,

1) thermal utilisation is decreased (f);

2) resonance-escape probability is increased considerably (p);

3) fast-fission factor is increased (ε).

The double advantage arising from the increase in p and ε offsets the relatively small decrease in f by a considerable margin. It may be remarked that lumping the fuel into a fuel element (1) decreases f and (2) increases p relative to their values, were the fuel homogeneously distributed throughout the moderator. Thus the net result of selecting a heterogeneous system is the maximisation of multiplication constant K_∞. This becomes rather inevitable when the reactor system is to be charged with natural uranium.

This places very great emphasis on the accurate calculation of the four factors in K_∞, since even with the best possible arrangement of fuel (natural uranium) and moderator (graphite), the resulting multiplication constant is greater than unity by only a few percent. In these circumstances small errors in the estimation of f, p. ε and η are bound to lead to large errors in the calculation of quantities dependent on

$$\delta K = K_\infty - 1 \qquad 1.2.1$$

for example, material buckling, reactivity available and so on. When these quantities are known with the

required accuracy, the K_∞ for the system is known and suitable expressions can be obtained for the effective diffusion length, migration area of the lattice and hence the estimates of the overall size of the reactor-core and reflector configurations. For thermal-reactor systems, the diffusion theory treatment of the neutron-behaviour in the multiplying system is sufficiently accurate provided the transport theory corrections are applied to the diffusion coefficients, extrapolation distances, etc.

1.3 METHODS USED FOR REACTOR ANALYSIS

The basis of reactor analysis is essentially the fact that, for the maintenance of a self-sustaining nuclear chain reaction in a reactor assembly in the steady-state, the Neutron Production in the fissile material should balance the neutron losses due to the absorption in the fuel, the moderator and the structural materials and the leakage out of the system, provided there is no extraneous neutron source present. The practical possibility of a reactor system is characterised by the 'Four-factor formula"

$$K_\infty = \eta \varepsilon p f \qquad 1.3.1$$

The infinite multiplication constant K_∞ may, therefore, be defined as the ratio of the number of neutrons

available for absorption in the fuel in any one generation to the number of neutrons absorbed in the fuel in the previous generation in an infinite system which has the same nuclear properties as the multiplying system under consideration.

If such a reactor system is in a critical state then the effective multiplication factor is unity. The sequence of events in the neutron life cycle in a critical steady state may be summarised briefly as

(1) production of fast neutrons by fission in U^{235} and fast fission in U^{238}.

(2) slowing down to thermal energies and resonance capture in U^{238} and leakage out of the system during slowing down and in process (3),

(3) thermal neutron absorption in different materials including fuel leading to production of fast neutron i.e. process (1).

The exact and detailed knowledge of the last-mentioned process is very essential for the of reactor system. Complete details of the competing processes going on in a reactor system will be discussed in the succeeding chapters in greater detail. Therefore one could say that the purpose of any worthwhile method for reactor analysis is the determination of the conditions under which a reactor will become critical and fairly accurate knowledge of the neutron flux distribution in

the reactor.

Various methods are used for this purpose, their approach may be different but basically they are different forms of one or other of the two analytical concepts described below.

(a) Unit-cell Model of Wigner - Seitz and

(b) Source-Sink Method of Feinberg-Galanin.

Herein they will be referred to briefly as Homogeneous Method and Heterogeneous Method respectively because of the very principles involved in the formulation of each. A short description of each less mathematical details, would suffice here.

1.4(a) HOMOGENEOUS METHOD OR UNIT-CELL MODEL OF WIGNER-SEITZ

Originally conceived for the calculation of wave-functions of crystal lattices, this method has been used very extensively for reactor analysis. The essential feature of the method is that the lattice may be regarded as a periodic array of identical lattices, each having a fuel element symmetrically located in it. On account of the symmetry of the cells, a single lattice is taken as the representative of the infinite reactor system. The methods based on this model are concerned with the analysis of any one equivalent-cell of the infinite system. This assumes

(i) The net neutron current is zero at the boundary of the cell;

(ii) The source term is constant in the moderator and zero in the fuel, while the flux fine structure is the same as it would be in an infinite lattice with the same type of cells;

(iii) The neutron flux distribution in the unit-cell is obtained under the boundary conditions detailed in section 3.2.1. with the help of diffusion theory or transport theory depending on the size of the cell. Having determined both the energy spectrum and neutron flux distribution in the cell, the thermal utilisation and resonance-escape probabilities may then be computed. The calculation of fast-fission factor ε and η is a separate problem using the flux distribution in detail. ε and η are combined with f and p to give the infinite multiplication factor of the reactor system. Equivalent cylindricalization of the actual cell (may be square, rhombus or any other) is the most commonly used procedure,

while the fuel channel boundary is kept intact. The overall nuclear properties are the average of all the materials present in the lattice-cell.

There are a few obvious advantages in the procedure, but serious errors may arise in the flux fine

structure. Newmarch (31) has shown that the effect of cylindrical cell approximation in lattice calculations is to overestimate the ratio of the flux in the moderator to the flux in the fuel and has demonstrated that it gives a flux in the moderator which is considerably higher than in the fuel, even when the cell dimensions in units of mean free path tend to zero; whereas, for the case of real cells (e.g. square or hexagonal), the flux ratio must tend to unity. Also as the actual cell is replaced by an equivalent cylindrical one, the effect of the cell-shape both on flux fine structure and related parameters is completely ignored. In actual practice, a lattice cell is often a square or rhombus. In the equivalent cell approximation the cell shape being replaced by a circle, the high flux regions at the corners of the cell as shown in section 3.2.1 are replaced by comparatively low flux regions at the sides. This leads to an underestimation of the excess absorption term in the moderator; the underestimation being least in the rhombic cell.

Clark-Newmarch's (27) and Cohen's (28) exact treatment of a square-cell are variations of the same idea. Inspite of quite a few complicated mathematical details, their use remains limited in scope and the equivalent cell approximation procedure stands out quite marked for its inherent simplicity in computation and the good results

obtained justify its use as such.

1.4(b) HETEROGENOUS METHOD OR SOURCE-SINK METHOD OF FEINBERG-GALANIN

The homogenised model discussed in the last section is based on the gross properties of the unit-cell and all calculations resulting from the consequent relationships have an inherent assumption that the reactor system is infinite in extent. If the size of the multiplying system is reduced, the unit-cell concept cannot predict the criticality of the system with sufficient accuracy. In these cases the detailed arrangement of the fuel elements is an essential feature of the nuclear configuration which must be included in the criticality considerations.

A model with such considerations has been developed by Feinberg-Galanin (12, 13). Here the existence of heterogeneity is treated as such and the problem of computing the multiplication constant of a given multiplying system is treated as an integral system and the basic assumption of the Wigner-Seitz model, that the system should be infinite, is removed. The fuel elements are regarded as a collection of line or point sources in a matrix of moderator material of infinite extent. The fast (fission) neutrons produced by these sources slow down in the moderator. Feinberg and Galanin have assumed that the resulting spatial distribution of thermal neutrons may be re-

presented by the Fermi-age solution appropriate to the source geometry. Then the one-velocity diffusion equation is used to describe the distribution of thermal neutrons in the moderator. The source term in this context is obtained by super-imposing the contributions from all the fuel elements in the assembly and additional absorption term due to the fact that the fuel elements are 'sinks' for thermal neutrons. The properties of the fuel elements as neutron sources and sinks are described in terms of "The THERMAL CONSTANT" defined as the ratio of total net current of thermal neutrons into the fuel element to the value of the thermal flux at the surface. Feinberg and Galanin used the results obtained from diffusion theory.

However, a neglect of a small term by Galanin in computing the lumping effect led to inconsistent results for various cell shapes, which neglect obscured the significance of his method. This was later pointed out by Feinberg and elucidated by Kronrod.

The original formulation of the method as propounded by Feinberg-Galanin was applicable for fuel elements embedded in an infinite moderator medium. This method has been extended to finite media of rectangular shape by Meetz (30) and to those of cylindrical shape by Jonsson (16, 17). This general approach to the overall problem is both elegant and precise; besides, the method

offers great flexibility in treating complex heterogeneous arrays involving various lattice geometries, irregularities in rod size and spacing. It is also very helpful in control rod effectiveness studies and those of voids and channels. However, it should be mentioned, too, that the mathematical treatment is much more complicated than that involved in the unit-cell method. Also the analysis of large regular geometries by this method offers no significant advantage over the Wigner-Seitz model.

1.5.1 PRESENT WORK AND ITS STATUS

The diffusion theory has been used fairly extensively by several authors as the basis for reactor analysis. The aim of the diffusion theory in calculating the critical size of reactors is to account correctly for the neutron balance between production, absorption and leakage in the steady state of the reactor. In the analysis of the present work the validity of the diffusion theory was assumed throughout. However, the diffusion theory parameters were defined in a way appropriate to heterogeneous lattices and boundary conditions considered carefully. In particular, it should be emphasised that, although homogeneous diffusion equations are used, any real reactor system consists of a whole number of finite cells.

The lattice experiments which have been performed to date can be summarized according to moderator, and degree of enrichment of fuel (uranium). The fuel available with the sub-critical assembly at Imperial College is Natural Uranium and that settles the enrichment problem. The graphite components (Appendix A-1.1) are of such dimensions that they give a lattice pitch of 8" square. Consequently the fuel to moderator volume ratio is fixed except for slight variations which can be created.

The experimental work reported here involves the determination of relaxation lengths in case of partially filled sub-critical assembly and relaxation length and extrapolation length in case of full assembly by measuring the neutron flux distribution in vertical and horizontal directions. The flux distributions are fitted to the appropriate expressions and one arrives at a measured value of the material buckling for the system and hence K_∞ for the reactor system.

The experiments had been designed to see whether the measurements on small numbers of fuel elements will give sufficient accuracy in the measured parameters of a reactor system so that the necessity of filling the whole assembly or the use of a critical reactor could be avoided if possible. If this idea is practicable, then, to what extent ? The answer to that question will provide a check for the extra fuel needed.

Though the BICEP group (23) have done quite extensive measurements on different sizes of exponential stacks, little attention has been paid to the two-zone experiments. If core and reflector regions are treated as separate, the partially filled assembly cases could be called two-zone experiments. Only few experiments have been carried out involving measurements on single fuel rods and no further. At Winfrith King (22) has done some measurements on two-zone exponential graphite moderated lattices on the basis of substitution method. In this method, measurements are made on a full stack of reference fuel, part of which is then progressively replaced by test fuel the measurements of the relaxation length being made at each loading. Despite the fact that the measurements provide very valuable information about the behaviour of lattices under the conditions, their application remains very limited in extent because there are very few institutions rich in the availability of fissile materials of one sort or the other for substitution purposes.

Further to reduce any mathematical details the slab system has been used leading to an inefficient use of the available fuel.

Zink (25) and Stuart (26) have also done some calculations on single fuel measurements. The methods developed are

excellent exercises in the mathematics of the subject but it would appear too much to expect too accurate parameters from the analysis since there are very intense variations of neutron flux over a small region so that the assumptions simply break down. This lack of interest in the reflected sub-critical assembly measurements is rather surprising, as it could be a very powerful procedure for reactor analysis if an accurate measurement of the relaxation length could be obtained for the system under consideration.

With these points in mind the following experimental measurements were carried out.

1) Measurement of b_{11} and λ_r for the fueled assembly. This served to ascertain the accuracy of the lattice parameters calculated by the model (7) adopted as the basis for analysis.

With the available graphite components (details are given in Appendix A-1.1) four fueled assemblies of varying channel diameter could be created. All were investigated.

In five fueled assembly cases for control rod effectiveness studies, flux measurements were carried out by creating one vacancy or by filling it with control rod (mild steel) per 9, 4 and 2 lattices.

2) Careful and detailed considerations led to the selection of "square core region" in reducing the size

of the core in the sub-critical assembly. Flux measurements for four sets of 100, 64, 36, 16 and 4 fuel elements in the central region of the assembly, were done to find the relaxation lengths in the vertical direction and flux measurements in the horizontal direction for comparison with theory, and fourteen pairs of similar experiments for steel and vacancies.

This arrangement in the text is referred to as "The reflected core system". Another lattice, slightly different from one of the four lattices with 121, 81, 49, 25 and 9 fuel elements in the assembly were investigated.

3) Mild steel was used as the control rod for control rod effectiveness studies referred to in 1) and 2) above.

The full details of these measurements will follow in the succeeding chapters.

1.5.2 METHOD OF ANALYSIS

The theoretical characteristic parameters for the full assembly cases were calculated according to Syrett's (7) model. The measured relaxation lengths were combined with extrapolation lengths to give a measured value of B_m^2 (material buckling) and K_∞. The extrapolated lengths were assumed to be the same for vacancy cases as for their corresponding full assembly cases.

The twenty-nine "clean" core cases were also analysed by solving two group diffusion equations by finite difference methods.

The twenty-five partially filled cases of assembly were analysed on the basis of

(i) Homogeneous model of Wigner-Sietz both for modified one-group theory and two-group theory of neutrons, and

(ii) Two-group heterogeneous theory of Feinberg-Galanin for finite reactor systems in moderator of finite size.

In the first case the problem was reduced to the calculation of reflector savings for the particular combination of core size in the assembly and the reflector thickness. Then the reflected core in the assembly is replaced by an equivalent bare homogeneous reactor system and the measured relaxation lengths are combined to give the material buckling of the system and hence the measured value of K_∞ is predicted.

Two energy group analysis, on the basis of heterogeneous theory (source-sink) for finite reactor system is used. The measured axial buckling is used in conjunction with the heterogeneous set of equations to predict the criticality of the system. The problem is treated as an Eigen-value problem where K_{eff} is the eigen-value and the flux is the eigen-vector.

The controlrod effectiveness calculations were carried out on the basis of "super-cell concept" and the heterogeneous concept of reactor systems. In both, two energy groups of neutrons were used for analysis.

The relevant vacancy cases were studied only on the basis of modified one-group theory in conjunction with super-cell calculations. Full details of the analysis are given in the succeeding chapters.

CHAPTER 2

THE APPARATUS AND THE EXPERIMENTAL METHOD

2.1.1 THE SUB-CRITICAL ASSEMBLY

The general arrangement of the sub-critical assembly is shown in FIG. (2.1.1). The graphite assembly is of parallel shape with square cross-section, i.e. 8' x 8' x 9 ft 3 inches high and is supported on the 6 inch thick bedplate. The graphite lattice region consists of a 12 x 12 array of fuel channels with an 8 inch pitch. The lower 2 feet of the graphite assembly form the pedestal, which consists of solid graphite blocks arranged for structural stability. Its function is to slow down and diffuse the relatively fast neutrons emanating from four antimony-beryllium sources. The main part of the graphite structure above the pedestal is similar to that in an actual reactor core and it can be stacked either with the channels vertical, as shown, or horizontal. The neutron flux measurements can be made either in the axial or transverse directions with the detection equipment described in section (2.2).

2.1.2 NEUTRON SOURCES

Four antimony-beryllium (γ,n) neutron sources are used giving a flux of 10^5 n/cm^2-sec at the bottom instead of the more generally used Ra-Be or

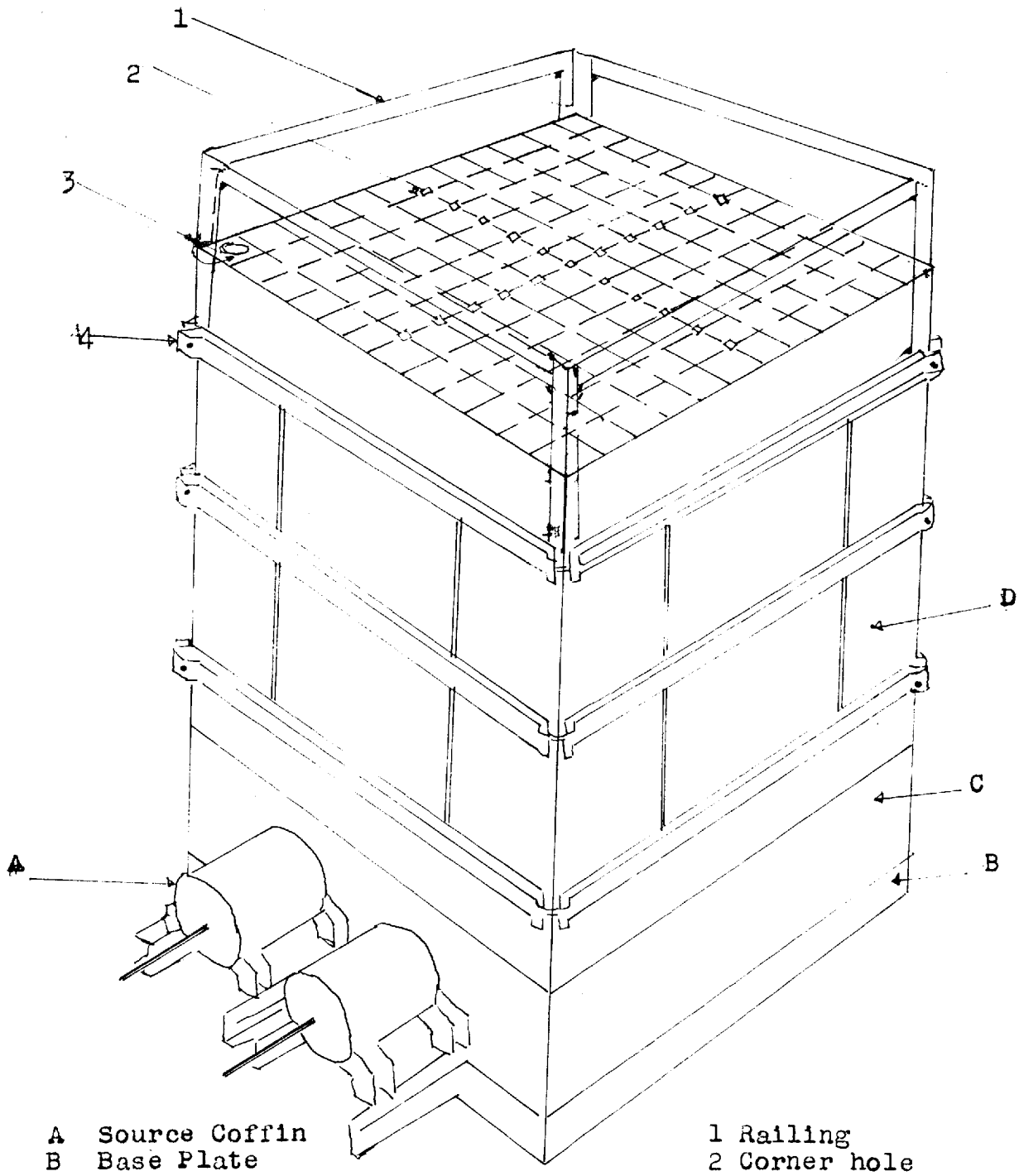

A Source Coffin
B Base Plate
C Pedestal
D Cd. facing

1 Railing
2 Corner hole
3 Fuel channel
4 Bracing

FIG. 2.1.1 SUB-CRITICAL ASSEMBLY

Po-Be sources. The beryllium component is in the form of a sintered metallic sleeve, permanently located inside a high-purity lead shielding block, built into the graphite pedestal structure. The antimony component is in the form of a metal slug of approximately 1.0 inch diameter and 8.0 inches length, contained in a stainless-steel sheath. The antimony sources are normally irradiated in a reactor to a level of approximately 25 curies for the Sb^{124} isotope. The practical advantage of this type of neutron source is that the emission rate can be varied by simply adjusting the position of the Sb γ-sources in the Be sleeves and this is of great benefit in balancing the sources, to make the distribution "cosine" in the assembly, especially when the Sb sources vary in strength. When inserted, the source centres are 1 ft from the pedestal-core interface. They are positioned horizontally at the nodes of the third harmonics. When not in use, the Sb-sources are withdrawn by a long handling rod into lead-filled coffins, which provide adequate shielding.

2.1.3 GRAPHITE COMPONENTS

The graphite basic raw material was purchased through the industrial group of U.K.A.E.A. and the machining has been carried out by Powell Duffryn Carbon Products Ltd. The basic lattice block has a 4.25 ins. diameter hole

along its axis, and a 0.625 ins. square section cut from each corner along the full length of the block. These give a 1.250 ins. square hole for flux measurements when assembled. The overall size of the block is 8 x 8 x 29 inches. The square-hole channels can be filled with square section graphite bars which are connected by graphite links.

The blocks on the extreme sides of the assembly do not have a 0.625 in. square hole along two sides of the block so that the boundary on the outside is linear.

The density of graphite in the assembly can be increased by inserting (i) a graphite sleeve, or (ii) a graphite sleeve and a plug. Full details of these components and the nomenclature of the possible lattices which have been investigated are given in Appendix A-1.1 and shown here for reference.

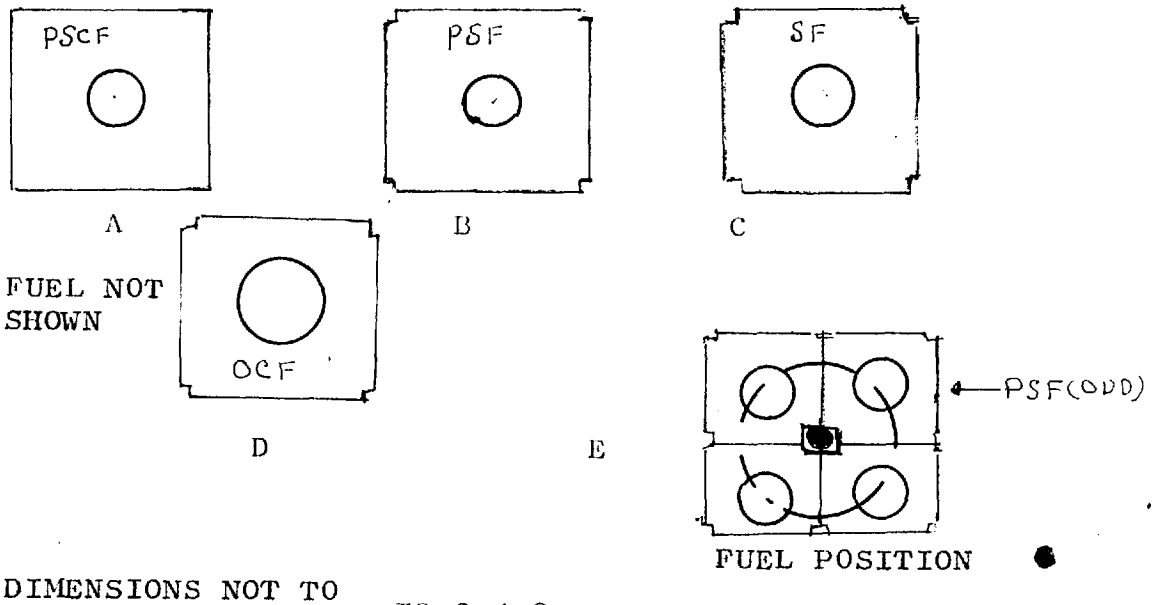

DIMENSIONS NOT TO SCALE

FIG.2.1.2

Since the sleeves are slightly smaller than the channels, they are centralised in the channels by means of graphite collars.

2.1.4 FUEL

The fuel consists of natural uranium slugs, 1 inch in diameter, 11.5 inches long and covered in aluminium of 1/32" thickness. The slugs are loaded into aluminium tubes, 8 to a tube, and the tubes inserted in the channels. In case of lattices (C) and (D), each Fuel Element Al. tube is located in the centre of a graphite channel by means of three thin aluminium spiders (to match the channel) situated near the top, centre and bottom of the channel.

The assembly is completely shielded with Cd, 0.015 in. thick, which serves to give an ideal boundary condition and also to reduce the thermal neutron flux level in the surroundings. Steel corner posts connected with cross-braces support the cadmium and prevent the blocks from shifting. The top is covered by Cd sheets and there are four corner posts, connected by chains, as a safety precaution for the personnel working at the top.

The physical dimensions of all components of the assembly are given in A-1.1.

2.2 FLUX MEASUREMENTS

The flux measurements, to evaluate the neutron buckling as defined by a relaxation length b_{11} and by a radial extrapolation length λ_r, are required in vertical and horizontal planes. These measurements were carried out by a BF_3 proportional counter, of the type 12EB40. The counter 2.5 cms in diameter is enriched to 96% of B^{10} and has a sensitivity of 3 cps/n/cm^2-sec. It has been shown previously by Brown (8), and confirmed by Macdonald (4), that the difference between bucklings obtained with 5 EB/40 counter and 12EB/40 is negligible. Brown reports that the change in relaxation length caused by the introduction of the boron counter has been measured as $0.04 \pm 0.03\%$ in a typical case. Errors caused by variations in the local flux depression produced by the counter and its cable are negligible.

The electronic equipment for counting was standard one, and special attention was paid to the reduction of instrument sensitivity drift and spurious pulses.

The counter is rigidly attached to an aluminium positioning rod which can be moved along the axis of the measuring hole and can be locked at 2" axial intervals. The positioning holes in the rod have been calibrated and found to have a random error corresponding to less than 0.1% of the flux for the minimum relaxation length.

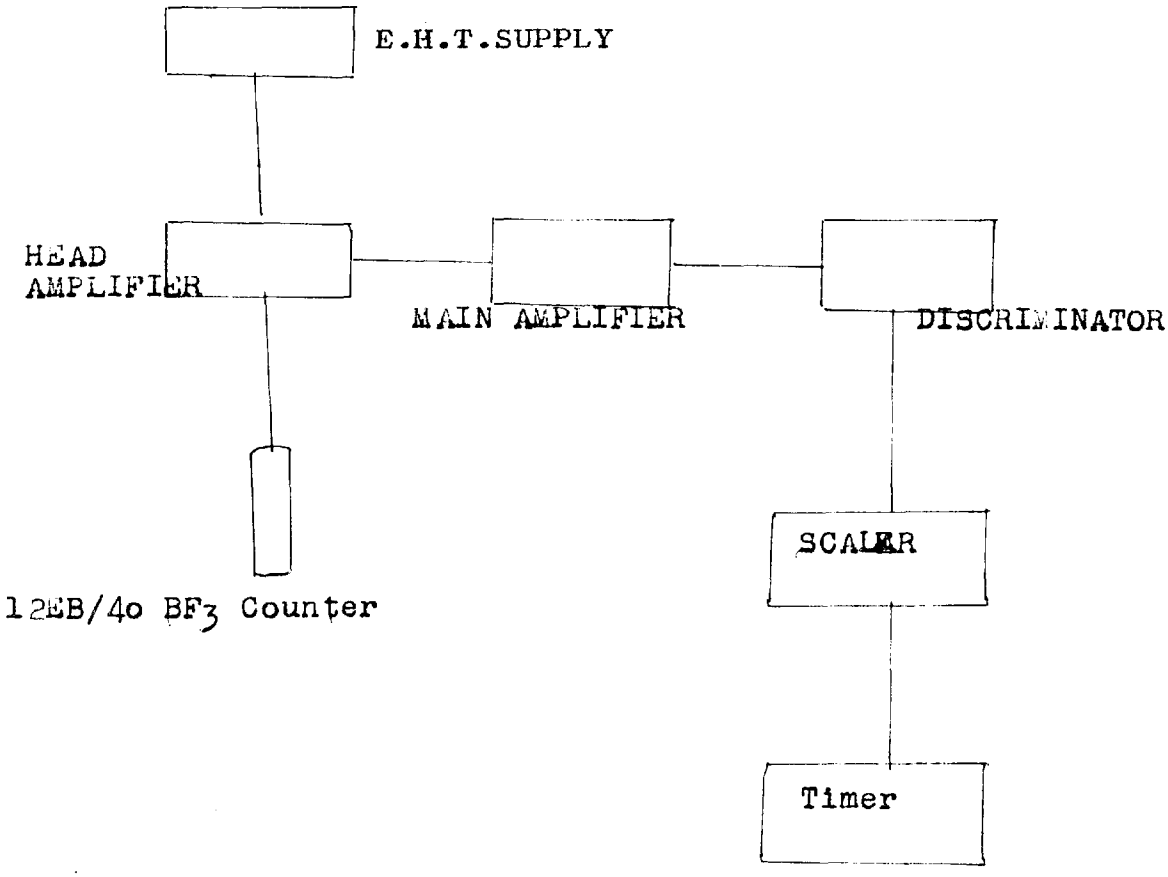

FIG. 2.2.1

DIAGRAM OF DETECTION EQUIPMENT CIRCUIT

The rod is constrained in the transverse direction by a collar just above the counter. In case of PSF (ODD) measurements the flux distribution was measured with an identical positioning plate but with a circular cylindrical cross-section to fit in the plug holes normally occupied by fuel elements. It was necessitated as a consequence of making a symmetrical configuration of squares of odd numbers of fuel elements. The fuel elements were placed in the corner-holes and the measurements had to be made in the inner plug-holes.

The overall measuring procedure has been detailed elsewhere (29). The pulses from the counter are fed to the main counting unit through a head amplifier. (Fig.2.2-1). The counting equipment is the standard one (4) consisting of main amplifier (NE 5202), discriminator (D 4019/1), scaler (ETL 127A type 4) and an ETL 127A type 4 timing unit. The overall dead time of the unit is (2.0 $\pm$ .02) μsecs. Special attention was paid to the reduction of instrument sensitivity drift and spurious counts. With the help of filters and constant voltage transformers the mains supplies to all the instruments were kept constant. Since the counting system was found to be quite stable, the bias and H.T. curves were plotted only once in a fortnight, but the counting system was checked very often before and after or during the actual experiment. The reproducibility of the counting numbers

within statistical accuracy was used as the best criterion for the true working of the system. For example, a repeat measurement was often done at F_6 and the analysis always gave identical relaxation lengths.

The relaxation length measurements in the z-direction were confined to flux distribution in the constant Cd ratio region and for reasons discussed in the next section. The readings in each hole were taken from the 3'4" position (measured from the pedestal-stack interface) to 5'6" position, in 2"intervals, this being dictated more by boundary effects and harmonics considerations. Each reading was of 10^5 counts, corresponding to a statistical accuracy of 0.316%. Since all the four sources used to be balanced at the start when the sources had been newly irradiated and the holes chosen were almost identical except the central one so that systematic error could be checked any time during the experiment.

The flux plots in the X and/or Y-directions were limited to 8" interval. To calculate the extrapolation lengths, the maximum number of points could be eleven. The measured values of the extrapolated lengths are given in Table 2.5.1.

2.3 HARMONICS CONSIDERATIONS

The ultimate aim of an exponential experiment is to determine the material buckling of the lattice under study from measurements of the thermal neutron flux distribution in a sub-critical assembly in which the flux is maintained by means of neutron sources (1). There are, however, some inherent disadvantages in an exponential experiment. First of all, the system is in a steady state rather than in a critical state, higher order eigen-functions would be present in the solution of diffusion equation. Secondly, the introduction of sources, to maintain the steady-state and to counteract the excessive loss of neutrons by leakage on account of smaller size, will give rise to a region of non-asymptotic flux distribution both on the approach of the boundaries and on the source plane. Thus, theoretically speaking, the measured thermal flux distribution will not be free of harmonics other than the fundamental asymptotic flux distribution.

A rigorous investigation into this problem has been done by Macdonald (4) and also the BICEF group. The conclusions of the BICEP (23) group could be summarised briefly in the next few lines.

According to the group, measurements and harmonic analysis of the flux distribution to obtain the harmonic

coefficients and the application of harmonic corrections to the vertical line flux distributions occupies considerable time required to obtain the material buckling of a given lattice. The resultant change in the value of the material buckling is much less than 1%. They concluded that the effort is not worth making. The group decided to restrict their measurements so that they have not to apply any harmonic corrections.

Macdonald (4) has done extensive studies on the sub-critical assembly under investigation for the measurement and reduction of harmonics and their effect on buckling measurements. As stated before the exponential assembly is in a steady-state rather than in a critical state, all eigen solutions of the steady-state diffusion equation should be considered and the equation for the thermal flux is

$$\varphi(x,y,z) = \sum_{m,n=1,3,..} A_{mn} \cos\left(\frac{m\pi x}{a}\right) \cos\left(\frac{n\pi y}{b}\right) \frac{1}{\sinh(c/b_{mn})} \times \sinh\left((c-Z)/b_{mn}\right) \qquad 2.3.1$$

which is a solution of the well-known diffusion equation in rectangular coordinates,

$$\nabla^2 \varphi(x,y,z) - \kappa^2 \varphi(x,y,z) = 0 \qquad 2.3.2$$

the origin of axes being the centre of the assembly at

the stack-pedestal interface .

The solution (2.3.1) of the diffuion equation 2.3.2 is true only for positive values of z. C is the extrapolated height of the sub-critical assembly. The axial bucklings are related for the vertical assembly to the x and y direction eigen-values by the equation

$$\gamma_{mn}^2 = \frac{1}{b_{mn}^2} = \kappa^2 + \left(\frac{m\pi}{\bar{a}}\right)^2 + \left(\frac{n\pi}{\bar{b}}\right)^2 \qquad 2.3.3$$

where

$$\kappa^2 = \frac{M_z^2}{M_R^2}\left(\frac{1}{b_{11}}\right)^2 - \left(\frac{\pi}{\bar{a}}\right)^2 - \left(\frac{\pi}{\bar{b}}\right)^2 \qquad 2.3.4$$

$\bar{a}$ and $\bar{b}$ are the extrapolated lengths of the assembly and they have been kept separate for the purpose of better understanding, though they are equal in the present case. κ^2 corresponds to the first harmonic. The normal procedure is to reduce the higher order functions in equation 2.3.1 to a negligible level. In the case of the exponential assembly the sources have been positioned to remove the third harmonic, namely A_{31}, and A_{13} by placing the sources at the nodal points of the third harmonic.

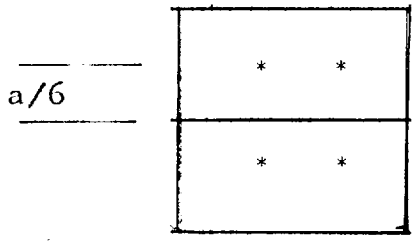

FIG.2.3.1

In this way, the harmonic A_{33} is removed as well. However, the higher harmonics still remain in the present set-up to varying degrees, if the flux distributions are to be analysed in terms of b_{11}, $\bar{a}$ and $\bar{b}$.

Attempts here have been made to correct the harmonics, but, in the present investigation, Macdonald's study is very instructive. He has done measurements for the symmetric harmonic coefficients for the vertical fueled and unfueled sub-critical assembly at a number of heights, all the measurements being in the region of asymptotic flux distribution. Each harmonic measurement consisted of 81 readings taken at the intersections of a 9 x 9 measuring hole lattice. The measurements were fitted to the function

$$\varphi(x,y)_z = \sum_{m,n=1,3\ldots} A_{mn} \cos\left(\frac{m\pi x}{\bar{a}}\right) \cos\left(\frac{n\pi y}{\bar{b}}\right) \qquad 2.3.5$$

Values of A_{mn} were obtained relative to A_{11}, the values of $\bar{a}$ and $\bar{b}$ having been measured in a harmonic free region, and a typical result he obtained for the solid diffusion stack at a height of "2 feet" above the pedestal for the first 16 symmetrical harmonics A_{17} to A_{71} is directly quoted here.

TABLE 2.3.1

m=	1	3	5	7
n=1	100.00 ± .04	-0.25 ± .05	-1.09 ± .06	-0.03 ± .07
3	- 0.06 ± .05	0.08 ± .06	0.12 ± .07	0.02 ± .08
5	- 1.06 ± .06	-0.14 ± .07	-0.02 ± .08	-0.02 ± .09
7	- 0.11 ± .07	0.01 ± .08	0.21 ± .09	0.00 ± .011

The only harmonic present to a level for detection purposes is A_{51} and A_{15} at a height of 2 feet above the pedestal. About this measurement for the two fueled stacks, he remarks that only the A_{15}, and A_{51} harmonics were present in detectable quantities at the levels measured. He has not quoted any figures for them, implying thereby that they could safely be neglected.

He has drawn curves for the experimental and theoretical values for the harmonic ratio $(A_{51} + A_{15})/A_{11}$ as a function of the height above the pedestal. His measurements indicate that the ratio $(A_{15} + A_{51})/A_{11}$ is less than or of the order of, 0.2% at 3 feet above the pedestal and the ratio ranges within 0.1 to 0.5% for fuel and practically no channels, and fuel-open channels, at this level respectively, which are the two extreme cases in the present investigation. The same ratio is of the order of 0.1 to 0.6% for the diffusion stacks

at 3 feet level above the pedestal interface. The latter measurement is not of very great importance in the present study which is concerned mostly with fueled lattices. In his analysis, he remarks, that the only harmonics present in measurable quantities were A_{15} and A_{51}; the harmonic content was small and the experimental errors relatively large. To overcome this he studied the "grouped" harmonics in the y-direction due to a single, non-central source at various heights along the line x=0. He introduced the harmonics simply for the purpose of measurement and exact knowledge of their magnitudes. Even then, his measurements indicate that the ratio (A_{m5}/A_{m1}) was less than 0.4% at a level of 3 feet and stabilising at 0.2% beyond for a solid diffusion stack. Thus, according to his measurements, the harmonic content present in fueled stacks for all practical purposes were the A_{51} and A_{15} harmonics and their coefficients are negative. The magnitude is of the order or less than 0.4% relative to the fundamental at a height of 3 feet above the pedestal and even less farther than 3 feet.

In view of the aforementioned considerations, it was decided not to apply any harmonic corrections, because even when it is

necessary to apply the corrections one should bear in mind the following considerations pointed out by the BICEP group.

1) The perturbations to the first harmonic cosine flux distribution caused by the presence of higher harmonics are, in general, only of the order of two or three times the standard deviation of the measured value of the flux. For this reason the harmonic coefficients are, in any case, subject to large errors (30 - 50%) and it is important to combine these errors with the other experimental errors of the measured flux values to which the harmonic corrections are applied. Failure to do this will lead to incorrect weighting of the flux values and can produce errors of the order of 1% in the value of the relaxation length.

2) The calculated values of the harmonic coefficients are very sensitive to the values used for the stack widths. For example, according to the group's calculations, a change in width of 2.7 cms has been shown to increase the coefficients by a factor of two in a particular case. It is, therefore, important that the widths should be taken as the physical width plus twice the mean value of the extrapolation lengths. , In the present work the width is of paramount importance because in the reflected fueled systems the flux distribution

is no longer cosine any more. And, in fact, there is no possible analytical solution of a square core surrounded by a square assembly with reflector around. In the analysis (Chapters 4 and 5) the whole idea is to determine the size of an equivalent bare system. As such, it seemed impossible to apply any harmonic correction to a partially filled assembly case.

3) The measurements in the harmonic plane should be confined to the region of equilibrium spectrum. Measurements on the BICEP stacks have shown that, while in an individual experiment the cadmium ratio at the outer points may not vary significantly, the results of a large number of experiments may show a systematic variation.

In view of these considerations, the following procedure was adopted throughout the measurements.

Seventeen measuring corner-hole points, shown in FIG. 2.3.2, were selected and the thermal flux distribution was analysed for the fundamental relaxation length and

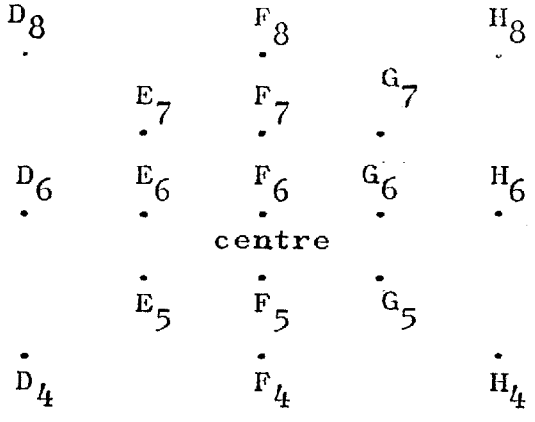

NOTATION EXPLAINED IN FIG.2.5.1(c)

FIG. 2.3.2

the mean of all these measurements was taken. It could be seen that these are practically all the available measuring holes in the central region of the assembly. According to Macdonald the measurements could still be extended beyond these points and still retain the desired accuracy but this was thought the best arrangement. Secondly, the measurements of the flux distribution in the vertical direction were confined to a region of an asymptotic flux distribution extending from 3'4" to 5'6". The flux distribution in this region, has an harmonic content of the order of 0.1%, which one can safely neglect without much consideration. This, however, increases to 0.4% in case of open-channel fuel cases. Experience showed that the nodal points and the central points often used to vary in the opposite directions from the mean and therefore did cancel the extreme variations.

2.4 SOURCES OF ERRORS IN THE DETERMINATION OF THERMAL NEUTRON FLUX

The possible sources of error other than the harmonics may be briefly summarised below :-

1) Counting Statistics and Counter Drift.

At each position a total of 10^5 counts were taken, so that the standard deviation due to counting statistics is 0.316%. No evidence of counter drift was observed.

Any random error in counter position was due only to lateral movement of the counter caused by a small difference between the size of the counter locating collar and the measuring channel.

2) Dead Time of Counting Equipment

The dead time error has the maximum effect. When the sources are newly irradiated the correction is of the order of 3½%, which corresponds to an error of approximately ± .03 cms for b_{11} = 70 cms due to the dead time error of ± .02 μs. This in comparison to a typical fitting error of 0.32 cms is considered negligible.

3) Counter Position

The counter could be positioned with an accuracy of ± .1 cms and errors arising due to the counter position were negligible.

4) Background

In the horizontal direction the background flux distribution is the same (cosine) and therefore is of no consequence, and in the vertical direction it is negligibly small. For example, usually it was planned that the experiments should be performed as soon as possible after the sources have been newly irradiated, and under these conditions a count rate of 10 to 15 thousand per sec was reasonable in the region of measurement, and background of 5 to

10 counts per sec is not worth applying.

The necessity for a small harmonic correction was excluded by selecting the position of the measuring holes and taking the mean value of the relaxation lengths over the whole region of the stack. The dead time correction was always applied at each measuring position for all flux distributions.

2.5.1 EXPERIMENTALLY FITTED VALUES OF RELAXATION LENGTHS AND OF EXTRAPOLATION LENGTHS TO THE MEASURED FLUXES

The relaxation lengths b_{11} were fitted to the expression

$$\varphi(z) = A \frac{\sinh((c-z)/b_{11})}{\sinh(c/b_{11})} \qquad 2.5.1$$

and for extrapolation length in the X and/or Y directions to

$$\varphi(x) = A \cos\left(\frac{\pi x}{a'}\right) \qquad 2.5.2$$

The description of the programmes used for the purpose is given in A-2.1 and A-2.2. The expressions 2.5.1 and 2.5.2 have been fitted to the experimentally measured thermal flux distributions by the method of least square fitting, i.e. by minimising the sum of the residuals of the theoretical and the experimental flux distributions.

The thermal flux distributions have been analysed for b_{11} for fixed height; the experimental error increases to 2-3 times in case of variable height analysis as compared to the fixed height case.

Macdonald had done separate measurements to find out the extrapolated height of the sub-critical assembly. Therefore, his independent measurements for extrapolation length for height were taken as such. As a test measurement, average b_{11} was found to be in very close agreement with his measurement, e.g.

	(4)	(present)
	b_{11} cm	b_{11} cm (av. of 17)
PSF	69.94 - .08	69.92 - .07

Radial extrapolation lengths have been determined by measurements in the horizontal plane and fitting to the expression 2.5.2 by least squares method. The results are reported in Table 2.5.1 below.

EXTRAPOLATION LENGTHS IN VERTICAL AND HORIZONTAL DIRECTIONS

LATTICE	λ_z (axial)	λ_R (radial)
PSCF	2.78 $\pm$ .11 cms	2.52 $\pm$ .04 cms
PSF	2.78 $\pm$ .11 cms	2.80 $\pm$ .04 cms
SF	5.3 $\pm$ .15 cms	3.20 $\pm$ .06 cms
OCF	7.0 $\pm$ .2 cms	3.80 $\pm$ .07 cms

TABLE 2.5.1

The rejection of individual measurement φ_i was carried out if the value of the residual was

$$(\varphi_{ti} - \varphi_{mi})^2/\sigma_i^2 > 4.00$$

This amounts to setting a confidence limit of 95%. The results of measurements for the relaxation lengths in the vertical direction are tabulated in Tables 2.5.2 for all cases under investigation. In the first column is the number of fuel elements symmetrically placed in square array in the central part of the sub-critical assembly. In vacancy cases the apparent quoted number is the same but the corresponding number of fuel elements have been taken out, e.g. in case of $^1/9$ vacancy PSCF quoted under 1/4 fuel elements the actual number of fuel elements is 128 and there are sixteen vacancies created thereby. It is sometimes written for clarity as

CASE PSCF $\quad \frac{M_z^2}{M_R^2} = 1.010 \pm .002$

No. of Fuel Rods	b_{11} cm	γ_{11} $10^{-2}cm^{-1}$	γ_{11}^2 $10^{-4}cm^{-2}$	$\frac{M_z^2}{M_R^2}\gamma_{11}^2$ $10^{-4}\ cm^{-2}$
144	70.378,3 ±0.304,0	1.420,89 ±.004,60	2.018,94 ±.015,58	2.039,56 ±.016,25
100	68.996,3 ±0.290,4	1.449,35 ±.004,57	2.100,62 ±.016,16	2.122,08 ±.016,86
64	64.677,6 ±0.244,2	1.546,13 ±.004,38	2.390,52 ±.017,99	2.414,94 ±.018,79
36	57.086,3 ±0.175,0	1.751,73 ±.004,02	3.068,57 ±.022,15	3.099,91 ±.023,20
16	48.841,9 ±0.119,5	2.047,42 ±.003,76	4.191,94 ±.029,22	4.234,75 ±.030,69
4	42.577,5 ±0.086,0	2.348,66 ±.003,55	5.516,20 ±.037,42	5.572,54 ±.039,38

CASE PSF $\quad \frac{M_z^2}{M_R^2} = 1.036 \pm .002$

No. of Fuel Rods	b_{11} cm	γ_{11} $10^{-2}cm^{-1}$	γ_{11}^2 $10^{-4}cm^{-2}$	$\frac{M_z^2}{M_R^2}\gamma_{11}^2$ $10^{-4}\ cm^{-2}$
144	69.918,5 ± .298,5	1.430,24 ±.004,58	2.045,58 ±.015,74	2.120,02 ±.016,82
100	68.840,8 ± .288,5	1.452,63 ±.004,56	2.110,12 ±.016,22	2.186,91 ±.017,33
64	64.790,3 ± .247,5	1.543,44 ±.004,42	2.382,21 ±.018,02	2.468,90 ±.019,27
36	57.400,1 ± .180,1	1.742,16 ±.004,10	3.035,11 ±.022,10	3.145,56 ±.023,37
16	49.181,4 ± .120,5	2.033,29 ±.003,73	4.134,26 ±.028,74	4.284,71 ±.030,91
4	42.955,3 ± ..087,6	2.328,00 ±.003,56	5.419,59 ±.036,78	5.616,81 ±.039,63

TABLES 2.5.2.

CASE SF $\quad \frac{M_z^2}{M_R^2} = 1.182 \pm .003$

No. of Fuel Rods	b_{11} cm	γ_{11} $10^{-2}cm^{-1}$	γ_{11}^2 $10^{-4}cm^{-2}$	$\frac{M_z^2}{M_R^2}\gamma_{11}^2$ $10^{-4}cm^{-2}$
144	73.6614 ± .3356	1.357,56 ± .004,64	1.842,98 ± .014,28	2.177,62 ± .017,75
100	72.0972 ± .3175	1.387,02 ± .004,58	1.923,81 ± .014,81	2.273,13 ± .018,43
64	69.0804 ± .2850	1.447,59 ± .004,48	2.095,51 ± .024,61	2.476,01 ± .019,87
36	63.7487 ± .2305	1.568,67 ± .004,25	2.460,72 ± .018,25	2.907,52 ± .022,80
16	57.2593 ± .1750	1.746,44 ± .004,00	3.050,06 ± .021,95	3.603,88 ± .027,50
4	51.6308 ± .1362	1.936,83 ± .003,83	3.751,30 ± .026,41	4.432,45 ± .033,17

CASE OCF $\quad \frac{M_z^2}{M_R^2} = 1.330 \pm .004$

No. of Fuel Rods	b_{11} cm	γ_{11} $10^{-2}cm^{-1}$	γ_{11}^2 $10^{-4}cm^{-2}$	$\frac{M_z^2}{M_R^2}\gamma_{11}^2$ $10^{-4}cm^{-2}$
144	75.7544 ± .3600	1.320,06 ± .004,70	1.742,55 ± .013,60	2.317,36 ± .019,38
100	74.6497 ± .3572	1.339,59 ± .004,80	1.794,50 ± .014,15	2.386,46 ± .020,14
64	72.0851 ± .3152	1.387,25 ± .004,55	1.924,46 ± .014,76	2.559,29 ± .021,09
36	67.7611 ± .2641	1.475,77 ± .004,31	2.177,91 ± .016,27	2.896,34 ± .023,32
16	61.7472 ± .2109	1.619,51 ± .019,21	2.622,80 ± .019,21	3.487,99 ± .027,62
4	56.7867 ± .1692	1.760,98 ± .622,12	3.101,04 ± .022,12	4.123,98 ± .031,93

TABLES 2.5.2

CASE PSF(ODD) $\frac{M_Z^2}{M_R^2} = 1.027 \pm .002$

No. of Fuel Rods	b_{11}	γ_{11}	γ_{11}^2	$\frac{M_Z^2}{M_R^2}\gamma_{11}^2$
	cm	$10^{-2}cm^{-1}$	$10^{-4}cm^{-2}$	$10^{-4}cm^{-2}$
121	69.0721 ±.2890	1.447,76 ±.004,54	2.096,02 ±.016,07	2.152,23 ±.017,02
81	66.8243 ±.2605	1.496,46 ±.004,37	2.239.40 ±.016,85	2.299,46 ±.017,02
49	62.8606 ±.2365	1.590,82 ±.004,49	2.530,71 ±.019,28	2.598,58 ±.020,44
25	52.8997 ±.1450	1.890,37 ±.003,88	3.573,50 ±.025,34	3.669,34 ±.026,98
9	45.5223 ±.1005	2.196,73 ±.003,64	4.825,60 ±.033,10	4.955,02 ±.035,33

TABLES 2.5.2

CASES OF $^{1}/_{9}$ VACANCY

No. of Fuel Rods	b_{11}	γ_{11}	γ_{11}^2	$\frac{M_z^2}{M_R^2}\gamma_{11}^2$
	cm	$10^{-2}cm^{-1}$	$10^{-4}cm^{-2}$	$10^{-4}cm^{-2}$
PSCF128 VAC 16	67.3076 ± .2705	1.485,72 ± .004,48	2.207,35 ± .016,80	2.227,48 ± .018,20
PSCF8 VAC 1	65.5381 ± .1649	1.800,57 ± .004,01	3.242,03 ± .023,35	3.271,603 ± .025,49
PSF128 VAC 16	67.4012 ± .2745	1.483,63 ± .004,53	2.201,23 ± .016,85	2.272,84 ± .018,61
PSFD 72 VAC 9	64.4498 ± .2405	1.551,60 ± .004,34	2.407,44 ± .018,04	2.472,01 ± .019,87
PSFD 8 VAC 1	45.4968 ± .0991	2.197,96 ± .003,59	4.831,01 ± .032,92	4.960,57 ± .036,76
SF 128 VAC 16	72.2314 ± .3195	1.384,44 ± .004,59	1.916,68 ± .014,77	2.228,67 ± .018,81
SF 32 VAC 4	63.0804 ± .2257	1.585,28 ± .004,25	2.513,10 ± .018,64	2.922,179 ± .023,89

	ASYMMETRY FACTOR
PSCF 128 VAC 16	1.009 ± .003
PSF 128 VAC 16	1.033 ± .003
PSFD 128 VAC 16	1.026 ± .003
SF 128 VAC 16	1.163 ± .004

TABLES 2.5.2

CASE OF $^{1}/_{9}$ STEEL

No. of Fuel Rods	b_{11} cm	γ_{11} $10^{-2}cm^{-1}$	γ_{11}^2 $10^{-4}cm^{-2}$	$\frac{M_z^2}{M_R^2}\gamma_{11}^2$ $10^{-4}cm^{-2}$
PSCF 128 STEEL 16	55.4454 ±.1685	1.803,58 ±.003,99	3.252;89 ±.023,37	3.287,53 ±.025,52
PSCF 8 STEEL 1	49.4681 ±.1210	2.021,50 ±.003,70	4.086,48 ±.028,30	4.130,00 ±.031,08
PSF 128 STEEL 16	55.8529 ±.1611	1.790,42 ±.006,71	3.205,59 ±.022,69	3.309,89 ±.025,33
PSFD 72 STEEL 9	54.0161 ±.1506	1.851,30 ±.006,94	3.427,32 ±.024,25	3.519,23 ±.026,93
PSFD 8 STEEL 1	43.6271 ±.0907	2.322,20 ±.008,70	5.392,59 ±.037,15	5.533,39 ±.041,41
SF 128 STEEL 16	61.7631 ±.2105	1.619,09 ±.006,28	2.621,45 ±.023,63	3.048,16 ±.029,41
SF 32 STEEL 4	57.2166 ±.1721	1.747,74 ±.003,98	3.054,61 ±.021,81	3.551,83 ±.028,16

THE ASYMMETRY FACTORS IN THE PRESENT CASE ARE THE SAME AS IN THE CORRESPONDING VACANCY CASES.

TABLES 2.5.2

CASE PSCF108VAC36. $\frac{M_z^2}{M_R^2} = 1.008 \pm .003$

No. of Fuel Rods	b_{11}	γ_{11}	γ_{11}^2	$\frac{M_z^2}{M_R^2} = \gamma_{11}^2$
	cm	$10^{-2}cm^{-1}$	$10^{-4}cm^{-2}$	$10^{-4}cm^{-2}$
144	63.2050 ± .2285	1.582,15 ± .004,29	2.503,21 ± .018,65	2.522,62 ± .020,24
100	62.4394 ± .2207	1.601,55 ± .004,24	2.564,97 ± .019,01	2.584,86 ± .020,64
64	59.1301 ± .1901	1.691,19 ± .004,09	2.860,11 ± .020,82	2.882,30 ± .022,67
36	53.5117 ± .1485	1.868,75 ± .003,89	3.492,23 ± .034,77	3,519,30 ± .027,07
16	46.9293 ± .1087	2.130,86 ± .033,70	4.540,58 ± .031,42	4.575,79 ± .034,47
4	41.9502 ± .0835	2.383,44 ± .003,56	5.680,77 ± .038,54	5.724,82 ± .042,41

CASE PSCF 108 STEEL 36 $\frac{M_z^2}{M_R^2} = 1.008 \pm .003$

No. of Fuel Rods	b_{11}	γ_{11}	γ_{11}^2	$\frac{M_z^2}{M_R^2} \gamma_{11}^2$
	cm	$10^{-2}cm^{-1}$	$10^{-4}cm^{-2}$	$10^{-4}cm^{-2}$
144	44.8926 ± .4105	2.227,54 ± .004,19	4.961,93 ± .036,19	5.000,40 ± .020,24
100	44.6577 ± .1002	2.239,26 ± .003,78	5.014,27 ± .035,01	5.053,14 ± .038,35
64	44.0723 ± .0975	2.269,00 ± .003,76	5.148,37 ± .035,93	5.188,27 ± .039,36
36	43.4651 ± .0914	2.300,70 ± .003,63	5.293,20 ± .036,26	5.334,24 ± .039,85
16	42.1520 ± .0841	2.372,37 ± .003,56	5.628,12 ± .038,14	5.671,76 ± .041,98
4	40.7128 ± .0755	2.456,23 ± .003,41	6.033,07 ± .040,11	6.079,84 ± .044,28

TABLES 2.5.2

CASE PSCF 72 VAC 72 $\frac{M_z^2}{M_R^2} = 1.005 \pm .003$

No. of Fuel Rods	b_{11}	γ_{11}	γ_{11}^2	$\frac{M_z^2}{M_R^2}\gamma_{11}^2$
	cm	$10^{-2}cm^{-1}$	$10^{-4}cm^{-2}$	$10^{-4}cm^{-2}$
144	55.6166 ± .1640	1.798,02 ± .003,97	3.232,89 ± .023,19	3.249,99 ± .025,25
100	55.1451 ± .1604	1.813,40 ± .003,95	3.288,41 ± .023,52	3.305,81 ± .025,62
64	53.1196 ± .1475	1.882,54 ± .003,92	3.543,97 ± .025,24	3.562,72 ± .027,51
36	49.4999 ± .1220	2.020,21 ± .003,73	4.081,23 ± .028,37	4.102,83 ± .031,03
16	44.9764 ± .0975	2.223,36 ± .003,61	4.943,35 ± .033,80	4.969,50 ± .037,07
4	41.3376 ± .0795	2.419,11 ± .003,49	5.852,07 ± .039,32	5.883,03 ± .043,25

CASE PSCF 72 STEEL $\frac{M_z^2}{M_R^2} = 1.005 \pm .003$

No. of Fuel Rods	b_{11}	γ_{11}	γ_{11}^2	$\frac{M_z^2}{M_R^2}\gamma_{11}^2$
	cm	$10^{-2}cm^{-1}$	$10^{-4}cm^{-2}$	$10^{-4}cm^{-2}$
144	33.9959 ± .0510	2.941,53 ± .003,35	8.652,61 ± .056,95	8.698,39 ± .062,86
100	33.9145 ± .0506	2.948,59 ± .003,30	8.694,19 ± .056,80	8.740,19 ± .062,77
64	35.4822 ± .0564	2.818,31 ± .003,36	7.942,90 ± .052,36	7.984,92 ± .057,78
36	34.3343 ± .0529	2.912,54 ± .003,36	8.482,89 ± .055,97	8.527,77 ± .061,75
16	37.2606 ± .0637	2.683,80 ± .003,44	7.202,78 ± .048,06	7.240,89 ± .052792
4	39.0452 ± .0695	2.561,15 ± .003,42	6.559,41 ± .043,62	6.594,11 ± .048,07

TABLES 2.5.2

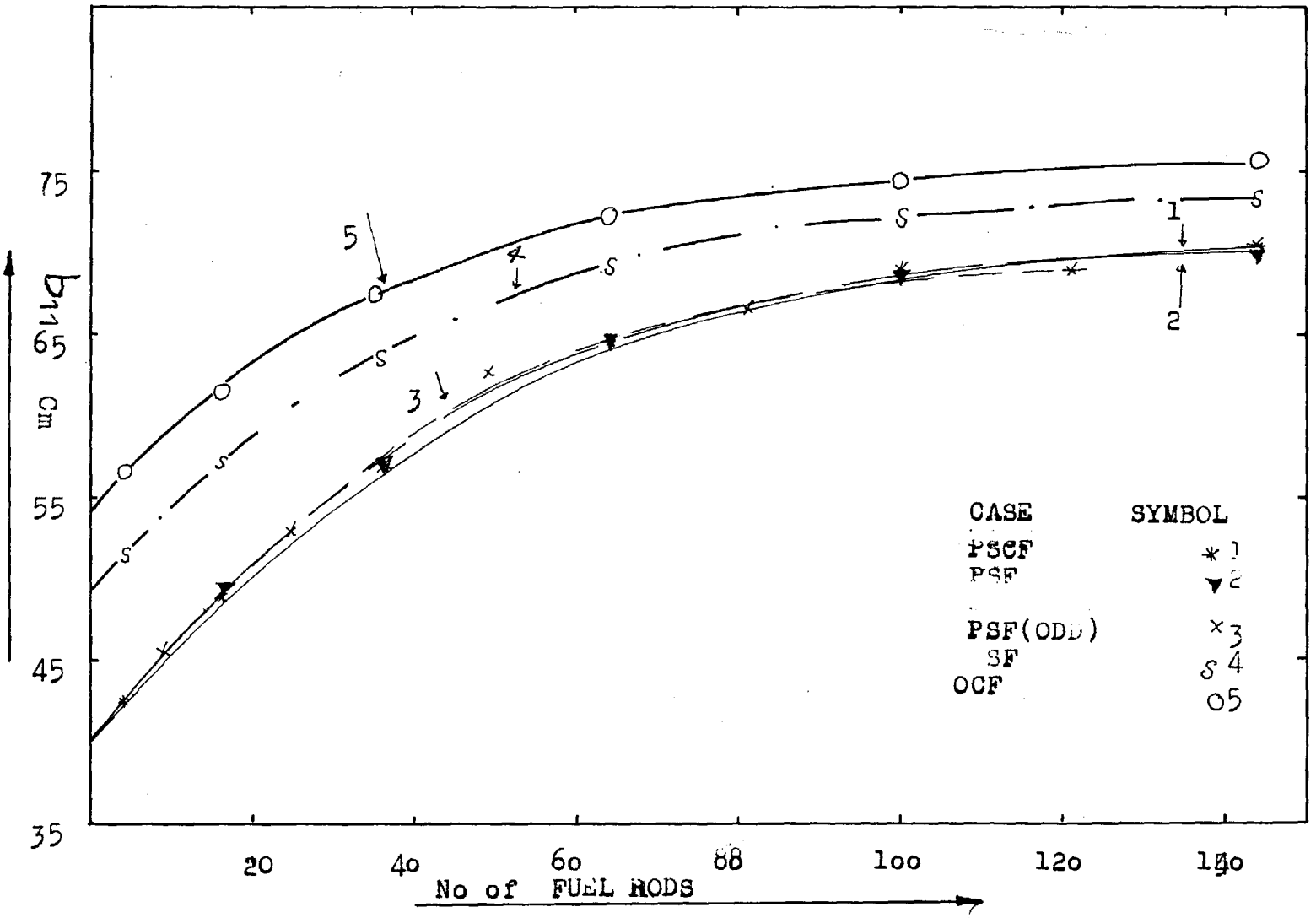

FIG. 2.5.1 (A) B11 (RELAXATION LENGTH) AS A FUNCTION OF NO OF FUEL RODS.

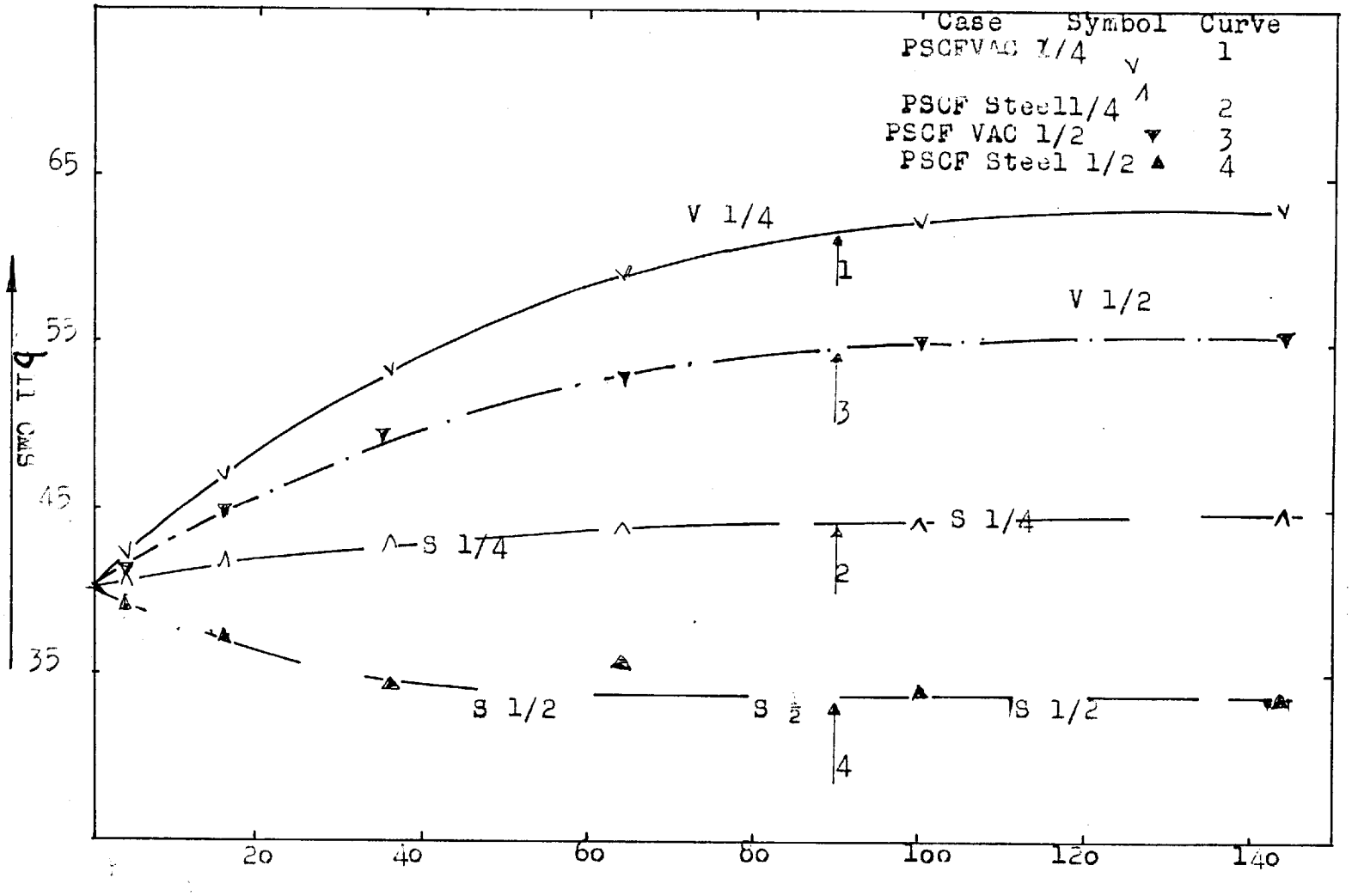

(B)

FIG. 3.1 B11 (RELEXATION LENGTH) AS FUNCTION OF NO OF FUEL RODS

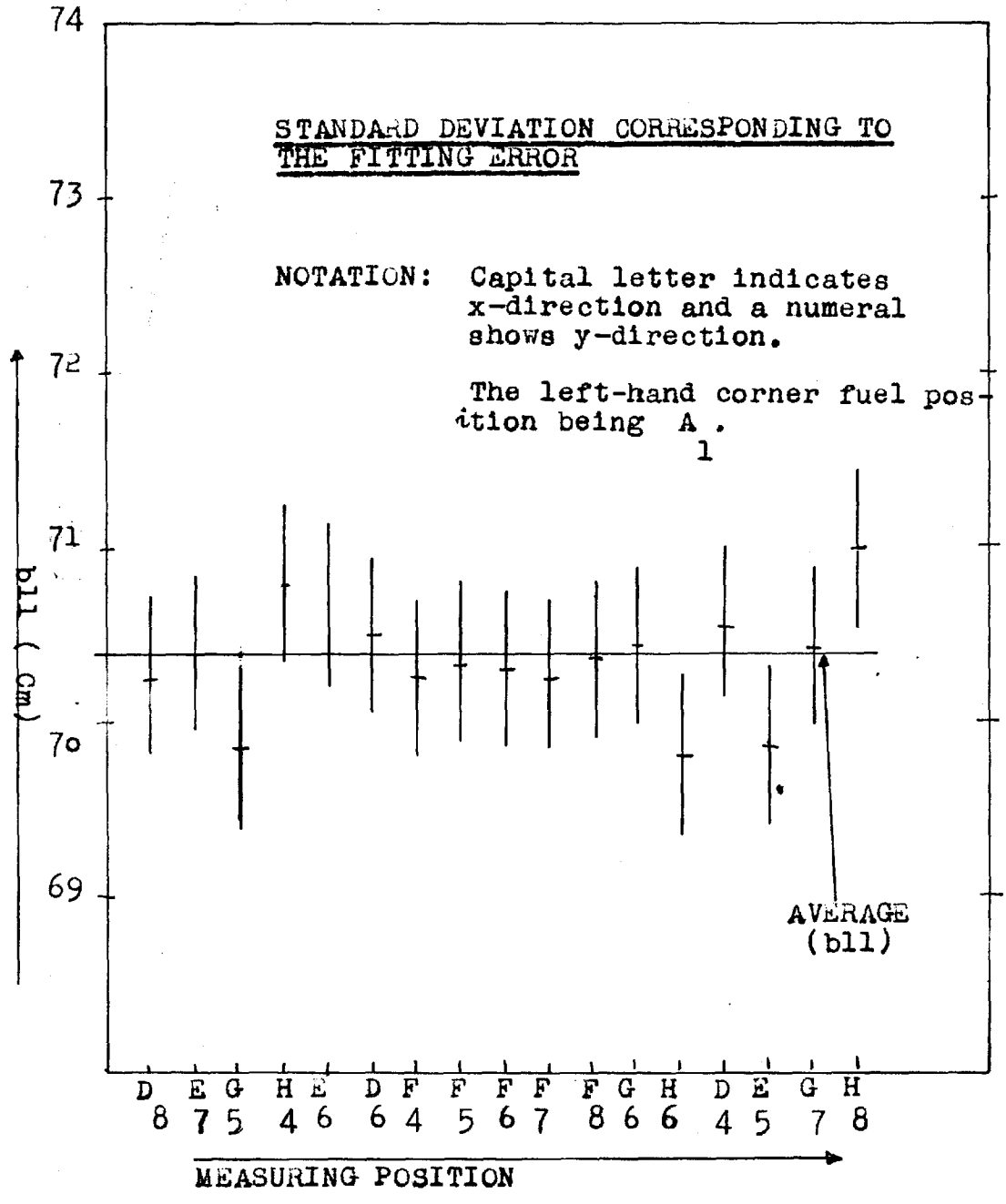

FIG. 2.5.1 (C) b11 VS MEASURING POSITION

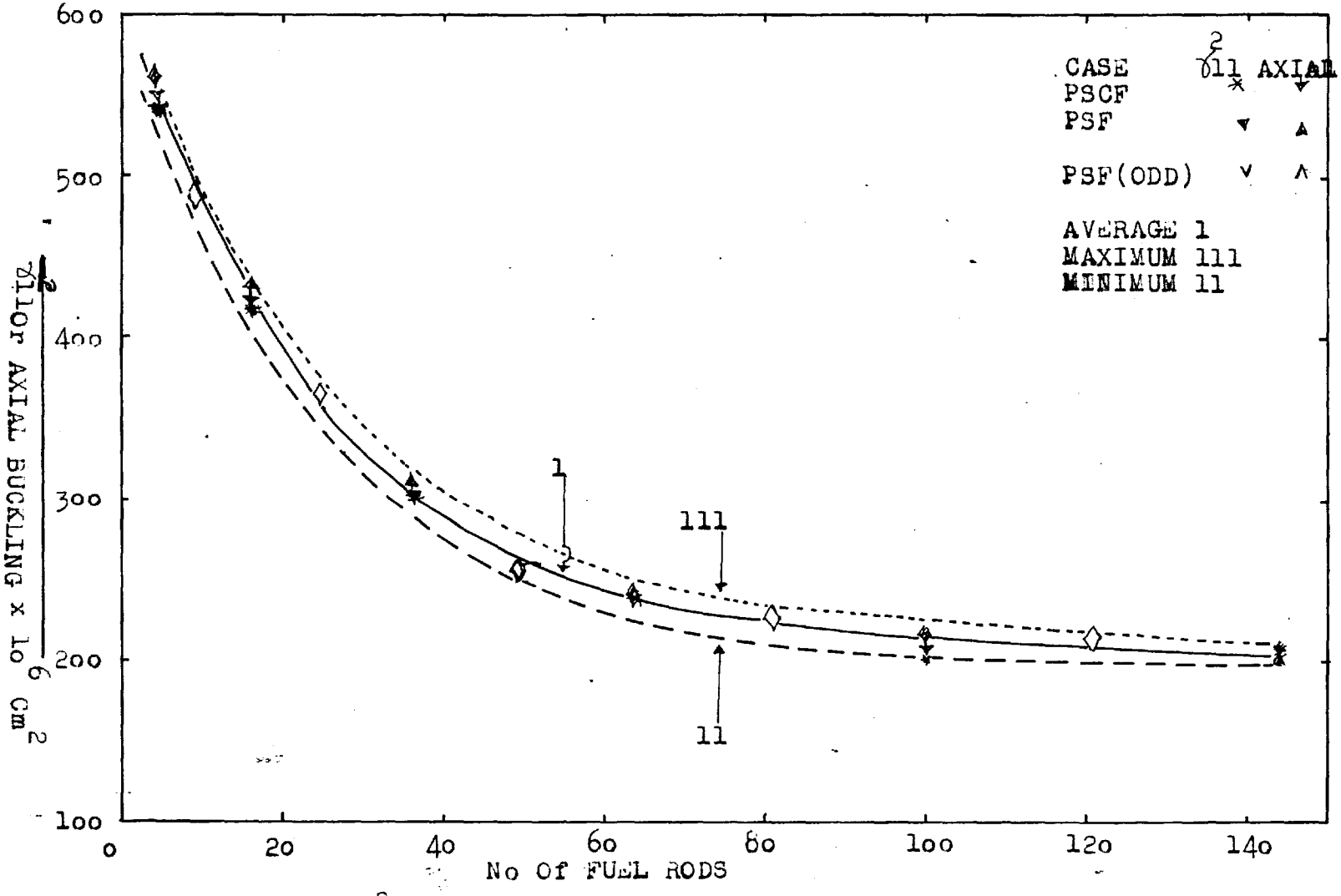

FIG. 2.5.1 (D) γ_{11}^2 ANDAXIAL BUCKLING V.S NO OF FUEL RODS

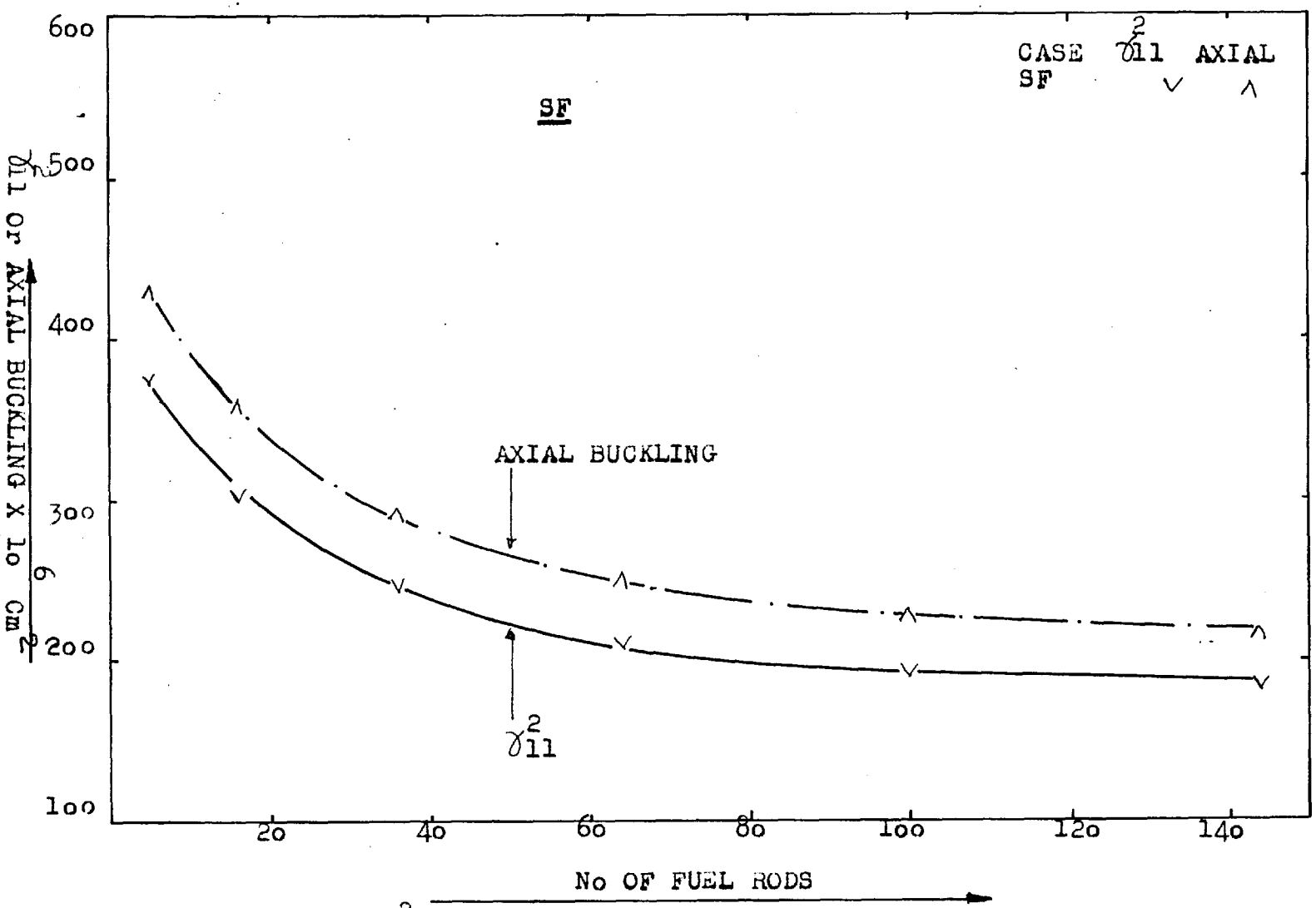

FIG. 2.5.1 (E) γ_{11}^2 AND AXIAL BUCKLING V.S NO OF FUEL RODS

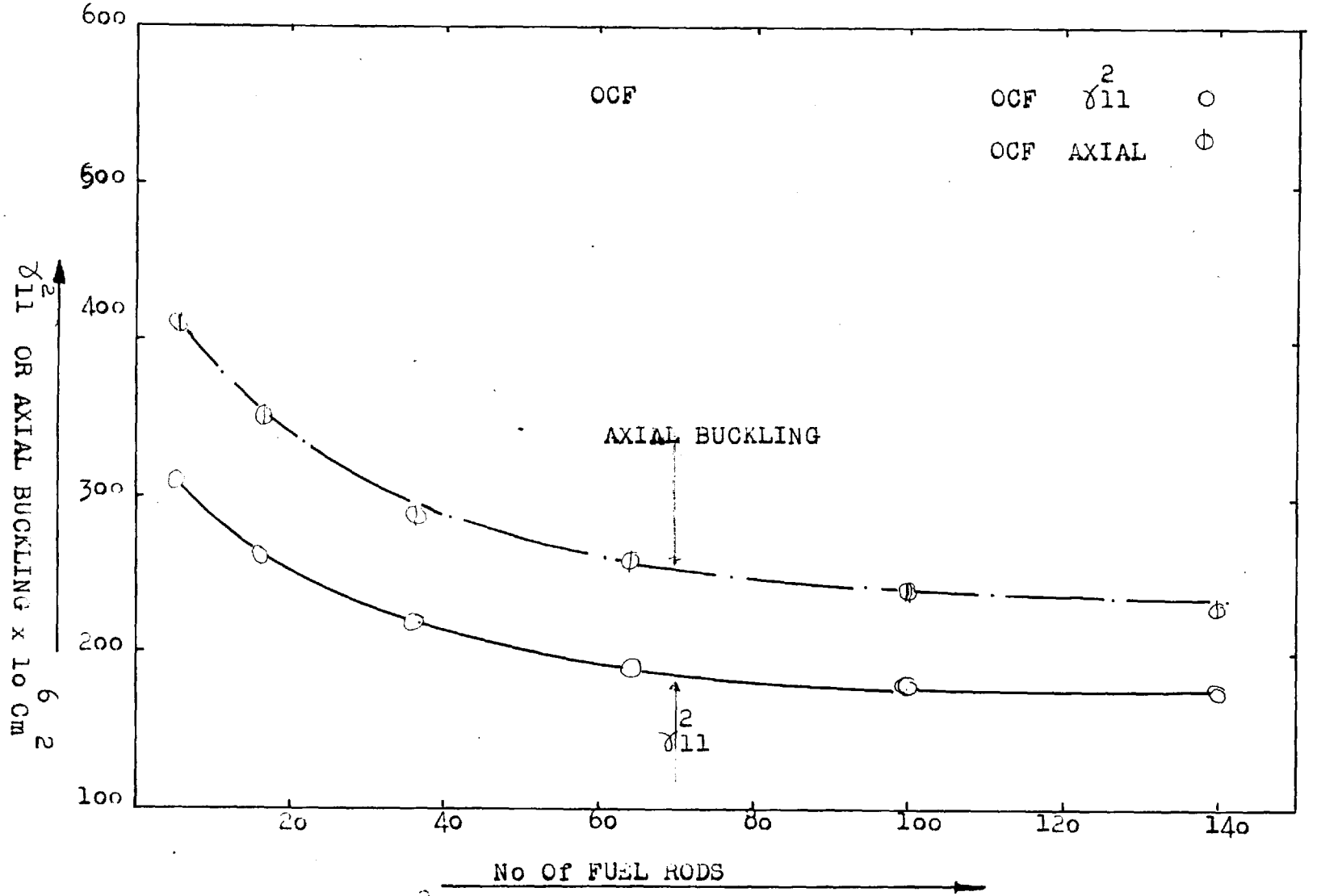

FIG. 2.5.1 (F) γ_{11}^2 AND AXIAL BUCKLING V.S. NO OF FUEL RODS

PSCF 128 VAC 16 and so on. In the next columns the symbols b_{11}, γ_{11}, γ_{11}^2 and $(M_z^{-2}/M_R^2\ \gamma_{11}^2)$ are pretty well known.

The error quoted under b_{11} is the fitting error but in calculating the errors in γ_{11} and the related parameters take into consideration that it is not one solitary measurement but an average of 17 fitted b_{11}'s, independently measured thermal flux distributions. The details of calculation of errors are given in the next section.

Curve (A) shows the variation of the relaxation length experimentally measured as a function of the number of fuel rods and is an indication of the build-up of the steady-state condition from the ordinary diffusion stack condition. It is instructive to note that from the graph we have the value of b_{11} for no fuel and the experimentally fitted value for the diffusion stack as

CASE	b_{11} (Graph)	b_{11} (Experiment)
PSCF	40.15 $\pm$ 0.10 cms	39.84 $\pm$ 0;07 cms
PSF	40.20 $\pm$ 0.10 cms	40.30 $\pm$ 0.07 cms
or PSFD SF	49.30 $\pm$ 0.12 cms	48.98 $\pm$ 0.12 cms
OCF	54.40 $\pm$ 0.14 cms	54.35 $\pm$ 0.15 cms

Even though the extrapolation method is subject to large errors, these values agree quite well within reasonable accuracy of fitting error in b_{11}.

A similar conclusion is reached if we extrapolate the measured thermal flux distribution in the horizontal direction for radial extrapolated length in comparion to values in Table 2.5.1. Curve (B) is an identical curve to the case (A) but herein the lattice under study is PSCF and has vacancy or steel in it, one per four lattices or two lattices, and their interpolation to zero number of fuel elements gives

	b_{11} (Graph)	b_{11} (experiment)
All Cases	40.15 ± 0.10 cm	39.80 ± 0.07 cm.

The purpose of the curve (C) is to show the variation of b_{11} (relaxation length) obtained in a typical experiment of 17 measurements. The letters indicate the number of the lattice in the x-direction and integers show the number of the lattice position, (specifically corner hole position in the y-direction).

The curves D, E and F indicate the effect of asymmetry factor introduced because of the streaming corrections applied to the square of the inverse of the relaxation length (γ_{11}^2). The value of the experimentally measured axial buckling (γ_{11}^2) increases to ($M_z^2/M_R^2\ \gamma_{11}^2$) henceforth referred to as "Axial".

In case of PSCF, PSF and PSF(ODD) the points practically coincide on the graph and therefore their extreme variations as "maximum" of axial and "minimum" of γ_{11}^2

curve indicated and the central one marked "average", indicates the variation of γ_{11}^2 over the whole spectrum of number of fuel rods, and it is revealing that they seem to fit a pretty well defined curve, though in case of PSF compared to PSCF, the streaming factors have increased considerably because of the removal of corner holes (void increase $\approx$ 2.5%) while in case of PSF(ODD) even the lattice has undergone a slight change in its configuration. The curves E and F are very clearly marked and show the streaming effect quite distinctly and follow a similar pattern.

2.5.2 ERRORS ARISING IN THE CALCULATION OF THE RELAXATION LENGTH AND THE RELATED PARAMETERS FROM THE FLUX

In analysing the flux distribution to obtain the value of b_{11}, the standard deviation of b_{11} is taken equal to the fitting error which very often ranges from 0.4 to 0.5% and the accuracy is in reasonable agreement with other measurements (23). This may be due to

1) possible harmonic contributions and
2) error in counter positioning.

The magnitude of the final error given in Table 2.5.2 depends on the number of measured flux points and on the number of relaxation lengths over which the flux is measured. Since, in a typical experiment, 17 measurements of relaxation length are made the average of all

those has been reported unless rejected, the error is reduced by a factor of $\sqrt{17}$. In a normal distribution (42) the probability that an observation lies within 3σ of the mean is 0.9973. Then the range of a distribution conforming to the normal type is effectively 6σ. The range ($\bar{x} \pm 3.09\sigma$) is the 99.8% zone and that an observation lies outside this range is 2 in 1000. It is for this reason that the actual fitting error in b_{11} is reported, which gives an idea of the fitting error in b_{11} and, at the same time, a fair idea of the range within which a measured value of b_{11} should lie in an experimental measurement.

In this context, therefore, it should be remembered that the standard deviation is equal to $(3.09/\sqrt{17})$ of the figure quoted in the Tables under the value of b_{11}, the relaxation length and the error in γ_{11} and γ_{11}^2 is calculated in a normal way. To calculate the error in the axial buckling namely $\frac{M_z^2}{M_R^2}\gamma_{11}^2$, the asymmetry factor comes in, which has not been measured during this study. However, these measurements have been done by Macdonald (4), and his results are

Lattice	M_z^2/M_R^2
PSF	$1.027 \pm .002$
OCF	$1.306 \pm .003$

In the light of this information, the following errors

in the asymmetry factors were assumed.

Lattice	$\sigma(M_z^2/M_R^2)$
PSCF PSF PSF(ODD)	0.002
SF	0.003
OCF	0.004
PSCF 128 VAC 16 PSF 128 VAC 16 PSFD 128 VAC 16	0.003
SF 128 VAC 16	0.004
PSCF 108 VAC 36 PSCF 72 VAC 72	0.003

TABLE 2.5.3

The asymmetry factors were calculated according to Syrett's model (7) and are reported in detail in the next chapeter. The errors in asymmetry factors in some cases were increased knowingly, since his measurements were done with stack fueled, while in the present study the assembly is often partially filled with fuel elements. The errors in γ_{11}^2 and M_z^2/M_R^2 were assumed to be interdependent and therefore the combined error in the axial buckling (42) was aalculated by the expression

$$\sigma^2_{axial} = \sigma^2_{\gamma_{11}^2} \left(\frac{\delta AX}{\delta \gamma_{11}^2}\right)^2 + \sigma^2_{\xi} \left(\frac{\delta AX}{\delta \xi}\right)^2 \qquad 2.5.3$$

where

$$\text{axial} = AX = \frac{M_z^2}{M_R^2} \gamma_{11}^2$$

$$AX = \xi \gamma_{11}^2 \qquad 2.5.4$$

In Table 2.5.4 the errors arising in γ_{11}^2 and $\frac{M_z^2}{M_R^2} \gamma_{11}^2$ both

1) due to fitting error in b_{11} and

2) due to the maximum possible error of 0.5 % in b_{11}

are given. These have been tabulated side by side for the sake of comparison. Only the four representative core cases have been given; the rest have been left. In no case was it found that the fitting error was greater than the maximum possible error of 0.5 % in b_{11}.

2.5.3 DISCUSSION

The conclusion which can be drawn from the present experimental results, tabulated in Section 2.5.2 and plotted in FIGS. 2.5.2, could be summed up by saying that the results are accurate to the extent that an experiment can predict a measured axial and material buckling (Chapter 3) for the neutron flux. The accuracy of the measurements is compatible with the accuracy reported by others (4, 23). In all cases, the maximum possible error due to an error

PSCF

Case	γ_{11}^2		$M_z^2/M_R^2\ \gamma_{11}^2$	
No. of Fuel Rods	Fitting Error in b_{11}	0.5% error in b_{11}	Fitting Error in b_{11}	0.5% error in b_{11}
144	1.558	1.676	1.625	1.740
100	1.616	1.761	1.687	1.828
64	2.799	2.070	2.879	2.145
36	2.215	2.829	2.320	2.923
16	2.922	4.178	3.069	4.303
4	3.742	5.888	3.938	6.049

PSF

	γ_{11}^2		$M_z^2/M_R^2\ \gamma_{11}^2$	
	Fitting Error in b_{11}	0.5% Error in b_{11}	Fitting Error in b_{11}	0.5% Error in b_{11}
144	1.574	1.704	1.682	1.813
100	1.622	1.771	1.733	1.884
64	1.802	2.061	1.927	2.189
36	2.210	2.790	2.370	2.955
16	2.874	4.106	3.091	4.335
4	3.678	5.759	3.963	6.066

SF

144	1.428	1.496	1.775	1.851
100	1.481	1.578	1.843	1.952
64	1.595	1.756	1.987	2.168
36	1.825	2.147	2.280	2.642
16	2.195	2.807	2.750	3.441
4	2.641	3.636	3.317	4.441

OCF

144	1.359	1.394	1.938	1.981
100	1.415	1.447	1.014	1.053
64	1.476	1.579	2.109	2.236
36	1.627	1.843	2.332	2.601
16	1.921	2.325	2.762	3.265
4	2.212	2.866	3.193	4.008

TABLE 2.5.4

The errors in γ_{11}^2 and $(M_z^2/M_R^2\ \gamma_{11}^2)$ have been multiplied by $(\underline{10^6\ cm^2})$.

of 0.5 cm% in the b_{11} has been considered. The fitting error in b_{11} and the extrapolated length measurements has been always less than the maximum errors quoted in the literature.

CHAPTER 3

HOMOGENEOUS REACTOR THEORY (Unit Cell Method), DERIVATION OF CHARACTERISTIC PARAMETERS AND THE EXPERIMENTAL RESULTS

3.1 THE METHOD AND THE BASIC ASSUMPTIONS

The essential feature of the unit cell method of Wigner and Seitz is that it represents a typical lattice element of a heterogeneous array by an Equivalent unit cell. The lattice is regarded as a periodic array of identical unit cells, each having a fuel element symmetrically located in it. In view of the symmetry of the cells, a single cell may be taken as representative of the infinite array. In this way, K_∞, L^2, L_s^2, etc. are calculated, and for macroscopic behaviour of the reactor, the lattice is replaced by a homogeneous material having the same characteristic values as the actual lattice. In the case of big coolant channels as in the present cases streaming corrections in axial and transverse directions need to be applied. However, the basic assumptions behind this treatment are that

i) the reactor is large and the neutron flux does not change appreciably over a distance of one lattice pitch, implying that there is no interaction between microscopic and macroscopic fluxes;

ii) the neutron energy spectrum is the same in the finite

reactor as in an infinite array.

In performing a calculation based on this model, the usual procedure is to specify that the net neutron current at the boundary of the cell is zero. The neutron flux distribution in the unit cell is obtained with the aid of diffusion theory (for more accurate work transport theory may be used) depending on the size of the lattice. Having determined both the energy spectrum and spatial distribution of the neutron population in the cell, thermal utilisation, resonance escape-probability, ε fast fission factor and η the reproduction constant can be evaluated and finally the infinite multiplication constant K_∞. Most of the calculations reported in this chapter have been carried out according to the procedure laid down by Syrett (7).

In sections 3.2 and 3.3. of the present chapter details of theoretical calculation of flux distribution and all the lattice parameters are given without any reference to actual computed numbers. In section 3.4 are given the computed results on the basis of theory outlined in sections 3.2-3. The computation has been carried out by the programme described in Appendix A-2.2. The experimental results have been compared with theory and discussed in the same section.

3.2.1 CALCULATION OF FLUX AND THE LATTICE PARAMETERS

Let us consider the case of cylindrical fuel rods embedded in a moderator with a square lattice pitch. If we assume the uranium rods to be infinite in length and then the lattice is replaced by a cylindrical one equivalent in cross-sectional area keeping the fuel channel boundary intact,

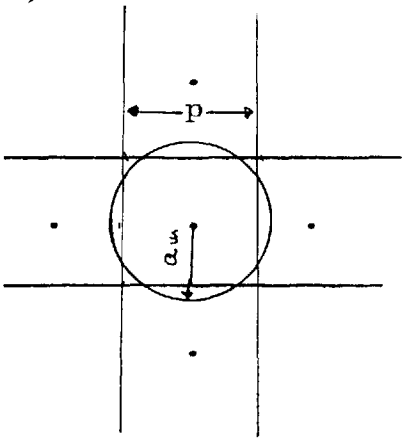

then $p^2 = \pi a_m^2$ 3.2.1

Now we have a uranium rod of radius a_o in a lattice cell moderator of radius a_m. Since the production of thermal neutrons by the slowing down process is such that no thermal neutrons are produced in uranium and therefore, the production rate of thermal neutrons is constant at all points in the moderator. Thus the steady-state diffusion equations in the uranium and moderator are

$$\nabla^2 \varphi_u - \kappa_u^2 \varphi_u = 0 \qquad 3.2.2$$

$$\nabla^2 \varphi_m - \kappa_m^2 \varphi_m + \frac{S}{D_m} = 0 \qquad 3.2.3$$

Solving these two equations by the usual procedure under the boundary conditions

i) flux is finite and symmetrical everywhere in the lattice;

ii) $\varphi_u = \varphi_m$ at uranium-graphite interface, i.e. $r = g_m = a_o$;

iii) The neutron current in and out of urnaium-graphite interface is equal i.e.

$$D_m \frac{\delta\varphi_m}{\delta r} = D_o \frac{\delta\varphi_o}{\delta r} \quad \text{at } r = a_o = g_m.$$

iv) Zero current at the boundary of the lattice, i.e.

$$D_m \frac{\partial\varphi_n}{\delta r} = 0 \quad \text{at } r = a_m.$$

The expressions for flux in Uranium and Moderator would be

$$\varphi_u = A\, I_o(\kappa_u r) \qquad 0 \leq r \leq a_o \qquad 3.2.4$$

$$\varphi_m = C\, I_o(\kappa_m r) + F\, K_o(\kappa_m r) + \frac{S}{\Sigma_{am}}$$

$$a_o \leq r \leq a_m \qquad 3.2.5$$

The shape of the flux distribution would be as in Fig. 3.2.1. (upper distribution)

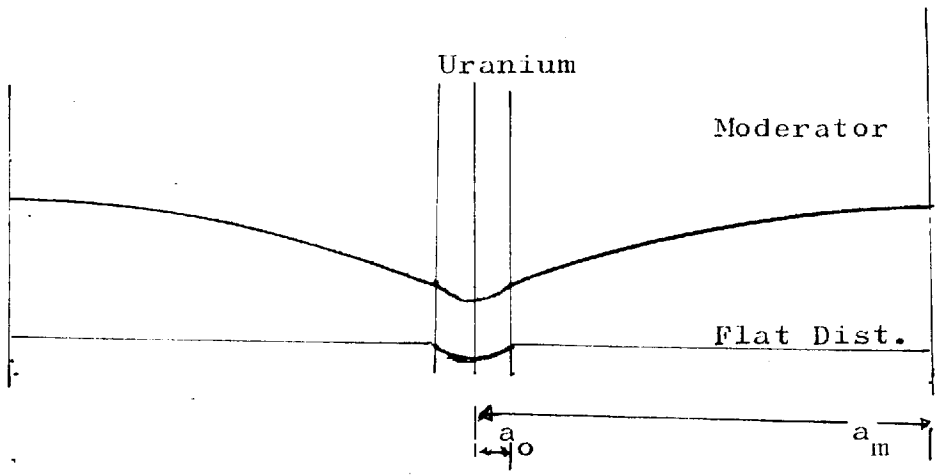

FIG. 3.2.1

Knowing A, C, F, the flux distribution can be plotted.

3.2.2 CALCULATION OF THERMAL UTILIZATION

The thermal utilisation is defined as

$$f = \frac{\text{absorption in fuel}}{\text{total absorption in the unit cell}}$$

Since we assume that there is no net loss of neutrons from the cell, therefore total absorption in the unit cell is equal to total thermal source term SV_m, V_m being volume of the moderator, then

$$f = \frac{V_o \Sigma_{au} \bar{\varphi}_u}{S V_m} \qquad 3.2.6$$

where

$$\bar{\varphi}_U = \text{AV. flux in uranium} = \frac{\int_o^{a_o} \varphi_u 2\pi r \, dr}{\pi a_o^2}$$

$$\bar{\varphi}_{u} = \frac{2A}{\kappa_{u} a_{o}} \cdot I_{1}(\kappa_{u} a_{o}) \qquad 3.2.7$$

On substitution in eq. 3.2.6 we have

$$f = \frac{V_{o}}{V_{m}} \cdot \frac{\Sigma_{au} \cdot 2A}{(\kappa_{u} a_{o}) \cdot S} \cdot I_{1}(\kappa_{u} a_{o})$$

$$\frac{1}{f} = \frac{V_{m} \cdot (\kappa_{u} a_{o})}{V_{o} \cdot 2\Sigma_{au}} \cdot \frac{1}{I_{1}(\kappa_{u} a_{o})} \cdot \left(\frac{S}{A}\right) \qquad 3.2.7$$

if we make use of the boundary conditions (ii) and (iii) of section 3.2.1 for $r = a_{o}$, and $r = a_{m}$

$$\frac{S}{A} = \Sigma_{a} \left[I_{o}(\kappa_{m} a_{o}) - \frac{D_{u} \kappa_{u}}{D_{m} \kappa_{m}} \cdot M_{o}(\kappa a) \right] \qquad 3.2.8$$

where

$$M_{o}(\kappa a) = I_{1}(\kappa_{u} a_{o}) \left[\frac{I_{o}(\kappa_{m} a_{o}) K_{1}(\kappa_{m} a_{m}) + K_{o}(\kappa_{m} a_{o}) I_{1}(\kappa_{m} a_{m})}{I_{1}(\kappa_{m} a_{o}) K_{1}(\kappa_{m} a_{m}) - K_{1}(\kappa_{m} a_{o}) I_{1}(\kappa_{m} a_{m})} \right]$$

Ultimately the expression for f reduces to

$$\frac{1}{f} = 1 + \frac{V_{m}}{V_{o}} \cdot \frac{\Sigma_{am}}{\Sigma_{au}} \cdot G + X \qquad 3.2.9$$

where

$$G = \frac{\kappa_{u} a_{o}}{2} \cdot \frac{I_{o}(\kappa_{u} a_{o})}{(\kappa_{u} a_{o})} \qquad 3.2.10$$

$$X = \frac{\kappa_{m}(a_{m}^{2} - a_{o}^{2})}{2 a_{o}} \left[\frac{I_{o}(\kappa_{m} a_{o}) K_{1}(\kappa_{m} a_{m}) + K_{o}(\kappa_{m} a_{o}) I_{1}(\kappa_{m} a_{m})}{I_{1}(\kappa_{m} a_{m}) K_{1}(\kappa_{m} a_{o}) - I_{1}(\kappa_{m} a_{o}) K_{1}(\kappa_{m} a_{m})} \right] - 1$$

3.2.11

X is the excess absorption term which arises due to flux rise in the moderator and would be zero if the flux were

flat. In general for a complicated reactor lattice we can write

$$\frac{1}{f} = 1 + \sum_{\substack{i \\ \text{all components}}} \frac{V_i \Sigma_i}{V_o \Sigma_{au}} \cdot \frac{\bar{\varphi}_i}{\bar{\varphi}_o} \qquad 3.2.12$$

The method can be extended to include epithermal neutron absorption, and flux fine-structure distribution in the lattice.

Following Syrett (7), it is assumed that thermal neutron spectrum is Maxwellian and the fast neutron spectrum follows $^1/E$ law. It is assumed that the fast flux is constant throughout the lattice. Westcott's definition for the neutron flux and the cross-sections is used, which is defined as the reaction-rate of a $^1/v$ detector, having unit cross-section at a neutron velocity of 2200 m/sec (.0253 eV). The slow neutron group includes only those neutrons which have a Maxwellian velocity distribution. Epithermal absorption and epithermal fission are associated with slowing down and resonance absorption in the epithermal range which extends from thermal velocities to fission threshold velocity of U^{238}.

The thermal utilization factor f_5 for U^{235} is calculated by

$$f_5 = \frac{\Sigma_{5f}}{\Sigma_{5a} + \Sigma_{xa}} \qquad 3.2.13$$

where Σ_{xa} includes the absorption in everything other than U^{235} and the quantity $(f\eta)$ is replaced by its numerically equivalent quantity $(f_5\eta_5)$.

If we now expand the expression (3.2.12) it would be written as

$$\frac{1}{f_5} = 1 + A_8 + A_g + A_n \qquad 3.2.14$$

where

$$A_8 = \frac{\Sigma_{80}}{\Sigma_{50}} \cdot \frac{(1+\beta'_u)}{N'}$$

$$A_g = \frac{V_g \Sigma_{ag}}{V_u \Sigma_{50}} \cdot \frac{(CRSG + \beta'_u)}{N'}$$

$$A_n = \frac{V_n \Sigma_{mn}}{V_u \Sigma_{50}} \frac{(G.B + \beta'_u)}{N'}$$

and

$$N' = \frac{\sigma_{5M}}{\sigma_{50}} + \beta'_u \frac{\sigma_{5e}}{\sigma_{50}}$$

$$\beta'_u = \sqrt{\frac{4}{\mu}} \cdot \frac{\eta_{5M} \varepsilon p}{\xi_g} \cdot \frac{V_v}{V_g} \cdot \frac{\Sigma_{5M}}{\Sigma_{sg}} \qquad (b)$$

$$\eta_{5M} = \eta_{50} \frac{g_{f5}(T)}{g_{a5}(T)} ;$$

B, C, G, R and S are the flux ratios defined in the latter part of the present section.

$T \rightarrow$ is the room temperature

$$\eta_{50} = 2.033.$$

Values of g's have been taken from Tables (7).

The inverse diffusion length in graphite is calculated from the expression

$$\kappa_g(T_o) = 0.00933\ S_g \sqrt{\sigma_g}\ \ cm^{-1} \quad (a) \qquad 3.2.15$$

$$T_o = 20.4^oC$$

σ_g is in millibars, which is calculated according to

$$\sigma_{g(in\ air)} = 1.0775 x \sigma'_g + \left(\frac{1.52}{d} - 1.0691\right) \quad (b) \qquad 3.2.15$$

where σ'_g is the Gleep value for A-grade reactor graphite. σ'_g = 4.1 mb has been used for the graphite which is of the same vintage as the graphite used in the early BICEP work (23). This is the quantity defined as "old σ_g" by Syrett (7). Equation 3.2.15 is the correction to the graphite absorption cross-section on account of air (nitrogen) present in the pores of the graphite. The inverse diffusion length for the natural uranium fuel is

$$\kappa_u(T_o) = 0.89\ S_u \qquad 3.2.16$$

There is no need to apply any correction for temperature and enrichment for the fuel available (natural uranium). The parameters $[\lambda_u \kappa_u^{\ 2}]$ and $[\frac{\lambda_u \kappa_u^{\ 2}}{\lambda_g}]$ are defined as

$$[\lambda_u \kappa_u^{\ 2}] = 0.64\ S_u \left(1 + \frac{a_o}{g_m}\right) \qquad 3.2.17$$

$$[\lambda_u \frac{\kappa_u^{\ 2}}{\lambda_g}] = 0.20\ S_u S_g \left(1 + \frac{a_o}{g_m}\right) \qquad 3.2.18$$

The ratio of maximum to mean flux in a uranium rod G is given by

$$G = \frac{\kappa_u a_o}{2} \cdot \frac{I_o(\kappa_u a_o)}{I_1(\kappa_u a_o)} \qquad 3.2.19$$

while B, the ratio of mean flux in sheath outside fuel to maximum flux in the uranium, is

$$B = 1 + \frac{a_o}{3G}[\lambda_u \kappa_u^2] \cdot C_1 \qquad 3.2.20$$

where C_1 is a temperature dependent constant. C, the ratio of the flux at the outer edge of the sheath outside the fuel to the flux at the outer edge of the uranium, is given by

$$C = 1 + \frac{[\lambda_u \kappa_u^2]}{3G} \cdot C_2 \qquad 3.2.21$$

C_2 = temperature dependent constant.

Similarly for R and S

$$R = 1 + \frac{[\lambda_u \kappa_u^2]}{3GC} \cdot a_o^2 \left(\frac{1}{a_n} - \frac{1}{g_n}\right) \qquad 3.2.22$$

$$S = 1 \quad \left[\frac{\lambda_u \kappa_u^2}{\lambda_g}\right] \cdot \frac{a_o^2}{GCRS} \frac{X}{\kappa_g^2} \qquad 3.2.23$$

X is given by eq. 3.2.11. Symbols R and S denote respectively the ratio of the flux at the inner edge of the moderator to the flux at the outer edge of the sheath outside the fuel and the ratio of the mean flux in the moderator to the flux at the inner edge of the moderator.

3.2.3 CALCULATION OF FAST FISSION FACTOR

When U^{235} undergoes fission, fast neutrons of average energy 2 MeV are emitted. Though the energies of the prompt neutrons cover a considerable range (up to 10 MeV) yet the majority, however, have energies of about 1-2 MeV. Those with energy above U^{238} fission threshold (1.1 MeV) cause fission and the "fast fission factor ε" is defined as

$$\varepsilon = \frac{\text{Neutrons slowing down past } U^{238} \text{ fission threshold}}{\text{Neutrons produced by thermal fission}}$$

The main contribution to this fact comes from

i) neutrons colliding with Uranium atoms in the same fuel element, and

ii) neutrons colliding with uranium atoms in the neighbouring fuel elements.

The contribution from the second effect in the present case is so small that we can simply neglect it, since the lattice pitch is 20.32 cms and the scattering mean free path for graphite is 2.57 cm, and it is improbable that a fast neutron from one fuel element would reach another fuel element as a "Fast neutron" with energy above U^{238} fission threshold. However, in closely packed lattices this would be predominant. The main contribution to this effect in the present lattices studied comes from the first effect and it is

therefore sufficiently accurate to calculate the fast fission factor in "a single isolated fuel element". Following the usual slowing down process of fission neutron in a uranium rod (1), we will arrrive at the expression for fast fission factor as given below

$$\varepsilon = 1 + \frac{Q(\nu_{8F} - 1 - \frac{\sigma_{CF}}{\sigma_{8fF}}) \frac{\sigma_{8fF}}{\sigma_{uF}} (p + \Delta p)}{1 - \frac{Q\nu_{8F}}{\sigma_{uF}} \frac{\sigma_{8fF}}{} + \sigma_{eF} (p+\Delta p)} \qquad 3.2.24$$

where

Q = fraction of neutrons born with energy above U^{238} fission threshold, and is taken as equal to 0.522

p = the probability that a fast fission neutron will make a collision inside the fuel rod in which it was created is given as a function of $(N_{u\,uF} a_o)$ (7)

$$\Delta p = (1-p)^2 \frac{V_u \Sigma_{uF}}{V_g \Sigma_{gF}} \sum_{n=0}^{\infty} \left[1 - \frac{V_u \Sigma_{uF}}{V_g \Sigma_g} (1-p)\right]^n (a_n + a_{n+1} + .. a_\infty) \qquad 3.2.25$$

The summation term is also given as a function of $\frac{V_u}{V_g} \cdot \frac{\Sigma_{uF}}{\Sigma_{gF}} \cdot (1-p)$. The other terms have their usual significance.

3.2.4 RESONANCE ESCAPE PROBABILITY

During the slowing down process, some of the neutrons are captured in non-fission processes (especially, U^{238}), so that not all the neutrons reach thermal energies. The probability, that a neutron will escape capture in slowing down from E_o (fission energy) to E is called the resonance escape probability p for neutrons of energy E, and is equal to the ratio of the slowing down density at E with absorption to the slowing down density at energy E without absorption. If we consider the resonances as narrow and widely spaced, then the expression for the resonance escape probability at energy E can be derived (1) to be

$$p(E) = \exp\left[-\int_{E}^{E_o} \frac{\Sigma_{a_m}}{\varsigma\,(\Sigma_{a_m} + \Sigma_s)} \frac{dE}{E'}\right] \qquad 3.2.26$$

Σ_s = macroscopic scattering cross-section which is constant for graphite over the whole energy range

$\Sigma_{a_m} = N_m \sigma_{a_m}$

and if we define

$$RI = \int_{E}^{E_o} \left(\frac{\sigma_{a_m} \Sigma_s}{\Sigma_{a_m} + \Sigma_s}\right) \frac{dE'}{E'} = \text{Resonance Integral} \qquad 3.2.27$$

$$\therefore\ p(E) = \exp\left[-\frac{N_m}{\varsigma \Sigma_s} \cdot RI\right] \qquad 3.2.28$$

Where RI and $\varsigma\Sigma_s$ have their physical significance as

(a) $N_u RI$ = effective absorption cross-section for resonance neutrons, and

(b) $\varsigma\Sigma_s$ = removal cross-section (slowing down cross-section) beyond the resonance region.

In a heterogenous lattice like the present one the two processes are competing. However the separation of fuel elements from the moderator leads to self-shielding of the resonance neutrons and p is considerably higher than if the same proportions were intimately mixed together. The resonance escape probability is therefore almost identical with the calculation of f and is given by the expression

$$p(E) = \exp\left[-\frac{V_u}{V_g}\frac{N_u}{\varsigma\Sigma_s} \cdot RI \cdot \frac{(\bar{\varphi}_{res})_u}{(\bar{\varphi}_{res})_m}\right] \qquad 3.2.29$$

Thus the calculation of resonance escape probability boils down to the calculation of $\frac{(\bar{\varphi}_{res})_u}{(\bar{\varphi}_{res})_m}$ and RI. Since all other quantities in the expression are known, the ratio $\frac{(\bar{\varphi}_{res})_u}{(\bar{\varphi}_{res})}$ cannot be calculated very reliably. Therefore, it is best to ignore this, because it is of the order of unity and the expression for p reduces to

$$p(E) = \exp\left(-\frac{V_u}{V_g} \cdot \frac{N_u}{\varsigma\Sigma_s} RI\right) \qquad 3.2.30$$

The effective resonance integral is calculated experimentally and depends upon the surface area and mass of the uranium material, and can, therefore, be written as

$$RI = A + B\frac{S}{M} \qquad 3.2.31$$

where A and B are constants, the units being barns, and barns.gm.cm^{-2} respectively. For natural uranium the effective resonance integral (7) at room temperature is

$$RI = [5.65 + 40.7\ (\frac{S}{M})]\ \text{barns} \qquad 3.2.32$$

$\frac{S}{M}$ is the surface to mass ratio of the fuel (cm^2/gm). The surface area of the fuel element includes the area of the ends.

3.2.5 THERMAL FISSION FACTOR (η)

The average number v of fast neutrons released per slow neutron fission is (2.5 ± 0.1); but since all neutrons captured in fuel do not necessarily lead to fission; the valu of η (thermal fission factor) differs from v. Assuming v to be constant, the differential fission cross-section data may be combined with directly measured variation of η with energy defined as

$$\eta = v\frac{\Sigma_f}{\Sigma_a} \qquad 3.2.33$$

Though the value of η varies with the relative energy

of the neutron, for thermal reactors only "thermal neutron fission" is predominantly important. Thus an effective η-value in a thermal reactor spectrum can be uniquely defined as

$$\eta = \frac{\int (M(E) + \lambda F(E))\ \sigma_a(E)\eta(E)\ dE}{\int (M(E) + \lambda F(E))\ \sigma_a(E)\ dE} \qquad 3.2.34$$

where the flux distribution is given by

$$\varphi(E) = M(E) + \lambda F(E)$$

ν is assumed independent of energy

$M(E) = \frac{E}{E_T^2} e^{-E/E_T}\ dE$ is the Maxwellian thermal flux distribution, and $F(E)$ denotes the epithermal flux, where λ, characterises the intensity of the epithermal component to the thermal component, which, when integrated, yields unity. Thus the two parameters, namely, the temperature, T, of the Maxwellian thermal distribution and λ, the relative intensity of the epithermal distribution define completely the energy variation of the flux. λ is given by

$$\lambda = \frac{\beta'_u}{b} \qquad (a) \qquad 3.2.35$$

$$b = \frac{4}{(\mu\pi)^{\frac{1}{2}}} \quad : \quad \mu = 2.813 \qquad (b)$$

and thus $b = 1.345$.

Rewriting the expression for

$$\eta = \frac{v\int (M(E) + \lambda F(E)\ \sigma_f\ dE}{\int (M(E) + \lambda F(E)\ \sigma_a\ dE}$$

$$\eta = \frac{v\ \sigma_{fo}}{\sigma_{ao}} \quad \frac{(g_f + rs_f)}{(g_a + rs_a)} \qquad 3.2.36$$

$$\eta = \eta_o\ (\frac{g_f + rs_f}{g_a + s_a}) \qquad 3.2.37$$

$\eta_o = \eta$ - value for 2200 m/sec neutrons.

$$r = \frac{\lambda}{1+\beta'_u} \qquad 3.2.38$$

The entries of Tables (7) can be used directly to obtain the effective value of η at a point where the flux is characterised by a Maxwellian temperature and a value for λ.

3.3.1 DIFFUSION AREA L_o^2

The effect of lumping the materials in heterogeneous reactors complicates the evaluation of diffusion area (diffusion length square) since it is difficult to compute accurately the overall influence on the thermal non-leakage probability. The apparent nuclear properties would vary with direction (due to flux arising from various sources and non-symmetries in the shape and

arrangement of the fuel lumps) and the form (2) $(1+B^2L^2)^{-1}$ for non-leakage would hold only approximately. However, in case of the present lattice, under study, the form $(1+B^2L^2)^{-1}$ would be a good approximation to the thermal non-leakage probability and it would be also acceptable to use the general form

$$L^2 = \frac{D}{\Sigma_a} \qquad 3.3.1$$

Thus $$D = \frac{1}{3\Sigma_{tr}} = \frac{1}{3(\Sigma_{tr}^{(m)}+\Sigma_{tr}^{F})} \qquad 3.3.2$$

along with $$\Sigma_{tr}\bar{\varphi}V_{cell} = \Sigma_{tr}^{F}\bar{\varphi}_F V_F + \Sigma_{tr}^{(m)}\bar{\varphi}_m V_m \qquad 3.3.3$$

and $$\Sigma_a\bar{\varphi}V_{cell} = \Sigma_a^{F}\bar{\varphi}_F V_F + \Sigma_a^{(m)}\bar{\varphi}_m V_m \qquad 3.3.4$$

Then with the help of usual simplifications such as $V_{cell} \approx V_m$; $\bar{\varphi} \approx \bar{\varphi}_m$

$$\frac{\bar{\varphi}_m}{\bar{\varphi}_F} = \varsigma \text{ and } \frac{\Sigma_{tr}^{F} V_F}{\Sigma_{tr}^{(m)} V_m} \cdot \frac{1}{\varsigma} \ll 1$$

one arrives at the expression for diffusion area as

$$L_o^2 = L_m^2(1-f) \qquad 3.3.5$$

We define the average diffusion coefficiant for a mixture of materials in a lattice given by

$$D_{cell} = \frac{\Sigma_J V_j W_{jm}}{\Sigma_J \frac{V_j W_{jm}}{D_{Jm}}} \qquad 3.3.6$$

and the average macroscopic absorption cross-section in the cell as

$$\Sigma_{cell} = \frac{\Sigma_J (\Sigma_J V_J W_J)}{\Sigma_J V_J W_J} \qquad 3.3.7$$

where $\Sigma_J = \Sigma_{Jo}(g_j + r'S_J)$

and $W_J = W_{JM} + W_{Je}$

By definition for all materials in the lattice we have

$$f_5 = \frac{V_u \Sigma_5 W_5}{\Sigma_J V_J \Sigma_J W_J} \qquad 3.3.8$$

$$A_J = \frac{V_J \Sigma_J W_J}{V_u \Sigma_5 W_5}$$

$$A_{JM} = \frac{V_J \Sigma_{JM} W_{JM}}{V_u \Sigma_{5M} W_{5M}}$$

$$L^2_{JM} = \frac{D_{JM}}{\Sigma_{JM}}$$

By substitution of these expressions into the original expression for diffusion area eq. 3.3.1 (uncorrected for streaming) we would get

$$L_o^2 = f_5 \frac{\left[\sum_{J\neq c} \frac{A_{JM}}{\Sigma_{JM}}\right]\left[\sum_{J\neq c} \frac{A_J}{\Sigma_J}\right]}{\left[\sum_{J\neq c} \frac{A_{JM}}{\Sigma^2_{JM} \, l^2_{JM}}\right]} \qquad 3.3.9$$

The summation does not include the gas spaces. The values of L^2_{JM}, g, s factors have been taken from Tables (7).

3.3.2 SLOWING DOWN AREA L_{so}^2

The calculation of slowing down area is analogous to the one presented in the previous section (diffusion area) in connection with the average distance travelled by a thermal neutron from the point at which it enters the thermal range to the point at which it is absorbed. Here, the problem is to compute the average distance travelled by a neutron (fission neutron) while it slows down through a given lethargy range or energy range. In the case of a heterogeneous combination of the reactor lattice, allowance has to be made in this parameter for the different slowing down properties of the various materials used in the reactor.

In this case the quantity analogous to the absorption cross-section is the transfer cross-section from fast group to the thermal group of neutron and it is estimated from the slowing down process caused by scattering.

The transfer cross-section can be shown (43) to be

$$\Sigma_1 = \frac{V_m}{V_{cell}} \cdot \frac{\mu^{\frac{1}{2}}}{2} \quad \frac{V_T}{V_o} \; \varsigma \overline{\Sigma}_s \qquad 3.3.10$$

where $\varsigma \overline{\Sigma}_s$ is an average cross-section over all the materials in the cell. By using the volume weighted cross-sections and assuming that the fast flux is constant across the cell, we have

$$L_{so}^2 = L_{sg}^2 \; \frac{(\Sigma_J \; \frac{V_J}{V_g})^2}{(\Sigma_J \; \frac{V_J I_{trg}}{V_g I_{trJ}})(\Sigma_J \; \frac{V_J \varsigma_J I_{sg}}{V_g \varsigma_g I_{sJ}})} \qquad 3.3.11$$

where

$$L_{sg}^2 = \frac{363.9 - 84.6\ (p + \Delta p)}{S_g^2} \qquad 3.3.12$$

It may be pointed out that, to be more exact in a system of two-group equations, the slowing down area should include epithermal absorption, bringing it into line with the corresponding definition of L_o^2 (diffusion area).

3.3.3 CALCULATION OF STREAMING FACTORS

The presence of channels or cavities, whether regularly or randomly distributed, serves, effectively, to increase the total path traversed by a neutron from

point of birth to point of capture (or escape from the reactor). The problem of computing this increase in path length is further complicated by considerations of anisotropy, which occur in graphite-moderated reactors with large parallel coolant channels, since a neutron entering a hole at a small angle will travel a long way before encountering any solid materials.

An elementary approach for estimating the increase in the average path length consists of applying a uniform correction factor to all macroscopic cross-sections to account for the effective reduction in density due to the presence of holes. On this basis, the corrected diffusion length L is related to the diffusion length L_0 of the reactor materials without holes, by

$$L^2 = L_o^2 (1+\varphi)^2 \qquad 3.3.12$$

Similarly for the slowing down area where φ is the ratio of the volume of the holes to the volume occupied by the solid materials.

It has been shown by Behrens that the estimate by (3.3.12) is the first order isotropic correction for small holes in a more general result which takes into account the distribution and shape of the holes. According to Behrens, if we consider the case of a uniform mixture moderator and the fissile material, inter-

spersed with a random arrangement of holes of given size and shape, then the mean square free path is increased by the presence of the holes in a ratio

$$1 + 2\varphi + \left(\frac{r\varphi}{\lambda}\right)\{\coth(r/\lambda\varphi) + Q - 1\} \qquad 3.3.13$$

where

r is hydraulic radius defined as

$$r = \frac{2 \text{ volume of the hole}}{\text{total surface area}} \qquad 3.3.14$$

λ is the mean free path of neutron in the solid material and Q is a geometric function of the shape of the hole (the ratio of the mean square of the length of straight passages through the hole to the square of the mean length of such passages). It may be pointed out that the mean passage length through any hole is twice its hydraulic radius, and that Q is inherently greater than unity. For a hole of given hydraulic radius r and given volume ratio, φ, if $\frac{r}{\lambda}$ becomes very small, the expression reduces to $(1+\varphi)^2$; already referred to as the density correction. If, on the other hand, $\frac{r}{\lambda}$ is at least somewhat larger than φ (which is very often the case), the hyperbolic cotangent becomes approximately unity, and we may write the expression in the form

$$1 + 2\varphi + Qr\varphi/\lambda \qquad 3.3.15$$

However, the holes in a reactor are not randomly dispersed

throughout the lattice, but they are situated immediately surrounding the uranium rods. This results in a lowering of the streaming (factors) correction, since fewer thermal neutrons emerge from the rods than strike them (owing to the capture in the uranium), and thus the number of neutrons crossing the hole from the core to the outer boundary is less than it would be if the cores of the holes were not strong (fuel) absorbers, which leads to the evaluation of φ and Q to be modified (Q^*, φ^*). This fact, therefore, brings in the nuclear properties (absorption) of the fuel in the application of streaming corrections.

The treatment outlined in the last paragraph is correct for determining the diffusion length of thermal neutrons, it certainly does not apply in the case of fast neutrons. For fast neutrons, capture in the rods is not a very probable event and the "Equivalent Capture Width" of the rod may reasonably be treated as vanishing In this case Q^* and φ^* reduce to the original values φ and Q.

The following parameters are required for each hole in the lattice:

$$\phi_i = \frac{\text{volume of hole i}}{\text{volume of solid material}} \qquad 3.3.16$$

$$r = \frac{2 \times \text{volume of hole i}}{\text{Surface area of hole i}} = a_i - g_i \text{ for cylindrical annuli} \qquad 3.3.17$$

$$S = \frac{4(a_g^2 - g_g^2)}{3L_g^2} I_{gM} \quad \frac{1-f_5 A_g}{f_5 A_g} \qquad 3.3.18$$

$$\not{s} = \frac{S}{a_o + g_g} \qquad 3.3.19$$

$$\mu_i = \frac{g_i}{a_i} \qquad 3.3.20$$

$$\varphi_i^* = \varphi_i (1 - \varphi_{1i} \not{s}) \qquad 3.3.21$$

$$Q_i^* = \frac{Q_i (1-\not{s})(1-\varphi_{2i}\not{s})}{(1-\varphi_{1i}\not{s})^2} \qquad 3.3.22$$

$$Q_i = \frac{4}{3} F(\mu_i) \qquad 3.3.23$$

The values of $F(\mu_i)$, φ_1 and φ_2 as a function of μ are given in (7)

The streaming factors are then given by

$$S_{MR} = 1+2(\varphi_1^*+\varphi_2^*+ ..)+ \frac{3}{4}\left(\frac{Q_1^* r_1 \varphi_1^*}{I_{gM}} + \frac{Q_2^* r_2 \varphi_2^*}{I_{gM}} + ..\right) \quad \text{(a)} \quad 3.3.24$$

$$S_{MZ} = S_{MR} + \frac{3}{4}\left(\frac{Q_1^* r_1 \varphi_1^*}{I_{gM}} + \frac{Q_2^* r_2 \varphi_2^*}{I_{gM}} + ...\right) \quad \text{(b)} \quad 3.3.24$$

$$S_{FR} = 1+2(\varphi_1+\varphi_2+ ..)+ \frac{3}{4}\left(\frac{Q_1 r_1 \varphi_1}{I_{gF}} + \frac{Q_2 r_2 \varphi_2}{I_{gF}} + ..\right) \quad \text{(a)} \quad 3.3.25$$

$$S_{FZ} = S_{FR} + \frac{3}{4}\left(\frac{Q_1 r_1 \varphi_1}{I_{gF}} + \frac{Q_2 r_2 \varphi_2}{I_{gF}} + ...\right) \quad \text{(b)} \quad 3.3.25$$

I_{gM} and I_{gF} are the mean free paths for thermal and

fast neutrons in graphite respectively and are given by

$$I_{gM} = \frac{2.70}{S_g} \quad \text{and} \quad I_{gF} = \frac{3.50}{S_g} \qquad 3.3.26$$

3.3.4 MIGRATION AREA ASYMMETRY, SLOWING DOWN AND DIFFUSION AREAS

In a graphite-moderated reactor the isotropic effect is very marked because the neutrons, which travel almost parallel to the rod, and so suffer collisions in uranium instead of in the moderator, are not slowed down appreciably by these collisions. Consequently, their mean number of slowing-down collisions is increased. This leads to the pronounced anistropic effect in this type of reactor.

If we calculate the asymmetric effect as

$$\left(\frac{M_z^2}{M_R^2}\right)_{th} = \frac{L_o^2 S_{MZ} + L_{so}^2 S_{FZ}}{L_o^2 S_{MR} + L_{so}^2 S_{FR}} \qquad 3.3.27$$

it needs a correction factor. It has been found that the experimentally determined value of M_z^2/M_R^2 very roughly fits the empirical formula

$$\left[\left(\frac{M_z^2}{M_R^2}\right)_o - 1\right]_{experimental} = A \times \left[\left(\frac{M_z^2}{M_R^2}\right)_{th} - 1\right]_{theory} \qquad 3.3.28$$

The value of A in the present study has been taken to be equal to 1.73 (7). Thus, knowing the "Experimental

asymmetric factor" we derive corrected streaming factor as

$$S'_{MR} = S_{MR} \qquad S'_{MZ} = S_{MR} \left(\frac{M_z^2}{M_R^2}\right)_{expt.}$$

$$S'_{FR} = S_{FR} \qquad S'_{FZ} = S_{FR} \left(\frac{M_z^2}{M_R^2}\right)_{expt.}$$

and hence the corresponding areas, are modified as

$$L_R^2 = L_o^2 S_{MR} \text{ (a)} \qquad L_Z^2 = L_o^2 S'_{MZ} \text{ (b)} \qquad 3.3.29$$

$$L_{SR}^2 = L_{so}^2 S_{FR} \text{ (a)} \qquad L_{SZ}^2 = L_{so}^2 S'_{FZ} \text{ (b)} \qquad 3.3.30$$

3.3.5 CORE THERMAL AND EPI-THERMAL GROUPS

The thermal group diffusion coefficients are

$$D_{MR} = \Sigma_2 L_R^2 \frac{V(solid)}{V(core)} \text{ (a)} \qquad 3.3.31$$

$$D_{MZ} = \Sigma_2 L_Z^2 \frac{V(solid)}{V(core)} \text{ (b)}$$

where

Σ_2 is defined as

$$\Sigma_2 = \frac{\sum_{j \neq c} V_j \, {}_j W_j}{\sum_{j \neq c} V_j W_j}$$ namely equation 3.3.7 for the lattice materials and c means that it does not apply to gas spaces.

The fast group of diffusion coefficients are

$$D_{FR} = D_{Fg}\, S'_{FR}\, \frac{V(solid)}{V(core)} \quad \text{and} \qquad \text{(a)} \qquad 3.3.32$$

$$D_{FZ} = D_{Fg} S'_{FZ}\, \frac{V(solid)}{V(core)} \qquad \text{(b)} \qquad 3.3.32$$

where

$$D_{Fg} = \frac{(I_{tr})_{eg}}{3} \cdot \frac{V_e}{V_o} \qquad \text{(a)} \qquad 3.3.33$$

$$\frac{V_e}{V_o} = \left(\frac{\mu T}{4T_o}\right)^{\frac{1}{2}} \ln \left(\frac{2.321 \times 10^{10}}{\mu T}\right) \qquad \text{(b)} \qquad 3.3.33$$

at $T = T_o = 293.40^{o}K$

$$\frac{V_e}{V_o} = 14.385$$

and $(I_{tr})_{eg} = (I_{tr})_g$ according to Syrett and is equal to $\frac{2.57}{Sg}$.

3.3.6 REFLECTOR THERMAL AND EPITHERMAL GROUPS

For the reflector an identical set of calculations were performed, taking into consideration the obvious changes, e.g.

$$D_{MR} = D_{Mg}\, S_{MR}\, \frac{V(solid)}{V(reflector)}$$

where

$$D_{Mg} = L_g^{\,2} \Sigma_g = \frac{.951}{Sg} \quad \text{for } T = T_o \qquad 3.3.34$$

$S = 0$ for the reflector. The calculation of streaming factors is almost identical to the core system except

that more streaming corrections have to be applied because of the additional channels created on account of the removal of fuel elements from the system. The diffusion area and slowing down in this case becomes a simpler problem because

$$L_o^2 = \left(\frac{1}{\kappa_g}\right)^2 \qquad 3.3.35$$

and $$L_{so}^2 = L_{sg}^2 = \frac{363.9 - 84.6\ (P + \Delta P)}{sg^2} \qquad 3.3.36$$

where κ_g is given by eqn. 3.2.15 and $(P + \Delta P)$ is the same as for the core case. Full details of the constants for the reflector are given in Appendix A-1.2.

3.3.7 TWO GROUP DIFFUSION EQUATION

The distribution of neutrons can be based on the classification of neutron energies into "thermal" and "fast or epithermal energies". In the present scheme the order of events may be summed up as below:-

1) Production of fast neutrons by fission in U^{235}.
2) Fast fission in U^{238}.
3) Resonance Capture in U^{238}.
4) Fast and epithermal neutron leakage, slowing down, capture and fission,
5) Thermal neutron capture, fission and slowing down.

This is based on the recognition that a large proportion

of fast neutron leakage occurs at energies below the U^{238} resonance region which is consistent with a system of effective cross-section data such as that of Westcott.

Denoting epithermal (fast) flux by φ_F and thermal flux φ_m, the two group diffusion equations are,

$$D_F \nabla^2\varphi_F + K_\infty \Sigma_m \varphi_m - \Sigma_F \varphi_F = 0 \quad \text{Fast} \qquad 3.3.37$$

$$D_M \nabla^2\varphi_m + \Sigma_F \varphi_F - \Sigma_m \varphi_m = 0 \quad \text{Thermal} \qquad 3.3.38$$

If the buckling of the system is B^2, then

$$K_\infty = (1+B^2L^2)(1+B^2L_s^2) \qquad 3.3.39$$

where

$$K_\infty = (\varepsilon p f_5 \eta_5) \text{ or } (\varepsilon p \eta f)$$

ε is determined by fast fission in U^{238} produced by neutron of energy such that energy > U^{238} fission threshold. The resonance escape probability is fairly well-defined since resonance capture takes place over a definite energy range. However η and f in two energy group are not very clearly defined since absorption in fuel takes place above and below the U^{238} resonance region. Anyway an average value of f and η can be calculated for each energy region but the weighting factors used in obtaining the average values depend upon the size of the reactor system through the relative neutron leakage in the two groups.

3.3.8 SOLUTION OF TWO-GROUP EQUATION FOR A BARE HOMOGENEOUS REACTOR

The critical condition defined by the equation 3.3.39 is quadratic in B^2, one being real and positive and the other being negative and imaginary. The general solution of the equations 3.3.37-38 will have a linear combination of the corresponding two roots of the critical condition. The solution for the two neutron fluxes can be written for a slab reactor with a reflector on either side and being infinite in the other two directions y and z.

$$\varphi_{Fc} = A\cos(\mu x)+C\sin(\mu x)+F\cosh(vx)+G\sinh(vx) \qquad 3.3.40$$

$$\varphi_{mc} = S_1[A\cos(\mu x+C\sin(\mu x)]+S_2[\cosh(vx)+G\sinh(vx)] \qquad 3.3.41$$

c denotes the core and A, C, F and G are arbitrary constants which have to satisfy the boundary conditions detailed in section 3.2 of the present chapter. S_1 and S_2 are the coupling constants given by

$$S_1 = \frac{\Sigma_{Fc}}{\Sigma_{mc}} \quad \frac{1}{1+L^2\mu^2} \qquad (a) \qquad 3.3.42$$

and

$$S_2 = \frac{\Sigma_{Fc}}{\Sigma_{mc}} \quad \frac{1}{1-v^2L^2} \qquad (b) \qquad 3.3.42$$

$$v^2 = \mu^2 + \left(\frac{1}{L^2} + \frac{1}{L_s^2}\right) \qquad (c) \qquad 3.3.42$$

μ^2 is the real positive root of the eqn. 3.3.39.

In the symmetrical case under study, the reflector thickness is zero and the two fluxes should be zero at the extrapolated boundaries of the assembly, i.e.

$$\varphi_{Fc}\left(\pm \frac{a}{2}\right) = \varphi_{mc}\left(\pm \frac{a}{2}\right) = 0$$

at $x = \pm a/2$ so that the arbitrary constants $F = C = G = 0$ and the flux distributions in the assembly without much loss of generality can be written as

$$\varphi_{Fc} = \cos(\mu x) \qquad 3.3.43$$

$$\varphi_{mc} = S_1 \cos(\mu x) \qquad 3.3.44$$

The constant A has been put equal to unity for the purpose of normalisation of flux distribution.

It may be remarked that the real positive root μ corresponds to the asymptotic flux distribution and the imaginary root $(-v^2)$ to a non-asymptotic transient brought about by a sudden change of the boundary conditions. These considerations will be taken up in Chapter 5 in greater detail where the case of non-aymptotic flux distribution has also been taken into consideration.

3.4.1 RESULTS OBTAINED FROM EXPERIMENT AND THEORY

All theoretical results and the experimentally measured thermal flux distributions and the material

bucklings for the various cases of fuelled (completely) sub-critical assembly are given in Tables 3.4.1 (A to F).

The errors in the experimentally measured material bucklings and the resulting K_∞ were calculated on the basis of modified one-group theory and correspond to the maximum possible error of 0.5 cm% in the measured relaxation length and an error of 0.5 cm in the width measurements. These errors are considerably higher than the fitting errors reported in Chapter 2.

The asymmetry factors for the lattices under study have not been measured. They have been calculated according to the recipe in section 3.3.4 and corrected by the fitting factor (7) of A= 1.73 and error has been assumed to be of the same order of magnitude as reported by Macdonald and in some cases somewhat more. For example, cases PSCF, SF and OCF (Table 2.5.3) have errors .002, .003 and .004 respectively.

The errors in the material buckling have been calculated on the principle that the flux measurements in the horizontal direction (extrapolation lengths) and the vertical direction (relaxation lengths) are independent of each other. Therefore they have been combined directly.

The error in K_∞ is evaluated according to the

dependency of errors in the material bucklings and the migration area, i.e.

$$\sigma_{K_\infty}^2 = \sigma_{B_m^2}^2 \left(\frac{\delta K_\infty}{\delta B_m^2}\right)^2 + \sigma_{M_R^2}^2 \left(\frac{\delta K_\infty}{\delta M_R^2}\right)^2 \qquad 3.4.1$$

on the basis of modified one group theory.
The error in the migration area, $\sigma_{M_R^2}$ was checked by changing the graphite absorption cross-section from 4.1mb to a possible or of $\pm$ .01 mb since the other nuclear properties of fuel and can are fairly well-known. The slowing down area did not change at all because it is a function of the scattering cross-section and the density of graphite. The following changes in the radial diffusion area were observed.

The particular case is PSCF, the corresponding change in f_5 is also tabulated.

	σ_g = 4.09 mb.	σ_g = 4.1 mb.	σ_g = 4.11 mb.
$L_R^2(cm^2)$	301.50	301.42	301.33
f_5	0.56385	0.56369	0.56353

The rest of the parameters did not change. However, the error in the migration area comes mainly from the uncertainty of the streaming corrections. Therefore, a pessimistic estimate of 1.5% error in case of PSCF and PSF cases, and 1.75% in the case of SF and OCF cases was made. Even with these large

(A) K_∞(Exp.), K_∞ (Theory), Fast fission factor, Resonance Escape Probability, Thermal utilisation and η_5 for lattices.

Case	ε	p	η_5	f_5	K_∞(Theory)	K_∞(expt.)
PSCF	1.02891	0.91910	2.02040	0.56369	1.07701	1.072220 ± .001312
PSF	1.02902	0.91709	2.02011	0.56538	1.07783	1.069814 ± .001269
PSF (ODD)	1.02902	0.91704	2.02011	0.56585	1.07867	1.068728 ± .001251
SF	1.02964	0.90560	2.01849	0.57622	1.08450	1.081987 ± .001661
OCF	1.02991	0.90049	2.01779	0.57929	1.08405	1.078661 ± .001594
PSCF 128 VAC 16	1.02845	0.92772	2.02167	0.55494	1.07042	1.064055 ± .001178
PSF 128 VAC 16	1.02855	0.92591	2.02140	0.55682	1.07190	1.063156 ± .001160
PSF 128 (ODD) VAC16	1.02855	0.92587	2.02140	0.55738	1.07294	*
SF 128 VAC 16	1.02910	0.91558	2.01990	0.56907	1.08305	1.081288 ± .001662
PSCF 108 VAC 36	1.02787	0.93866	2.02333	0.54071	1.05554	1.048454 ± .000897
PSCF 72 VAC 72	1.02682	0.95870	2.02653	0.49868	0.99483	0.994239 ± .000108

TABLES 3.4.1

(B) FLUX FINE STRUCTURE

CASE	B	C	R	S	β'u
PSCF	1.03775	1.07115	1.01620	1.31210	0.10087
PSF	1.03775	1.07115	1.01620	1.30420	0.10328
PSF (ODD)	1.03545	1.06682	1.05705	1.25002	0.10334
SF	1.02700	1.05088	1.16365	1.07274	0.11692
OCF	1.02575	1.04[illegible]	1.17322	1.05077	0.12292
PSCF 128 VAC 16	1.03775	1.07115	1.01620	1.32395	0.09051
PSF 128 VAC 16	1.03775	1.07115	1.01620	1.31575	0.09270
PSF 128 (ODD)VAC16	1.03545	1.06682	1.05750	1.26020	0.09274
SF 128 VAC 16	1.02700	1.05088	1.16365	1.07720	0.105,08
PSCF 108 VAC 36	1.03775	1.07115	1.01620	1.34132	0.07730
PSCF 72 VAC 72	1.03775	1.07115	1.01620	1.38371	0.05250

TABLES 3.4.1

(C) STREAMING FACTORS

CASE	FAST		THERMAL		AXIAL ADJUSTED	
	SFR	SFZ	SMR	SMZ	SFZ	SMZ
PSCF	1.00858	1.01381	1.00866	1.01542	1.01889	1.01897
PSF	1.02227	1.04118	1.02639	1.05088	1.05947	1.06374
PSF(ODD)	1.02993	1.04409	1.02791	1.04588	1.05755	1.05548
SF	1.42318	1.56611	1.38247	1.53635	1.68160	1.63349
OCF	1.85186	2.18901	1.80312	1.17011	2.46271	2.39790
PSCF 128 VAC 16	1.00761	1.01224	1.00770	1.01368	1.01681	1.01689
PSF 128 VAC 16	1.01974	1.03649	1.02340	1.04510	1.05293	1.05672
PSF 128 (ODD)VAC16	1.02765	1.04131	1.02624	1.04360	1.05449	1.05304
SF 128 VAC 16	1.36824	1.49114	1.33296	1.46549	1.50096	1.54995
PSCF 108 VAC 36	1.00641	1.01030	1.00649	2.00152	1.01420	1.01430
PSCF 72 VAC 72	1.00426	1.00685	1.00434	1.00768	1.00956	1.00964

TABLES 3.4.1

(D) CHARACTERISTIC AREAS

CASE	L_o^2	L_{so}^2	L_R^2	L_{sR}^2	L_z^2	L_{sz}^2
PSCF	298.83	325.32	301.42	328.11	304.50	331.46
PSF	305.42	342.25	313.48	349.87	324.88	362.61
PSF(ODD)	300.05	338.44	308.43	348.56	316.70	357.91
SF	253.34	345.00	350.24	491.00	413.84	580.15
OCF	217.35	316.14	391.90	585.45	521.18	778.57
PSCF 128 VAC 16	336.10	326.56	338.69	329.05	341.78	332.05
PSF 128 VAC 16	343.60	343.59	351.65	350.37	363.09	361.77
PSFD 128 VAC 16	337.84	340.18	346.71	349.59	355.76	358.72
SF 128 VAC 16	293.52	357.32	391.26	488.90	454.95	568.48
PSCF 108 VAC 36	396.76	328.13	399.34	330.24	402.44	332.80
PSCF 72 VAC 72	576.17	330.91	578.67	332.32	581.73	334.08

TABLES 3.4.1

(E) DIFFUSION COEFFICIENTS(CORE).

	THERMAL		FAST		
CASE	DMR	DMZ	DRF	DFZ	M_z^2/M_R^2
PSCF	0.90588	0.91513	12.91831	13.05032	1.010,214
PSF	0.94492	0.97930	13.43444	13.92330	1.036,391
PSFD	0.93531	0.96040	13.37504	13.73387	1.026,819
SF	1.11733	1.32021	16.48596	19.47941	1.181,577
OCF	1.26013	1.67579	18.59719	24.73170	1.329,871
PSCF 128 VAC 16	0.91084	0.91916	12.93910	13.05720	1.009,120
PSF 128 VAC 16	0.94831	0.97918	13.43565	13.87304	1.032,535
PSFD 128 VAC 16	0.94113	0.96570	13.39781	13.74763	1.026,109
SF 128 VAC 16	1.11868	1.30078	16.39304	19.06154	1.162,777
PSCF 108 VAC 36	0.91734	0.92446	12.96514	13.06574	1.007,756
PSCF 72 VAC 72	0.92975	0.93466	13.01061	13.07932	1.005,291

TABLES 3.4.1

Case	B_m^2 10^{-6} cm^{-2}	β_U' Theory	Flux Ratio Fast/Thermal
PSCF	114.721 ± 1.173	0.1009	0.0800
PSF	105.245 ± 1.080	0.1033	0.0824
PSF (ODD)	104.611 ± 1.079	0.0927	0.0815
SF	97.460 ± 0.995	0.1169	0.1003
OCF	80.484 ± 0.824	0.1229	0.1074
PSCF 128 VAC 16	95.928 ± 1.021	0.0905	0.0721
PSF 128 VAC 16	89.963 ± 0.954	0.0927	0.0742
SF 128 VAC 16	92.356 ± 0.973	0.1051	0.0905
PSCF 108 VAC 36	66.414 ± 0.721	0.0773	0.0656
PSCF 72 VAC 72	-6.324 ± 0.072	0.0525	0.0450

TABLES 3.4.1. Measured material buckling for each lattice. The axial buckling corresponds to the values given in Tables 2.5.2.

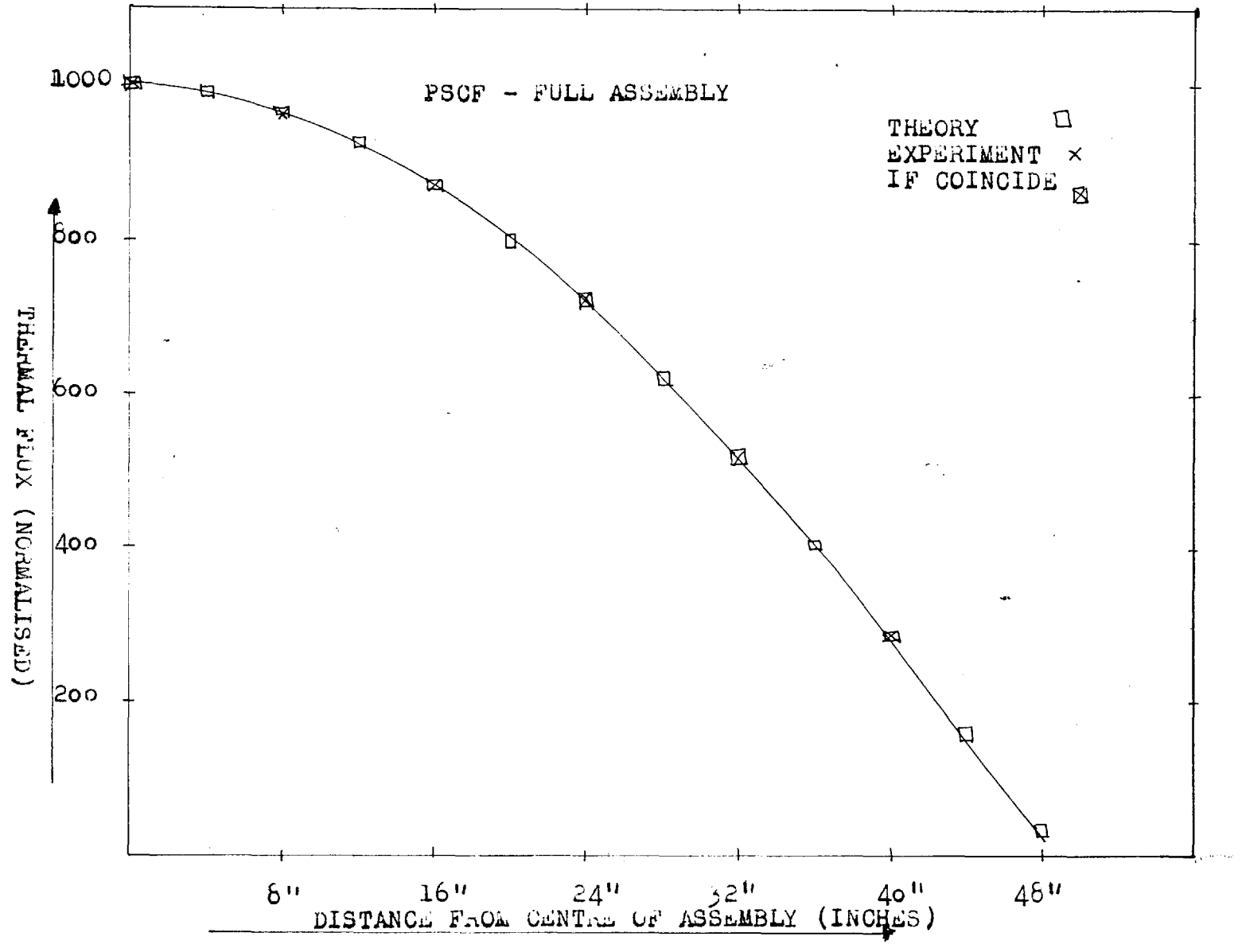

FIG. 3.4.1 COMPARISON OF THEORETICAL (TWO -GROUP) AND EXPERIMENTAL FLUX DISTRIBUTION.

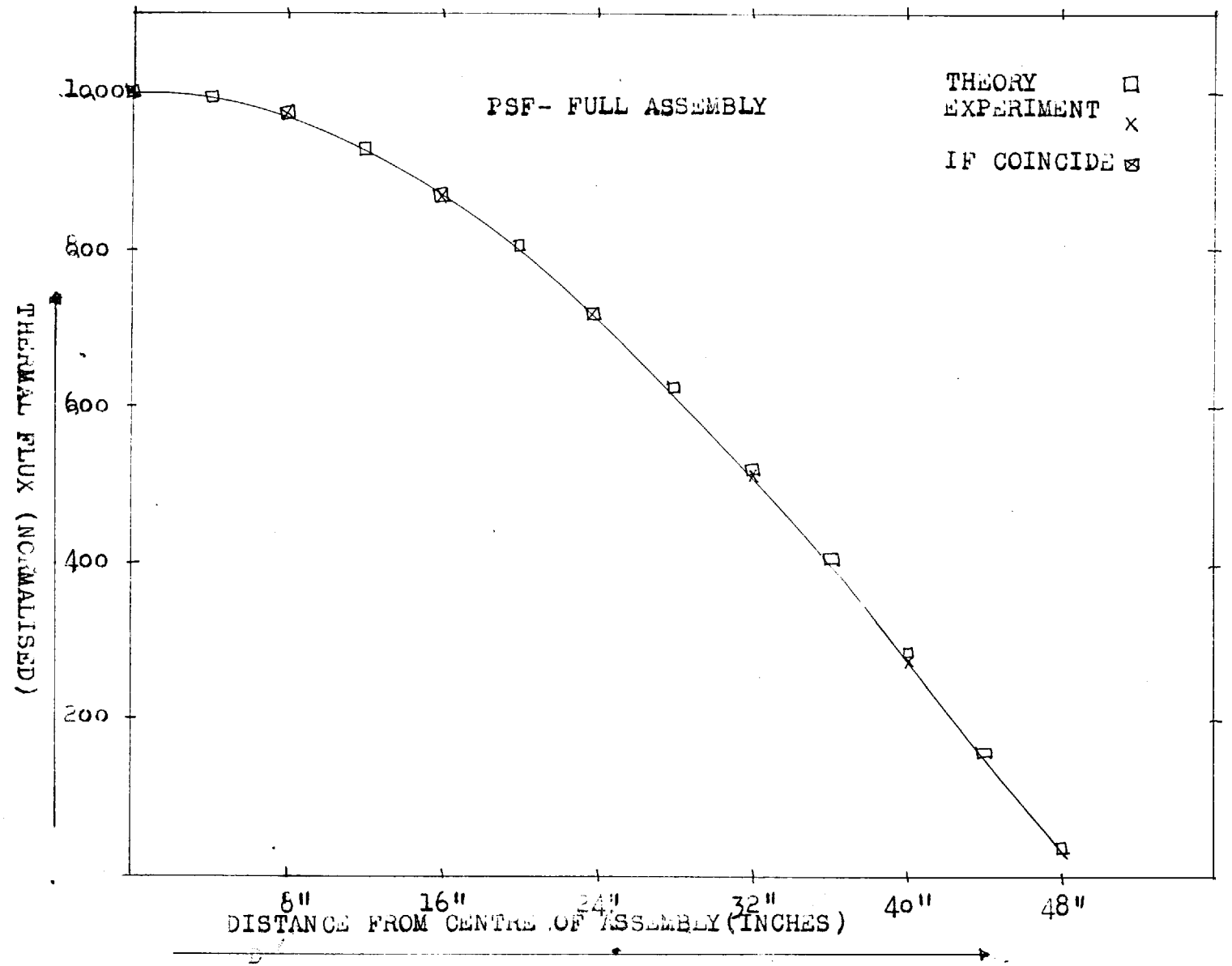

FIG. 3.4.1 COMPARISON OF THEORETICAL (TWO-GROUP) AND EXPERIMENTAL FLUX DISTRIBUTION

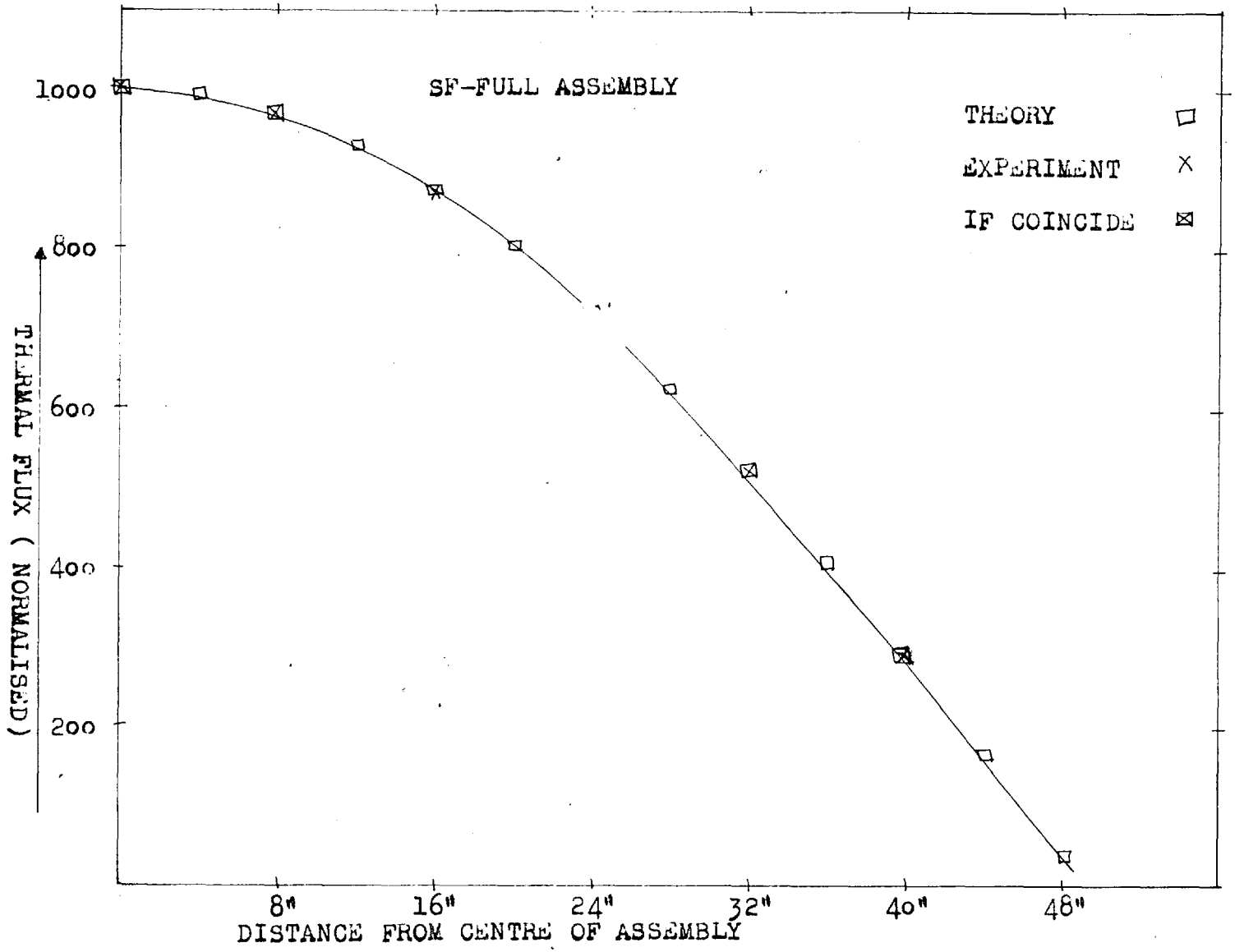

FIG. 3.4.1 COMPARISON OF THEORETICAL (TWO-GROUP) AND EXPERIMENTAL FLUX DISTRIBUTION

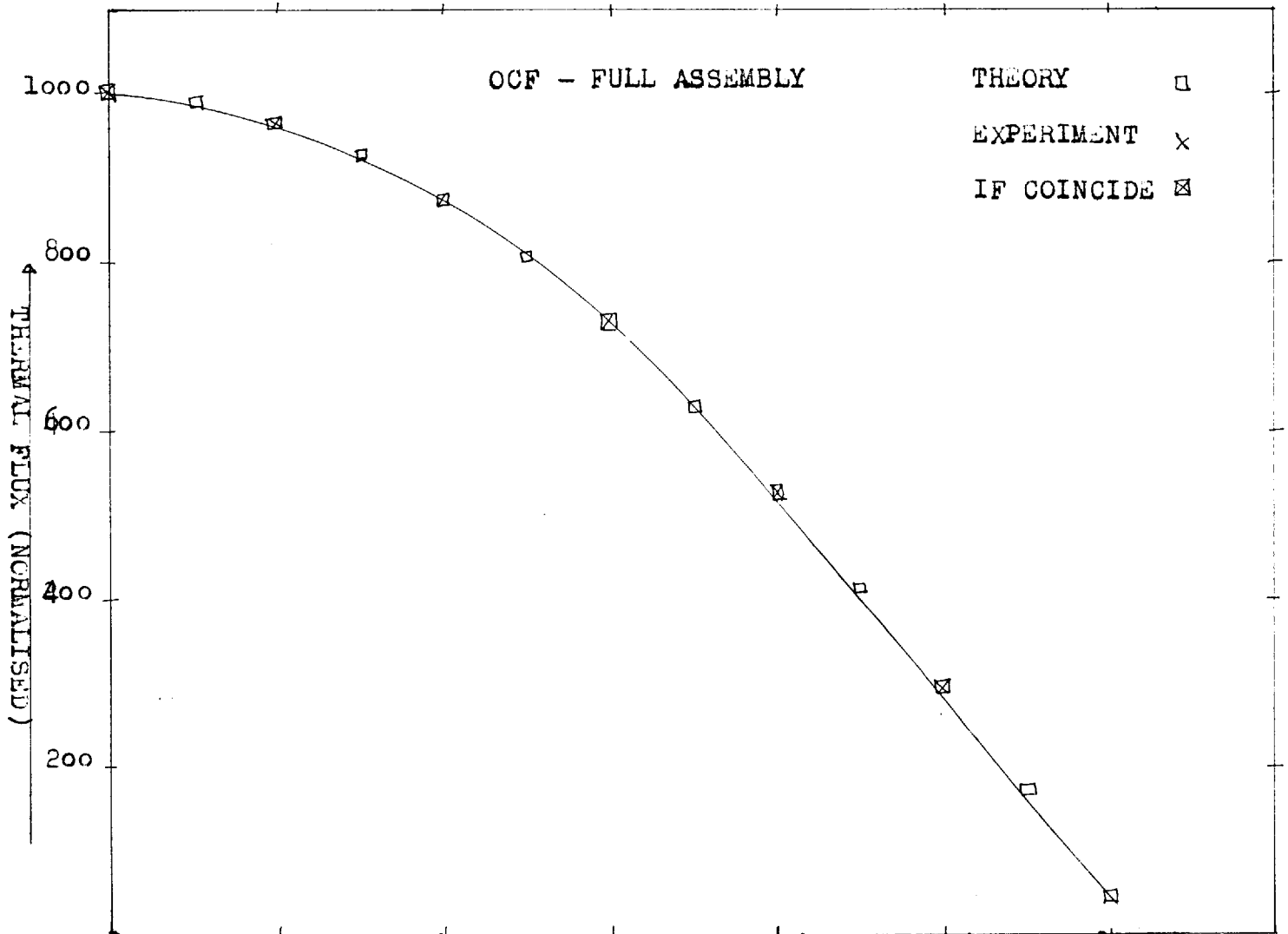

FIG.3.4.1 COMPARISON OF THEORETICAL (TWO-GROUP) AND EXPERIMENTAL FLUX DISTRIBUTION

possible errors the resulting error in the calculated K_∞ is never larger than 0.15% in case of SF and in all other cases it is always of the order of 0.1% of K_∞ predicted by experiment.

The experimental errors reported in the thermal flux measurements are the statistical errors corresponding to a total ccunt of 10^5 counts at a position, i.e. 0.316%. The error arising due to errors in dead time, harmonics and the other related causes have been reduced to a negligible level by the procedure detailed in Chapter 2.

3.4.2 CRAM - RESULTS FOR FULL ASSEMBLY CASES

The results tabulated in section 3.4.1 have been compared with the results obtained from CRAM, described in Appendix A-2.3. The programme solves two-group diffusion equations by the finite difference method. The input to the programme is the constants from the Tables 3.4.1, and the resultant K-effectives for the system predicted are given below and the same quantity obtained from experiment is tabulated below.

	EXPERIMENT	CRAM
PSCF	1.004,492 $\pm$.001,312	1.005,017
PSF	1.007,411 $\pm$.001,269	1.005,588
PSF(ODD)	1.009,320 $\pm$.001,251	1.009,379
SF	1.002,322 $\pm$.001,661	0.981,736
OCF	1.004,996 $\pm$.001,594	0.960,947

TABLE 3.4.2

The accuracy in K-effective from CRAM is a function of various quantities detailed in the Appendix. The disagreement between the results in case of SF and OCF is rather large, most probably due to the uncertainties in the diffusions and the slowing down areas because of large streaming corrections.

3.4.3 DISCUSSION OF RESULTS

The experimentally measured thermal flux distributions tabulated in the Tables 3.4.3 and plotted in FIGS. 3.4.1. are in good agreement with the predictions of theory on two-group theory and the predictions of CRAM based on the finite difference methods. One-group theory and two-group theory practically coincide with each other, so it is not reported here. Only the points where measurements have been carried out are tabulated. CRAM results for thermal flux are not quoted here since they are practically identical with those of two-group theory. They are tabulated in A.2.6 for comparison purposes of one-group, two-group and the CRAM results of flux distributions. The results for various other cases of vacancies have not been reported since the theory predicts only a macroscopic picture of the flux distributions, while, in actual practice, there are vacancies where the flux rises distinctly because of the absence of fuel elements. This, however, emphasises the inadequacy of the homogenised methods in the case of lattices with defects in them.

In Tables 3.4.1 the ultimate predicted parameter K_∞ (theory) is in very good agreement with the experimental predictions in case of SF, OCF, SF 128 VAC 16 and PSCF 72 VAC 72, reasonable in the case of PSCF, PSCF 128 VAC 16

PSCF

CASE DIST.	TWO-GROUP EXPERIMENT FAST	THERMAL	THERMAL
0.0	80.00	1000.00	1000.00±3.16
20.32	77.38	967.28	961.26±3.04
40.64	69.70	871.28	871.38±2.75
60.96	57.46	718.26	720.11±2.28
81.28	41.46	518.25	519.09±1.64
101.60	22.75	284.33	284.96±0.90

PSF

	TWO-GROUP EXPERIMENT FAST	THERMAL	THERMAL
0.0	82.40	1000.00	1000.00±3.16
20.32	79.72	967.43	968.16±3.06
40.64	71.84	871.84	872.24±2.76
60.96	59.29	719.46	721.92±2.23
81.28	42.87	520.22	514.14±1.63
101.60	23.66	287.09	274.69±0.87

SF

0.0	100.26	1000.00	1000.00±3.16
20.32	97.01	967.64	967.44±3.057
40.64	87.49	872.64	869.88±2.75
60.96	72.30	721.17	722.28±2.28
81.28	52.44	523.01	521.74±1.65
101.60	29.18	291.01	288.71±0.91

OCF

0.0	107.42	1000.00	1000.00±3.16
20.32	103.97	967.94	964.33±3.05
40.64	93.86	873.83	869.88±2.75
60.96	77.74	732.69	722.28±2.28
81.28	56.63	527.16	521.74±1.65
101.60	31.88	296.82	288.71±0.91

TABLE 3.4.3 EXPERIMENTAL THERMAL FLUX DISTRIBUTION IN COMPARISON TO TWO-GROUP THEORY FLUXES

and PSCF 108 VAC 36 and not very good in case of PSF, PSF (ODD) and PSF 128 VAC 16 however acceptable in the extreme limiting cases.

Case PSCF 72 VAC 72 is the limiting case in the process of homogenisation, as explained in the Appendix A-1.2 but the K_∞ predicted by experiment is in such a close agreement it is rather surprising. Perhaps the negative and positive assumptions of one sort or the other produce such a close experimental fit.

The seemingly irregular changes in the Flux Fine structure especially constants B and C, are indeed true according to the constants fed in the programme. At one stage some fault in the programme was suspected and the calculations were checked against hand calculations and the results agreed well in accordance with the theoretical explanations. In the last table of 3.4.1 are given the measured material buckling, and β_u', the ratio of fast flux to the average thermal flux in uranium given by eqn. 3.2.14 (b) is compared to the ratio of fast flux to the thermal flux in the lattice.

The possible sources of error in the experimentally predicted values of K_∞ may be ascribed to the following causes.

1) The use of one-group modified theory to calculate the K_∞ for the reactor system is open to objection

because in the expression

$$K_\infty = (1 + B_m^2 L_R^2)(1 + B_m^2 L_{SR}^2)$$

We neglect a small term which in theory we should not. Therefore K_∞ was calculated on the basis of two-group theory and is given in the tables below for comparison. The errors in K_∞ are not tabulated.

	K_∞ (theory)	K_∞Exp(ONE)	K_∞Exp(TWO)
PSCF	1.077,01	1.072,220	1.073,494
PSF	1.077,83	1.069,814	1.071,119
PSF (ODD)	1.078,67	1.068,728	1.069,908
SF	1.084,50	1.081,987	1.083,621
OCF	1.084,05	1.078,661	1.080,147
PSCF 128 VAC 16	1.070,42	1.064,055	1.065,080
PSF 128 VAC 16	1.071,90	1.063,156	1.064,153
SF 128 VAC 16	1.083,05	1.081,288	1.085,080
PSCF 108 VAC 36	1.055,54	1.048,454	1.049,037
PSCF 72 VAC 72	0.944,83	0.994,239	0.994,247

Generally the agreement improves by 0.1 to 0.2% in all cases.

2) The error may well be due to the error in the fitting factor Λ=1.73. There is absolutely no criterion for its genuineness. Some workers have tried to improve upon

their works by arbitrarily changing the value of 1.73 to 1.84 (4) or 1.93 (23), but there is no such theoretical reasoning for taking any arbitrary value of A so that it fits pretty well "the experiment". Perhaps it would be better to fix the value of A once for all.

3) Asymmetry Factor

The information about the asymmetry of neutron leakage is deduced by measuring the bucklings in exponential assembly with the axis of the exponential relaxation parallel to, and perpendicular to, the axis of the channels. This has been done for the sub-critical assembly under study by Macdonald (7) on the basis of one-group analysis of the experiments and the asymmetry is expressed in terms of the ratio $\frac{M_z^2}{M_R^2}$ of the migration areas in the axial and radial direction. However this analysis is open to criticism because in experiments with air channels vertical, i.e. parallel, to the axis of the exponential relaxation, there may be direct streaming from the region of high flux near the source and therefore the experiments tend to underestimate the asymmetry. This point has been investigated by Smythe(9) and he derives a relationship for the relative contribution M to the flux at the height Z as

$$M = \frac{D_z r_o^2 p \cosh(h/b_{11})}{b_{11} Z^2 D_m \kappa_m \sinh\left(\frac{h-Z}{b_{11}}\right)}$$

r_o - radius of the channel at the base and

$$p = \frac{K_1(\kappa_m b)\, I_o(\kappa_m b) + K_o(\kappa_m b)\, I_1(\kappa_m b)}{K_1(\kappa_m b)\, I_1(\kappa_m r_o) - K_1(\kappa_m r_o)\, I_1(\kappa_m b)}$$

b - is the radius of the lattice cell of infinite length. He did some experiments with 0.015" thick cadmium discs at the base of the channels and agrees with Grant's conclusion in a similar experiment that there is no significant change in the ratio of readings taken. However his experiments are inconclusive for various practical difficulties in this regard.

In the author's opinion it was not reasonable to change some constants arbitrarily so that it fits certain other parameters well. It was decided to accept the results for the full sub-critical assembly as best with the existing methods of calculations. To support this view was the fine agreement between theoretical and experimental flux distributions. Secondly, as outlined in Chapter 1, section 1.4, the aim of the project was not to fit one experimental result but a series of experiments which could be done with the facility available in the College, so that this could be taken as the basis of the validity of the methods of reactor analysis.

CHAPTER 4

CALCULATION OF FLUX, K-INFINITY AND THE REFLECTOR SAVING FOR A PARTIALLY FILLED (Core) SUB-CRITICAL ASSEMBLY ON THE BASIS OF ONE-GROUP THEORY

4.1 INTRODUCTION

In a homogeneous reactor small-scale composition is uniform and isotropic. All cross-sections are independent of position in a homogeneous reactor. In a non-uniform (reflected core reactor) reactor the cross-sections are position dependent and the reactor calculations are more complex than those for uniform reactors, both in the analytical sense and with regard to the mechanics of computation. The non-uniformity usually consists of:

1) The presence of a reflector which serves to deflect neutrons back into the fueled core and hence reduces the fast nuetron leakage.

2) The presence of control rods which serves to regulate power level of the reactor.

3) Non-uniform fuel loadings, which increase the efficiency of the reactor by flattening the power distribution.

In the present work the sub-critical assembly comes under the first heading, namely, "Reflected core reactor". The material composition in such a non-uniform reactor

usually changes abruptly and causes a mathematical discontinuity. This makes the analytical treatment of the system a difficult problem (1-3). The neutron flux at the interface between two different materials has to adjust itself to a status between the two different characters it would exhibit in an infinite system composed purely of either of the two adjacent materials. The fundamental assumptions used in the diffusion theory of non-uniform reactor are:-

1) The diffusion balance equation can be set up in each different material and gives the neutron flux for each region.

2) At the boundary between the two regions, the flux and the current are continuous.

3) The flux is zero at the extrapolated boundary of the external region.

To simplify the mathematical details the problem is considered in one dimension only as a symmetrical case and the results are supposed to hold for the other dimension as well. To do this we have enough experimental evidence to prove that the flux distribution is identical in shape and magnitude both in X and Y-directions and the distribution in the Z-direction is α well-known exponential. Since measurements of thermal flux distribution (Chapter 2) for the determination of relaxation

length were carried out in the central zone of the sub-critical assembly, when the number of fuel elements used were less, some parts of the measuring region were in the reflector region. However the fitted values of b_{11} were always the same within experimental error.

The difficulties in evaluating the neutron flux distribution in X and Y-directions as said earlier, stem from the fact that the multiplying and slowing-down properties of the fueled region (core) are different from those of the reflector. The neutron energy spectrum changes appreciably at the core-reflector interface; while in the case of a uniformly filled reactor the neutron spectrum remains fairly uniform (in the macroscopic sense) and can be described mathematically by standard geometric functions.

The problem in case of a reflected sub-critical assembly is made much more complicated by the presence of harmonics. Further, the smaller size of the assembly reduces the asymptotic measuring region because of boundary effects and the presence of the sources at the bottom. As discussed in Chapter 2, the measurements were confined to the asymptotic distribution of the neutron spectrum in the light of Macdonald's harmonic analysis.

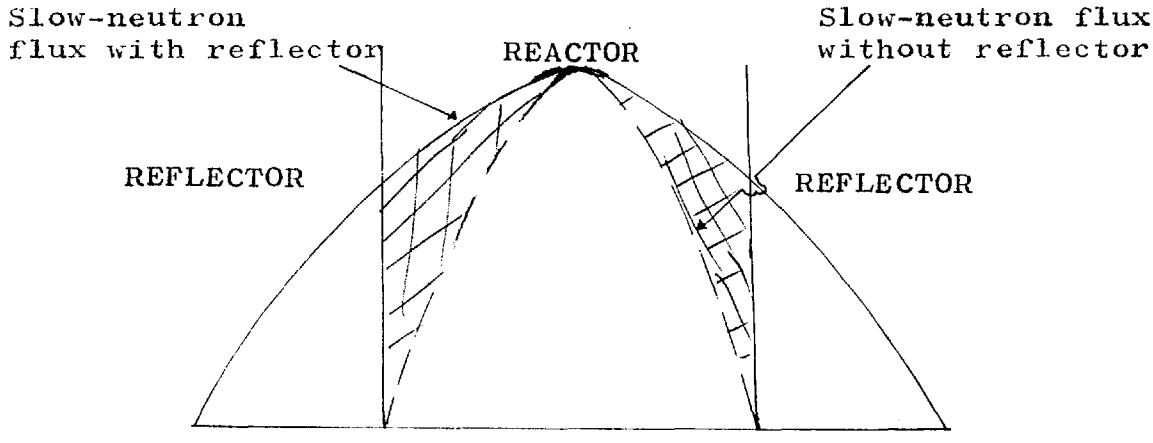

FIG.4.1 A typical graph of Thermal Flux in a Reflected Core System.

Fig.4.1 shows the effect of a reflector on the thermal neutron flux. For the sake of simplicity, only thermal flux has been considered and the fast flux has been neglected. The cross-hatched area under the curves represents the gain in flux integral introduced by the reflector. A careful consideration of this fact leads one at once to the conclusion that for a given core composition, the dimensions of a critical reflected core are smaller than those of a critical bare core. The difference between the two sizes, δ, is called the Reflector Saving.

Thus, to summarize, the effect of a reflector outside the core region is to reduce the bare equivalent reactor size. In the present chapter it will be assumed that the reactor is all thermal, i.e. there is only one energy group "Thermal". The solution of the diffusion equation in the core and the reflector region would lead us to an expression for a reflector saving for the system, the problem being treated as a plane infinite slab system.

The "core region" would then be replaced by an "Equivalent bare reactor system" each side being equal to a $+2\delta$.

The material buckling for such a system would be given by

$$B_m^2 = 2\left(\frac{\pi}{a+2\delta}\right)^2 - \frac{M_z^2}{M_R^2}\gamma_{11}^2 \qquad 4.1.1$$

for the sub-critical assembly with vertical air channels.

The K_∞ for the system has been calculated by the one-group modified expression,

$$K_\infty = 1 + B_m^2 M_R^2 \qquad 4.1.2$$

Two-group theory expression

$$K_\infty = (1+B_m^2 L_R^2)(1+B_m^2 L_{SR}^2) \qquad 4.1.3$$

and the Age-one group expression

$$K_\infty = e^{B_m^2 L_{SR}^2}(1+B_m^2 L_R^2) \qquad 4.1.4$$

were also used for the purpose of comparison.

Throughout the mathematical analysis, it is assumed the neutron flux distribution $\varphi(X,Y,Z)$ is separable in three directions; for this assumption there is ample experimental evidence.

4.2 ONE-GROUP THEORY FORMULATION AND BOUNDARY CONDITIONS

In one-group theory the basic assumption is that all production, diffusion and absorption takes place at a single energy well-known in the reactor field as "Thermal Energy" for thermal reactors. The source term in this case is equal to the production rate $(\varphi_m \Sigma_{am} K_\infty)$. This would imply either that fission neutrons are born thermal or that the distance it would take to slow down was exactly zero, both to a large extent unrealistic situations. Only in a fast reactor, one could find a semblance of validity of this concept, which reactor operates as a result of fissions by fast neutrons. However, less need to say the picture represented is a gross over-simplification of the complicated situation existing in a reflected reactor.

Writing the basic diffusion equation in steady state for thermal neutrons in the reactor core (c) and the reflector (r) regions we have

$$D_c \nabla^2 \varphi_c - \Sigma_{ac} \varphi_c + K_\infty \Sigma_{ac} \varphi_c = 0 \qquad 4.2.1$$

$$D_t \nabla^2 \varphi_r - \Sigma_{mr} \varphi_r = 0 \qquad 4.2.2$$

The source term in the reflector region is zero since it does not contain any fissile material. The two equations for the thermal flux φ_c and φ_r are solved under the boundary conditions:-

a) The flux distribution is symmetrical.

b) The flux shall be finite and non-negative.

c) The neutron flux and the neutron current are continuous across the core-reflector interface.

d) The flux is zero at the extrapolated boundary of the reflector.

The details of the mathematical solution for the flux in the sub-critical assembly with reflector is given in the next section.

4.3 APPLICATION OF ONE GROUP THEORY TO THE SUB-CRITICAL ASSEMBLY WITH A CORE IN THE CENTRAL REGION

Writing equations (4.2.1) and (4.2.2) in the core and reflector regions for the sub-critical assembly in reactngular co-ordinates

$$\nabla^2 \varphi_c(X,Y,Z) + B_c^2 \varphi_c(X,Y,Z) = 0 \qquad 4.3.1$$

$$\nabla^2 \varphi_r(X,Y,Z,) - \kappa_r^2 \varphi_r(X,Y,Z) = 0 \qquad 4.3.2$$

where

$$\nabla^2 = \frac{\partial^2}{\partial x^2} + \frac{\partial^2}{\partial y^2} + \frac{D_{MZ}}{D_{MR}} \frac{\partial^2}{\partial z^2} \qquad 4.3.3$$

The diffusion coefficients D_{MZ} and D_{MR} are direction dependent because of streaming of neutron flux in the vertical channels where the material buckling B_c^2 and κ_r^2 (square of inverse diffusion length) are

$$B_c^2 = \frac{K_\infty - 1}{M_R^2} \qquad (a) \qquad 4.3.4$$

and

$$\kappa_r^2 = \frac{\Sigma_{mr}}{D_{mr}} = \frac{1}{L_r^2} \qquad (b)$$

in the reflector.

Since we assume that the neutron flux can be separated by the principle of separation of variables:

$$\varphi(X,Y,Z) = X(x).Y(y).Z(z) \qquad 4.3.4$$

This holds both for the neutron flux in the core and the reflector regions. The equations 4.3.1 and 4.3.2 can be written as

$$\frac{1}{X_c} \frac{\partial^2 X_c^z}{\partial x^2} + \frac{1}{Y_c} \frac{\partial^2 Y_c}{\partial y^2} + \frac{D_{cz}}{D_{cR}} \frac{1}{Z_c} \frac{\partial^2 Z_c^2}{\partial z^2} + B_c^2 = 0 \qquad 4.3.5$$

$$\frac{1}{X_r} \frac{\partial^2 X_r^2}{\partial x^2} + \frac{1}{Y_r} \frac{\partial^2 Y_r}{\partial x^2} + \frac{D_{rz}}{D_{rR}} \frac{1}{Z_r} \frac{\partial^2 Z_r^2}{\partial z^2} - \kappa_r^2 = 0 \qquad 4.3.6$$

where each of the first three terms is a function of one variable only and, therefore, it will be independent

of the value of the other terms. Thus,

$$\frac{1}{X_c}\frac{\partial^2 X_c}{\partial x^2} = \frac{1}{Y_c}\frac{\partial^2 Y_c}{\partial y^2} = -\alpha^2 \qquad \text{(a)} \qquad 4.3.7$$

$$\frac{1}{Z_c}\frac{\partial^2 Z_c}{\partial Z^2} = \gamma^2 \qquad \text{(b)} \qquad 4.3.7$$

So that

$$B_c^{\,2} = 2\alpha^{\,2} - \frac{D_{cZ}}{D_{cR}}\gamma^2 \qquad \text{(c)} \qquad 4.3.7$$

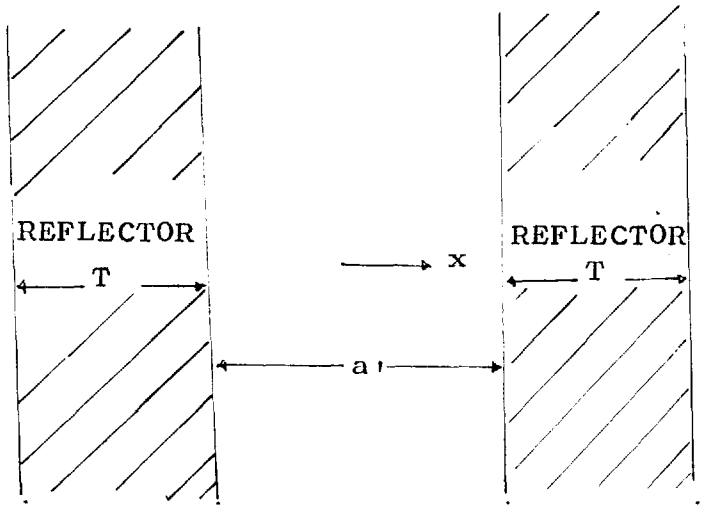

FIG.4.3.1. Infinite Slab Reactor with Reflector

Equation 4.3.7(a) is true since the flux distribution is identical in both X and Y-direction. α^2 and γ^2 are positive real quantities. γ^2 is positive since there is net inflow of neutrons from the sources and α^2 is negative for the fact that there is net leakage of neutrons

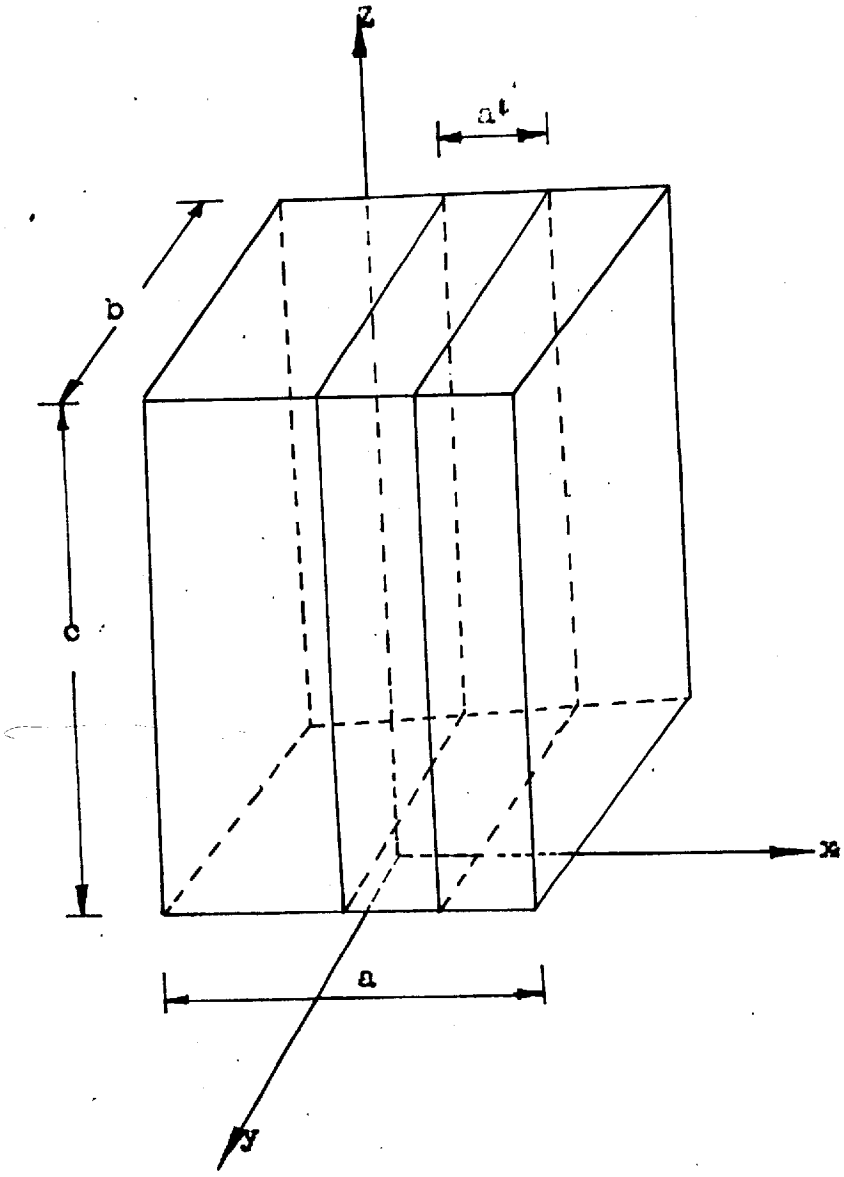

FIG. 4.3.2 SUB-CRITICAL ASSEMBLY IN THE SLAB SYSTEM

in the X or Y-direction.

The solution along the Z-axis is the well-known exponential distribution,

$$Z_c(x) = A_1 \frac{\sinh(C-Z)\gamma}{\sinh(\gamma c)} \qquad \text{(a)} \qquad 4.3.8$$

All the harmonics have been neglected and γ is the inverse relaxation length corresponding to the fundamental. Treating the sub-critical assembly as an infinite plane slab system shown in FIG.4.3.2 (y and z being infinite), the general solution for eq. 4.3.7 (a) in the core region would be written as

$$\varphi_c(x) = A_c \cos(\alpha x) + C_c \sin(\alpha x)$$

Since the flux shall be finite, symmetrical and non-negative, therefore, $C_c = 0$ and the solution for the present case in the core region would be

$$\varphi_c(x) = A_c \cos(\alpha x) \qquad \text{(b)} \qquad 4.3.8$$

It may be remarked that the flux distribution in the Z-direction is the same for the reflector as for the core; namely,

$$Z_r(z) = A_1 \frac{\sinh(C-Z)\gamma}{\sinh(\gamma c)}$$

For the reflector in the X-direction, we solve

$$\frac{1}{X} \frac{\partial^2 X}{\partial x^2} - \kappa_r^2 = 0 .$$ The general solution would be

$$X(x) = A_r \cosh(\kappa_r x) + C_r \sinh(\kappa_r x)$$

subject to the boundary condition that the flux is zero at the extrapolated boundary of the reflector, i.e.

$$\text{when } x = \frac{a'}{2} + T \quad \text{then}$$

$$\varphi_r(x) = C \sinh \kappa_r\left(\frac{a'}{2} + T - x\right) \quad (b) \quad 4.3.8$$

A and C in eq. 4.3.8 are arbitrary constants. A similar solution for y-direction would exist both for the core and the reflector; since the position of the core region is symmetrical at the centre of the assembly it involves only a change of the co-ordinates treating the others to extend to infinity.

The arbitrary constants A and C can be calculated by introducing the boundary conditions that the neutron flux and current density shall be continuous at the core-reflector interface, i.e.

$$\varphi_C\left(\frac{a'}{2}\right) = \varphi_r\left(\frac{a'}{2}\right) \quad (a)$$

and 4.3.9

$$D_C \frac{\partial \varphi_C\left(\frac{1}{2}a'\right)}{\partial x} = D_r \frac{\partial \varphi_r\left(\frac{a'}{2}\right)}{\partial x} \quad (b)$$

The substitution of these boundary conditions leads to the criticality condition,

$$D_C \alpha \tan\left(\alpha \frac{a'}{2}\right) = D_r \kappa_r \coth(\kappa_r T) \qquad 4.3.10$$

Consequently, the normalised thermal flux distribution

in the core and reflector regions in the direction of x (similarly for y) are

$$\varphi_c(x) = \cos(\alpha x) \qquad \text{(a)}$$

$$\varphi_r(x) = C/A \sinh\left(\frac{a'}{2} + T - x\right) \qquad \text{(b)} \qquad 4.3.11$$

For the Z-direction the flux distribution is the same both for the core region and the reflector region, namely,

$$\varphi(z) = A_1 \frac{\sinh(C-Z)\gamma}{\sinh(\gamma c)} \qquad 4.3.12$$

4.4.1 COMPUTATION OF RESULTS

The net result of the analytical solution for the partially filled sub-critical assembly on the basis of one-group theory for an infinite slab reactor system as outlined in the previous section is the critical condition which should be satisfied for the reactor system to be critical, namely, the equation 4.3.10 written here as

$$\coth(\kappa_r T) = \frac{D_c}{D_r} \cdot \frac{1}{\kappa_r} \cdot \alpha \tan\left(\alpha \frac{a'}{2}\right) \qquad 4.4.1$$

This equation defines the critical size of a reflected reactor system for a specified core size a' and thickness T of the reflector.

The decrease in the critical size of the reactor, defined in section 4.1 as reflector saving, can be written

$$\delta = \frac{\pi}{2\alpha} - \frac{a'}{2}$$

or $\frac{a'}{2} = (\frac{\pi}{2\alpha} - \sigma)$. On substitution in eq. 4.4.1 we have

$$\coth (\kappa_r T) = \frac{D_c}{D_r} \cdot \frac{1}{\kappa_r} \alpha \tan(\frac{\pi}{2} - \alpha\delta)$$

or

$$\tan (\alpha\delta) = \frac{D_c}{D_r} \cdot \frac{\alpha}{\kappa_r} \cdot \tanh (\kappa_r T) \qquad 4.4.2$$

Thus, we end up with a transcendental relationship involving the critical size of the reactor (π/α) and the reflector thickness T and the respective diffusion parameters for the two regions.

The following two procedures to compute the critical size and therefore the corresponding reflector saving can be adopted.

1) If either T, the reflector thickness, is small or the reactor core is large so that the quantity

$$\alpha\delta = \frac{\pi}{a}\delta = \text{small} \quad \text{then}$$

$\tan(\alpha\delta) \approx \alpha\delta$ and the expression 4.4.2 approximates to

$$\delta = \frac{D_c}{D_r} \frac{1}{\kappa_r} \cdot \tanh (\kappa_r T) \qquad 4.4.3$$

2) No approximation is used and equation 4.4.2 is solved for critical size.

Both these methods of calculations have been used in

the present study and the computation has been carried out by the programme described in Appendix A-2.4, under the title, "One-Group Theory Criticality Calculations".

In the first case the calculations are straightforward. Given the constants D_c, D_r, κ_r and T, the corresponding reflector saving is obtained and the material buckling for the system is calculated by the relation 4.3.7 (c) in combination with the measured axial buckling from experiment.

In the second case the equation 4.4.2 being transcendental in nature, cannot be solved directly. Two guess values obtained from the first approximation (1) for the given core and reflector thickness are used to give a better estimate for the critical size or reflector saving, the two being inter-dependent

The process is repeated till the required accuracy is reached.

Having obtained the critical size and the reflector saving for the particular combination of the core size and reflector thickness, the calculation of the thermal flux distribution is a fairly easy matter. The thermal flux distribution in core and reflector are calculated by the expressions

$$\varphi_c(x) = \cos(\alpha x) \qquad \text{(a)}$$

$$\varphi_r(x) = C/A \sinh\left(\frac{a'}{2} + T - x\right) \qquad \text{(b)} \qquad 4.4.4$$

A is used as the normalising constant determined by the power level in the reactor. If we use the boundary condition (C) of section 4.4.2, of equal fluxes at the core-reflector interface we would get

$$C/A = \cos\left(\frac{a'}{2}\alpha\right)/\sinh\left(\varkappa_r T\right) \qquad 4.4.5$$

The results of computations on the basis of these two procedures are given in the next section and discussed.

The results referred to as A and B are a variation of the first approximation. It is seen from equation 4.4.3, that there are three constants which we assume should predict the right reflector saving for a given core and thickness, namely the constants D_c, D_r and $\varkappa_r$.

The constant D_c (diffusion coefficient for the core region) and $\varkappa_r$ (inverse diffusion length) are known quite accurately as the average values of the materials in the reactor core, and the latter as reported in section 3.3.6. But there is some doubt about the value of D_r (diffusion coefficient) in the reflector region, partly because of the errors in the streaming factor. In the calculation of streaming factor for any gaps, e.g. between plugs-sleeves, the term 2φ is neglected in Syrett's model since it is assumed that this is corrected for by the density correction and only the term $(\phi_T Q/\lambda)$ is considered.

Then in calculating the diffusion coefficient the volume of solids is taken as the "Actual" volume of solids and the gaps are then leftout for no theoretical ason. Once the process of homogenisation has been applied then it should be considered as a "Solid" and no argument holds for its neglect; so this leads to an under-estimation of D_{mr}. Therefore the results marked "A" correspond to the value of D_{mr} with volume of solids equal to the volume of solids actually present in one lattice, while "B" corresponds to the value of D_{mr} wherein the volume of solids is equal to the "Actual homogenised volume". More will be said about this point in section 6.7. The results marked "C" correspond to the reflector saving as a result of iterations of the expression 4.4.2, so that the transcendental equation holds true. In this case no approximation as to the size of the core or the reflector thickness is used.

The thermal flux distributions are plotted in graphs of FIGS. 4.4.1 for the case A. The experimental measurements of the flux distributions are also plotted alongside.

The input constants for the core are taken from Tables 3.4.1 for the lattices, and reflector constants are tabulated in Appendix A-1.2. The constants

(A) PSCF K_∞ (Theory) = 1.07701

Case	Ref. Thickness cm	Ref. Savings cm	$\frac{M_z^2}{M_R^2}\gamma_{11}^2$ $10^{-4}cm^{-2}$	B_m^2 $10^{-4}cm^{-2}$	K_∞ (Exp.)	% Error From Theory
144	2.52	2.52	2.03998 ± .01741	1.14678 ± .01176	1.07222 ± .001312	-0.4472
100	22.84	20.8815	2.12208 ± .01828	1.16742 ± .01211	1.07344 ± .00134	-0.3266
64	43.16	34.5083	2.41494 ± .02145	1.26585 ± .01365	1.07969 ± .00147	0.2487
36	63.48	42.7212	3.09992 ± .02923	1.49069 ± .01735	1.09384 ± .00178	1.5629
16	83.80	47.0768	4.23475 ± .04303	2.17889 ± .02826	1.13717 ± .00272	5.5856
4	104.12	49.2309	5.57255 ± .0605	4.62897 ± .06885	1.29141 ± .00616	19.9068

PSF K_∞ (Theory) = 1.07783

144	2.80	2.80	2.11872 ± .01812	1.05375 ± .01080	1.069841 ± .00127	-0.7357
100	23.12	21.7253	2.18691 ± .01884	1.05772 ± .01094	1.07016 ± .00128	-0.7113
64	43.44	35.9063	2.46890 ± .02189	1.12459 ± .01206	1.07460 ± .00138	-0.2997
36	63.76	44.6468	3.15533 ± .02955	1.26956 ± .01476	1.08422 ± .00161	0.5925
16	84.08	49.3994	4.28471 ± .04335	1.80231 ± .02308	1.11956 ± .00236	3.8713
4	104.40	51.8124	5.61680 ± .06066	3.86757 ± .05641	1.25651 ± .00537	16.5820

TABLES 4.4.1

(A) SF K_∞ (Theory) = 1.08450

Case	Ref. Thickness cm	Ref. Savings cm	$\frac{M_z^2}{M_R^2}\gamma_{11}^2$	B_m^2 $10^{-4}cm^{-2}$	K_∞(Exp.)	% Error From Theory
144	3.20	3.20	2.17762	0.974598 $\pm$.009503	1.08198$\pm$.00166	-0.2317
100	23.52	20.3454	2.27313	1.04535 $\pm$.01083	1.08794$\pm$.00179	0.3171
64	43.84	34.6324	2.47601	1.19690 $\pm$.01277	1.10069$\pm$.00206	1.4926
36	64.16	44.7593	2.90752	1.50779 $\pm$.01701	1.12684$\pm$.00264	3.9042
16	84.48	51.2307	3.60388	2.24288 $\pm$.02751	1.18868$\pm$.00403	9.6063
4	104.80	55.0964	4.43245	4.24391 $\pm$.05824	1.35702$\pm$.00794	25.1281

OCF K_∞ (Theory) = 1.08405

144	3.80	3.80	2.31736	0.804838 $\pm$.003590	1.078661$\pm$.00159	-0.4971
100	24.12	19.3371	2.38646	0.987588 $\pm$.010273	1.09652 $\pm$.00197	1.1505
64	44.44	33.0440	2.55929	1.21639 $\pm$.01302	1.11888 $\pm$.00244	3.2133
36	64.76	43.3459	2.89634	1.63945 $\pm$.01845	1.16023 $\pm$.00333	7.0275
16	85.08	50.4159	3.48799	2.46389 $\pm$.02997	1.24081 $\pm$.00513	14.4604
4	105.40	54.9705	4.12398	4.58142 $\pm$.06192	1.44765 $\pm$.00990	33.5515

TABLES 4.4.1

(A) PSFD K_∞ (Theory) = 1.078,67

Case	Ref. Thickness cm	Ref. Savings cm	$\frac{M_z^2}{M_R^2}\gamma_{11}^2$ $10^{-4}cm^{-2}$	B_m^2 $10^{-4}cm^{-2}$	K_∞(Exp.)	%Error From Theory
121	12.96	12.4546	2.15223 ± .01852	1.04611 ± .01080	1.06873 ± .00125	-0.9216
81	33.28	29.0452	2.29946 ± .02010	1.09994 ± .01158	1.07226 ± .00132	-0.5938
49	53.60	40.2226	2.59859 ± .02338	1.38200 ± .01522	1.09080 ± .00169	1.1241
25	73.92	46.6479	3.66934 ± .03586	1.52733 ± .01859	1.10034 ± .00194	2.0093
9	94.24	50.0091	4.95502 ± .05205	2.66217 ± .03646	1.17490 ± .00355	8.9214

TABLES 4.4.1

(B) PSFD $K_\infty = 1.07867$

Case	Ref. Thickness	Axial 10^{-4} cm^2	B Saving	B B_m^2	B K_∞	C Saving	C B_m^2	C K_∞
121	12.96	2.15223	11.6590	1.08748	1.071446	12.3529	1.05135	1.06907
81	33.28	2.29946	27.1899	1.20710	1.079305	27.7394	1.17485	1.077186
49	53.60	2.59859	37.6534	1.57226	1.103296	36.3629	1.67301	1.109915
25	73.60	3.66934	43.6632	1.86032	1.122221	39.1442	2.43057	1.159686
9	94.24	4.95502	46.8146	3.30477	1.217120	36.9889	5.88581	1.386692

TABLES 4 4.1

(B) PSCF K_∞ (Theory) = 1.07701

Case	Ref. Thickness cm	Axial 10^{-4} cm^{-2}	B Saving cm	B B_m^2 10^{-4} cm^2	B K_∞ (Exp.)	C Saving cm	C B_m^2 10^{-4} cm^{-2}	C K_∞ (Exp.)
144	2.52	2.03928	2.52	1.14678	1.072193	2.52	1.14678	1.072193
100	11.84	2.12208	20.0544	1.21229	1.076318	20.3990	1.19349	1.075134
64	43.16	2.41494	33.1418	1.35429	1.085257	32.1931	1.41758	1.089241
36	63.48	3.0992	41.0294	1.64428	1.103510	37.4986	1.99060	1.125314
16	83.80	4.23475	45.2125	2.46045	1.154893	37.7384	3.79824	1.239111
4	104.12	5.37255	47.2813	5.22587	1.328984	32.7497	11.94914	1.752234

TABLES 4.4.1

(B) PSF K_∞ (Theory) = 1.07783

Case	Ref. Thickness cm	Axial $10^{-4}cm^{-2}$	B Saving cm	B B_m^2 $10^{-4}cm^{-2}$	B K_∞(Exp.)	C Saving cm	C B_m^2 $10^{-4}cm^{-2}$	C K_∞ (Exp.)
144	2.80	2.11872	2.80	1.05375	1.069901	2.80	1.05375	1.069901
100	23.12	2.18691	20.3376	1.13199	1.075090	21.1906	1.08604	1.072043
64	43.44	2.46890	33.6128	1.26949	1.084211	33.369	1.3854	1.085267
36	63.76	3.15533	41.7931	1.51858	1.100735	38.9243	1.79093	1.118801
16	84.08	4.28471	46.2440	2.25246	1.149417	39.1948	3.45786	1.229377
4	104.40	5.61680	48.5029	4.80167	1.318519	33.9520	11.1372	1.738786

TABLES 4.4.1

(B) SF K_∞ (Theory) = 1.08450

Case	Ref. Thickness dm	Axial $10^{-4}cm^{-2}$	B Saving cm	B B_m^2 $10^{-4}cm^{-2}$	B K_∞(Exp.)	C Saving cm	C B_m^2 $10^{-4}cm^{-2}$	C K_∞ (Exp.)
144	0.999702	2.17762	3.20	0.974598	1.081987	3.20	0.9746	1.081987
100	0.987270	2.27313	18.8974	1.12558	1.094688	19.8947	1.07001	1.090014
64	0.968464	2.47601	32.1676	1.35823	1.114260	32.2978	1.34944	1.11352
36	0.934933	2.90752	41.5737	1.78640	1.15029	39.0085	2.03039	1.170805
16	0.865249	3.60388	47.5846	2.73614	1.230175	40.3255	3.92394	1.330098
4	0.709477	4.43245	51.1752	5.22175	1.439274	35.4443	11.43683	1.962111

TABLES 4.4.1

(B) OCF K_∞ (Theory) = 1.08405

Case	Ref. Thickness cm	Axial $10^{-4}cm^{-2}$	B Saving cm	B B_m^2 $10^{-4}cm^{-2}$	B K_∞(Exp.)	C Saving cm	C B_m^2 $10^{-4}cm^{-2}$	C K_∞(Exp.)
144	3.80	2.31736	3.80	0.80484	1.078661	3.80	0.80438	1.078661
100	24.12	2.38646	18.745	1.02087	1.09975	18.9427	1.00970	1.098683
64	44.44	2.55929	32.032	1.28412	1.125503	30.9507	1.35855	1.132778
36	64.76	2.89634	42.019	1.75711	1.171731	37.9636	2.14644	1.209783
16	85.08	3.48719	48.872	2.67093	1.261044	39.8243	4.13391	1.404028
4	105.40	4.12398	53.288	4.98408	1.487119	35.3878	11.77749	2.151073

TABLES 4.4.1

PSCF

CASE	ONE GROUP	TWO GROUP	AGE DIFFU-SION
144	1.07219	1.07349	1.07424
100	1.07344	1.07484	1.07561
64	1.07969	1.08127	1.08218
36	1.09384	1.09604	1.09731
16	1.13717	1.14186	1.14465
4	1.29141	1.31260	1.32643

PSF

	ONE GROUP	TWO GROUP	AGE DIFFU-SION
	1.06990	1.07119	1.07183
	1.07016	1.07139	1.07211
	1.07460	1.07599	1.07680
	1.08422	1.08598	1.08703
	1.11956	1.12312	1.12526
	1.25656	1.27196	1.28371

SF

144	1.08199	1.08362	1.08482
100	1.08794	1.08982	1.09121
64	1.10069	1.10315	1.10499
36	1.12684	1.13073	1.13371
16	1.18868	1.19733	1.20412
4	1.35702	1.38799	1.41475

OCF

	1.07866	1.08015	1.08131
	1.09652	1.09876	1.10053
	1.11888	1.12228	1.12500
	1.16023	1.16640	1.17146
	1.24081	1.25474	1.26671
	1.44777	1.49592	1.54241

PSF (ODD)

121	1.06873	1.06991	1.07060
81	1.07226	1.07357	1.07434
49	1.09080	1.09285	1.09408
25	1.10034	1.10285	1.10436
9	1.17490	1.18252	1.18733

TABLE 4.4.3

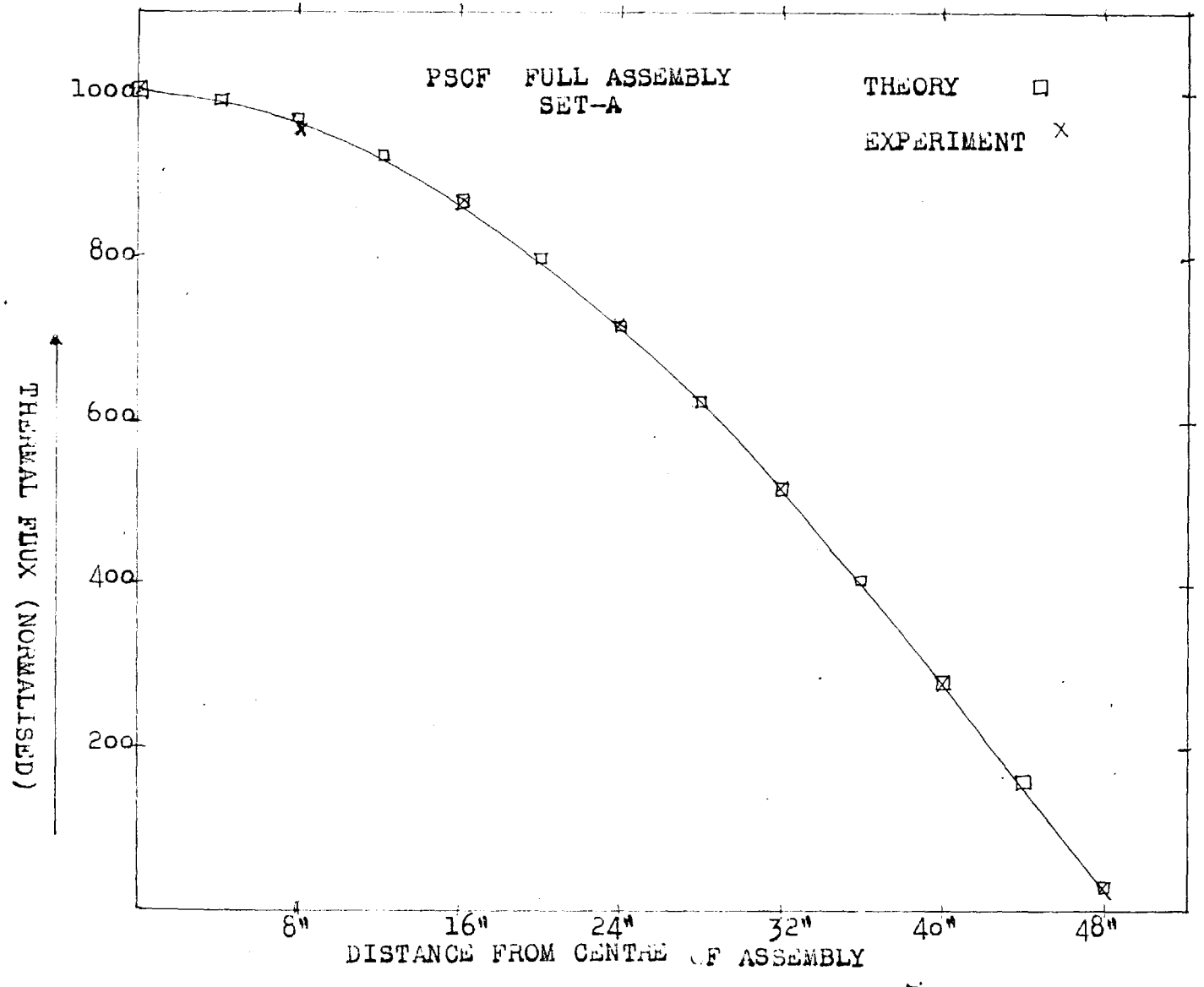

FIG. 4.4.1 COMPARISON OF THEORETICAL(ONE-GROUP) AND EXPERIMENTAL FLUX DISTRIBUTION

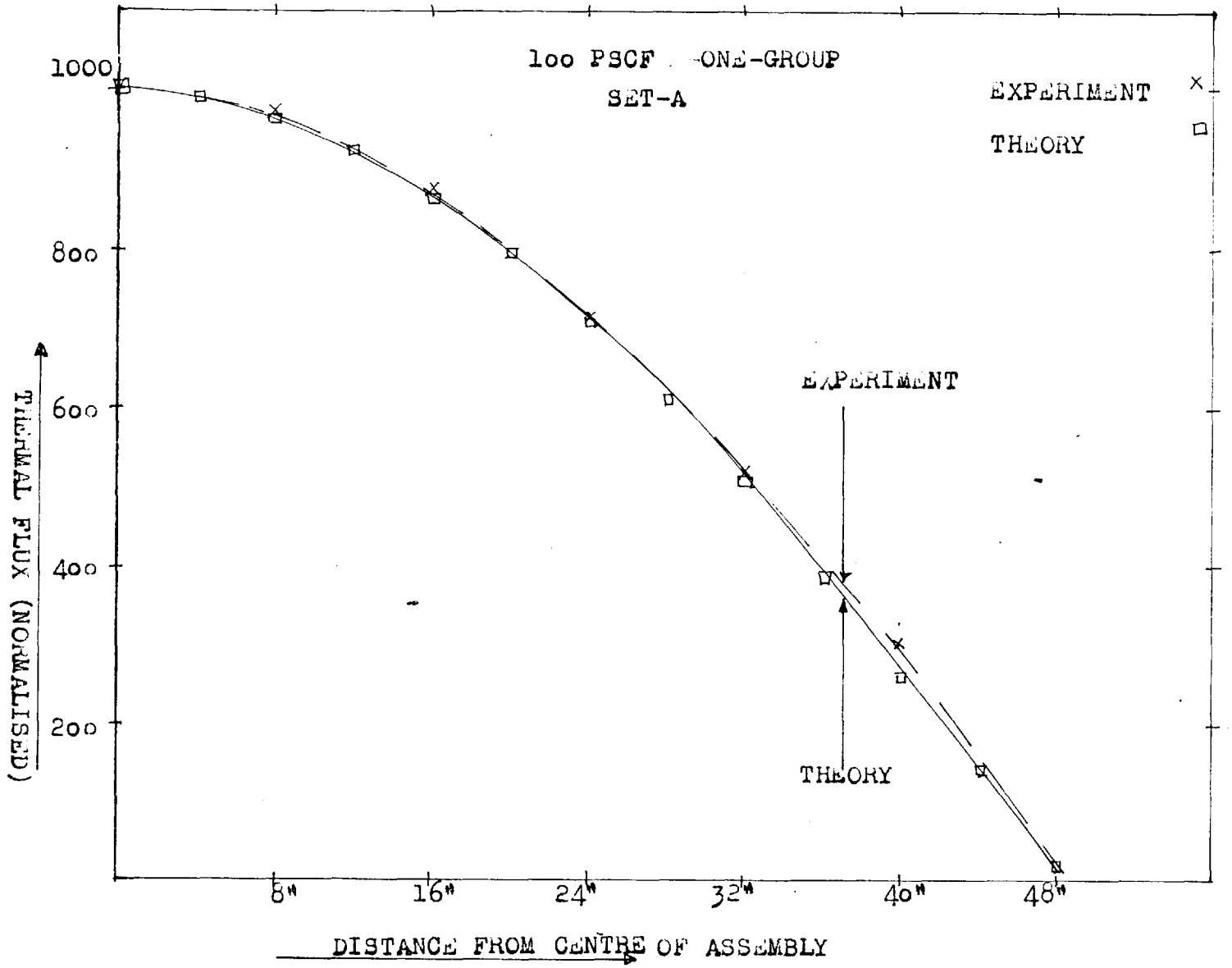

FIG.4.4.1 COMPARISON OF THEORETICAL (ONE-GROUP) AND EXPERIMENTAL FLUX DISTRIBUTION

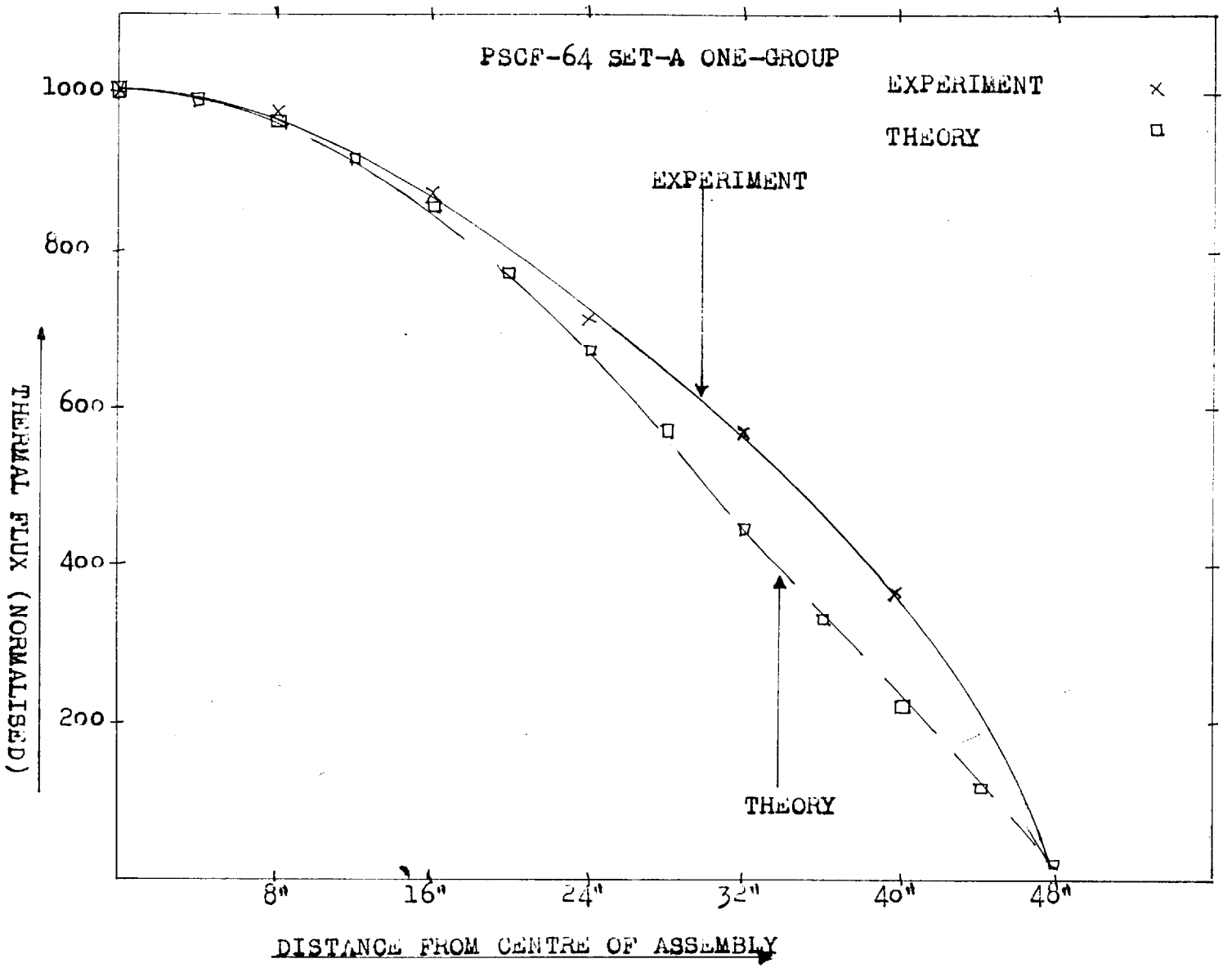

FIG. 4.4.1 COMPARISON OF THEORETICAL(ONE-GROUP) AND EXPERIMENTAL FLUX DISTRIBUTION

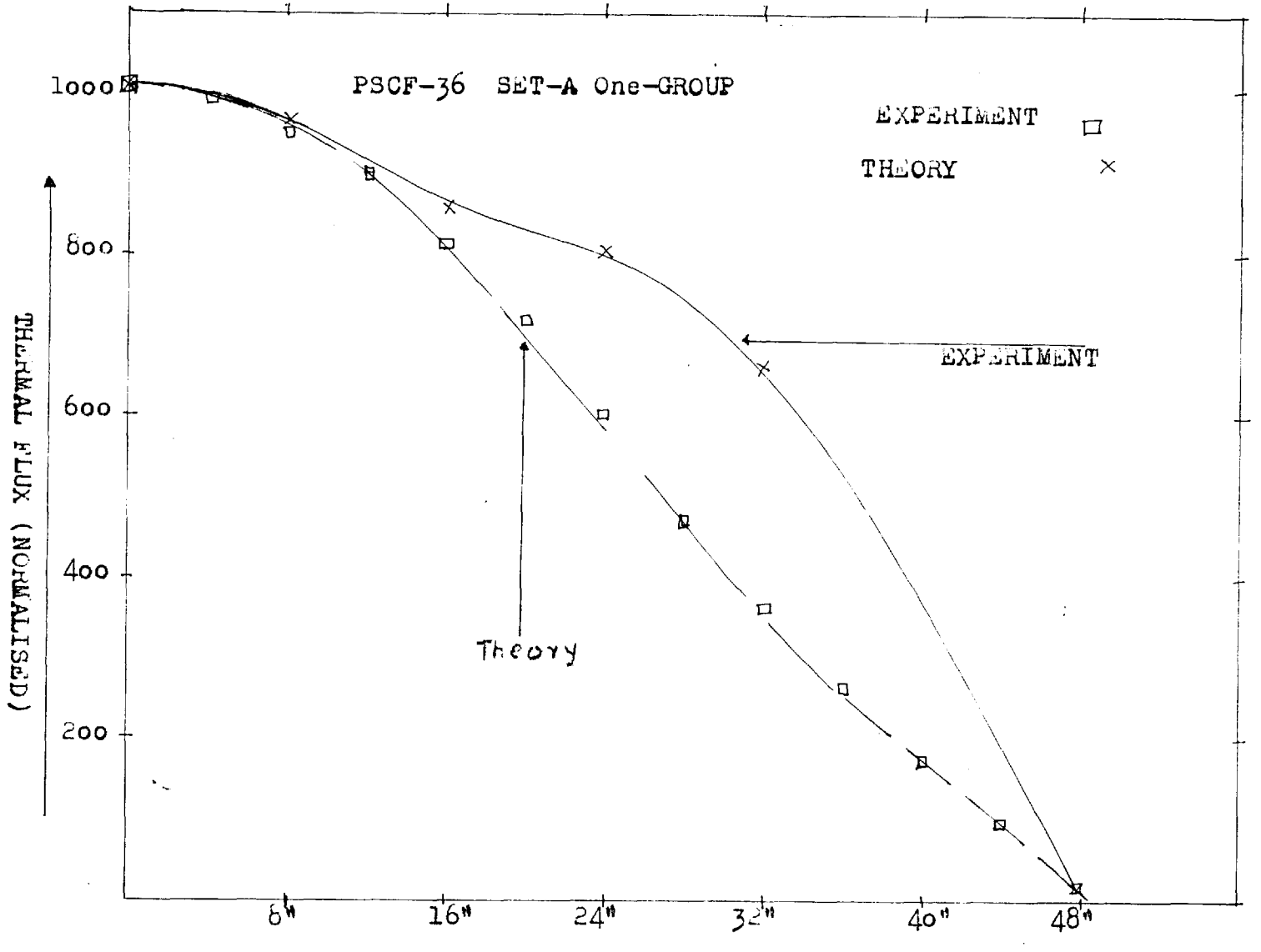

FIG.4.4.1 COMPARISON OF THEORETICAL (ONE-GROUP) AND EXPERIMENTAL FLUX DISTRIBUTION

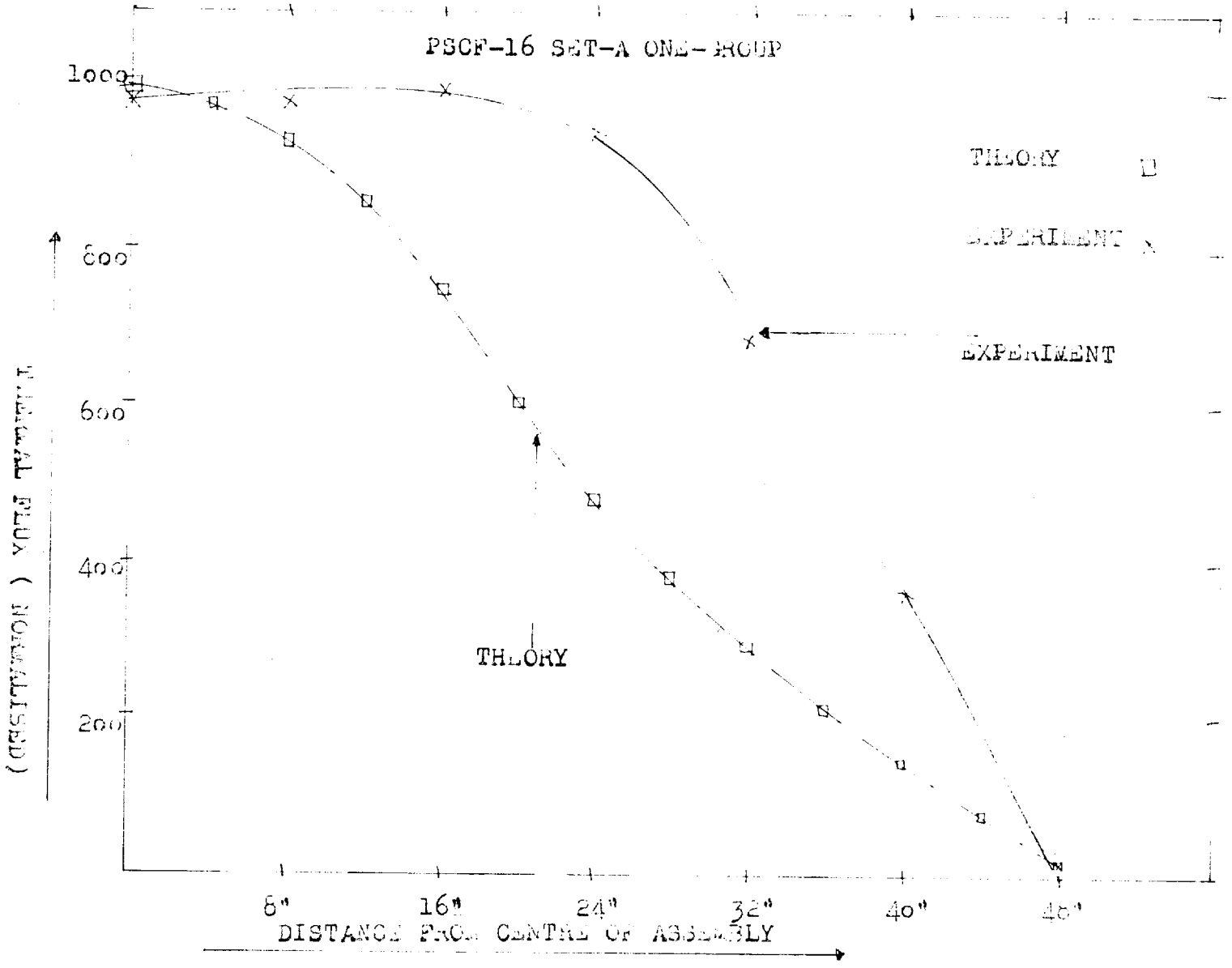

FIG.4.4.1 COMPARISON OF THEORETICAL(ONE-GROUP) AND EXPERIMENTAL FLUX DISTRIBUTION

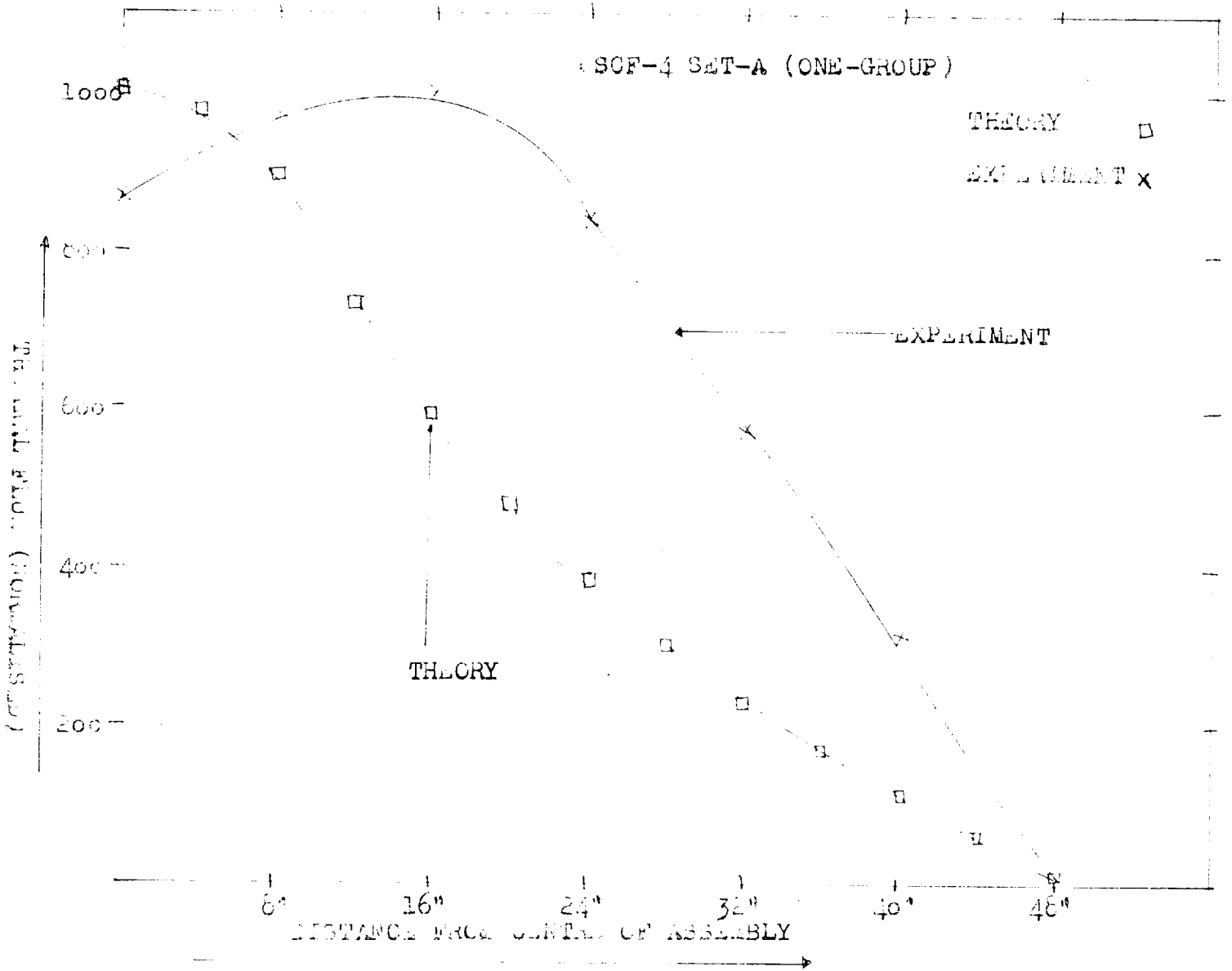

FIG.4.4.1 COMPARISON OF THEORETICAL (ONE-GROUP) AND EXPERIMENTAL FLUX DISTRIBUTION

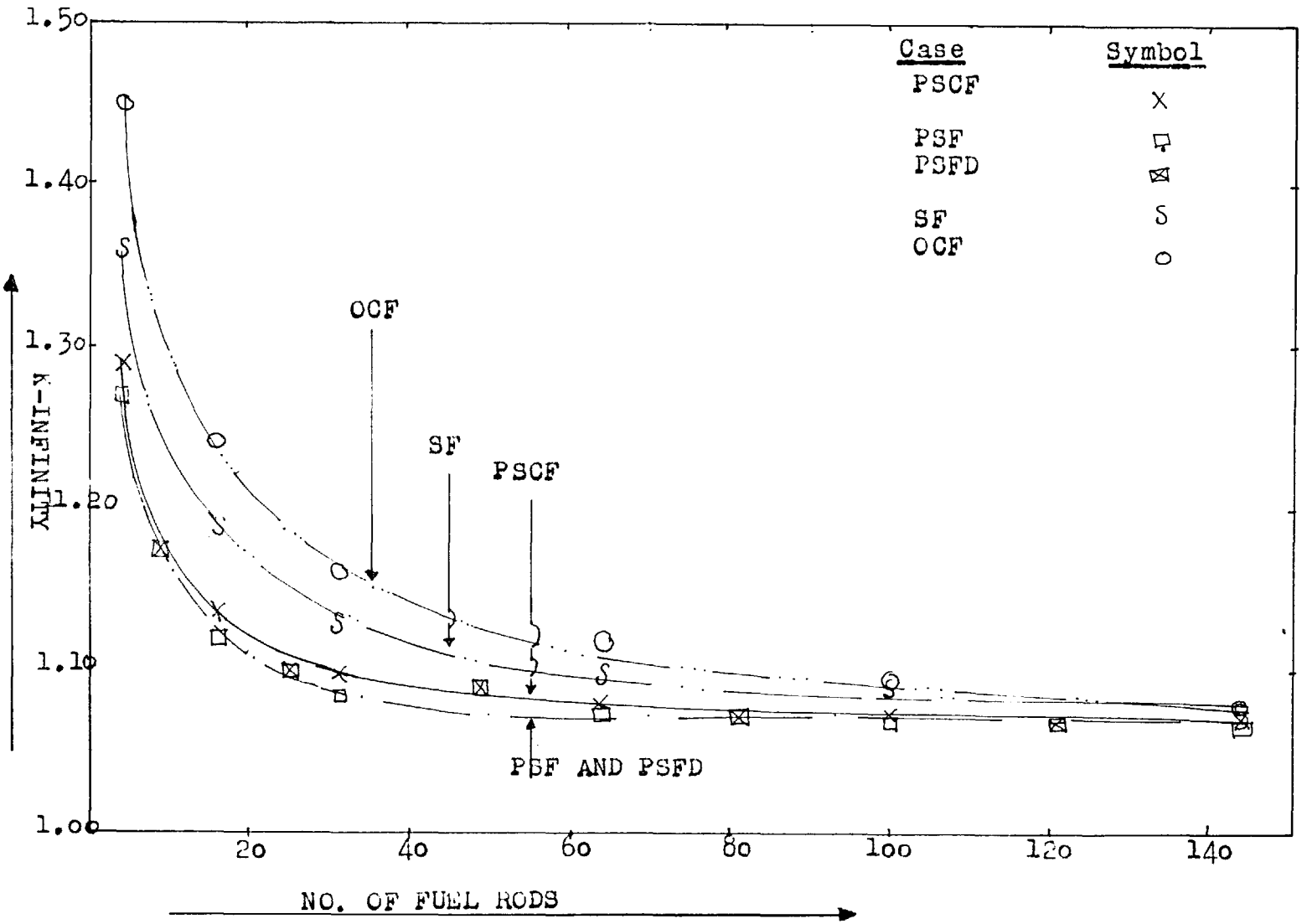

FIG. 4.4.1 K-INFINITY AS FUNCTION OF NO. OF FUEL RODS

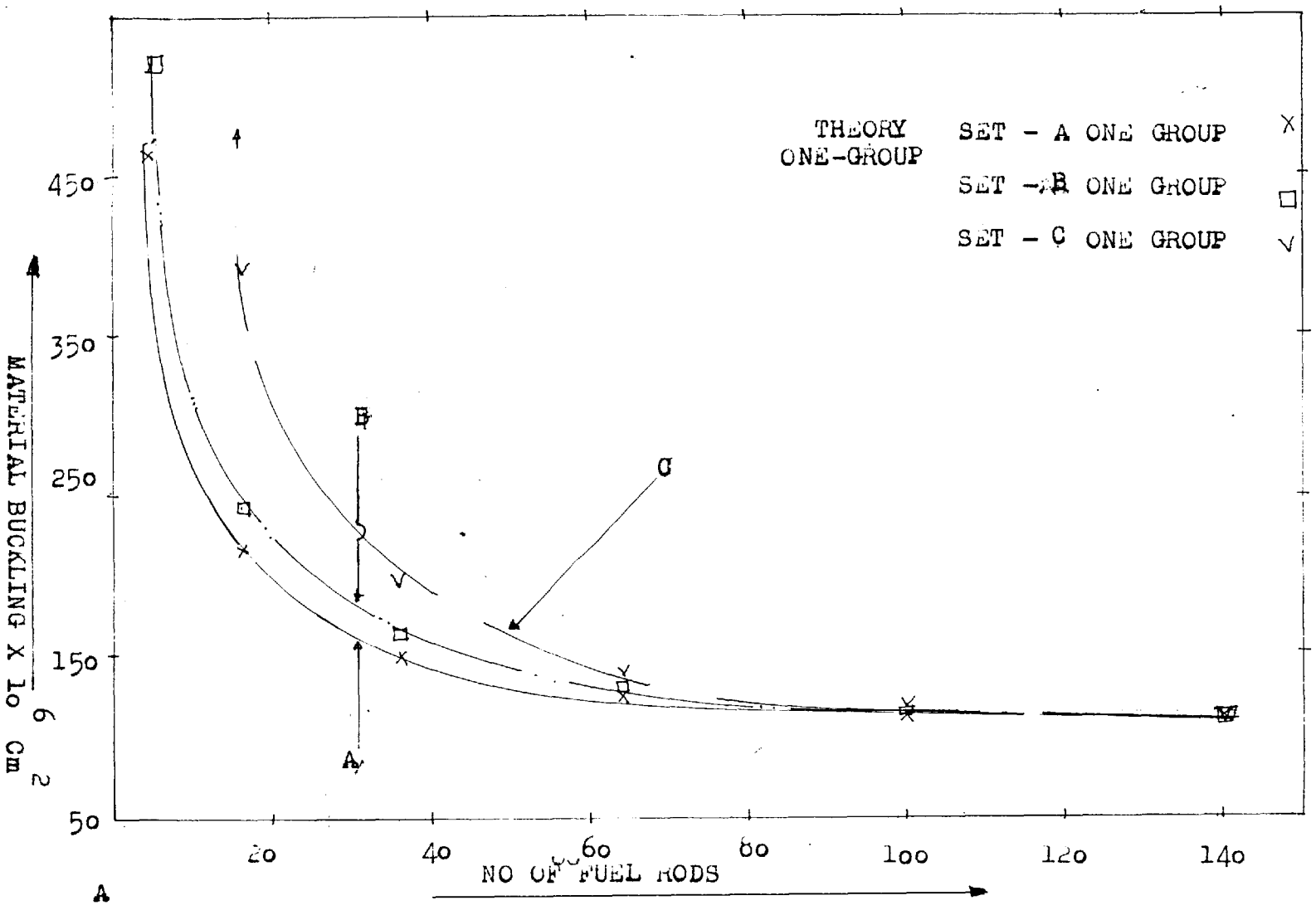

FIG. 4.4.1 MATERIAL BUCKLING AS A FUNCTION OF NO OF FUEL RODS

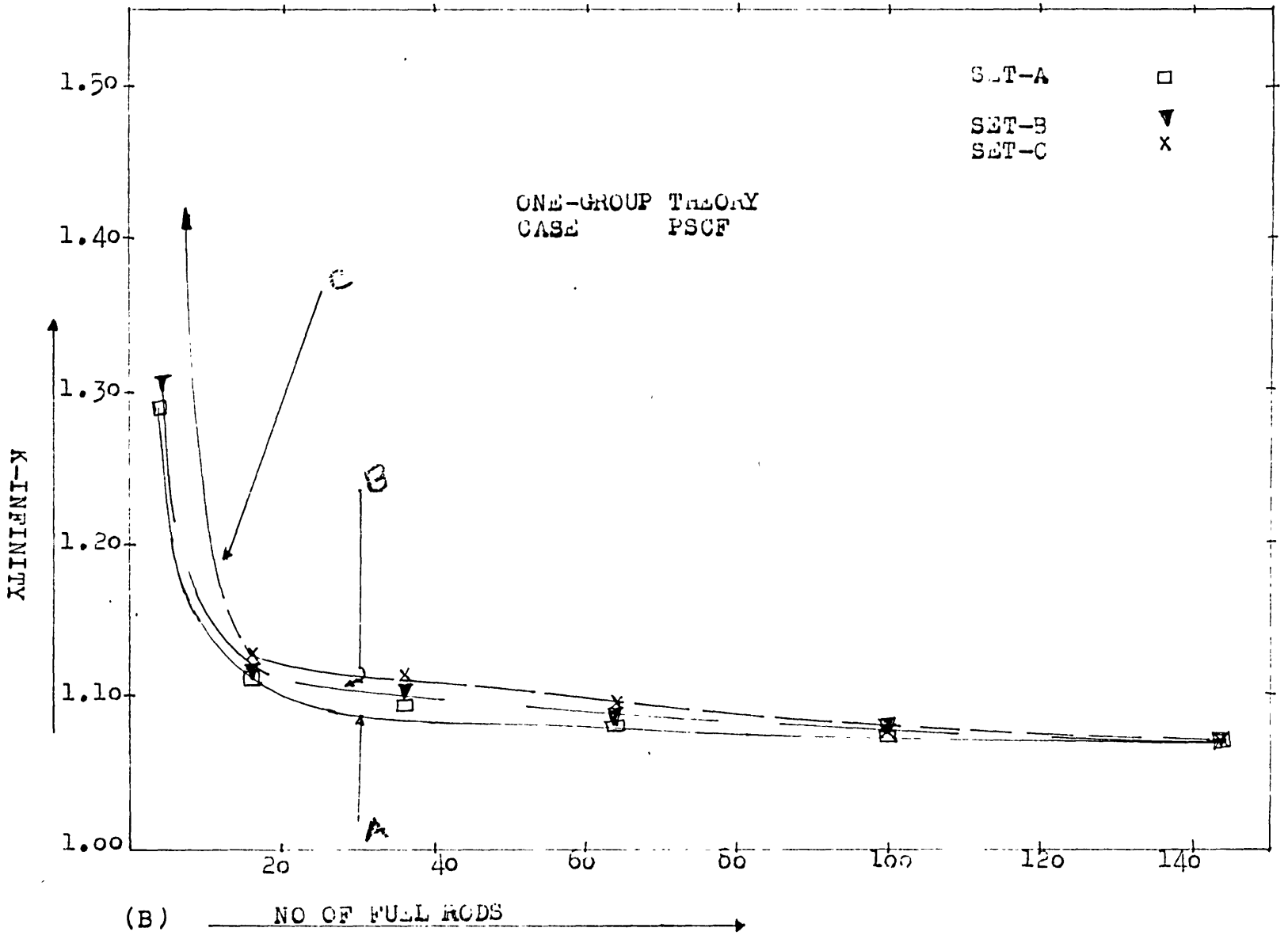

FIG. 4.4.1 K-INFINITY (ALL CASES) VS NO OF FULL RODS

used correspond to the radial direction.

4.4.2 CALCULATION OF ERRORS IN K_∞

The calculation of errors in K_∞ for partially filled sub-critical assembly is almost identical to the procedure given in section 3.4.1. In the case of a sub-critical assembly the uncertainty in the experimentally measured material buckling and therefore K_∞ is due to:-

1) the error in the measured relaxation length due to causes fully discussed in section 2 of Chapter 2, and

2) the error in the extrapolated dimensions of the assembly in X and Y-direction.

When the sub-critical assembly is full with fuel elements it is a simple matter of calculating how much the resulting error is. But when the sub-critical assembly is partially filled with the fuel and there is reflector surrounding the core, mathematically there is no analytical solution for the system in three dimensions and consequently we do not know the exact material buckling for the system. Thus the material buckling becomes a complicated function of the geometry of the system and the uncertainty as such is not in the experiment to find the relaxation length accurately, but in the theory used for the analysis. Hence, it is very important to distinguish between an experimental error in K_∞ or

material buckling and the theoretical error in the said quantities. At the moment our interest is in the experimental errors involved, assuming that the theory adopted is the right one for the analysis.

Therefore in the calculation of errors it was assumed that measurement of the relaxation length in the axial direction is independent of the measurements in the X or Y-directions. The combination of errors then onwards is almost the same as in the case of the sub-critical assembly full with fuel elements. However from the theoretical point of view the inaccuracies are reduced to zero. For example, in the calculation of the reflector saving it is assumed that there is no error in the analysis and hence it should give the right answer. But, the attitude in the present analysis could be summed up, "Had we the possibility to measure the width of the sub-critical assembly with reflector outside in X and Y directions so that in combination with the relaxation length measured it could give the material buckling of the system, then what error could we have expected in the experimental results so obtained?" Since the proposition is rather hypothetical, it was assumed that the equivalent width of the reactor calculated by the addition of reflector savings is subject to an error of 0.5 cms, the same maximum error as we assume in an experiment with

fully fueled sub-critical assembly. The accuracy which the programme , Appendix A-2.4. , assume is very high (10^{-6} cm).

The errors in b_{11} and equivalent width are then combined in the normal way, section 3.4. As it was found in the case of full assembly cases, the error introduced due to measurements in the X and Y-direction was very small, never more than 0.1%. of the error due to error in b_{11}. Only representative values of the widths were taken for the purpose. Thus the errors quoted in all K_∞'s in Chapters 4 and 5 correspond to the widths given by the core size and the corresponding reflector savings with an assumed error of 0.5 cms. for case A.

It was found that contribution due to the error in b_{11} in the resulting material buckling and K_∞ calculated was the most dominant. Therefore no more pedantically accurate but less revealing calculations were done for errors in K_∞ and B_m^2. Only the errors in the first set for K_∞, B_m^2 and axial buckling are tabulated, while in the latter case they have been omitted. The errors arising due to errors in thickness T have not been considered because the error in the function $\tanh(T\alpha_1)$ due to errors in thickness is diminishingly small.

4.4.3 DISCUSSION OF THE RESULTS

(a) Let us first of all consider the results quoted in section 4.4.1 all together. Obviously the best results with reference to the measured thermal flux distribution, best known values of the parameters, specifically material buckling and K_∞ etc., start to deviate seriously when the number of fuel elements is less than 36 in case of PSCF, PSF and PSF(ODD), while in case of SF and OCF, the process of degeneration starts from 64 fuel elements downwards. The latter case could conveniently be ascribed to the inaccuracies in the streaming (3.34) corrections and thus the corresponding characteristic constants are not known to the desired accuracy. Therefore the discussion would be concerned with the first three cases, namely PSCF, PSF and PSF(ODD). The thermal flux has been plotted in FIGS. 4.4.1 and it can be seen that the flux distribution calculated theoretically is in absolutely close agreement in case of 144, slightly affected near the core-reflector boundary in case of 100 fuel elements. The differences in flux distribution are quite large when the number of fuel elements is 64 or less, and there is no relationship when the number of fuel elements is 4. These deviations could be explained by considering the flux plots as a function of the number of fuel elements in conjunction with curves

for K_∞ vs number of fuel rods and that of B_m^2 vs number of fuel rods.

First of all if the calculation of reflector savings is true then the material buckling defined as

$$B_m^2 = 2\left(\frac{\pi}{a'+2\delta}\right)^2 - \frac{M_z^2}{M_R^2}\,\gamma_{11}^2$$

should be constant and be independent of the number of fuel elements in the sub-critical assembly. The fact, that it remains fairly constant over the range 144 to 64 fuel elements and starts to break down seriously when the number of fuel elements is reduced below 36, proves that the calculation and the concept of reflector savings is true. Below this number it is not the method but that the basic physical assumptions in the analysis break down.

In the theoretical analysis the problem is treated as infinite plane slab system, implying that the dimensions in y and z-directions are infinite. Mathematically it has the significance that there is zero flux curvature in these two directions and consequently there is no loss of neutrons from the reactor system. Thus in reducing the size of core-region in the assembly, we increase the loss of neutrons and consequently the material buckling increases leading to the increase in the value of K_∞ needed to make the system critical under the prevailing

conditions.

However, it is fortuitous combination of assumptions that the results are quite consistent over a wide range of fuel elements.

The rapid fall of thermal flux in comparison to the experimentally measured flux distribution is due to the fact that the basis of one group theory is not true that "all events leading to the production of thermal neutrons take place at a single energy". This will be considered in some detail in the next chapter.

(b) Now considering the individual sets of data and the computed results, for the sets A and B the reflector savings have been calculated by the expression

$$\delta = \frac{D_C}{D_r \kappa_r} \tanh (T\kappa_r) \qquad 4.4$$

while in case of (C) by solving the transcendental equation,

$$D_C \alpha \tan(\alpha \frac{a'}{2}) = D_r \kappa_r \coth (\kappa_r T)$$

for δ in case of given thickness and core-size.
In B the increase of D_r reduces the reflector saving or indirectly increases the radial leakage in the reflector region; therefore the agreement gets worse between theory and experiment in comparison with the set A. In case of 100 fuel elements the results for PSCF and PSF and

PSF(ODD) 84 the agreement between theory and experiment is improved; while the agreement in case of C is the worst as compared to A and B shown in FIG.4.4.1 (A,B) since, in accordance with theory, neither the analytical assumptions are absolutely true nor the use of consequent results should be absolutely true. However derivation of the eqn. 4.4 is a simple approach to the problem and has certain opposing processes (Chapter 5) going on so that the agreement is quite close.

In section 3.4.3 it was remarked that the basis of modified one group theory to compute K_∞ are approximate only. With that point in mind, all the results for A cases have been tabulated in Table 4.4.3 for the sake of comparison, in the use of modified one-group theory in comparison to two-group and age-diffusion theories. The material bucklings and the relevant constants are the same for the computation of K_∞. The expressions for K_∞ used are 4.1.2-4. The agreement between theoretical and experimental values improves considerably in case of full assembly case, 100 and 64 fuel elements, and the apparent disagreement in other cases is due to the neglect of other theoretical and physical reasons, which will be discussed in the next chapter.

CHAPTER 5

CALCULATION OF FLUX, K-INFINITY AND THE REFLECTOR SAVING FOR A PARTIALLY FILLED (Core) SUB-CRITICAL ASSEMBLY ON THE BASIS OF "TWO-GROUP THEORY"

5.1 FORMULATION OF TWO-GROUP THEORY DIFFUSION EQUATIONS

All the introductory remarks of the last chapter apply to the present chapter, except that here we will consider the two energy groups, namely, thermal and fast. Two-group theory is one of the most widely used methods for calculating criticality in a thermal reactor.

It can be applied to a reflected reactor and takes account of the slowing down process more rigorously than does the modified one-group theory of the last chapter. In order to set up the two-group neutron balance equations in the core and the reflector regions, we follow Syrett's model(7) in ordering the sequence of events briefly summarised below.

1) Production of fast neutrons by fission caused by thermal neutrons in U^{235} and fast fission in U^{238}.

2) Resonance capture in U^{238}, fast neutron leakage and slowing down of fast neutrons.

3) Thermal neutron capture, leading to the process (1) and the parasitic absorption as well.

The ordering of events in the two-group model is in line with the use of Westcott's formalism of effective cross-sections. The neutron-balance equations for the core region for the two energy groups can be written as

$$D_{fc}\nabla^2\varphi_c - \Sigma_{fc}\varphi_{fc} + K_\infty \Sigma_{mc}\varphi_{mc} = 0 \qquad 5.1.1$$

$$D_{mc}\nabla^2\varphi_c - \Sigma_{mc}\varphi_{mc} + \Sigma_{fc}\varphi_{fc} = 0 \qquad 5.1.2$$

f, m and c stand for fast, thermal and core regions respectively.

If we substitute φ_{fc} from eq. 5.1.2 in eq. 5.1.1 or vice versa, the resulting fourth order differential equation would be identical in φ_{mc} or φ_{fc} showing that any particular solution of φ_{mc} has a corresponding solution for the fast flux or vice versa.

Effect of resonance escape probability is assumed to be included in K_∞ and therefore the transfer cross-section from fast flux to thermal is the same in the two equations.

The fluxes in the reflector region can be written as

$$D_{fr}\nabla^2\varphi_{fr} - \Sigma_{fr}\varphi_{fr} = 0 \qquad 5.1.3$$

$$D_{mr}\nabla^2\varphi_{mr} - \Sigma_{mr}\varphi_{mr} + \Sigma_{fr}\varphi_{fr} = 0 \qquad 5.1.4$$

There is no source term in the fast group for the reflector because there is no fuel in the reflector region.

The process of regeneration, absorption and leakage could be followed much more clearly with reference to FIG.5.1.1 wherein the competing processes going on in such a system are shown diagramatically. Details of the method of solving these four differential equations are given in the next section.

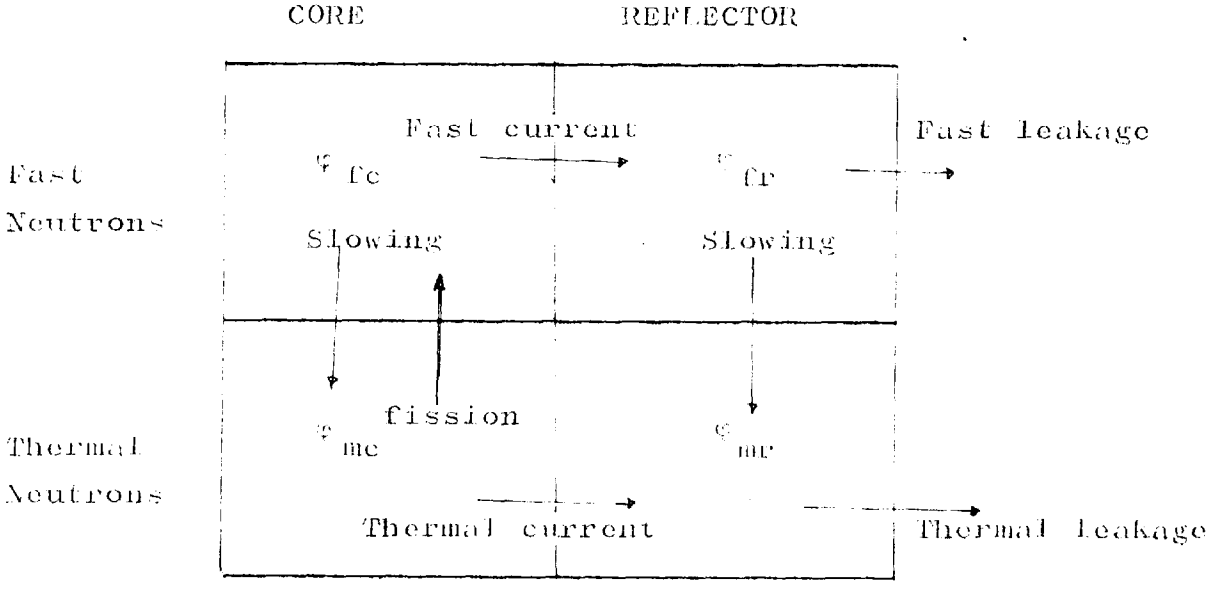

FIG. 5.1.1

TWO-GROUP REGENERATION, ABSORPTION AND LEAKAGE PROCESSES

5.2 SOLUTION OF TWO-GROUP DIFFUSION EQUATIONS FOR FLUXES IN THE SUB-CRITICAL ASSEMBLY AND CONDITION FOR CRITICALITY

In the present section, as in the last chapter, the problem of the square core in the square assembly (reflector core system) will be reduced to the case of "infinite plane system". The assumption is partly true; specifically, the fact

(a) that the flux distribution in x and y directions is identical because of the symmetrical position of the core, is in favour of this assumption while

(b) that the analytical solution of such a core reflected system in two dimensions is impossible; counts against it.

However there was ample experimental evidence to support that this can be assumed to be true for a square core of reasonable (section 5.3.4) dimensions.

Writing the two-group equations for thermal and fast fluxes in the core and the reflector region (section 5.1) in rectangular coordinates, we have

$$D_{fc}\nabla^2\varphi_{fc}(X,Y,Z)-\Sigma_{fc}\varphi_{fc}(X,Y,Z)+k_\infty\Sigma_{mc}\varphi_{mc}(X,Y,Z)=0 \qquad 5.2.1$$

$$D_{mc}\nabla^2\varphi_{mc}(X,Y,Z)-\Sigma_{mc}\varphi_{mc}(X,Y,Z)+\Sigma_{fc}\varphi_{fc}(X,Y,Z)=0 \qquad 5.2.2$$

$$D_{fr}\nabla^2\varphi_{fr}(X,Y,Z)-\Sigma_{fr}\varphi_{fr}(X,Y,Z)=0 \qquad 5.2.3$$

$$D_{mr}\nabla^2\varphi_{mr}(X,Y,Z)-\Sigma_{mr}\varphi_{mr}(X,Y,Z)+\Sigma_{fr}\varphi_{fr}(X,Y,Z)=0 \qquad 5.2.4$$

All of the balance equations are inhomogeneous excepting the fast flux equation for the reflector. The solution to an inhomogeneous differential equation is equal to the sum of the solution to its homogeneous part and a particular solution in accord with the nature of the inhomogeneous part, i.e.

$$\Phi = \Phi_{\text{homo.}} + \Phi_{\text{particular.}}$$

The homogeneous parts of the four balance equations are

$$\nabla^2\varphi_{fc}(X,Y,Z) - B^2\varphi_{fc}(X,Y,Z) = 0 \qquad 5.2.5$$

$$\nabla^2\varphi_{mc}(X,Y,Z) - B^2\varphi_{mc}(X,Y,Z) = 0 \qquad 5.2.6$$

(It is assumed bucklings for the fast and thermal fluxes in the core are equal.)

$$\nabla^2\varphi_{fr}(X,Y,Z) - \kappa_{fr}^2\varphi(X,Y,Z) = 0 \qquad 5.2.7$$

$$\nabla^2\varphi_{mr}(X,Y,Z) - \kappa_{fr}^2\varphi_{mr}(X,Y,Z) = 0 \qquad 5.2.8$$

Substituting equations 5.2.5 and 5.2.6 in the fast and thermal equations for the core, we have

$$-(D_{fc}B^2 + \Sigma_{fc})\varphi_{fc} + K_\infty\Sigma_{mc}\varphi_{mc} = 0$$

$$\Sigma_{fc}\varphi_{fc} - (D_{mc}B^2 + \Sigma_{mc})\varphi_{mc} = 0$$

Leading to the determinant for a non-trivial solution and the criticality condition is

$$k_\infty = (1+B^2L_R^2)(1+B^2L_{SR}^2) \qquad 5.2.9.$$

This is a second order equation in B^2 and has got two roots μ^2 (real, positive) and ν^2(negative and very large). The problem is to find the geometrical dimensions which give a geometrical buckling satisfying the boundary conditions outlined in section 4.2 for the neutron fluxes at the interface and at the extrapolated boundaries; besides that, the flux should be symmetrical and non-negative.

Making use of the fact that

$$\varphi(X,Y,Z) = X(x)\ Y(y)\ Z(z)$$

and rewriting the core equations 5.2.5-6.

$$\frac{1}{X_{fc}}\frac{\partial^2 X_{fc}}{\partial x^2} + \frac{1}{Y_{fc}}\frac{\partial^2 Y_{fc}}{\partial y^2} + \frac{D_{FZC}}{D_{FRC}}\frac{\partial Z^2}{\partial Z^2} + B^2 = 0 \quad (a)$$

$$\frac{1}{X_{mc}}\frac{\partial^2 X_{mc}}{\partial x^2} + \frac{1}{Y_{mc}}\frac{\partial^2 Y_{mc}}{\partial y^2} + \frac{D_{MZC}}{D_{MRC}}\frac{\partial Z^2}{\partial Z^2} + B^2 = 0 \quad (b) \qquad 5.2.10$$

The system under study is not "plane infinite slab"; it is finite in all directions and to complicate matters there are neutron sources at the bottom of the sub-critical assembly. However we proceed with our assumptions as before.

Since each term in the equations 5.2.10 (a,b) is independent of the other,

$$\frac{1}{Z_{fc}} \frac{\partial^2 Z_{fc}}{\partial z^2} = \frac{1}{Z_{mc}} \frac{\partial^2 Z_{mc}}{\partial z^2} = \gamma^2$$

and $$\frac{1}{X_{fc}} \frac{\partial^2 X_{fc}}{\partial x^2} = \frac{1}{Y_{fc}} \frac{\partial^2 Y_{fc}}{\partial y^2} = -\mu^2$$

μ^2 is the radial leakage in x-direction corresponding to asymptotic flux distribution. Therefore the material buckling of the system is

$$B^2 = \alpha^2 - \gamma^2 \frac{M_z^2}{M_R^2} \qquad (e) \qquad 5.2.10$$

Now considering the solution in the direction of x or y, the general solution to the core equation- is a linear combination of the two solutions corresponding to ν^2 and $-\nu^2$, satisfying the boundary conditions. The solutions would be

$$X_{fc}(x) = A \cos(\mu x) + C \cosh(\nu x) \qquad (a) \qquad 5.2.11$$

$$X_{mc}(x) = S_1 A \cos(\mu x) + S_2 C \cosh(\nu x) \qquad (b) \quad 5.2.11$$

The values of S_1 and S_2 are

$$S_1 = \frac{D_{FRC}}{D_{MRC}} \cdot \frac{L_{RC}^2}{L_{SR}^2} \cdot \frac{1}{1+L_{RC}^2 \mu^2} \qquad (c) \quad 5.2.11$$

$$S_2 = \frac{D_{FRC}}{D_{MRC}} \cdot \frac{L_{RC}^2}{L_{SRC}^2} \cdot \frac{1}{1-L_{RC}^2 \nu^2} \qquad (d) \quad 5.2.11$$

The fact that the flux distributions should be symmetrical and non-negative in the core, has been applied as the boundary

conditions.

Solution in the Z-direction both for the core and for the reflector regions for the equations 5.2.5-8 is

$$Z(z) = A_{11} \frac{\sinh(c-z)\gamma}{\sinh(c\gamma)} \qquad 5.2.12$$

The criticality condition (5.2.9) rewritten for the two groups

$$K_\infty = (1+B_R^2 L_{SR}^2 - \gamma^2 L_{SZ}^2)(1+B_R^2 L_R^2 - \gamma^2 L_Z^2)$$

relates the production and absorption of neutrons to the leakage and flux curvature in the core of the sub-critical assembly. This gives two values for the radial flux curvature, μ^2 being the real root and $-\nu^2$ the imaginary one. The real root is positive and very small and the other is negative but of very large magnitude. Physically the positive value describes the asymptotic distribution of the fast and the thermal fluxes, cos (μx), while the negative root corresponds to the non-asymptotic flux distribution, cosh (νx), or is the transient solution for the flux distribution near the interface of the core and the reflector. This is as a consequence of the fact that the nuclear properties of the core and the reflector are completely different from each other. However this transient dies out in a distance of the order of a migration length from the inter-face . Then the

flux distribution settles down according to the properties of the reflector region.

The asymptotic solution of the core flux is physically realizable since, on extrapolation, it reduces to zero at the extrapolated boundary of the assembly, while the transient solution is not. Therefore we can associate the two in a linear combination only. Regarding the magnitude of the roots, we have to assume a trial value of μ^2 and then

$$\nu^2 = \left(\frac{1}{L_R^2} + \frac{1}{L_{SR}^2}\right) + \mu^2$$

since we do not know the critical parameter K_∞ in the criticality conditions, which we have to calculate eventually.

Now the equations 5.2.7-8 for the fast and thermal fluxes in the reflector region written in rectangular co-ordinates by making use of

$$\varphi(X,Y,Z) = X(x)\ Y(y)\ Z(z)$$

are

$$\frac{1}{X_{fr}}\frac{\partial^2 X_{fr}}{\partial x^2} + \frac{1}{Y_{fr}}\frac{\partial Y_{fr}^2}{\partial y^2} + \frac{D_{FZr}}{D_{FRr}}\frac{1}{Z_{fr}}\frac{\partial Z^2}{\partial z^2} - \varkappa_{fr}^2 = 0 \quad (a)$$

$$\frac{1}{X_{mr}}\frac{\partial^2 X_{mr}}{\partial x^2} + \frac{1}{Y_{mr}}\frac{\partial^2 Y}{\partial y^2} + \frac{D_{MZr}}{D_{MRr}}\frac{1}{Z_{mr}}\frac{\partial^2 Z}{\partial z^2} - \varkappa_{mr}^2 = 0 \quad (b) \qquad 5.2.13$$

The solution for the flux in the x-direction as before is

$$X_{fr}(x) = F \sinh \kappa_{fr}\left(\frac{a'}{2} + T - x\right) \qquad (a)$$

$$X_{mr}(x) = G \sinh \kappa_{mr}\left(\frac{a'}{2} + T - x\right) + \qquad 5.2.14$$

$$+ S_3 F \sinh \kappa_{fr}\left(\frac{a'}{2} + T - x\right) \qquad (b)$$

where the coupling constant S_3 is

$$S_3 = \frac{D_{FRr}}{D_{MRr}} \cdot \frac{1}{\left(\frac{L_{SRr}^2}{L_{Rr}^2} - 1\right)} \qquad (c)$$

and $$\kappa_{fr}^2 = \frac{1}{L_{SRr}^2} \qquad (d)$$

and $$\kappa_{mr}^2 = \frac{1}{L_R^2} \qquad (e)$$

It may be remarked that the flux distribution in the z-direction is the same as for the core region. The same expressions for the flux distribution in the y-direction would hold true except for the values of y's in place of x's because of the symmetrical position of the core in the sub-critical assembly. The thermal and the fast neutron flux distributions in the core have been obtained under the conditions that the flux is finite, symmetrical and non-negative, while those for the reflector region have been obtained under the boundary condition that the fluxes go to zero at the extrapolated boundary

of the assembly. However it is assumed that fast and thermal fluxes have the same extrapolation lengths.

To find the constants A, C, F and G we apply the boundary condition of equal current and equal fluxes at the core-reflector interfaces both for fast and thermal fluxes in the two regions, i.e.

$$\varphi_{fc}\left(\frac{a'}{2}\right) = \varphi_{fr}\left(\frac{a'}{2}\right)$$

and

$$D_{fc}\frac{\partial \varphi_{fc}\left(\frac{a'}{2}\right)}{\partial x} = D_{fr}\frac{\partial \varphi_{fr}\left(\frac{a'}{2}\right)}{\partial x}$$

similarly for thermal fluxes.

For a non-trivial solution of the resulting four equations for the arbitrary constants A, C, F and G, by Cramer's rule the determinant so formed should be equal to zero. Written in full it would be

$$\Delta A = \begin{vmatrix} X & Y & -Z_1 & 0 \\ S_1X & S_2Y & -S_3Z_1' & Z_2 \\ X' & Y' & -p_1Z_1' & 0 \\ S_1X' & S_2Y' & -p_2Z_1' & -p_2Z_2' \end{vmatrix} = 0 \qquad 5.2.15$$

where $p_1 = \frac{D_{FRr}}{D_{FRc}}$; $p_2 = \frac{D_{MRr}}{D_{MRc}}$

$$X = \cos(\mu x)$$

$$Y = \cosh(\nu x) \qquad 5.2.16$$

$$Z_1 = \sinh \kappa_{fr}\left(\frac{a'}{2} + T - x\right)$$

$$Z_2 = \sinh \kappa_{mr}\left(\frac{a'}{2} + T - x\right)$$

The prime indicates the corresponding derivations. All these functions are evaluated at the "Core-Reflector Interface", i.e. $x = \frac{a'}{2}$. To solve the determinant (5.2.15) it becomes easy if the following notation is used.

$$\alpha = \frac{X'}{X} = -\nu \tan(\nu x)$$

$$\beta = \nu \tanh(\nu x) \qquad \gamma = -\kappa_{fr} \coth(\kappa_{fr} T)$$

$$\delta = -\kappa_{mr} \coth(\kappa_{mr} T)$$

$$C_1 = S_1 (p_1 \gamma - \beta)$$

$$C_2 = S_2 (\beta - p_2 \delta)$$

$$C_3 = S_3 p_2 (\delta - r)$$

Then the value of the determinant on expansion can be written

$$\Delta = D_{MRc} D_{FRc} (C_1 + C_2 + C_3)(\alpha - \alpha') \qquad 5.2.17$$

where

$$\alpha' = \frac{C_1 p_2 \delta + C_2 p_1 \gamma + C_3 \beta}{C_1 + C_2 + C_3}$$

The coupling constants S_1 and S_2 have to be modified to take into account the curvature of the neutron-flux distribution in the axial and y-directions, so that in

expressions for S_1 and S_2

$$\mu^2 = \overline{\mu}^2 = 2\sigma^2 - \frac{M_Z^2}{M_R^2}\gamma_{11}^2 \qquad \text{(a)}$$

5.2.18

and $$\nu^2 = \overline{\nu}^2 = \overline{\mu}^2 + \frac{1}{L_{SR}^2} + \frac{1}{L_R^2} \qquad \text{(b)}$$

where μ^2 is any guessed value. Then the expression 5.2.15 is iterated so that $\Delta \approx 0$. In the end having obtained μ and ν, the radial bucklings (guessed values) for the fluxes, it boils down to iterating 5.2.15, details are given in Appendix A-2.5, for improved guesses of μ so that

$$\Delta = 0 \qquad 5.2.19$$

Or at best has the least possible value for the combination of T (reflector thickness) and the equivalent size of the bare critical system ($a' + 2\delta$) where δ is the reflector saving for the reflected core-system under study. The value of μ or $(a + 2\delta)$ which satisfies the condition 5.2.19 is taken as the equivalent size of the bare critical system and the material buckling is calculated so that

$$B_m^2 = 2\left(\frac{\pi}{a+2\delta}\right)^2 - \frac{M_Z^2}{M_R^2}\gamma^2 \qquad 5.2.20$$

and the infinite multiplication constant K_∞ is calculated by the relationship below

$$K_\infty = (1+2\alpha^2 L_R^2 - \gamma^2 L_Z^2)(1+2\alpha^2 L_{SR}^2 - \gamma^2 L_{SZ}^2) \qquad 5.2.21$$

5.? COMPUTATION DETAILS AND RESULTS

The mathematical solutions of the four differential equations 5.2.1-4 have been programmed (Appendix A-2.5) to solve the critical condition in the form of determinant 5.2.15 for given reflector thickness and core size.

It may be mentioned that, having obtained the general solution in the form of equations 5.2.11 (a,b) and 5.2.14(a, b), it is purely a geometrical problem and involves the interplay between the core and the reflector. This is done by making these four equations (last section) to satisfy the condition of equal fluxes and equal currents.

The input constants for the two-group criticality calculations are taken for the core from Tables 3.4.1 and for the reflector from tables in Appendix A-1.2. The results are marked 'A' and 'B' for the same reasons as in section 4.4.1; specifically, the diffusion coefficients D_{mr} and D_{fr} correspond to homogenised graphite volumes but not to the actual volume of the solid graphite, i.e. in case of B,

$$D_{mr} = D_{mg} S_{MR} \frac{V(\text{solid})}{V(\text{lattice})}$$

V(Solid) = volume of the homogenised graphite. The computed results are tabulated in Tables 5.3.1 along with

fast and thermal flux distributions at some representative points, for comparison with experiment for twenty-nine clean core cases. Tables 5.3.2 Also are given the constants A,C,F, etc. in the case of the case PSCF (A-set) to give a general idea about their magnitudes. The flux plots for 5-PSCF cases (100, 64, 36, 16, 4 fuel rods cases) are given in FIGS. 5.3.1. The flux distributions in all other cases are almost identical in shape though different in magnitudes and are therefore omitted. The parameter K_∞ vs. number of fuel rods is also plotted along with the graph of reflector thickness (T) vs. core size and reflector savings, calculated both on one-group theory and two-group theory for the sake of comparison in the case of PSF (PSF (ODD) is also included). The graph giving the material buckling vs. number of fuel rods is omitted, because it is almost identical to the one given in FIG. 4.4.1 except for slight differences in magnitude.

The errors quoted in K_∞ are the same as in Chapter 4 for the reasons given there. The errors in the axial and material buckling are not tabulated here to avoid duplication every so often. The error in the calculation of reflector saving is approximately zero (10^{-6}cm) according to theory so it is not quoted here. In set-B even the error in K_∞ is omitted.

PSCF

TWO-GROUP THEORY RESULTS

CASE	REFLECTOR Thickness	Axial	A Saving	A B_m^2	A K_∞	B Saving	B B_m^2	B K_∞
FUEL	cm	$\times 10^{-4}$ cm^{-2}	cm	$\times 10^{-4}$ cm^{-2}		cm	$\times 10^{-4}$ cm^{-2}	
144	2.52	2.03998	2.52	1.14678	1.073494±.001312	2.52	1.14678	1.073494
100	22.64	2.12208	21.418	1.13880	1.072937±.001340	20.605	1.20428	1.075813
64	43.16	2.41494	34.978	1.23618	1.079333±.001471	33.749	1.34174	1.084467
36	63.48	3.09918	41.779	1.57680	1.101723±.001781	40.436	1.74612	1.109924
16	83.80	4.23475	43.274	2.77337	1.182199±.002719	42.065	3.11924	1.196366
4	104.12	5.57255	40.911	7.58982	1.534773±.006155	40.020	8.98184	1.565434
PSF								
144	2.80	2.11872	2.80	1.05375	1.071119±.001270	2.80	1.05375	1.071119
100	23.12	2.18691	22.246	1.03051	1.069524±.001279	20.884	1.12254	1.074464
64	43.44	2.46890	36.216	1.10569	1.074687±.001376	34.168	1.25879	1.083502
36	63.76	3.15533	46.280	1.38616	1.094058±.001606	41.060	1.62760	1.107967
16	84.08	4.28471	44.840	2.46904	1.170470±.002358	42.832	2.92726	1.194180
4	104.40	5.61681	42.312	6.96290	1.515058±.005368	40.839	8.52563	1.565548

TABLES 5.3.1

PSF(ODD)

REFLECTOR			A			B		
CASE FUEL	Thickness cm	Axial $\times 10^{-4}$ cm^{-2}	Saving cm	B_m^2 $\times 10^{-4}$ cm^{-2}	K_∞	Saving cm	B_m^2 $\times 10^{-4}$ cm^{-2}	K_∞
121	12.96	2.15223	12.798	1.02848	1.068707-.001251	12.066	1.08481	1.071271
81	33.38	2.29946	29.714	1.06250	1.071019±.001334	28.122	1.17437	1.077155
49	53.60	2.39859	40.198	1.38379	1.092972±.001690	38.224	1.56708	1.102966
25	73.92	3.66934	44.182	1.80062	1.121785±.001938	42.243	2.09577	1.137869
9	94.24	4.95502	43.726	4.00676	1.280499±.003552	42.121	4.72514	1.310437
SF								
144	3.20	2.17762	3.20	0.974598	1.083621±.001661	3.20	0.974598	1.083621
100	23.52	2.27313	21.598	0.978194	1.083935±.001788	20.120	1.08049	1.090895
64	43.84	2.47601	36.060	1.10805	1.095325±.002064	33.793	1.28267	1.107904
36	64.16	1.90752	44.832	1.50175	1.130211±.004032	42.312	1.77564	1.149374
16	84.48	3.60388	48.269	2.63886	1.233967±.004032	45.952	3.15874	1.265726
4	104.80	4.43245	47.039	6.44371	1.613474±.007939	45.315	8.03082	1.675585

TABLES 5.3.1

OCF

REFLECTOR A B

CASE FULL	Thickness cm	$\times 10^{-4}$ cm^{-2}	Saving cm	B_B^2 $\times 10^{-4}$ cm^{-2}	K_∞	Saving cm	B_B^2 $\times 10^{-4}$ cm^{-2}	K_∞
144	3.80	2.31736	3.80	0.804838	1.080147±.001594	3.80	0.804838	1.080147
100	24.12	2.38646	20.329	0.905840	1.090415±.001965	20.213	0.959952	1.093821
64	44.44	2.55929	34.690	1.09736	1.110014±.002438	33.944	1.18906	1.116216
36	64.76	2.8937	44.147	1.57053	1.59155 ±.003333	43.088	1.72679	1.68768
16	85.08	3.46799	46.521	2.71961	1.282770±.005131	47.540	3.05016	1.298108
4	105.40	4.12398	48.351	6.33892	1.711727±.009900	47.621	7.57915	1.740749

TABLES 5.3.1

TABLE 5.3.2

A-SET

CONSTANTS FOR CRITICALITY

CASE	A	C	F	G	S_1	S_2	S_3
			PSCF				
100	0.534220	-0.000010	0.079399	9.032287	12.666	-13.747	-15.546
64	0.298007	-0.000079	0.020641	4.126455	12.630	-13.705	"
36	0.226595	-0.000470	0.006420	2.453277	12.506	-13.559	"
16	0.187073	-0.002569	0.002073	1.555528	12.090	-13.071	"
4	0.152418	-0.013758	0.000641	0.933968	10.662	-11.417	"
			PSF				
100	0.499938	-0.000011	0.079312	8.765040	12.340	-13.723	-15.497
64	0.280712	-0.000086	0.021318	4.038422	12.312	-13.688	"
36	0.214247	-0.000497	0.006859	2.421305	12.208	-13.560	"
16	0.177677	-0.002616	0.002292	1.550418	11.824	-13.087	"
4	0.145169	-0.013460	0.007310	0.938491	10.456	-11.432	"
			PSF (ODD)				
121	1.029888	-0.00003	0.212324	19.028858	12.265	-13.805	-15.495
81	0.355637	-0.000032	0.039659	5.636632	12.252	-13.790	"
49	0.243890	-0.000207	0.012080	3.091376	12.136	-13.642	"
25	0.196506	-0.001133	0.003992	1.944491	11.988	-13.456	"
9	0.164065	-0.005944	0.001332	1.241310	11.262	-12.548	"
			SF				
100	0.467285	-0.000016	0.095511	8.833731	10.176	-14.078	-14.923
64	0.250697	-0.000120	0.029184	4.106143	10.132	-13.993	"
36	0.186269	-0.000631	0.011026	2.539899	9.999	-13.742	"
16	0.152728	-0.002960	0.004366	1.697533	9.935	-13.062	"
4	0.123572	-0.013323	0.001622	1.072308	8.587	-11.209	"
			OCF				
100	0.463979	-0.000021	0.102105	8.940216	9.540	-14.015	-14.486
64	0.243782	-0.000157	0.032897	4.187893	9.472	-13.867	"
36	0.177878	-0.000771	0.013263	2.622637	9.306	-13.515	"
16	0.144166	-0.003369	0.005634	1.781821	8.928	-12.731	"
4	0.115163	-0.013961	0.002220	1.136333	7.913	-10.764	"

PSCF

CASE DIST. cm	TWO-GROUP EXPT. FAST	THERMAL	THERMAL
0.0	80.00	1000.00	1000.00±3.16
20.32	77.38	967.28	961.26±3.04
40.64	69.70	871.28	870.28±2.75
60.90	57.46	718.26	720.28±2.28
81.28	41.46	518.25	519.09±1.64
101.60	22.75	284.33	284.96±0.9

PSCF-100

	TWO-GROUP EXPT. FAST	THERMAL	THERMAL
0.0	78.95	1000.00	1000.00±3.16
20.32	76.31	966.53	970.15±3.07
40.64	68.56	868.36	871.68±2.76
60.90	56.22	712.06	721.34±2.28
81.28	40.11	508.09	515.19±1.63
101.60	21.32	270.12	302.51±0.96

PSCF-64

0.0	79.13	1000.00	1000.00±3.16
20.32	76.17	962.57	962.07±3.04
40.64	67.49	853.08	864.13±2.73
60.46	53.76	679.74	708.48±2.24
81.28	36.00	455.55	568.03±1.80
101.60	8.72	354.42	367.24±1.16

PSCF-36

0.0	79.62	1000.00	1000.00±3.16
20.32	75.79	952.34	963.69±3.05
40.64	64.67	813.93	859.67±2.72
60.46	47.32	598.10	800.63±2.53
81.28	11.76	606.41	662.22±2.53
101.60	3.60	330.27	

PSCF-16

0.0	80.39	1000.00	984.86±3.11
20.32	74.48	930.64	979.10±3.09
40.64	57.58	732.80	1000.00±3.16
60.96	14.33	805.83	946.69±2.99
81.28	4.70	546.14	678.56±2.14
101.60	1.44	280.65	361.34±1.14

PSCF-4

0.0	73.41	943.53	870.18±2.75
20.32	61.68	840.81	970.35±3.06
40.64	16.30	908.68	1000.00±3.16
60.96	5.38	666.77	830.37±2.63
81.28	1.77	424.33	584.68±1.85
101.60	0.38	163.87	315.15±1.00

TABLES 5.3.2.

PSF

CASE	TWO-GROUP EXPT.			PSF-100 TWO-GROUP EXPT.		
DIST. cm	FAST	THERMAL	THERMAL	FAST	THERMAL	THERMAL
0.0	82.40	1000.00	1000.00±3.16	81.03	1000.00	1000.00±3.16
20.32	79.72	967.43	968.16±3.06	78.36	966.97	973.42±3.08
40.64	71.84	871.84	872.24±2.76	70.50	870.07	875.47±2.77
60.96	59.29	719.46	721.92±2.23	57.99	715.70	715.72±1.62
81.28	42.87	520.22	514.14±1.63	41.65	514.06	511.81±1.62
101.60	23.66	287.09	274.69±0.87	22.56	278.46	

PSF-64 PSF-36

0.0	81.17	1000.00	1000.00±3.16	81.51	1000.00	1000.00±3.16
20.32	78.19	963.35	975.43±3.08	77.70	953.73	963.01±3.04
40.64	69.47	856.10	867.75±2.74	66.63	819.23	863.39±2.73
60.96	55.66	686.12	713.52±2.26	49.31	609.10	709.46±2.52
81.28	37.75	465.88	571.08±1.80	12.80	621.52	655.32±2.07
101.60	9.53	364.79		4.04	342.44	

PSF-16 PSF-4

0.0	81.99	1000.00	999.43±3.16	74.02	939.62	876.06±2.77
20.32	76.17	933.33	966.57±3.05	62.65	842.69	961.93±3.04
40.64	59.49	742.81	1000.00±3.16	17.32	915.84	1000.00±3.16
60.96	15.49	822.40	948.28±3.00	5.92	679.86	820.12±2.59
81.28	5.25	563.40	673.68±2.13	2.01	437.22	573.52±1.81
101.60	1.66	292.87		0.63	221.56	

TABLES 5.3.2

PSF-121

CASE DIST. cm	TWO-GROUP EXPT. FAST	THERMAL	THERMAL
10.16	80.87	1000.00	1000.00±3.16
30.48	75.58	934.67	940.67±2.97
50.80	63.37	808.35	814.81±2.58
71.12	50.88	629.21	631.87±2.80
91.44	33.07	408.97	410.20±1.30
111.76	13.10	162.04	163.13±0.52

PSF-81

TWO-GROUP EXPT. FAST	THERMAL	THERMAL
80.89	1000.00	1000.00±3.16
75.31	931.00	941.45±2.98
64.53	797.78	810.68±2.56
49.29	609.52	625.64±1.98
30.66	379.22	448.16±1.42
6.71	209.05	211.56±0.67

PSF-49

10.16	81.41	1000.00	1000.00±3.16
30.48	74.75	918.51	921.88±2.91
50.80	61.97	762.19	801.35±2.53
71.12	44.12	543.83	700.25±2.21
91.44	11.43	307.43	330.32±1.68
111.76	3.01	206.62	213.93±0.68

PSF-25

81.23	1000.00	1000.00±3.16
72.03	889.63	929.24±2.94
54.66	681.39	911.34±2.88
14.16	736.94	813.27±2.57
4.72	467.33	523.71±1.66
1.24	180.93	202.98±0.64

PSF-9

10.16	79.32	982.59	921.79±2.92
30.48	63.72	818.33	1000.00±3.16
50.80	16.87	913.94	987.85±3.12
71.12	5.76	657.23	762.78±2.41
91.44	1.92	391.89	478.14±1.51
111.76	0.51	148.06	186.18±0.59

These experimental flux distributions correspond to the line y=10.16 cm away from centre line while theoretical numbers at y=0.

TABLE 5.3.2

SF

CASE	TWO-GROUP EXPT.			SF-100 TWO-GROUP EXPT.		
DIST cm	FAST	THERMAL	THERMAL	FAST	THERMAL	THERMAL
0.0	100.26	1000.00	1000.00±3.16	98.26	1000.00	1000.00±3.16
20.32	97.01	967.64	967.44±3.057	94.98	966.63	967.44±3.06
40.64	87.49	872.64	869.88±2.75	85.36	868.74	869.88±2.75
60.96	72.30	721.17	722.28±2.28	70.04	712.87	722.28±2.28
84.28	52.44	523.01	521.74±1.65	50.05	509.43	521.74±1.65
101.60	29.18	291.01	288.71±0.91	26.71	271.99	313.0±0.91

SF-64 SF-36

0.0	98.59	1000.00	1000.00±3.16	99.21	1000.00	1000.00±3.16
20.32	94.96	963.28	966.75±3.06	94.70	955.25	962.8±3.04
40.64	84.34	855.82	869.63±2.77	81.57	825.08	890.98±2.82
60.96	67.51	685.54	730.14±2.28	60.99	621.38	870.15±2.75
81.28	45.71	464.98	607.06±1.65	19.54	666.29	757.88±2.39
101.60	13.97	373.06	408.48±1.29	7.17	381.63	444.39±1.41

SF-16 SF-4

0.0	99.17	1000.00	912.67±2.84	82.73	908.31	835.23±2.64
20.32	92.60	939.55	912.02±2.88	71.37	833.39	934.02±2.95
40.64	73.68	766.34	1000.00±3.16	24.30	951.69	1000.00±3.16
60.96	23.70	902.24	990.74±3.13	9.98	750.11	846.35±2.68
81.28	9.50	650.16	740.91±2.34	4.04	507.56	608.06±1.92
101.60	3.52	352.15	408.73±1.29	1.48	267.55	333.34±1.05

TABLES 5.3.2

OCF

CASE	TWO-GROUP EXPT.		
DIST. cm	FAST	THERMAL	THERMAL
0.0	107.42	1000.00	1000.00±3.16
20.32	103.97	967.94	964.33±3.05
40.64	93.86	873.83	876.65±2.79
60.96	77.74	732.69	728.73±2.28
81.28	56.63	527.16	522.63±1.65
101.60	31.88	296.82	291.37±0.92

OCF-100

	TWO-GROUP EXPT.		
	FAST	THERMAL	THERMAL
0.0	104.81	1000.00	1000.00±3.16
20.32	101.26	966.21	969.57±3.06
40.64	90.88	867.13	877.28±2.77
60.96	74.35	709.45	721.08±2.28
81.28	52.79	503.84	522.52±1.65
101.60	27.67	264.19	316.22±1.00

OCF-64

0.0	105.41	1000.00	1000.00±3.16
20.32	101.45	962.56	975.85±3.08
40.64	89.87	853.06	870.80±2.75
60.96	71.54	679.73	739.67±2.34
81.28	47.82	455.60	616.82±1.95
101.60	15.81	366.83	419.72±1.33

OCF-36

0.0	106.32	1000.00	1000.00±3.16
20.32	101.41	954.82	969.08±3.06
40.64	87.13	823.47	914.51±2.89
60.96	64.78	618.14	890.89±2.82
81.28	22.55	667.08	792.87±2.51
101.60	8.84	389.57	469.21±1.48

OCF-16

0.0	105.87	1000.00	892.09±2.81
20.32	98.83	940.74	897.77±2.84
40.64	78.57	771.00	995.94±3.15
60.96	27.52	915.16	1000.00±3.16
81.28	12.00	671.88	750.65±2.40
101.60	4.70	372.38	424.28±1.34

OCF-4

0.0	86.31	905.41	940.79±2.97
20.32	74.59	837.06	937.36±2.96
40.64	27.68	958.94	1000.00±3.16
60.96	12.30	772.22	858.64±2.71
81.28	5.36	534.06	616.90±1.95
101.60	2.10	288.21	*

TABLES 5.3.2

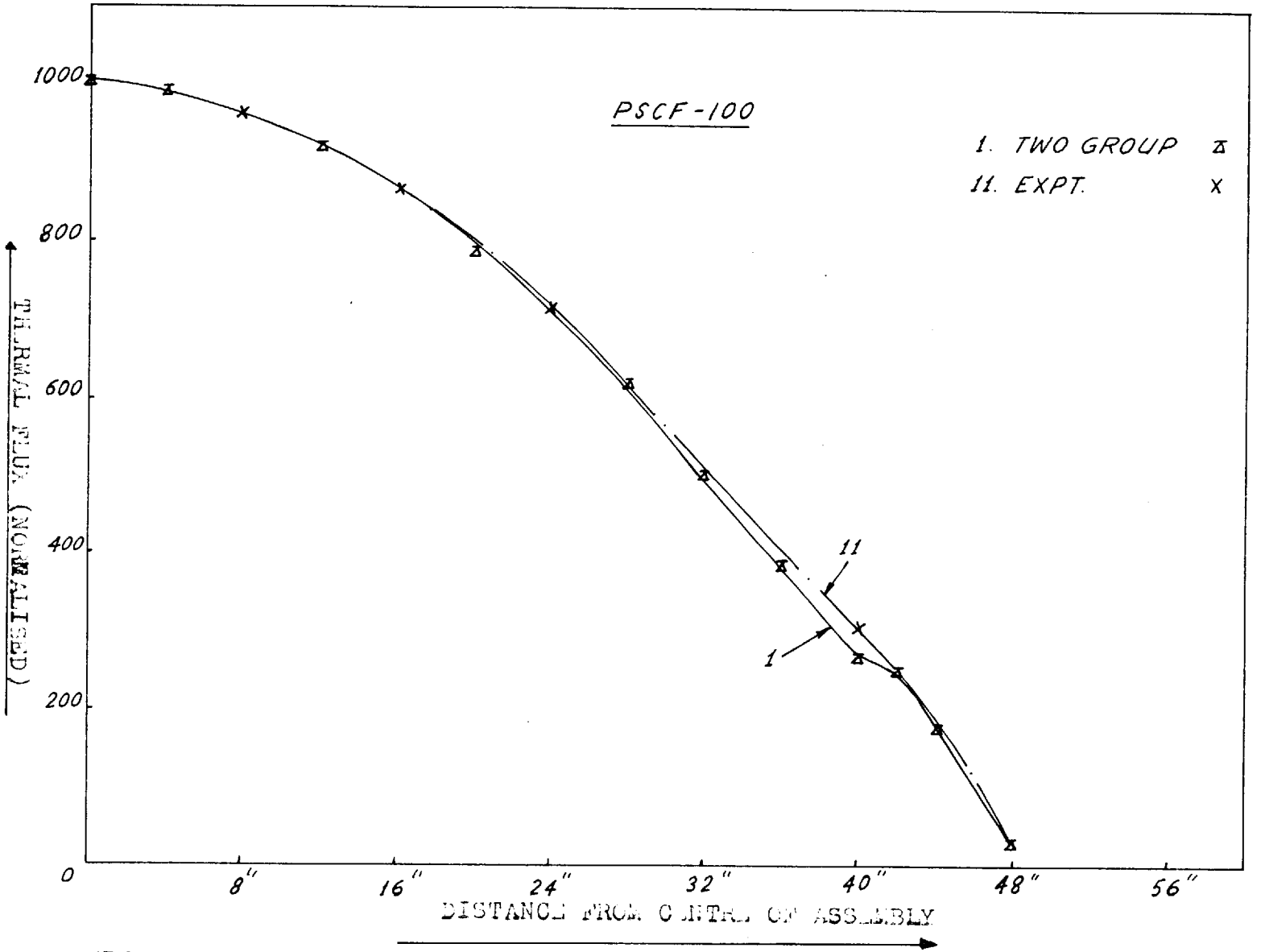

FIG. 5.3.1 EXPERIMENTAL AND THEORETICAL THERMAL FLUX DISTRIBUTIONS ON TWO GROUP THEORY

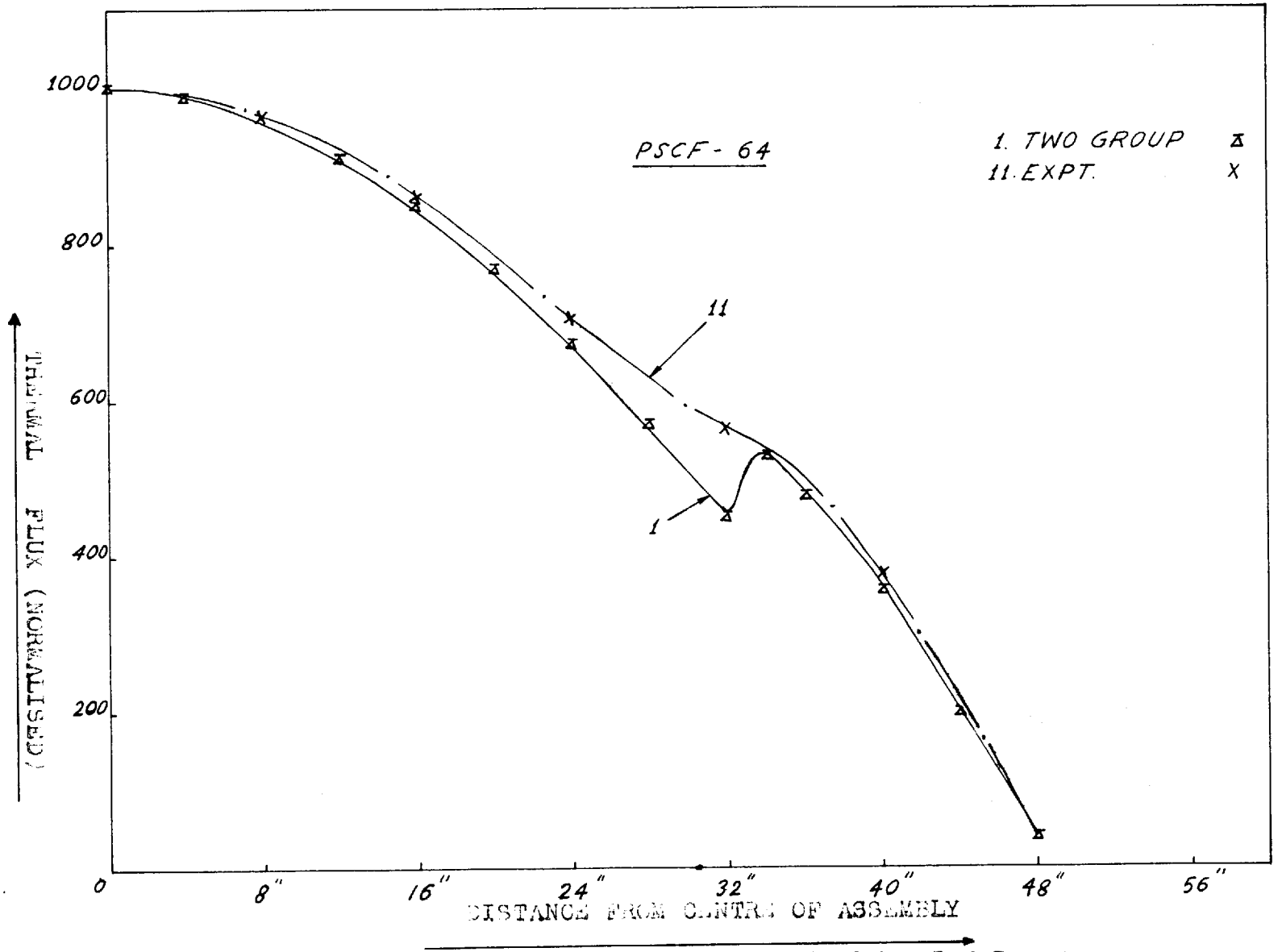

FIG. 3.3.1 EXPERIMENTAL AND THEORETICAL THERMAL FLUX DISTRIBUTIONS ON TWO GROUP THEORY

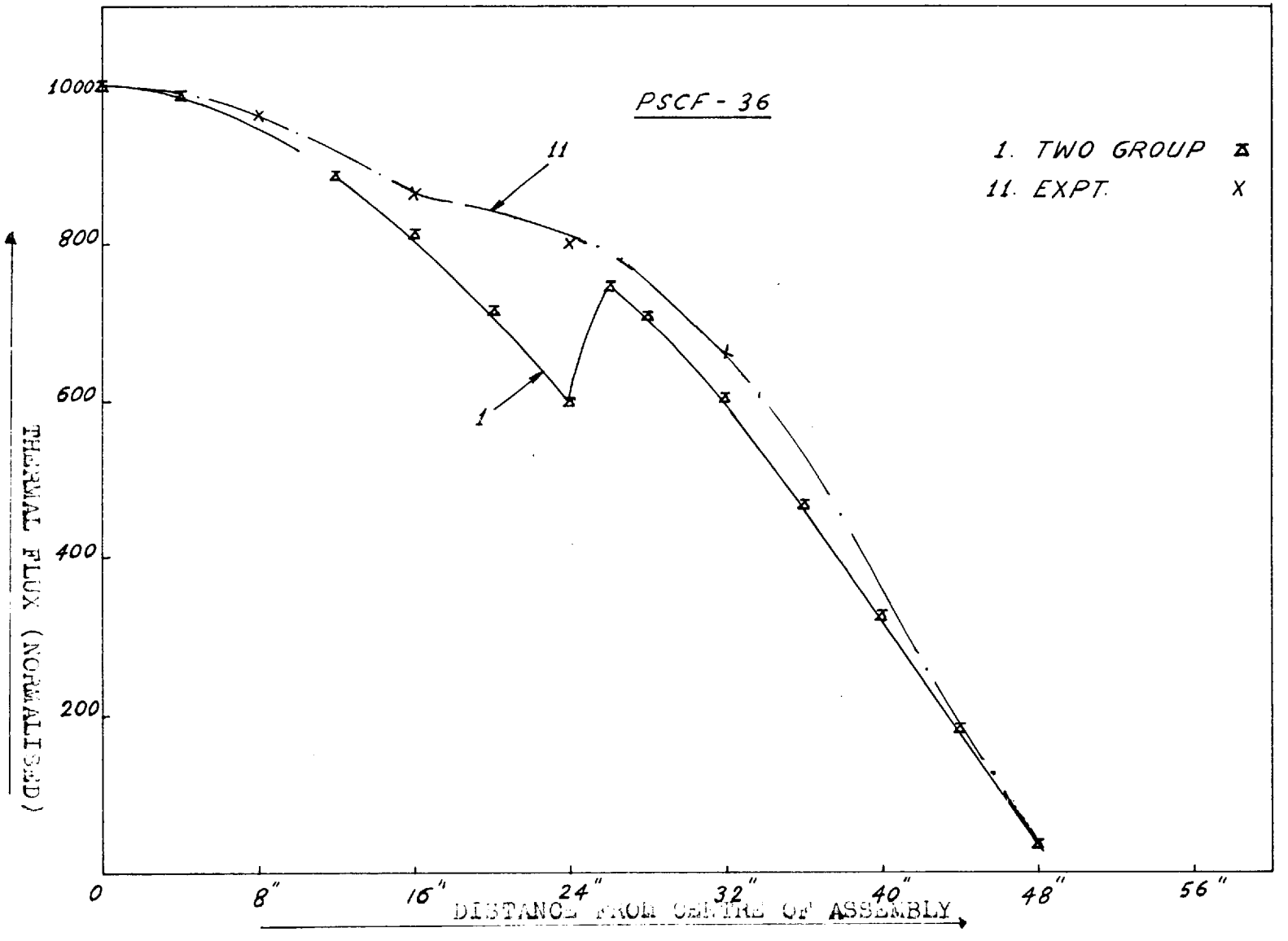

FIG. 5.3.1 EXPERIMENTAL AND THEORETICAL THERMAL FLUX DISTRIBUTIONS ON TWO GROUP THEORY

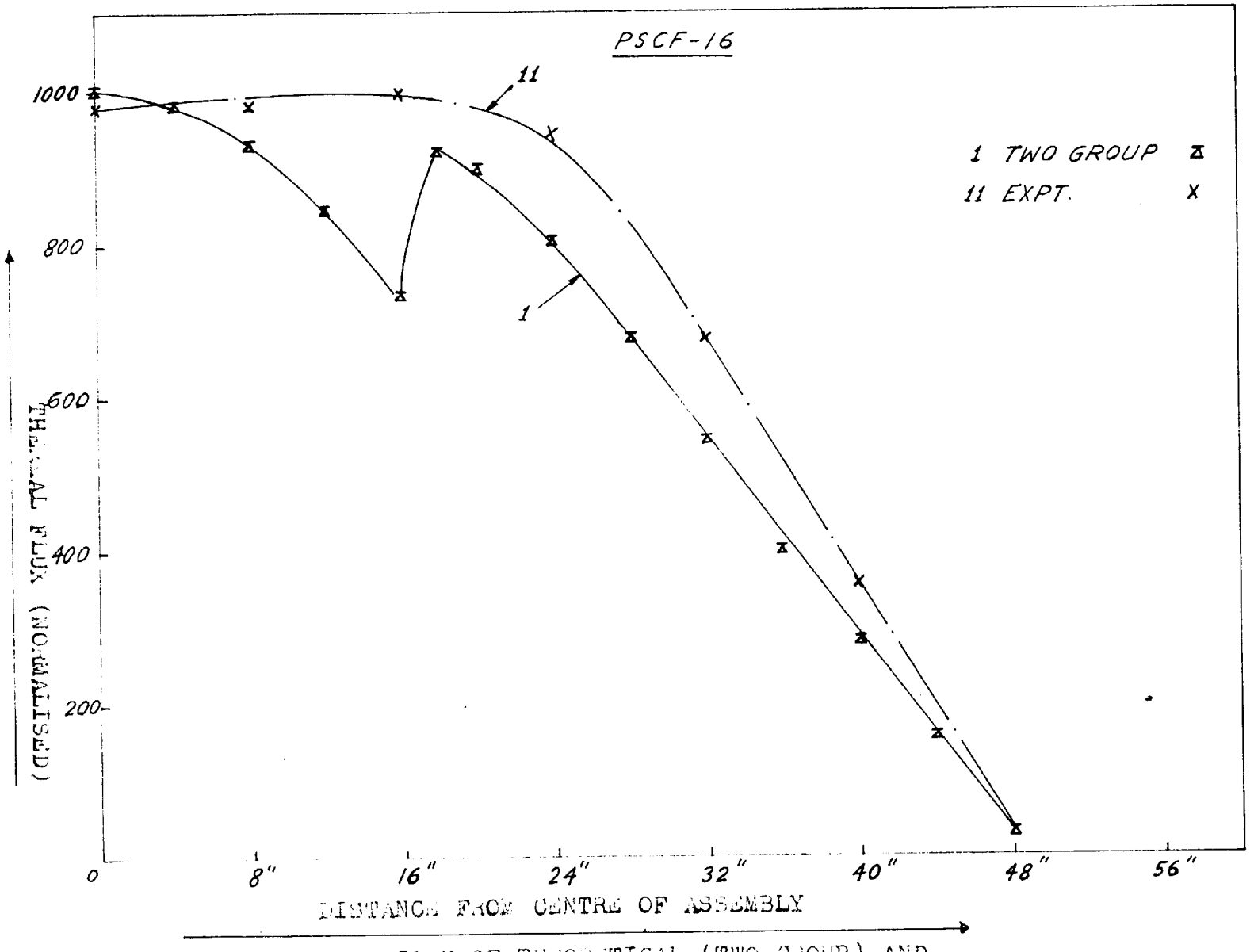

FIG. 5.7.1 COMPARISON OF THEORETICAL (TWO-GROUP) AND EXPERIMENTAL FLUX DISTRIBUTION

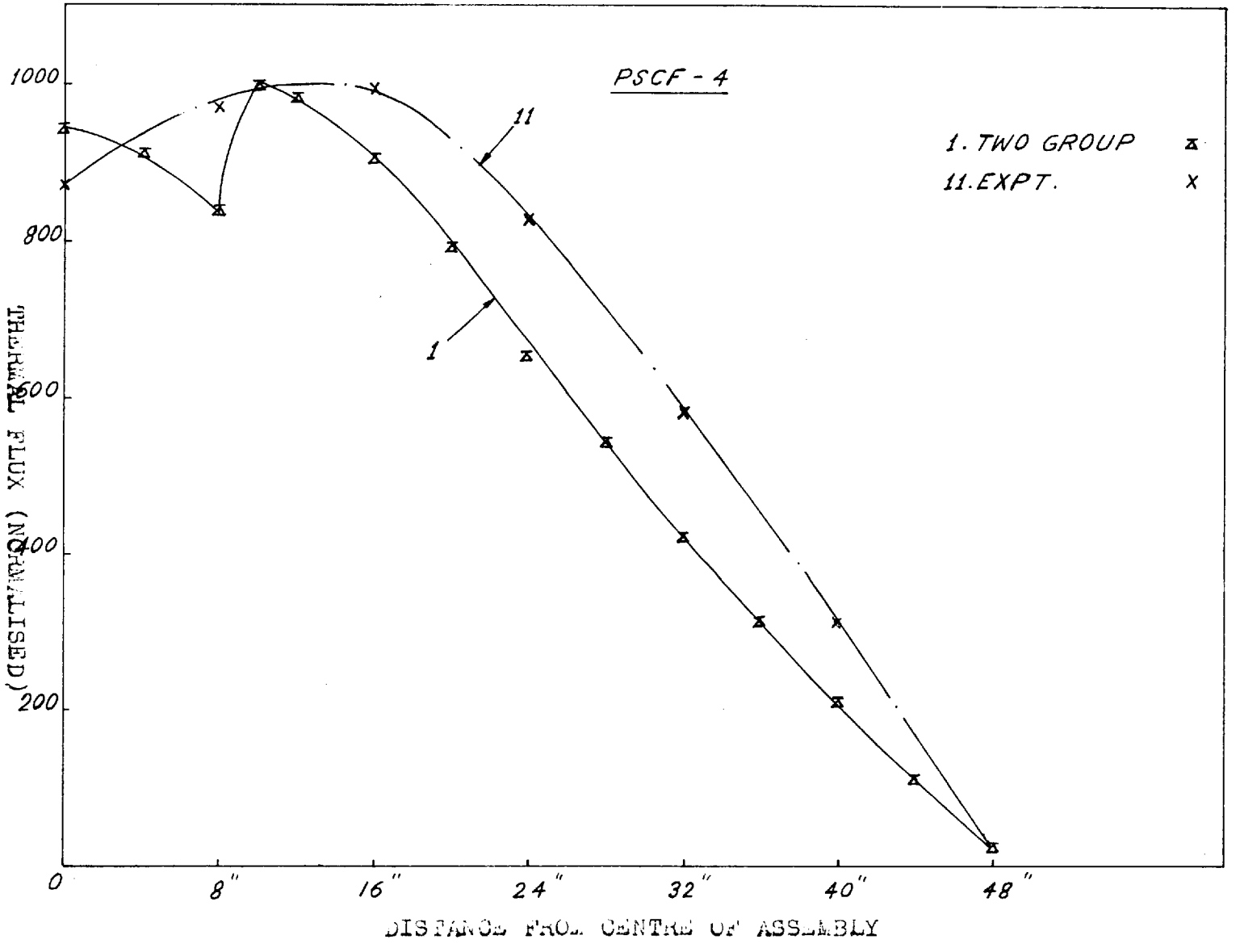

FIG. 5.3.1 EXPERIMENTAL AND THEORETICAL THERMAL FLUX DISTRIBUTIONS ON TWO GROUP THEORY

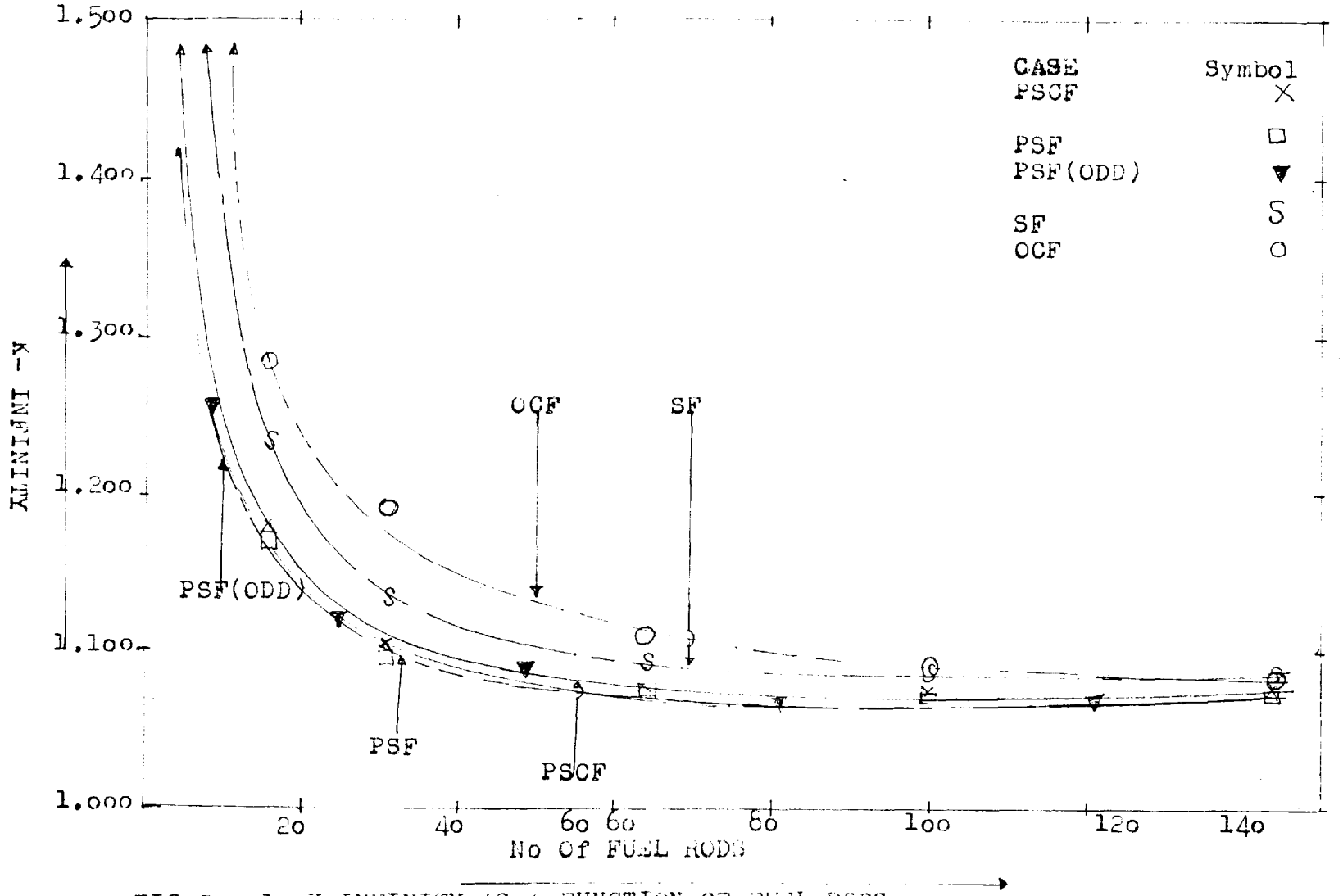

FIG.5.3.1 K-INFINITY AS A FUNCTION OF FUEL RODS

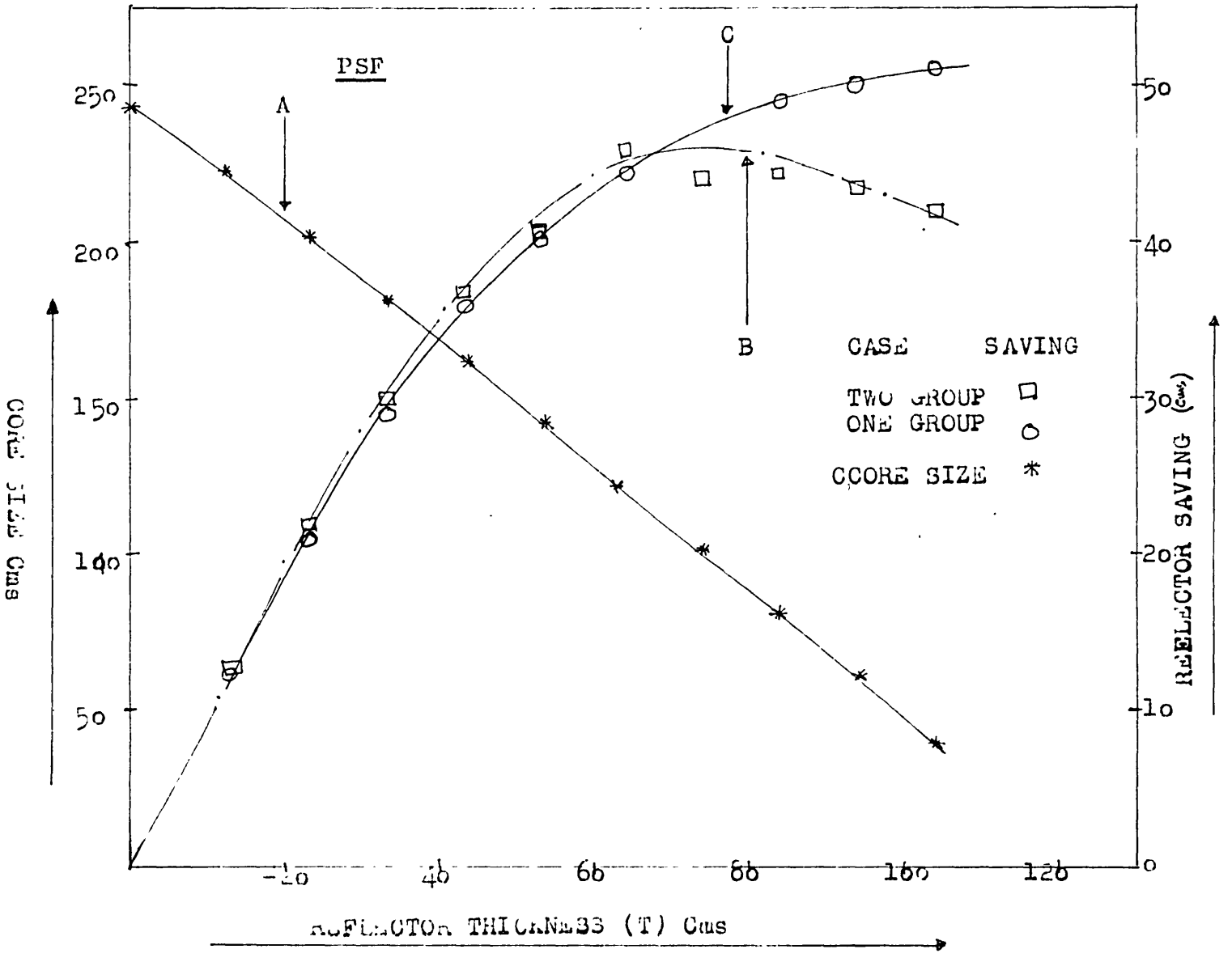

FIG. 3.3.1 REFLECTOR SAVING ON ONE-GROUP(C) AND TWO-GROUP (B) THEORY AND CORE SIZE VS REFLECTOR THICKNESS

5.4 DISCUSSION OF RESULTS

A close examination of the tables and graphs in Chapters 4 and 5 would convince that two-group theory is a distinct improvement over the modified one-group treatment of a reflected core system. Since the behaviour of different (meaning different channel diameters) core cases is almost identical, only representative case of PSCF or PSF would be pointed out.

Let us consider the flux plots first. In FIGS. 4.4.1 it was seen that the thermal flux distribution follows a cosine-distribution in the core defined by α and distribution from the core-reflector interface up to the boundaries of the assembly is given by the hyperbolic sine defined in Chapter 4, i.e. $\sinh (\kappa_r (\frac{a'}{2} + T - x))$. On the basis of one-group theory we neglect all events connected with the slowing down process and the fact that the neutrons are not born thermal. Therefore it does not make anydifference in this regard that the thermal flux distribution in the neighbourhood of the core-region should be affected in some way.

The nuclear properties of the core and the reflector are entirely different. Therefore, the passing of the core region must have some bearing on entering the reflector. Physically we understand that the thermal flux must show

a rise after having passed the core-reflector interface since on approaching the reflector there is no absorption due to the absence of the fuel from the region. The only absorption in the reflector is due to its own absorption which is very small compared to the absorption in the fuel. This is taken account of in the two-group theory. The boundary conditions that neutron fluxes and currents are equal at the interfaces implies that the behaviour of neutrons is passed over from one region to the other. Now, in the core region fast and thermal fluxes are so distributed that they follow the relationship

$$\varphi_{fc} = A \cos(\mu x) + C \cosh(\nu x) \qquad 3.4.1$$

$$\varphi_{mc} = S_1 A \cos(\mu x) + S_2 C \cosh(\nu x) \qquad 3.4.2.$$

The constant S_2C turns out to be positive and is in accordance with the physical interpretation that the term $(S_2C \cosh(\nu x))$ corresponds to the non-asymptotic flux distribution at the core-reflector interface, and consequently has a positive contribution to make to the overall asymptotic flux distribution. However this term should die out in a distance of the order of migration length. This thermal flux rise is, therefore, due to the flow into the core of thermalised neutrons, which leaked out of the core-region as fast neutrons.

Then the thermal flux follows the exponentials defined by equations 5.2.14(a,b) in the reflector.

Further, it may be argued that the thermal flux, according to theory, does not follow the experimental results strictly. About that it might suffice to say that the diffusion theory parameters are defined in a way appropriate to the heterogeneous nature of the lattice (Chapter 3) under the boundary conditions defined in section 3.1; the homogenised parameters are used in the diffusion equations. It should be remembered, however, that the actual lattice system consists of a finite number of lattice cells. The theory assumes that neutron absorption can occur at all points up to the core-reflector interface, while in practice fuel absorption ceases some 10 cms from the approach of the core-reflector interface; therefore the experimentally measured thermal flux is bound to be higher. It is for this reason that the term $S_2C \cosh(\nu x)$ cannot entirely cope with the situation on the theoretical side.

The agreement between theory and experiment is quite clear in the case of 100 fuel elements, less in the case of 64 fuel elements, and starts to deviate seriously for

36 and less number of fuel rods. For these cases the actual theory seems to break down. Because when the number of fuel elements is less than 36 or equal to 36, the core region is more like a cylinder than a "plane slab." It was thought advisable to analyse this region of fuel elements on the basis of an equivalent cylinder. It was left, so that the correlation of theoretical and experimental results should remain consistent.

The value of K_∞ predicted by experiment is quite consistent and is in agreement with theory down to 36 fuel elements in case of PSCF, PSF and PSF (ODD), while in case of SF and OCF it starts to deviate from 64 fuel elements downwards. Then the curve (especially PSCF, PSF cases) bends rather sharply at 36 fuel elements and for 4 fuel elements even the scale needs to be modified and shows the complete breakdown of the concept of unit-cell model and that of the concept of reflector savings as well on the basis of the model adopted here. This sudden rise in K_∞ and therefore material buckling is due to excessive leakage from the system of reference discussed previously in section 4.4.

The last graph, showing the variation of reflector savings as a function of reflector thickness, is very instructive. The curves (C) (reflector saving on the

basis of one-group theory) and B (reflector saving on the basis of two-group theory) show the variation of reflector saving with change of reflector thickness. In case of one-group theory, the curve continues to show a rise (though small comparatively for larger thickness) while in case of two-group theory, the curve starts to show a decrease in the reflector saving, which obviously is not true.

In case of one-group theory we neglect fast neutron events altogether while in two-group theory we take that into consideration as well. The agreement between theory and experiment improves precisely for this reason when the number of fuel elements is greater than 36 but when the size of the core is reduced beyond expectation of the unit-cell model it overestimates the outward leakage as well. This shows the limit to which we can extend the homogenised model and the consideration of reflector savings as the basis for analysis. Also, it tells us that the basic physical changes do not correspond to the theoretical details. In a simple but precise manner we are, therefore, led to the belief that 36 fuel elements is the absolute minimum number one should have to perform any worthwhile exponential experiment in an assembly of the size under study.

CHAPTER 6

ANALYSIS OF THE HETEROGENEOUS REFLECTED REACTOR SYSTEMS ON THE BASIS OF TWO-GROUP HETEROGENEOUS THEORY

6.1 INTRODUCTION

The heterogeneous method of reactor analysis is characterised by its explicit consideration of the individual fuel and/or control rods in the reactor core, as opposed to the usual methods which consider an equivalent homogenised problem. This detailed consideration of the fuel elements with regard to the flux distribution in a reactor is bound to give accuracy in calculating reactivity and power distribution within a core, as a function of the configuration and the characteristics of fuel and or control elements.

It was earlier pointed out in Section 1.4(b) of the first chapter that if the size of the multiplying system is reduced, the unit-cell model cannot predict the criticality of the system with sufficient accuracy. Therefore the detailed arrangement of the fuel elements is an essential feature of the nuclear configuration which must be included in the criticality consideration. In the present work we are faced precisely with this problem. The analytical models used to compute the flux distributions and reactivity of a "square" core surrounded by reflector

of square shape, have been outlined in Chapters 4 and 5 on the basis of homogenised model for one group and two group of neutrons respectively.

At every step in the analysis of such a sytem one has to assume something which actually is not the case. Though in many cases the contributions from the factors under assumption are often very small, yet the argument remains that we study a simplified picture of the system. Since the very first reports by Feinberg and Galanin, the fundamental equations relating the absorption in the fuel rods, thermal diffusion and slowing down kernels have been based on the group diffusion theory and Fermi-Age slowing down kernels for the appropriate geometry of the sources of neutrons. It is only recently that recourse to more than one energy group has been taken. Papers by Jonsson (16) and Aurbach (32) are the latest on the subject. Therefore, it was decided to analyse the present experiments on the basis of two group heterogeneous theory instead of the conventional one group theory in conjunction with the Age theory.

The heterogeneous reactor theory in two-group diffusion approximation defines two basic parameters for the lattice which specify the nuclear characteristics of the fuel elements, namely, γ_{th} (thermal constant) and η (the multiplication constant).

The thermal constant is defined as the number of thermal neutrons absorbed in the fuel element per unit thermal neutron flux on the fuel element surface. Thus $\varphi_m \gamma_h$ is the total number of neutrons absorbed, φ_m being the asymptotic thermal neutron flux defined by the diffusion theory.

The multiplication constant η is defined as the number of neutrons produced per neutron absorbed in the fuel element. Since the fast fission factor ε is not calculated separately, η is actually taken equal to $\varepsilon\eta$ where the value of ε is taken in the present study from Chapter 3 for the cases under study. The value for P, the resonance escape probability, was also taken from the values given in Chapter 3 for each case.

The finite size of the reactor system is characterised by the axial and the radial bucklings. The axial buckling will cause axial leakage in the moderator and streaming in channels and the radial buckling will produce a flux asymmetry around the axis of an eccentric rod, resulting in radial leakage and streaming. A second effect associated with finite systems is the energy dependence of the extrapolation lengths. It may be negligible in case of large reflected systems but in the case of small exponential assemblies the effect may not be negligible for the evaluation of critical bucklings.

The fuel elements are taken as the line neutron sources for fast neutrons and sinks for thermal neutrons.

The theoretical details of the two group diffusion equations are given in Section 6.3 of the present chapter. And the results are given in Section 6.7, the relevant details of computation and input data are given in Section 6.4-5 and in Section 6.6 experimental arrangement for thermal flux measurement at the fuel is described. The discussion of results in the present analysis follows in Section 6.8 of this Chapter.

6.2 CYLINDRICALISATION OF THE SUB-CRITICAL ASSEMBLY

In the heterogenous method, the reactor is regarded as an array of sources embedded in a great lump of moderator so that its heterogenous nature is taken into account explicitly. A reflector, therefore, requires no special treatment in this theory, provided it is made of the same material as the moderator. It is only regarded as a piece of the moderator which does not contain any sources or sinks other than its own absorption properties. From this consideration one can see that a lattice, whether regular or irregular, is of no significance and tends to lose the special importance attached in the homogenised concept of Wigner-Sietz.

To derive definite conclusions from the experimental measurements it was absolutely necessary to have a programme

which would handle the calculations successfully within the desired accuracy, and that it should have been tested separately that the procedure (the very method for solving diffusion equations) adopted does give the right answers.

In this respect the heterogeneous theory is pretty well-known for complications in computing and a slight error in the computing process might lead to absolutely discouraging results. Secondly, computing and programming is only a means to the end and it is not an end in itself. Initially attempts were made to write a programme for the heterogeneous calculations in autocode for the London University Atlas computer, for the square assembly, but it was not very successful. In the process a programme for IBM-7044 computer by Näslund (21) of Swedish Atomenergi became available and an IBM-7090 computer facility became available at the College as well.

Though Näslund had not done much computing with the programme for exponential cases, Näslund and Jonsson (16) had done quite complicated calculations for the criticality and power distribution in a heavy water moderated reactor core. They were perfectly satisfied with the numerical method(A-3.2) used for the purpose. Therefore the programme was made suitable to run on the IBM-7090 and it was decided to forego the explicit shape of the square sub-critical assembly in favour of an

equivalent cylinder. A few initial runs seemed to give very promising results and the change to cylindricalisation of the square sub-critical assembly did not affect the result as such. Thus it was decided to treat the sub-critical assembly as an equivalent cylinder and proceed with the analysis of the experiments.

An additional advantage of this choice was that infinite sums of cosines and sines could be avoided in favour of Bessel's functions which are much faster converging functions than the cosines or sines. Consequently there is much less comparative truncation error. The equivalent radius of the sub-critical assembly was taken equivalent to the buckling of the system corresponding to the extrapolated boundary of the assembly as given below.

CASE	a cms.	R cms.
PSCF	248.88	134.7143
PSF	249.44	135.0158
SF	250.24	135.4488
OCF	251.44	136.0984

The extrapolation lengths in the radial direction are given in Section 2.5.1 of Chapter 2. In some preliminary runs the radius equivalent to cross-sectional area was tried but it underestimated the leakage and therefore it was not tried any further.

In the succeeding sections there are the theoretical and computing details with the results obtained.

6.3.1 HETEROGENEOUS TWO-GROUP THEORY FOR A FINITE CYLINDRICAL REACTOR

Two group diffusion theory will be used to describe the neutron-balance in a reactor system as regards the absorption, leakage and reproduction in a steady-state. The basis of the heterogeneous method is an analytical solution of the diffusion equation assumed to hold in the moderator. The solution is subject to boundary conditions on the moderator surface i.e. the fuel-moderator interface. The basic assumptions are given below:

i) The problem is a two-dimensional one. This is achieved by assuming that the solution of the diffusion equation in three dimensions for the neutron balance can be separated into two functions; one describing the flux distribution in z-direction and the second in r,φ plane, that is

$$\varphi(\bar{r},z) = \varphi(\bar{r})\ Z(z) \qquad 6.3.1$$

where $\bar{r}$ is a plane-polar vector with components $\bar{r}$ and φ. In the case of the sub-critical assembly, the axial flux distribution is well-known to be

$$Z(z) = \sum_{m,n=1,3\ ..} \sum A_{mn}\ \frac{\sinh\ (c-z)\gamma_{mn}}{\sinh(\gamma_{mn}c)}$$

The harmonics have been included in this equation more to distinguish that this is the inverse relaxation length and is not to be confused with $\bar{r}$. which is a plane-polar vector and also to make it distinct from the thermal constant γ_n or γ_h.

ii) The fuel rods are line sources of fast neutrons and line sinks of thermal neutrons. The number of fast neutrons emitted by the fuel element for every thermal neutron absorbed is η. This assumption implies that the neutron-flux in the vicinity of a fuel rod possesses axial symmetry and is true if the distance between fuel elements is much larger than their dimension.

iii) The number of thermal neutrons absorbed by the fuel element is proportional to the flux at its surface. The constant of proportionality, i.e. the thermal constant γ_h is assumed to depend only on the nature of the fuel and the moderator.

iv) The reflector which may have a finite size must have the same physical properties as the moderator, i.e. there cannot be two types of moderators, one inside the core and the other one acting as a reflector outside. The restriction of an infinite reflector is removed by working with finite Fourier-Bessel Transforms when solving the diffusion equation in the moderator.

(v) Two-Group Theory is valid for the neutron flux in the moderator at least at some distance from the fuel elements.

6.3.2 DERIVATION OF THE CRITICAL CONDITION AND THE FLUX DISTRIBUTION

The two-group diffusion equations for the neutron balance in the system can be written for the fast group

$$\nabla^2\varphi_1(\bar{r},z) - \frac{1}{\tau_m}\varphi_1(\bar{r},z) + \frac{1}{D_{mf}} \sum_{n=1}^{N} \eta_n \gamma_n \varphi_{2n}(\bar{r},z)\delta(\bar{r}-\bar{r}_n) = 0 \qquad 6.3.2$$

and for the thermal flux

$$\nabla^2\varphi_2(\bar{r},z) - \frac{1}{L_m^2}\varphi_2(\bar{r},z) + \frac{D_{mf}}{D_{ms}\tau_m} \sum_{n=1}^{N} \varphi_{1n}(\bar{r},z) - \frac{1}{D_{ms}} \sum_{n=1}^{N} \gamma_n \varphi_{2n}(\bar{r},z)\delta(\bar{r}-\bar{r}_n) = 0 \qquad 6.3.3$$

n refers to the parameters of the nth fuel element. φ_{1n} and φ_{2n} are the fast and the thermal fluxes at nth fuel element.

Fast absorption in the fuel elements is neglected but a correction can be applied by the age in the actual lattice instead of τ_m. In principle the fast absorptions in the rods should be accounted for by a delta function sink term similar to the last term in equation (6.3.2) which gives the source of fast neutrons as a sum of con-

tributions of all fuel elements in the reactor. $\eta_n i_{2n}$ is the number of fast neutrons emitted by fuel element number n with position vector $\bar{r}_n$. $\gamma_n \varphi_{2n} = i_{2n}$ is the number of thermal neutrons absorbed by the nth rod, φ_{2n} being the thermal flux at its surface. It is to be pointed out that φ_{2n} is not the real (measured) flux but is the asymptotic flux given by diffusion theory and therefore the thermal constant γ_n should be calculated to give the true number of neutrons absorbed when combined with this flux. It will be discussed in Section 6.4 of the present chapter.

Substituting equation 6.3.1 in equations 6.3.2 and 6.3.3 we can write

$$\nabla^2 \varphi_1(\bar{r}) - \frac{1}{\tau} \varphi_1(\bar{r}) + \frac{1}{D_{mf}} \sum_{n=1}^{N} \eta_n \gamma_n \varphi_{2n}(\bar{r}) \delta(\bar{r}-\bar{r}_n) = 0 \qquad 6.3.4$$

and

$$\nabla^2 \varphi_2(\bar{r}) - \frac{1}{L^2} \varphi_2(\bar{r}) + \frac{D_{mf}}{\tau_m D_{ms}} \sum_{n=1}^{N} \varphi_{1n}(\bar{r}) -$$

$$- \frac{1}{D_{ms}} \sum_{n=1}^{N} \gamma_n \varphi_{2n}(\bar{r}) \delta(\bar{r}-\bar{r}_n) = 0 \qquad 6.3.5$$

where

$$\frac{1}{\tau} = \frac{1}{\tau_m} - \left(\frac{M_z^2}{M_R^2}\right) \gamma_{11}^2$$

and

$$\frac{1}{L^2} = \frac{1}{L_m^2} - \varsigma \gamma_{11}^2$$

Proper account will be taken of the cases when $\frac{1}{L_m^2} < \varsigma\gamma_{11}^2$ as described at the end of the present section.

To solve the equations 6.3.4 and 6.3.5 we first consider the solution for the fast group in the form of a Fourier series of the type

$$\varphi_1(\bar{r}) = \sum_{m=-\infty}^{+\infty} \varphi_{m1}(r)\, e^{im\varphi} \qquad 6.3.6$$

If we make this substitution in equation (6.3.4) it splits into an infinite number of equations for the Fourier components $\varphi_{m1}(r)$ subject to the boundary condition that the fast flux vanishes at the extrapolated boundary of the reactor, i.e.

$\varphi_1(R) = 0$, the equation 6.3.4 can then be written

$$\frac{1}{r}\frac{d}{dr}\left(r\frac{d\varphi_{1m}(r)}{dr}\right) - \frac{m^2}{r^2}\varphi_{1m}(r) - \frac{1}{\tau}\varphi_{1m}(r) + \frac{1}{2\pi D_{mf}} \sum_{n=1}^{N} \eta_n \gamma_n \varphi_n \int_0^{2\pi} \delta(\bar{r}-\bar{r}_n) e^{-im\varphi'}\, d\varphi' = 0 \qquad 6.3.7$$

If the finite Fourier-Bessel transform of the fast flux $\varphi_{1m}(x)$ in the interval (o,R) is defined to be (18)

$$\phi_\mu(\xi_i) = \int_o^R x\, \varphi_{1m}(x)\, J_\mu(x\,\xi_i)\, dx \qquad 6.3.8$$

where ξ_i is a root of the transcendental equation

$$J_\mu(R\,\xi_i) = 0 \qquad 6.3.9$$

Then at any point of (o,R) at which the function $\varphi_{1m}(x)$ is continuous

$$\varphi_{1m}(x) = \frac{2}{R^2} \sum_{i=1}^{\infty} \oint_{\mu}(\xi_i) \frac{J_\mu(x\,\xi_i)}{|J'_\mu(R\xi_i)|^2} \qquad 6.3.10$$

where the sum is taken over all the positive roots of equation (6.3.9). It may be mentioned that this is a limiting case of the m e general finite Hankel Transform. $\oint_{\mu}(\xi_i)$ (19) defined as

$$f(\xi_i) = \int_0^a x\, f(x)\, J_\mu(x\,\xi_i)\, dx \qquad 6.3.11$$

in which ξ_i is a root of the transcendental equation

$$\xi_i\, J'_\mu(\xi_i a) + H\, J_\mu(\xi_i\, a) = 0 \qquad 6.3.12$$

then at any point of the interval at which f(x) is continuous

$$f(x) = \frac{2}{a^2} \sum_{i=1}^{\infty}{}' \frac{\xi_i^{\,2} f_\mu(\xi_i)}{\pi^2 (\xi_i^{\,2} - \frac{\mu^2}{a^2})} \cdot \frac{J_\mu(x\,\xi_i)}{|J_\mu(a\xi_i)|^2} \qquad 6.3.13$$

where the sum is taken over all the positive roots of the equation (6.3.12). Following Jonsson (16, 17) the solution of equation (6.3.4) can be written as

$$\varphi_1(\bar{r}) = \frac{1}{2\pi D_{mf}} \sum_{n=1}^{N} \eta_n \gamma_n \varphi_{2n}(r_n) \left\{ K_o \left(\frac{|\bar{r}-\bar{r}_n|}{\sqrt{\tau}} \right) - \right.$$

$$\left. - \sum_{m=-\infty}^{\infty} e^{im(\varphi-\varphi_o)} I_m\left(\frac{r}{\sqrt{\tau}}\right) I_m\left(\frac{r_n}{\sqrt{\tau}}\right) \frac{K_m\left(\frac{R}{\sqrt{\tau}}\right)}{I_m\left(\frac{R}{\sqrt{\tau}}\right)} \right\} \quad 6.3.14$$

$\varphi_{2n}(r_n)$ is the thermal flux at the nth fuel element.

To solve the equation (6.3.5) for the thermal flux and the criticality condition, the fast flux $\varphi_{1n}(\bar{r})$ from the nth rod is substituted in equation (6.3.5), so that

$$\varphi_1(\bar{r}) = \sum_{n=1}^{N} \varphi_{1n}(\bar{r})$$

The ultimate solution of equation (6.3.5) will be

$$\varphi_2(\bar{r}) = \sum_{n=1}^{N} \gamma_n \varphi_n(\bar{r}_n) \left\{ \eta'_n F_n(\bar{r}, L, \tau) - f_n(\bar{r}, L) \right\} \quad 6.3.15$$

where $\eta'_n = \eta_n(P \frac{\tau}{\tau_m})$

$$f_n(\bar{r}, L) = \frac{1}{2\pi D_{ms}} \left\{ K_o\left(\frac{|\bar{r}-\bar{r}_n|}{L}\right) - \sum_{m=-\infty}^{\infty} e^{im(\varphi-\varphi_n)} \right.$$

$$\left. I_m\left(\frac{r}{L}\right) I_m\left(\frac{r_n}{L}\right) \frac{K_m\left(\frac{R}{L}\right)}{I_m\left(\frac{R}{L}\right)} \right\} \quad 6.3.16$$

and

$$F_n(\bar{r}, L, \tau) = \frac{1}{1-\frac{\tau}{L^2}} \left\{ f_n(\bar{r}, L) - \frac{D_{mf}}{D_{ms}} f_n(\bar{r}, \tau) \right\} \quad 6.3.17$$

The thermal sink and the fission to thermal source kernels, namely $f_n(\bar{r},L)$ and $F_n(\bar{r},L,\tau)$ are so normalised that they have unit thermal moderator absorption in an infinite moderator.

The equation (6.3.15) gives the criticality condition when $r = r_K$ (it is co-ordinate not γ_n) where K = 1, 2, ...N, resulting in N linear homogeneous equations for the unknown fluxes $\varphi_K(r_K)$. The Cramer's rule of vanishing determinant gives the critical parameter η_n (Eigenvalue) for the critical system. The corresponding Eigenvector will give the number of thermal absorption in the fuel elements, when multiplied by γ_n (the thermal constant).

When $\overrightarrow{r \to r_n}$, the diffusion kernel $f_n(r,L)$ is replaced so that $\bar{r}-\bar{r}_n = a_n$ and

$$f_n(\bar{r},L) = \frac{1}{2\pi D} K_o\left(\frac{a_n}{L}\right) \qquad 6.3.18$$

where a_n is the radius of the fuel element n.

In case of $\frac{1}{L^2}$ in equation (6.3.5) becoming imaginary the Bessel functions K and I (modified) change according to

$$I_n(z) = i^{-n} J_n(i\,z) \qquad (a) \qquad 6.3.19$$

$$Y_n(ix) = i^n \left(i\, I_n(x) - \frac{2}{\pi}(-1)^n K_n(x)\right) \qquad (b) \qquad 6.3.19$$

in particular for n = 0

$$I_o(x) = J_o(i\,x) \qquad (a) \qquad 6.3.20$$

and

$$Y_o(ix) = i\, I_o(x) - \frac{2}{\pi} K_o(x) \qquad (b) \quad 6.3.20$$

Otherwise the essential form of the Bessel function remains the same, or one could start with the new equation and get the solution on the same lines.

The general solution of the equations 6.3.2 and 6.3.3 has been programmed by Näslund (21) both for the case of 3-dimensional and two-dimensional heterogeneous systems. The programmatical details regarding input, output and the method of calculations has been discussed in detail in Appendix III. Originally the programme has been written and used for the computer IBM-7044. This was made suitable for use on the College computer IBM-7090. Details of the results obtained are given in Section 6.7 of the present chapter.

6.4.1 THERMAL CONSTANT (γ_h)

As referred to earlier in Section 6.3 the neutron flux is the same at every point on the surface of the fuel element. In case of cylindrical fuel elements it implies that the flux is independent of the azimuthal angle. Since the neutron current into the fuel element is proportional to the neutron flux on its surface, the constant of proportionality, i.e. the thermal constant, can be defined as

γ_n = ratio of total net current of thermal neutrons into the fuel element to the value of the thermal flux at the surface 6.4.1

If $J(\mathbf{r}_K)$ is the net current of thermal neutrons at the surface of the rod at $\mathbf{r}_K$ (the direction of neutron current is taken as positive when directed outward), then

$$\gamma_n = - \frac{2\pi\, a_o\, J(\mathbf{r}_K)}{\varphi(\mathbf{r}_K)} \qquad 6.4.2$$

where $\varphi(\mathbf{r}_K)$ is the thermal flux at the surface of the fuel element of radius a_o. Note that this expression is for unit length of rod.

The thermal constant can be calculated with varying degrees of accuracy, based on diffusion theory to one based on the transport theory formulation. The calculation is simple on the basis of diffusion theory and since all along diffusion theory has been supposed to be valid, therefore it was thought reasonable to calculate γ_n by the diffusion theory. The calculation uses the unit-cell concept as described in Chapter 3. By applying the continuity conditions for both the net current and the flux at the surface of the fuel rod, it is necessary to consider only the flux distribution on the inside of the fuel element. This is given by the differential equation (3.2.2) and the solution to this equation in cylindrical coordinates is given by (3.2.4), namely

$$\varphi_u(a_o) = A\, I_o(\kappa_u a_o) \qquad 6.4.3$$

where the requirement, that the neutron flux is finite at the centre, has been applied. The net current is

$$J(a_o) = -D_u \varphi_u'(a_o) = -AD_u \kappa_u I_1(\kappa_u a_o) \qquad 6.4.4$$

Substitution of (6.4.3) and (6.4.4) into (6.4.2) gives

$$\gamma_n = \frac{2\pi a_o \Sigma_a^u}{u} \cdot \frac{1}{I_o(\kappa_u a_o)} \qquad 6.4.5$$

if we put $G = \frac{\kappa_u a_o}{2} \cdot \frac{I_1(\kappa_u a_o)}{I_o(\kappa_u a_o)}$ = Disadvantage factor

then

$$\gamma_n = \frac{\pi a_o^2 \Sigma_a^u}{G} \qquad 6.4.6$$

where we can use G and Σ_a^u from Chapter 3 already calculated and the thermal constant used in the calculations is 1.564,639.

6.4.2 THERMAL MULTIPLICATION CONSTANT (η)

The value of η_5 calculated in Chapter 3 cannot be used directly in the present calculation since η_5 does not correspond to the natural uranium. The value of η, however, was derived from η_5 as below.

By definition

$$\eta_{nat.} = \nu \frac{\Sigma_{5f}}{\Sigma_{5a} + \Sigma_{80}} \qquad 6.4.7$$

or
$$\eta_{nat.} = \nu \frac{\Sigma_{5f}}{\Sigma_{5a}} \cdot \frac{1}{1 + \frac{\Sigma_{80}}{\Sigma_{50}}} \qquad 6.4.8$$

$$\eta_5 = \left(\frac{\nu \Sigma_{5f}}{\Sigma_{5a}} \right)$$

$$\Sigma_{5a} = N_5 \sigma_{50} (g_{a5} + r s_{a5})$$

$$\Sigma_{80} = N_8 \sigma_{80}$$

$$r = \frac{\beta'_u/b}{1+\beta'_u} \quad \text{because} \quad \lambda = \beta'_u/b$$

and $b = 1.345$

0 refers to the cross-sections at thermal energy of neutrons.

The value of η_5 and β'_u have been calculated in Chapter 3 and they have been directly used here to calculate the value of $\eta_{natural}$ and they are tabulated here for various cases. The value of η being used in the present context is $(\eta \epsilon)_{nat.}$ since the fast fission factor is not calculated in the heterogeneous method of calculations. The value of p, the resonance escape probability, was directly taken from Chapter 3 for each lattice.

TABLE 6.4.1

CASE	β_u	η_5	$\eta_{nat.}$	$\eta = \varepsilon\eta$
PSCF	0.10087	2.02040	1.290531	1.327840
PSF	0.10328	2.02011	1.290359	1.327805
PSFD	0.10334	2.02011	1.290359	1.327805
SF	0.11692	2.01849	1.289394	1.327612
OCF	0.12292	2.01779	1.288978	1.327531
PSCF 128 VAC 16	0.09051	2.02167	1.291287	1.328024
PSFD 128 VAC 16	0.09274	2.02140	1.291127	1.327988
SF 128 VAC 16	0.10508	2.01990	1.290234	1.327780
PSCF 108 VAC 36	0.07730	2.02333	1.292276	1.328292

INPUT CONSTANTS

6.5.1 CALCULATION OF DIFFUSION COEFFICIENTS AND CHARACTERISTIC AREAS

(a) THERMAL DIFFUSION COEFFICIENT AND DIFFUSION AREA FOR THE MODERATOR

In the present case the evaluation of the diffusion coefficients and diffusion area for the moderator does not present any special problem which it does in case of homogeneous model. Unless otherwise stated,

from Syrett's method for thermal neutrons

$$\frac{1}{L_g} = \kappa_g = .00933 \; S_g \sqrt{\sigma_g} \qquad 6.5.1$$

σ_g in millibarns

and $$D_{mg} = L_g^2 \Sigma_{ag} = \frac{0.951}{S_g} \qquad 6.5.2$$

and the values in the radial direction are corrected for streaming

$$D_{MR} = D_{mg} S_{MR} \frac{v(\text{solids})}{v(\text{lattice})} \qquad 6.5.3$$

$$L_R^2 = L_g^2 S_{MR} \qquad 6.5.4$$

(b) SLOWING DOWN AREA AND DIFFUSION COEFFICIENT FOR FAST NEUTRONS IN THE MODERATOR

The slowing down area uncorrected for streaming for the moderator is calculated by the expression

$$L_{sg}^2 = \frac{363.9 - 84.6 \; (P + \Delta P)}{S_g^2}$$

where $(P + P)$ is the value for the core and is equal to 0.407 and

$$L_{sg}^2 = \frac{329.468}{S_g^2} \qquad 6.5.5$$

The fast diffusion coefficient D_{Fg} is given by

$$D_{Fg} = \frac{(\lambda_{tr})}{3} \cdot \frac{\tilde{v}_e}{v_o}$$

$$\lambda_{tr} = \text{transport mean free path}$$

$$= 2.72/S_g \qquad 6.5.6$$

and

$$\frac{\tilde{v}_e}{v_o} = \mu^{\frac{1}{2}} \frac{v_T}{v_o} \ln \left[\frac{v(2\ \text{Mev})}{\mu^{\frac{1}{2}} v_T} \right] \qquad 6.5.7$$

at room temperature $T = 293.4^{o}K$

$$\frac{\tilde{v}_e}{v_o} = 14.385 \text{ and } \mu = 2.813$$

They are corrected for streaming in the same way as for thermal neutrons i.e.

$$D_{FR} = D_{Fg}\ S_{FR}\ \frac{v\ (\text{solids})}{v\ (\text{lattice})} \cdot \qquad (a) \qquad 6.5.8$$

$$L_{SR}^2 = L_{sg}^2\ S_{FR} \qquad (b) \qquad 6.5.8$$

The unknown quantity S_g, other than the streaming factors corresponds to graphite homogenised up to the can surface in each case. However, it may be remarked that the problem of heterogeneity is the two region "One". Since the core

has got fuel rods embedded in it and, therefore, the basic characteristic parameters do change to some extent. Because of this consideration and those due to the large channels leading to the inaccuracy in the calculation of characteristic areas, eight different sets of data were used to predict the computed results. These are detailed in Section 6.7 and discussed.

6.5.2 STREAMING FACTORS

Basically the method of analysis does not make any distinction between an infinite moderator or infinite moderator embedded with fuel elements distributed in any manner. The distinction between the fuel region and the moderator region is made by the fact that in the fuel region there is source of fast neutrons and additional sinks because of excessive absorption of neutrons by the fuel. The analysis is carried out under the appropriate boundary conditions at the fuel-moderator interfaces. Now, therefore, the problem becomes specially complicated in case of graphite-moderated systems by the fact that taking out the fuel element from the body of the moderator creates vacancies. There are two choices either (a) to fill the vacancies, or (b) leave them as they are and apply streaming corrections. In case of water-mod. systems there is no problem because there does not exist any streaming due to the large channels. In the first

by filling the vacancies we deliberately change the properties of the moderator, which is evidently an unwanted situation since in the analysis it is assumed that the moderator and the reflector are the same While in the second case we can try to correct the constants by the streaming factors. The following two types of corrections were applied.

1) On the basis of Syrett's model.

The streaming factors were taken direct from Chapter 3 for the core and the volume of solid was taken equal to the solid graphite volume plus fuel and can volumes.

2 Streaming factors due to Leslie.

A fuel rod inserted into the moderator in the heterogeneous theory is regarded as defining a surface on which appropriate boundary conditions have to be satisfied. In the present case only radial streaming will be considered because axial streaming is a single-cell problem. Leslie (15) has calculated the radial streaming by the introduction of dipoles as well as sources at the lattice points and derives an expression for the radial streaming factor given below

$$S_r = \frac{1 + \beta w'}{(1-w')(1 - \beta w')} + O(w'^3) \qquad 6.5.9$$

where $w' = \frac{\pi a_0^2}{p^2}$, p is the pitch of the lattice,

a_o is the radius of the hole

and

$$\beta = \tfrac{1}{2}\left[1 + \frac{a_o}{a_o + \ell}\right] \qquad 6.3.10$$

This definition of β is due to Carter and Javis (33).

Galanin and Kuckorov (34) have deduced an equivalent result by the same method and thus the expression (6.3.9) is the best available approximation to the radial streaming factor.

Theoretically expression (6.3.9) is all very well but this represents an idealised situation of a cylindrical hole of circular cross-section and infinite length in an infinite block of moderator. But in actual practice everything is finite and there may be more than one hole in each unit lattice. For example in case of PSCF there is one circular hole at the centre of the lattice and two cylindrical ones due to spaces between plug-sleeve and sleeve-block excluding the small space between the blocks and corner rods used to fill the corner holes. This complicates the very definition of β. The question is what should be taken as the radius of the equivalent hole? There are the following three possibilities:

(a) (b)

FIG. 6.5.2.1

(a) All the gas spaces are summed together and an equivalent radius of the hole is calculated.

(b) In β the term

$$\frac{a_o}{a_o + \ell} = \frac{1}{1 + \sum_{i=1}^{N} \frac{\ell}{a_o}}$$

is summed for all holes when the radius is the case of an annular channel, taken as the difference of the inner and the outer radii of the gas space.

(c) All holes are treated in situ. It means that the term

$$w\beta = \sum_{i=1}^{n} w_i \beta_i$$

where w_i and β_i correspond to each hole independently of the other. It is supposed that each hole is making its own contribution to the overall effect of streaming. On this basis for the case PSCF under consideration, following values were found

PSCF		a	b	c
S_r	=	1.124631	1.093634	1.091671

In (a) the effect is over-estimated, (b) is somewhat un-realistic because w the void factor has been considered constant and (c) seems to be a much more realistic approach. Therefore, throughout the assumption (c) was taken and the streaming factors, henceforth referred to as Leslie's streaming factor, were calculated. The streaming factors which were used in the calculations both according to Syrett (for core) and Leslie are tabulated in Table 6.5.1, along with the experimentally calculated streaming factors in combination with b_{11} for diffusion stacks and theoretical value of $L_o^2 = 2598\ cm^2$.

COMMON CONSTANTS

CASE	V RATIO	SFR	SMR	$\varepsilon_r(L)$	$S\gamma(EXP)$
PSCF	0.960,41	1.008,58	1.008,66	1.091,67	1.215,93
PSF	0.935,61	1.022,27	1.026,39	1.153,75	1.204,38
PSFD	0.935,61	1.029,93	1.027,91	1.155,01	1.204,38
SF	0.811,37	1.423,18	1.382,47	1.526,73	1.775,99
OCF	0.770,43	1.803,12	1.851,86	1.952,72	2.174,36

TABLE 6.5.1

$\varepsilon_r(exp) = \frac{L_R^2}{L_o^2}$.

L_R^2 = experimentally measured value of diffusion area.

L_o^2 = theoretical value corresponding to $\sigma_a = 4.1$ mb. $= 2498\ cm^2$.

V RATIO $= \frac{V(\text{solids including fuel \& can})}{V(\text{Lattice})}$.

6.6.1 MEASUREMENT OF THERMAL NEUTRON FLUX AT THE FUEL ELEMENTS

The basic usefulness of the heterogeneous method of reactor analysis lies in the fact that the neutron flux distribution is treated as a spatial problem depending upon the position of the fuel and moderator in comparison to the situation in case of homogenised model (unit cell model of Chapter 3) wherein we replace the reacting system by an "equivalent homogenised material" having the same characteristic nuclear properties as the actual lattice. Therefore, the flux distribution calculated at any point in this is the result of the overall average of the material, which excludes the consideration of the fact that "the actual lattice is heterogeneous with finite size of fuel, can and coolant channel surrounded by the moderator; even which (the moderator) is not perfectly solid in the present lattices under study.

Thus to compare the theoretical prediction, an attempt was made to measure the thermal neutron flux at the fuel elements. Since in the theoretical calculations it is assumed that the neutron flux is uniform over the fuel region treated as a line source.

Recourse to measurement of thermal neutron flux in between two slugs (though the flux is higher at that point because of the absence of fuel and aluminium being

in place instead) by Indium foils was taken. In the trial cases it was found impractical for a single person to carry out the experiment for the delicate nature of some 8 feet long uranium fuel rod placed in thin cylinder of aluminium. Besides, the statistical accuracy left much to be desired, at the same time radiation hazard was large. With these considerations the idea to measure the neutron flux "inside the fuel element" was given up in favour of an approximate measurement of thermal flux "At the fuel element" (on the surface of the fuel can) but it was practical for a single person to carry out the measurement in a day for one particular case involving, say, fifteen measurements.

The experimental details of flux measurements are given in the next section. They were carried out in channel $\frac{1}{2}$" x $\frac{3}{8}$" machined in the graphite plug surrounding the fuel element. As can be seen from the dimensional details given in Appendix A-1.1, the space between the can and the inner radius of the plug is 0.073 cm. In the experimental arrangement it was designed to reduce this (distance between detector and fuel) as much as possible. However in between the two being gas space it did not thermalize the neutron spectrum, so it was thought not to contribute any appreciable error in the experimental measurement.

6.6.2 EXPERIMENTAL ARRANGEMENT

The complete details of the experimental arrangement are schematically shown in FIGS. 6.6.1-4. The neutrons were detected by a BF_3 proportional counter, of active length 5 cms and 0.625 cms diameter (1/4") Type 5 EB 70/6, 20th Century Electronics Ltd. The sensitivity of the counter is 0.11 cps/n/cm^2/sec. The pulses from the counter were fed to the electronic equipment shown in FIG.2.2.1

FIG.6.6.1(A) and (B) show the BF_3 counter in position. (A) is the plan view of the counter as positioned in the channel and (B) details the position of the counter beside the fuel element. The counter was fitted to the end of an aluminium rectangular rod, of dimension 1/4" x 3/8" x 6', at the bottom by means of a locating shoe, so that the counter is securely and tightly held alongside the rod in the plug channel machined for the purpose. The rod was identically calibrated with the proportional counter BF_3 Type 12 EB/40 described in section 2.2. The counter is secured tight in the shoe by the screw S_1.

FIG. 6.6.3(A) and (B) shows the "Driving plate used to rotate the fuel rod and plugs assembly" by means of "Quick release clip", shown in FIG.6.6.4(A) and (B). The diagrams are sufficiently descriptive. The small curved part in FIG.6.6.4(B) shows

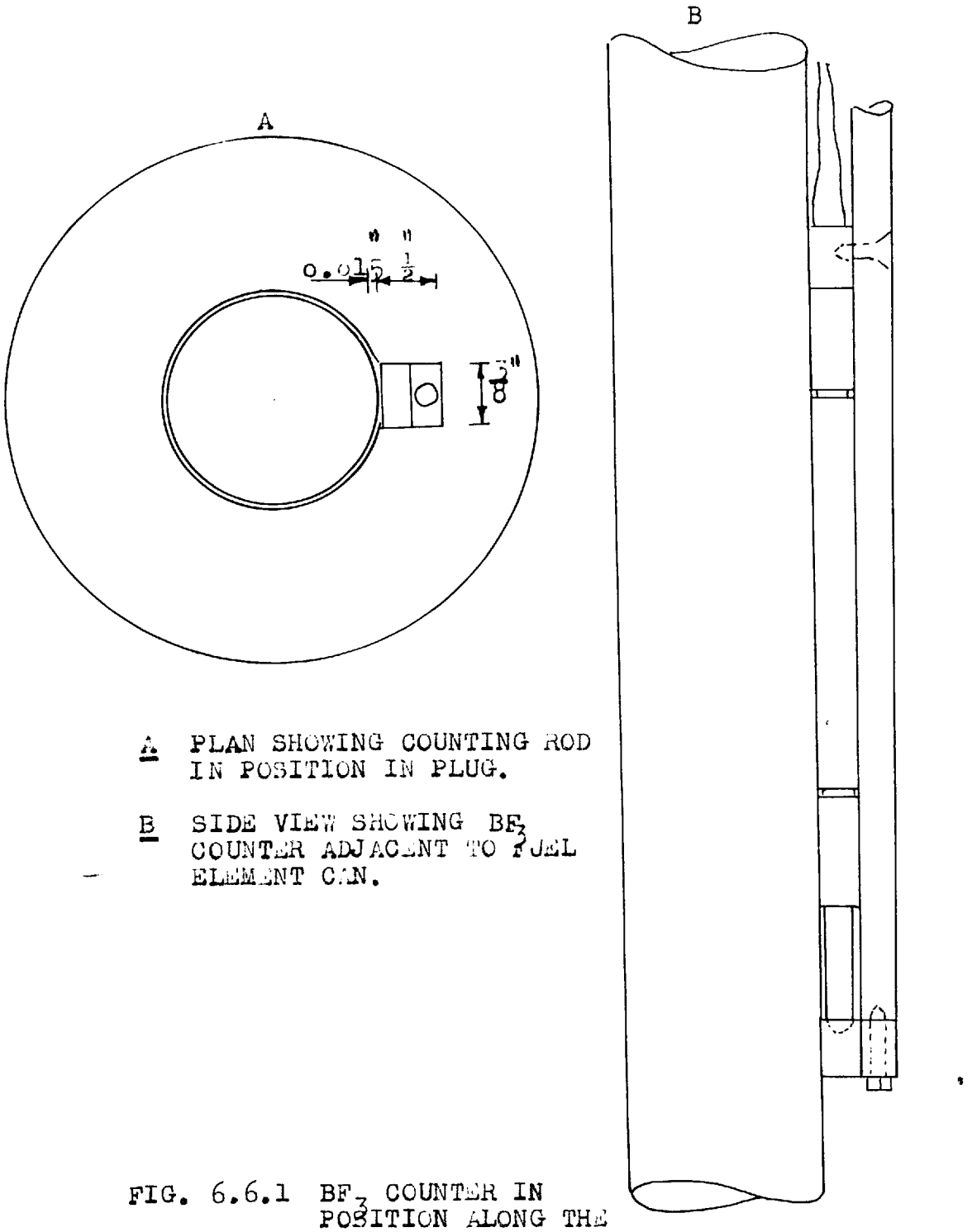

A PLAN SHOWING COUNTING ROD IN POSITION IN PLUG.

B SIDE VIEW SHOWING BF_3 COUNTER ADJACENT TO FUEL ELEMENT CAN.

FIG. 6.6.1 BF_3 COUNTER IN POSITION ALONG THE FUEL ELEMENT.

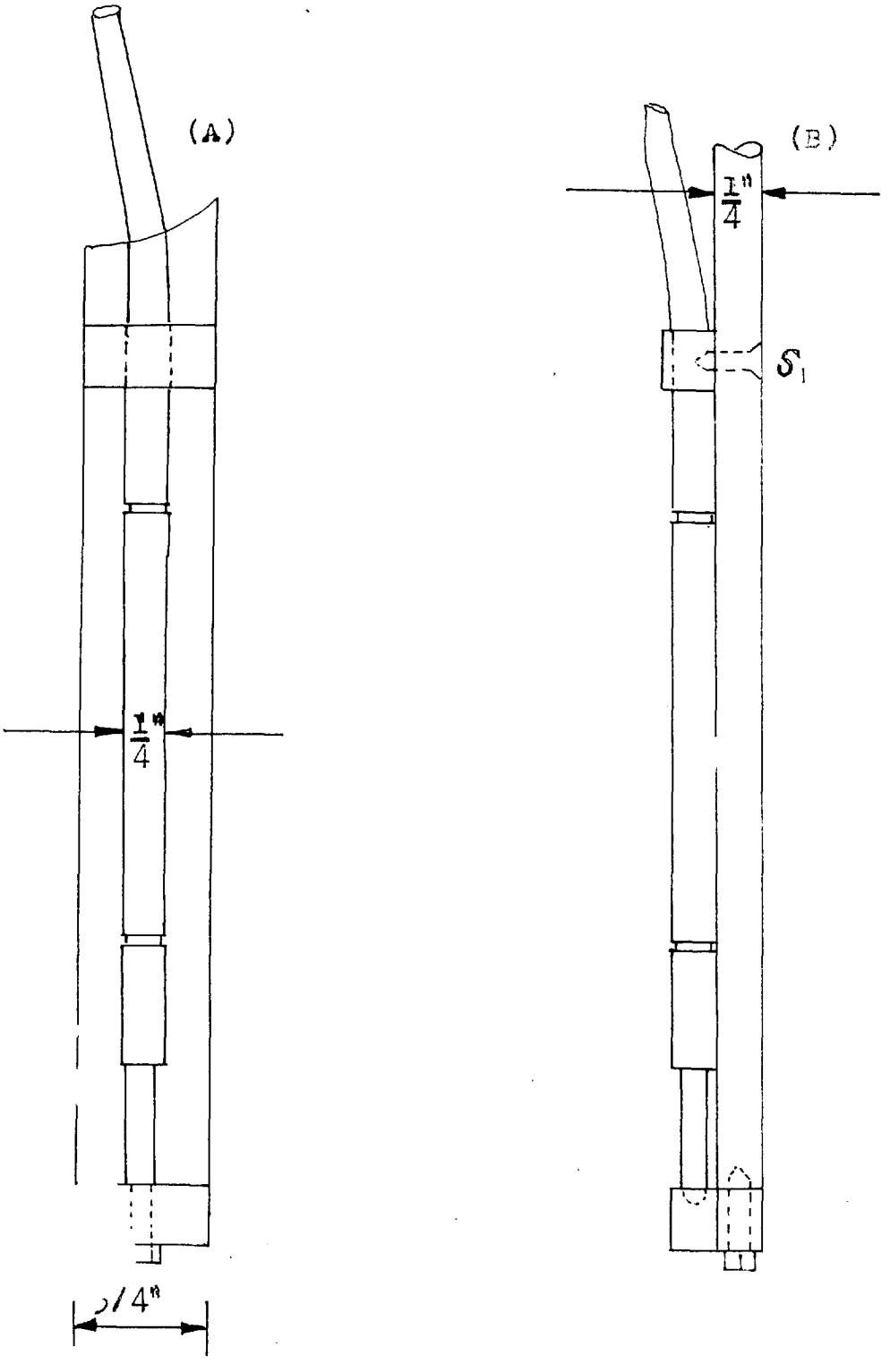

FIG. 6.6.2 MOUNTING ARRANGEMENT FOR BF_3 COUNTER

FIG. 6.6.3 DRVING PLATE ASSEMBLY

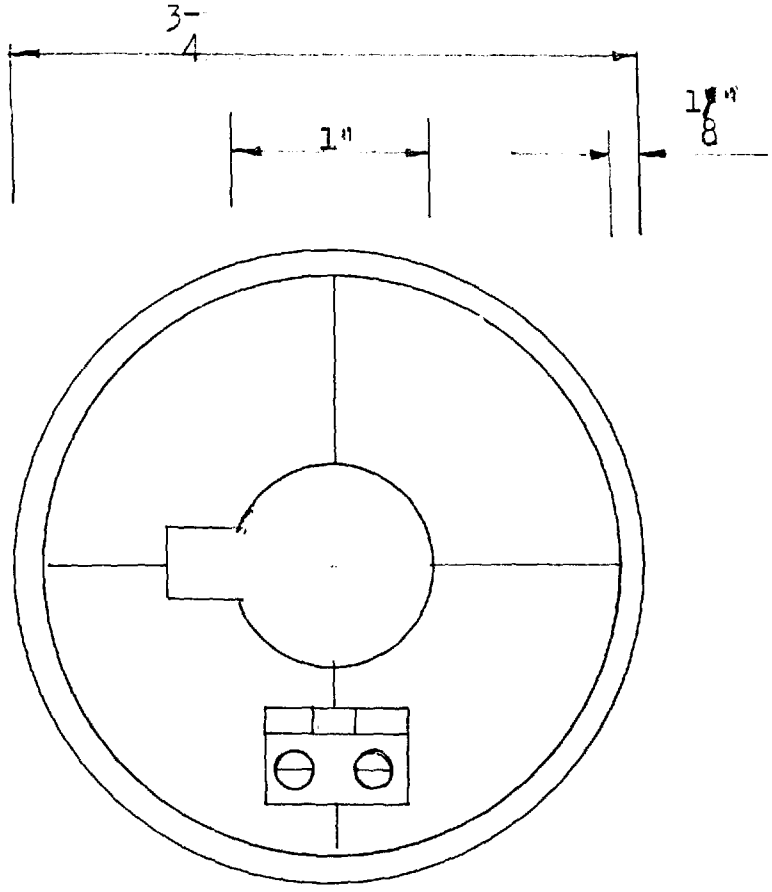

PLAN

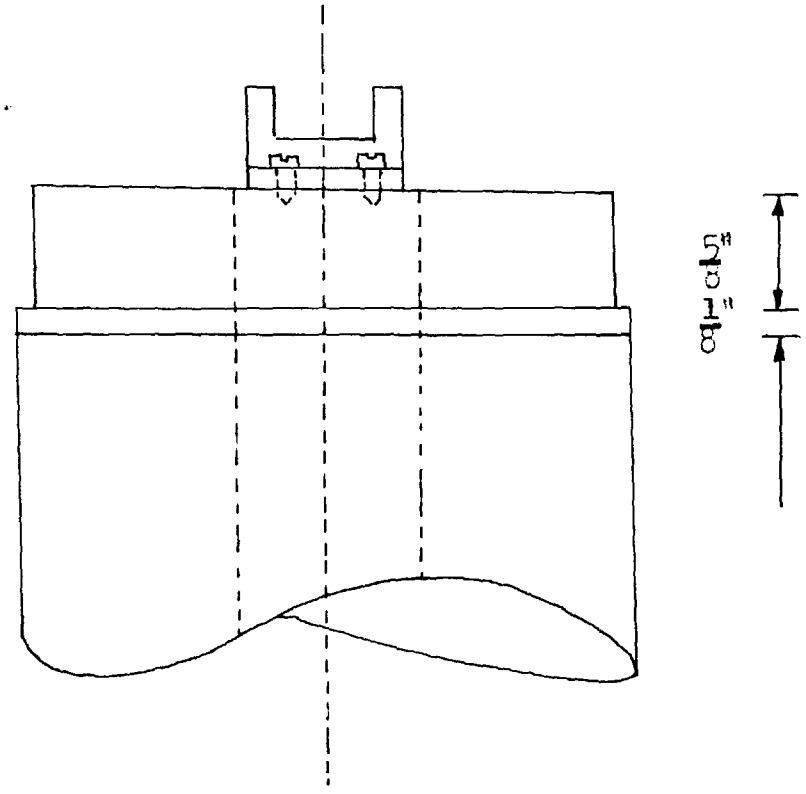

SIDE ELEVATION

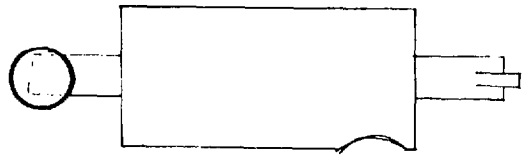

FRONT ELEVATION (B)

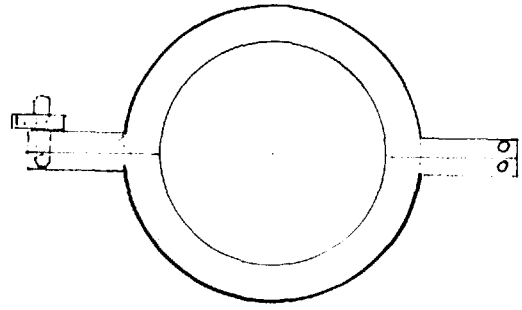

PLAN (A)

FIG. 6.6.4 QUICK RELEASE CLIP

the place whence the cable from the counter comes out of the driving plate assembly and is then fed to the pre-amplifier.

For every measurement of the thermal flux at the fuel element 4 readings of 100 seconds each were taken around the fuel at an angle of 90^{o} from the position of the first. The first reading was always such that the counter faced the centre of the assembly. To enable the counter to be taken at four positions of 90^{o} the fuel element and the plug assembly were locked together with quick release clip while the upper two plugs with channel machined are themselves joined to each other with two aluminium dowels and a similar arrangement for the small plug and driving plate at the top. Thus by simply sliding the quick release clip over the fuel element and engaging the driving plate assembly any rotation of the fuel element was transmitted to the graphite containing the counter in position all along.

The dead time of the counter was measured to be (20.69 ± 1.93) microseconds by the two source technique.

The sources of error in the determination of flux may be briefly summarized due to the following causes:-

1) Statistical Error. For each measurement of thermal flux 4 readings of 100 seconds were taken around the fuel

element and the statistical accuracy corresponded to within a range of 0.16% to 0.32%. For lower counter rates, however, it deteriorated still further when the number of counts per second decreased on the approach of boundaries of the assembly.

2) Error due to error in the dead time of the counter. The standard error in the dead time is 1.93 μsec which introduces a negligible error into the counting rate.

The error introduced due to the errors on account of these two causes is comparatively small as compared with the error due to the averaging process over the whole region.

The total sum of errors due to all these causes was usually of the order of 0.5% and, therefore, this was taken as a representative figure for the error quoted in the measured thermal flux distributions.

6.7 DETAILS OF INPUT DATA, RESULTS OF COMPUTATION AND EXPERIMENTS

The input (with regard to experiment) is precisely the same as given in Chapter 2 in full details, specifically the measured axial buckling and the extrapolation lengths in the horizontal direction in the form of external boundary condition of zero flux. From then on the problem

boils down to solving the set of homogeneous equations defined by the eq. 5.3.15 for K = 1, ... N number of fuel elements, the condition for criticality being the vanishing of the determinant. Since fast absorption and slowing down in the elements has been neglected, the input data and computing problem becomes simpler.

The problem is treated as an Eigen value problem. The complete details of the method of solving the determinant and the related parameters are given in Appendix-III and the programme "HETERO" used for the purpose is described in fuller detail.

As it can be seen from the description of the input data for the programme the constants, for example, coordinates, γ_h (thermal constant), η(the multiplication factor in the form of $(\eta\varepsilon)$ and various other input parameters for a certain lattice remain the same, with the exception of the "Moderator constants". We exclude the consideration of axial buckling and the external boundary condition as known parameter for a particular lattice case under investigation.

Had the system under study been a homogeneous mixture of fuel and moderator, or even water-moderated, the problem would have been rather simple. In the present case it is graphite with big or small channels and the problem does not end up there. It is complicated

by the fact that it is not solid, but has spaces in between two components designed to build up the lattices for investigation. Thus it amounts to applying corrections here and there for streaming gaps etc.

Additional complications in the moderator constants are due to varying size of the core region in the assembly. Consequently two extreme cases are: 1) constants conform to the core region entirely or 2) the constants are "clean" reflector parameters. In the present analytical model the first possibility is out of the question because of the basis of theory. The second is reasonably good, and the streaming factors are the main unknown parameters. However it should be remembered that the problem is a two-region "one" while we have to give parameters for the moderator.

In view of these considerations the following eight sets of data for the moderator were tried, namely D_{MR}, D_{FR}, L_R^2 and L_{SR}^2. The value of L_{SR}^2 is known fairly accurately while the others, specially thermal diffusion coefficient and area, are the controlling parameters in the whole set of homogeneous equations and, to put it precisely, are not known very accurately. All of them were so changed that they

remained consistent in respect of anisotropy, etc.

SET-1. In this case the constant Sg corresponds to density of graphite homogenised up to the surface of the can. Streaming factors are taken for the respective core cases from section 3.4.1.

SET-2. It was remarked in section 4.4.1 that in calculation of reflector constants (3.3.6) volume of solid is taken equal to the actual volume of the graphite present in the lattice while the process of homogenisation includes the gaps. There is no valid reason for this since the process of homogenization does imply a solid of reduced density spread over a greater volume and then when it comes to calculating diffusion constants the process is reversed. There is no valid argument to support this. Therefore in this set the diffusion coefficients (reflector) were adjusted so that they correspond to the volume of graphite homogenised. The corresponding areas L_R^2 and L_{SR}^2, however, remain unchanged. This set of data is marked B in Appendix A-1.2 and elsewhere in the text referred to as "SET B".

SET-3. They are entirely reflector constants, calculated according to the Syrett's model in the text, referred to as "SET A" and are given in A-1.2.

SET-4. This differs from Set 1 in respect of

application of streaming correction. In this case it was Leslie's streaming factors were used and assumed that the streaming due to thermal and fast neutrons is the same.

SET-5 and SET-6 Correspond to the theoretically calculated values of diffusion (both thermal and fast) coefficients and the corresponding diffusion area as basically defined (1,2,3). However slowing down area is precisely the same as in Set-1 (L_{So}^2). In Set 5 the streaming corrections are from section 3.3.6 for core and in Set 6 streaming factor due to Leslie has been used. It is assumed that thermal and fast streaming factors are equal.

SET-7 and SET-8. These are such that L_{So}^2 correspond to Sg as in Set-1, and theoretical value of L_o^2, is used to calculate the streaming factor in conjunction with the measured value of relaxation length in Table 2.5 and extrapolation length for the assembly when there is no fuel in it by the relation

$$\frac{1}{L_R^2} = \frac{M_z^2}{M_R^2}\,\gamma_{11}^2 - 2\left(\frac{\pi}{\bar{a}}\right)^2 \qquad 6.7.1$$

where $\bar{a}$ is the extrapolated dimension of the assembly and γ_{11} is the corresponding inverse relaxation length for the lattice (No Fuel) under study. The extrapolation lengths are given in Table 2.5.2. In Set-7, D_{mg} and D_{Fg} correspond

to Set-1, while in Set-8 they correspond to Set-5.

Finally the ratio $\frac{\tilde{V}_r}{V_o} = 14.385$ is common in all cases. The streaming factors used are tabulated in section 6.5 in table 6.5.1 but they have been referred to their original sources for clear understanding. The corresponding volume ratios are tabulated as well therein - the eight sets of constants are given in Tables 6.7.1.

All the results so computed giving the K_{eff} for the system have been tabulated in Tables 6.7.2 and plotted in case of Set-2 for all cases for the purpose of comparison. Since, as it can be seen, the values are a little in excess of unity (reasons discussed in next section) and the system is in steady-state, they have been normalised to unity and re-tabulated in 6.7.3 for the purpose of comparison.

The measured thermal flux and theoretical flux values normalised to 1000 are also plotted in FIGS. 6.7.1 and tabulated in Tables 6.7.4. The discussion of the results is given in section 6.8. The built-in accuracy in the programme for the Eigen-value (K_{eff}) is 10^{-6} and that in Eigen-vector is 0.1 per cent. Since from theoretical point of view these limits are quite accurate, they are omitted from tabulation.

The Bessel functions J's and Y's are periodic functions and in certain combinations of the general solution it eventually leads to the square root of a negative number, a situation which cannot be realised in practice. Therefore, for that particular combination of axial buckling and $(1/L_m^2)$ the results are not reasonable and are not quoted. They are indicated by a star all through the sets.

The infinite sum in the expression 6.3.14 has been truncated at 30 and, according to Näslund, gives absolute accuracy throughout the core.

In case of Tables 6.7.2-3, in case of lattice PSF (ODD) denoted as PSFD the number of fuel elements in the central region is 121, 81, etc. They are shown at the left-hand side of the K_{eff} quoted. The reason is that the lattice is almost identical to PSF and the number of fuel elements involved is nearest to the adjacent column of PSF.

CASE	DMR	DFR	L^2_{SR}	L^2_R
		SET-1		
PSCF	0.911,824	12.504,396	327.43	2688.45
PSF	0.931,014	12.717,470	349.37	2856.91
PSFD	0.923,393	12.812,764	351.99	2861.14
SF	1.244,818	17.575,223	638.52	5047.29
OCF	2.629,709	22.955,384	928.46	7437.00
		SET-2		
PSCF	0.971,625	13.272,056	337.00	2777.43
PSF	1.013,680	13.794,866	359.39	2949.24
PSFD	1.014,079	13.800,327	359.73	2955.66
SF	1.335,740	17.581,317	524.81	4448.92
OCF	1.567,285	20.117,227	634.80	5571.19
		SET-3		
PSCF	0.933,148	12.746,478	337.00	2777.43
PSF	0.948,931	12.913,717	359.39	2949.24
PSFD	0.955,239	12.999,588	359.73	2955.66
SF	1.240,674	16.330,041	524.81	4448.92
OCF	1.519,298	19.501,269	634.80	5571.19
		SET-4		
PSCF	0.988,749	13.560.548	354.40	2934.89
PSF	1.045,550	14.339,565	394.31	3211.42
PSFD	1.046,556	14.355,239	394.75	3211.93
SF	1.378,129	18.900,834	684.98	5573.97
OCF	1.628,617	22.336,224	979.03	8043.20

TABLE 6.7.1

CASE	DMR	DFR	L_{SR}^2	L_R^2
		SET-5		
PSCF	0.854,487	12.276,582	327.42	2503.71
PSF	0.869,106	12.437,611	349.37	2667.10
PSFD	0.870,393	12.530,808	351.99	2676.29
SF	1.163,145	17.204,776	638.53	4370.20
OCF	1.523,587	22.483,386	928.46	6569.87
		SET-6		
PSCF	0.924,818	13.039,340	354.40	2709.76
PSF	0.976.430	14.046,409	394.31	2998.05
PSFD	0.978,020	14.052,662	394.74	3001.33
SF	1.284,519	18.478,403	684.98	5051.22
OCF	1.649,801	23.707,912	979.03	7114.50
		SET-7		
PSCF	1.102,404	15.119,306	394.74	3037.39
PSF	1.091,433	14.968,842	411.61	3008.55
PSFD	1.091,433	14.968,842	411.61	3008.55
SF	1.599,154	22.004,194	796.82	4436.82
OCF	1.965,248	26.953,027	1090.15	5431.55
		SET-8		
PSCF	1.005,657	14.427,699	397.25	3037.39
PSF	0.980,373	14.086,479	395.69	3008.55
PSFD	0.980,373	14.086,479	395.69	3008.55
SF	1.129,098	16.223,428	602.10	4436.42
OCF	1.259,605	18.098,620	747.39	5431.55

TABLE 6.7.1

TWO GROUP HETEROGENEOUS RESULTS

SET-1

CASE	PSCF	PSF	PSFD	SF	OCF
100	1.012,170	1.017,126	1.018,461	*	0.999,412
64	1.010,890	1.016,288	1.018,392	1.015,212	1.007,446
36	1.004,996	1.013,754	1.004,899	1.015,023	1.013,545
16	0.948,907	1.002,472	*	1.005,988	1.031,195
4	0.882,908	0.937,899	0.985,356	0.953,368	1.040,570

121
81
49
25
9

SET-2

CASE	PSCF	PSF	PSFD	SF	OCF
100	1.008,193	1.010,964	1.011,729	*	1.003,474
64	1.007,349	1.010,518	1.011,835	*	1.004,812
36	1.002,608	1.009,153	0.998,534	0.996,770	0.995,573
16	0.985,733	1.001,293	*	0.969,654	0.972,800
4	0.897,007	0.953 084	0.987,880	0.854,990	0.847,534

121
81
49
25
9

TABLE 6.7.2

TWO-GROUP HETEROGENEOUS RESULTS

SET-3

CASE	PSCF	PSF	PSFD	SF	OCF
100	1.012,380	1.017,642	1.017,752	*	1.006,430
64	1.011,620	1.017,335	121 1.017,930	*	1.007,850
36	1.007,061	1.016,237	81 1.004,955	1.004,548	0.998,858
16	0.990,602	1.008,966	49 *	0.978,565	0.976,588
4	0.903,273	0.962,668	25 0.995,420	0.867,270	0.852,930
			9		

SET-4

CASE	PSCF	PSF	PSFD	SF	OCF
100	1.010,580	1.013,444	1.013,694	1.006,610	1.000,791
64	1.010,698	1.014,638	121 1.014,664	1.011,570	1.010,267
36	1.008,435	*	81 1.003,187	1.015,480	1.020,064
16	0.998,364	1.022,136	49 1.024,130	1.017,784	1.048,409
4	0.938,782	1.034,446	25 1.019,589	1.015,166	*
			9		

SET-5

CASE	PSCF	PSF	PSFD	SF	OCF
100	1.010,751	1.016,407	1.017,101	*	1.002,688
64	1.008,708	1.014,836	121 1.016,669		1.009,378
36	1.000,607	1.010,065	81 1.002,184	1.008,983	1.012,275
16	*	0.991,939	49 1.004,480	0.990,822	1.020,687
4	0.845,880	0.895,706	25 0.965,178	0.898,968	0.987,754
			9		

TABLE 6.7.2.

TWO-GROUP HETEROGENEOUS RESULTS

SET-6

CASE	PSCF	PSF	PSFD	SF	OCF
100	1.008,715	1.013,094	1.013,471	*	0.991,835
			121		
64	1.007,946	1.013,530	1.014,075	1.009,216	1.000,042
			81		
36	1.003,052	1.014,153	1.001,597	1.010,105	1.005,870
			49		
16	0.984,915	1.010,721	*	1.002,844	1.021,341
			25		
4	0.887,846	0.977,613	1.001,456	0.952,893	*
			9		

SET-7

CASE	PSCF	PSF	PSFD	SF	OCF
100	0.998,477	1.000,217	1.000,700	*	0.944,983
			121		
64	0.999,530	1.000,755	1.001,354	*	0.950,803
			81		
36	0.999,455	1.001,670	0.988,484	0.963,468	0.947,926
			49		
16	0.994,775	0.998,790	*	0.943,614	0.935,719
			25		
4	0.956,396	0.966,923	0.989,615	0.834,557	0.809,067
			9		

SET-8

CASE	PSCF	PSF	PSFD	SF	OCF
100	1.007,970	1.012,927	1.013,387	*	1.013,333
			121		
64	1.009,254	1.013,424	1.014,014	*	1.015,341
			81		
36	1.009,659	1.014,215	1.001,581	1.009,688	1.009,138
			49		
16	1.005,977	1.011,258	*	0.987,592	0.991,355
			25		
4	0.970,544	0.980,404	1.002,300	0.883,602	0.873,441
			9		

TABLE 6.7.2

TWO-GROUP HETEROGENEOUS RESULTS

SET-1

CASE	PSCF	PSF	PSFD	SF	OCF
100	1.000,000	1.000,000	1.000,000	*	1.000,000
64	0.998,735	0.999,176	0.999,932	1.000,000	1.008,039
36	0.992,912	0.996,848	0.986,684	0.999,813	1.014,141
16	0.973,065	0.985,593	*	0.990,914	1.031,801
4	0.872,292	0.922,107	0.967,495	0.939,082	1.041,182

* The original K is nearly equal to unity specifically equal to 0.999,412.

SET-2

CASE	PSCF	PSF	PSFD	SF	OCF
100	1.000,000	1.000,000	1.000,000	*	1.000,000
64	0.999,163	0.999,559	1.000,105	*	1.001,334
36	0.994,460	0.998,209	0.986,958	1.000,000**	0.992,126
16	0.977,723	0.990,434	*	0.972,796	0.969,432
4	0.889,716	0.942,748	0.976,428	0.857,761	0.844,660

** The original K for this case = 0.996,770

SET-3

CASE	PSCF	PSF	PSFD	SF	OCF
100	1.000,000	1.000,000	1.000,000	*	1.000,000
64	0.999,249	0.999,698	1.000,175 (121)	*	1.001,411
36	0.994,746	0.998,619	0.987,426 (81)	1.000,000	0.992,476
16	0.978,488	0.991,474	* (49)	0.974,135	0.970,349
4	0.892,227	0.945,979	0.978,058 (25)	0.863,344	0.847,481

(9)

TABLE 6.7.3

TWO-GROUP HETEROGENEROUS RESULTS

SET 4

CASE	PSCF	PSF	PSFD	SF	OCF
100	1.000,000	1.000,000	1.000,000	1.000,000	1.000,000
64	1.000,117	1.001,178	1.000,957 121	1.004,927	1.009,469
36	0.997,878	*	0.989,635 81	1.008,812	1.019,833
16	0.987,909	1.008,577	1.010,295 49	1.011,101	1.047,581
4	0.928,954	1.020,723	1.055,815 25	1.008,500	*
			9		

SET-5

CASE	PSCF	PSF	PSFD	SF	OCF
100	1.000,000	1.000,000	1.000,000	*	1.000,000
64	0.997,979	0.998,454	0.999,575	*	1.006,672
36	0.989,964	0.993,760	0.985,338	1.000,000	1.009,561
16	*	0.975,927	0.987,591	0.982,001	1.017,950
4	0.836,883	0.881,248	0.948,950	0.890,964	0.985,106

SET-6

CASE	PSCF	PSF	PSFD	SF	OCF
100	1.000,000	1.000,000	1.000,000	*	1.000,000
64	0.992,238	1.000,431	1.000,596	1.000,000	1.008,277
36	0.994,386	1.001,045	0.982,839	1.000,880	1.014,150
16	0.976,405	0.997,658	*	0.993,686	1.029,749
4	0.880,175	0.964,977	0.988,144	0.944,191	*

* The original K = 0.991,835.

TABLE 6.7.3

TWO-GROUP HETEROGENEOUS RESULTS

SET-7

CASE	PSCF	PSF	PSFD	SF	OCF
100	1.000,000	1.000,000	1.000,000	*	1.000,000*
64	1.001,054	1.000,558	1.000,654	*	1.006,159
36	1.000,979	1.001,453	0.987,793	1.000,000*	1.003,114
16	0.996,292	0.998,573	*	0.979,393	0.990,197
4	0.957,855	0.966,713	0.988 923	0.866,201	0.856,171

121
81
49
25
9

* Original K for these two cases is

	K
SF	0.963,468
OCF	0.944,983

SET-8

CASE	PSCF	PSF	PSFD	SF	OCF
100	1.000,000	1.000,000	1.000,000	*	1.000,000
64	1.001,274	1.000,491	1.000,619	*	1.002,317
36	1.001,676	1.001,272	0.988,350	1.000,000	0.996,193
16	0.998,023	0.998,352	*	0.978,116	0.978,638
4	0.962,870	0.967,892	0.989,060	0.875,124	0.862,237

121
81
49
25
9

TABLE 6.7.3

CASE	PSCF-100		PSCF-64	
POSITION	THEORY	EXPERIMENT	THEORY	EXPERIMENT
F_6	1000.00	1000.00 ± 5.00	1000.00	1000.00 ± 5.00
F_5	933.76	937.67 ± 4.39	929.16	933.17 ± 4.67
F_4	807.32	809.99 ± 4.05	798.42	800.21 ± 4.00
F_3	636.25	623.37 ± 3.12	647.21	640.17 ± 3.20
F_2	446.95	410.93 ± 2.05		
E_5	869.74	881.13 ± 4.40	862.37	867.84 ± 4.34
E_4	748.69	766.13 ± 3.83	736.18	742.07 ± 3.71
E_3	583.25	591.38 ± 2.95	591.75	595.73 ± 2.98
E_2	399.09	388.65 ± 1.94		
D_4	635.89	656.33 ± 3.28	624.02	635.21 ± 3.18
D_3	482.76	511.92 ± 2.55	486.89	510.28 ± 2.55
D_2	309.16	334.46 ± 1.67		
C_3	345.64	400.83 ± 2.00	354.36	401.97 ± 2.01
C_2	187.72	259.82 ± 1.30		
B_2	53.37	204.68 ± 1.02		
	PSCF-36		PSCF-16	
F_6	1000.00	1000.00 ± 5.00	999.54	1000.00 ± 5.00
F_5	924.61	918.94 ± 4.59	970.60	986.73 ± 4.93
F_4	821.16	820.43 ± 4.10		
E_5	853.27	852.96 ± 4.26	835.62	950.05 ± 4.75
E_4	754.65	764.26 ± 3.82		
D_4	654.62	670.28 ± 3.85		

TABLE 6.7.4

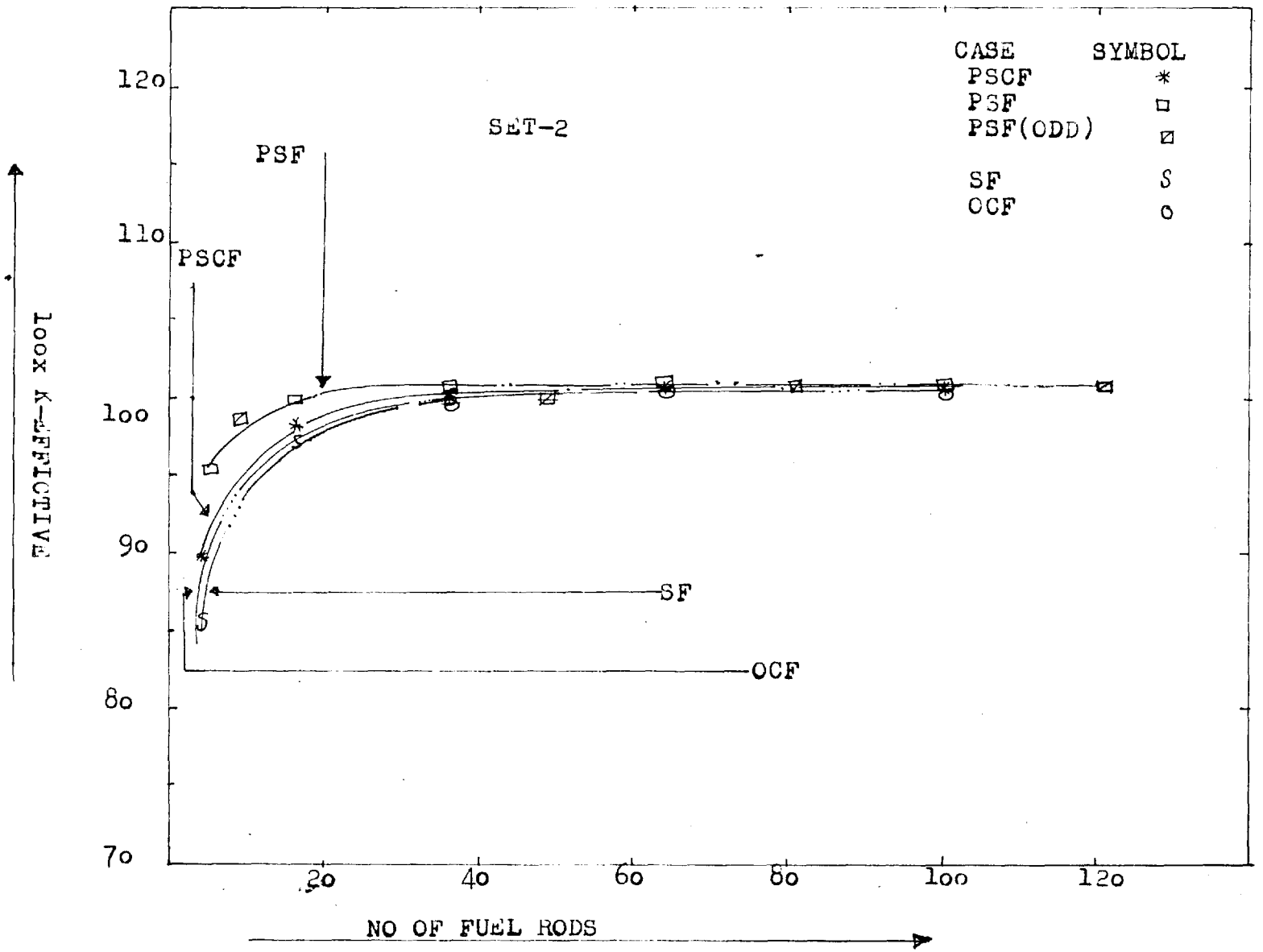

FIG. 6.7.1 (A) K_{EFF} VS NO OF FUEL RODS (ALL CASES)

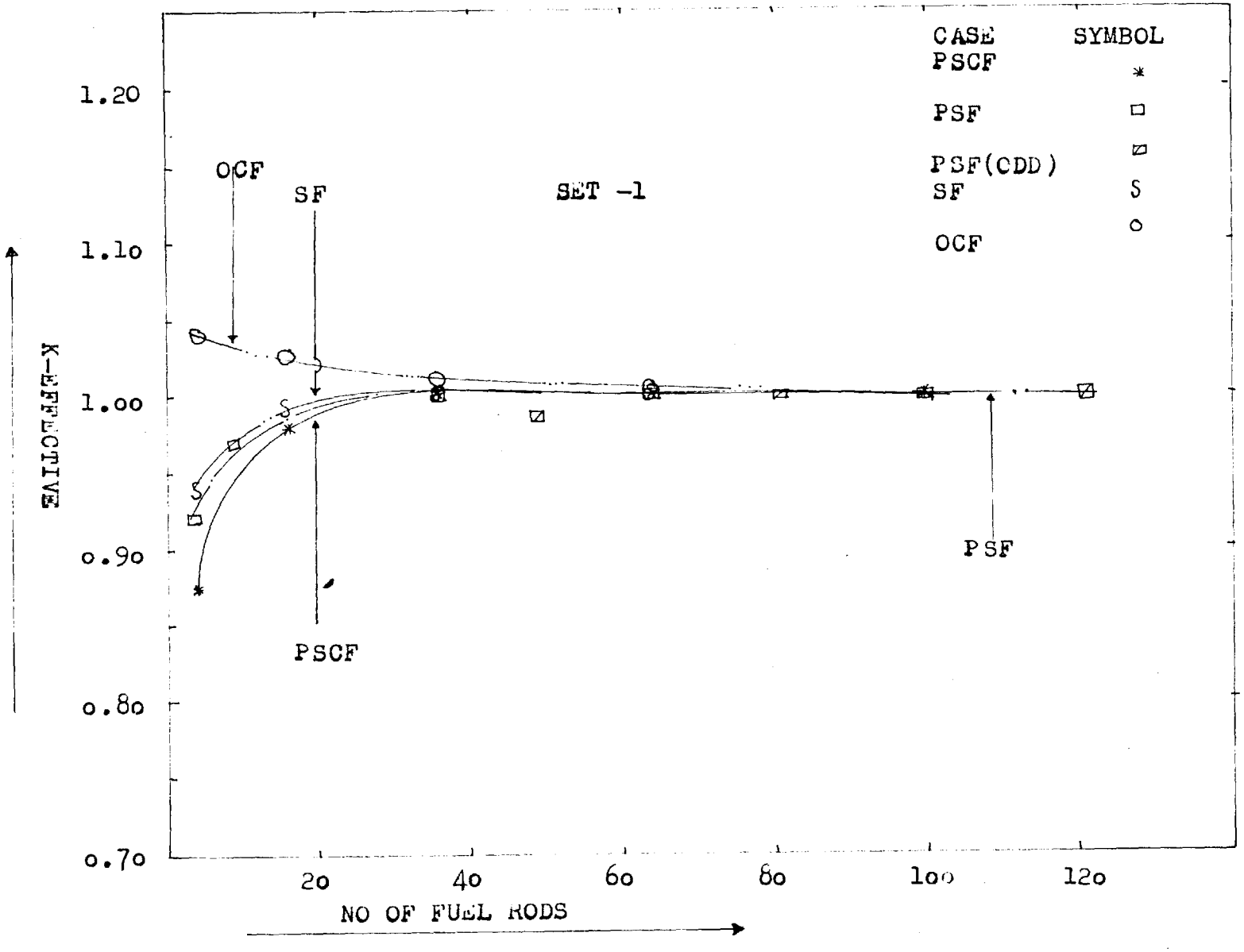

FIG. 6.7.1 (B) K-EFF. VS NO OF FUEL RODS (ALL CASES)

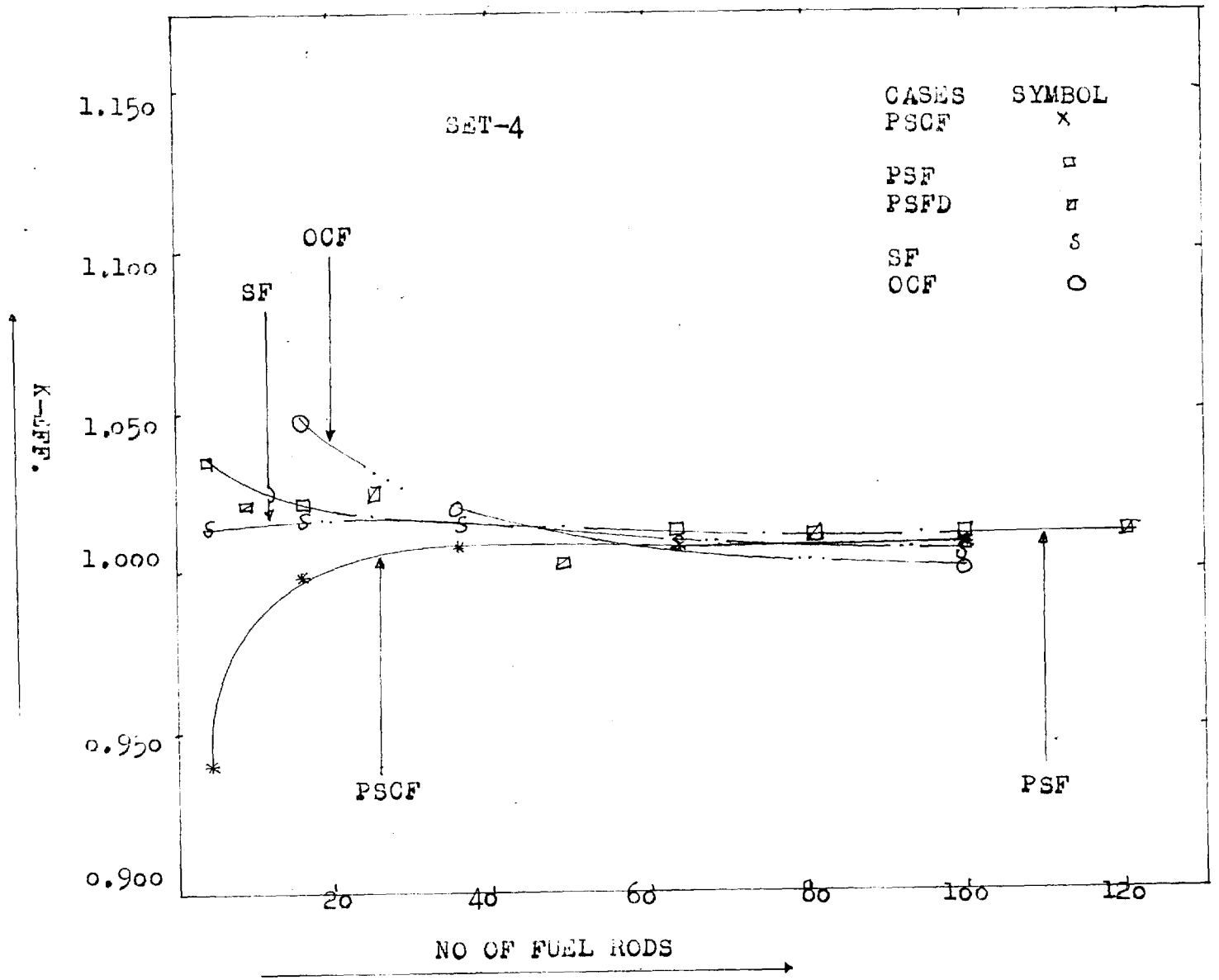

FIG. 6.7.1 (C) K-EFF. VS NO OF FUEL RODS (ALL CASES)

NOTATION; REFER FIG.3.3.1, LETTERS DENOTE X-Direction,
Numerals Y-Direction,
The Lefthand Corner Fuel Position is A_1

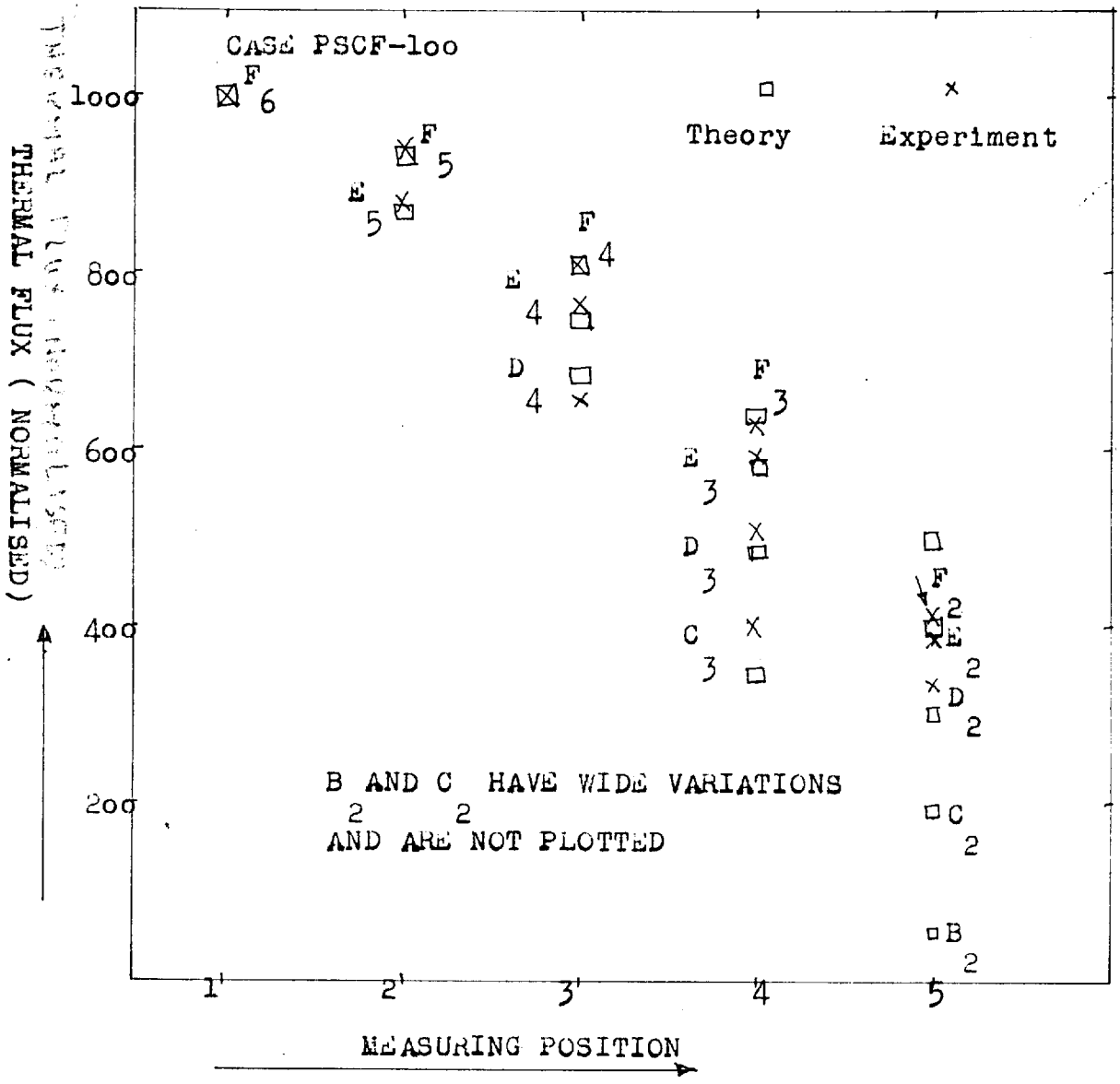

FIG. 6.7.1 THERMAL FLUX AT FUEL ELEMENTS
EXPERIMENT AND THEORY

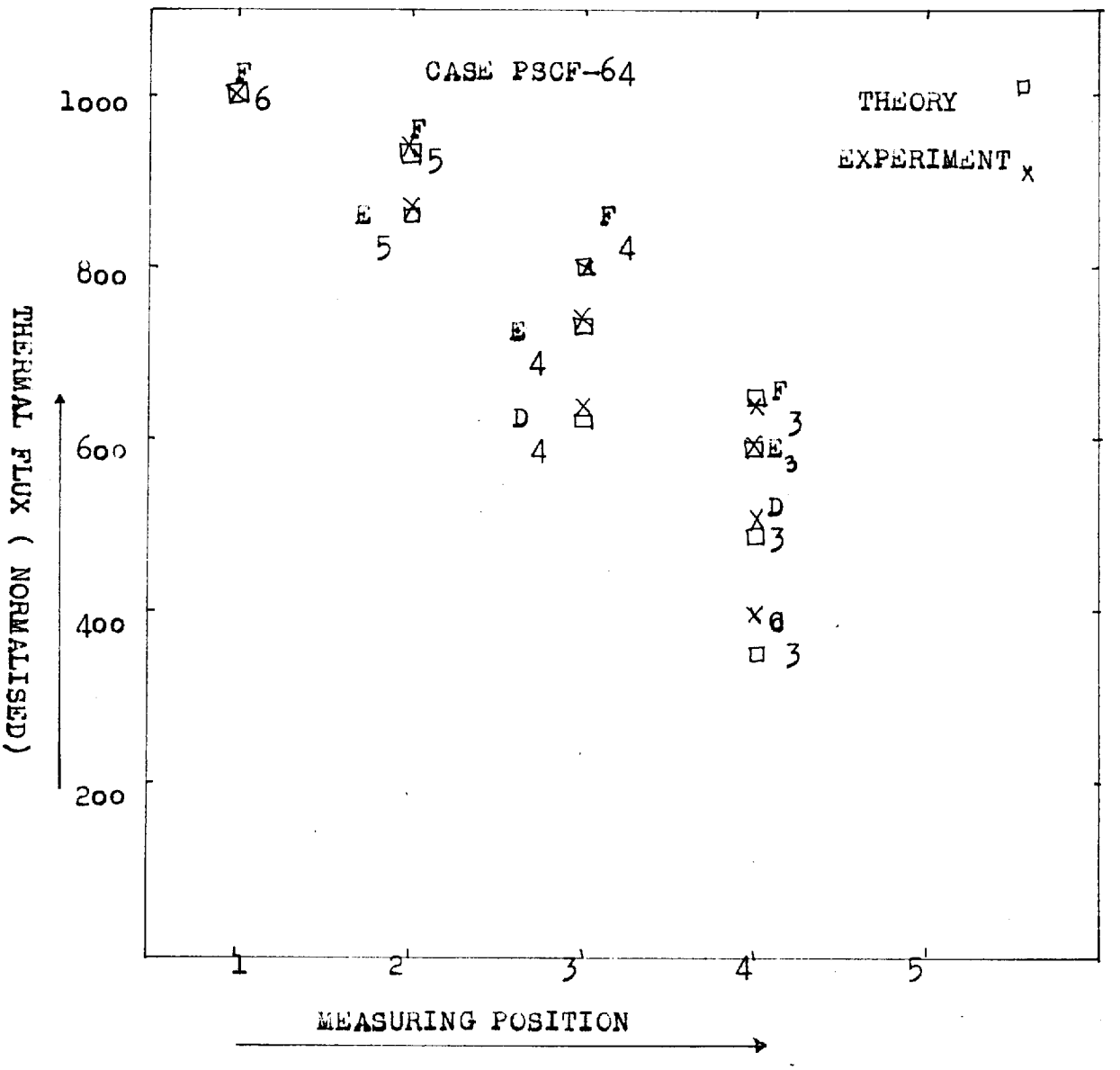

FIG. 6.7.1 THERMAL FLUX AT FUEL ELEMENTS, EXPERIMENT AND THEORY

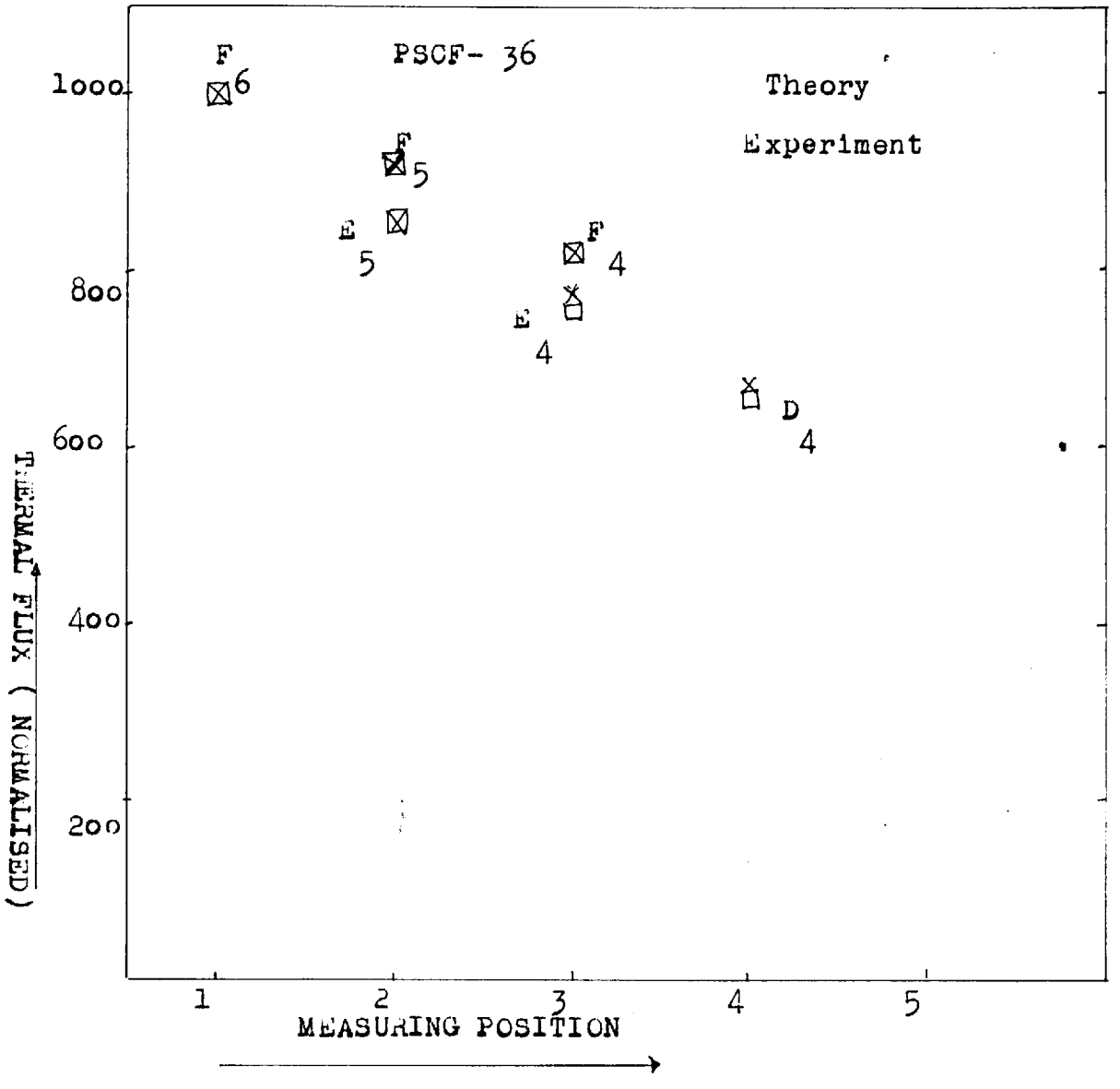

FIG. 6.7.1 THERMAL FLUX AT FUEL ELEMENTS EXPERIMENT AND THEORY

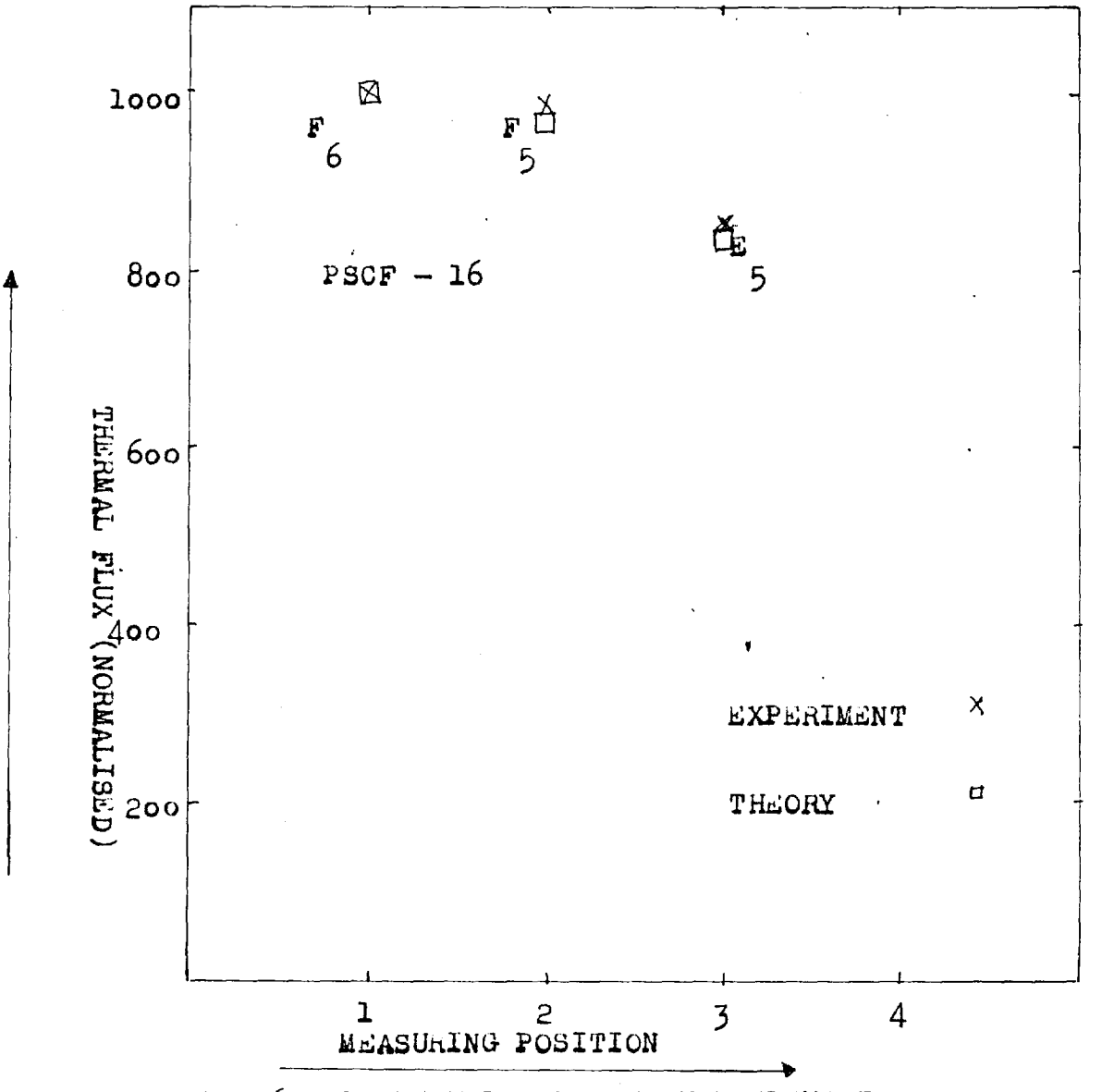

FIG. 6.7.1 THERMAL FLUX AT FUEL ELEMENTS
EXPERIMENT AND THEORY

6.8 DISCUSSION OF THE RESULTS

Detailed scrutiny of the results tabulated in section 6.7 and the corresponding spread of the values of K_{eff} predicted in combination with the flux plots shown in FIG.6.7.1. will convince that "Heterogenoues Two-group treatment is a distinct improvement over the whole range of fuel loadings in case of "all lattices investigated" as compared to homogenised concept.

(a) However there are discrepancies here and there which could possibly be due to the reasons discussed below.

(1) Thermal Constant. In section 6.4.1 the expression (6.4.5) is based on the fact that the flux is independent of the azimuthal angle, implying that the neutron flux is the same at every point on the surface of the fuel element. In case of small core it is however an approximation only because there are rapid variations of flux on account of excessive leakage. The definition of γ_h should therefore be modified to take into consideration this physical aspect of the situation. Or the heterogeneous technique suggested by Klahr (20) for the determination of γ_h may be more realistic.

(2) Resonance Escape Probability (p). The chief advantage in the change from homogeneous to heterogeneous systems is the marked increase in p, as remarked, in section 1.2. The increase of ε being less pronounced because

the system under study has natural uranium as fuel and this can be calculated (section 3.2.3) accurately. In any critical core system, however, the resonance escape probability changes from one group of fuel elements to the next and more so in the case of a reflected core system.

An element near a reflector, for example, would have a bigger resonance probability than the same element in an infinite lattice of similar elements because neutrons may bypass the resonance region while slowing down in the reflector. Precisely for this reason p increases in case of small number of fuel rods but it has been kept constant for the sake of fair comparison. Therefore it is felt that the results in case of 4 and, in some cases, 16 fuel elements can be improved upon by taking into consideration this change.

(3) The cylindricalization may have some bearing in case of 100 fuel elements but for less it is fairly good supposition.

(4) Streaming Factors. The basic streaming parameters, specifically S_{MR} and S_{FR} are the most disturbing ones and the errors may well be due to the inaccuracies in the streaming factor.

(b) Now let us consider all the results of 8-sets in comparison to each other. All the sets can be grouped

with regard to criticality parameter in the following categories.

Category-1. Sets 2, 3, 5 and 8. All vary in a reasonable way and are very good results.

Category-11. Sets 1, 6 and 7. The results are very reasonable and good when the graphite is fairly solid but they start to show inaccuracies in some cases of SF and OCF.

Category-111. 4. This is the worst set in comparison to the rest and is entirely inconsistent except for absolutely solid graphite case PSCF.

To study the systematic variation of these sets three representative curves, FIG.6.7.1, A, B, C have been plotted in their order of degeneracy. The sets selected are Set-2 (Curve A), Set-1 (Curve B) and Set-4 (Curve C).

In this context it should be remembered that Set-2 corresponds to the reflector data defined B (A-1.2) in text, Set-1 and 4 correspond to the graphite density homogenised up to can surface; thermal diffusion coefficients etc. correspond as given in section 6.5.1 But the difference between the two is that the streaming factors in Set-1 are directly taken from Chapter-3 (for core) while in Set-4 streaming factors are taken, in accordance with Leslie's formulation as detailed in

section 6.5.2(2). These two sets were specifically designed to see the effect of increased streaming factors. In Set-1 the effect of streaming as a consequence of (i) correction for density and (ii) streaming factors starts to deviate seriously in the case of extreme channeled case and this, therefore, puts a limit on channel diameter up to which the homogenization can be extended; while in the case of Set-4 the streaming corrections start to show up their effect as soon as the graphite is not quite solid. It is, therefore, felt that Leslie's formula overestimates streaming corrections. Set-3 is less accurate in comparison to Set-2.

The results of Sets 5 and 6 are very instructive because this is the simplest possible approach to the problem and the results are absolutely consistent and good and the effect of some incorrect parameters is shown in case of OCF-16 (specifically streaming corrections) fuel elements. There are no fitted parameters as in Syrett's model (7), e.g. κ_g, D_{mg}, etc. All that is required is the microscopic absorption cross-section, a fair knowledge of slowing down area and so on.

In Sets 7 and 8 the streaming factors are the experimentally calculated ones as explained before and Set-8 again emphasizes the simple approach detailed in the last paragraph. While Set-7 starts to deviate very

seriously in case of SF and OCF cases, which is more probably due to excessive leakage on account of streaming corrections.

(c) Thermal Flux Distribution at Fuel Elements.

Considering the flux plots and the table 6.7.4 giving the measured thermal flux distribution and the theoretical values, it seems that the effect of cylindricalisation of the assembly is maximum in the case of 100 fuel elements. However, predictions of flux on the line close to the centre line are fairly accurate. The agreement between theory and experiment improves as the number of fuel elements is reduced. This is the major advantage in going over to heterogeneous theory from the homogenised concept. As has been shown in Chapters 4 and 5, the agreement gets worse from 64 fuel elements and downwards, while in this case it improves considerably.

As a concluding remark it can be said that these results can still be improved upon by considering the reasons given in (a) of this section. However, even the neglect of various factors does not affect the results seriously.

It is felt that the Set-2 (defined in the text B and given in A-1.2) is the best for heterogeneous calculations of the present type. This confirms

the basic fact of the theory that fuel treated as a source-sink does not affect the properties of the moderator constants and the constants can be used directly for the purpose of analysis.

CHAPTER 7

CONTROL ROD CALCULATIONS .

7.1 INTRODUCTION

One of the many attributes ascribed to heterogeneous methods of reactor analysis is the study of control rod effectiveness. The simplicity of the control element analysis lies in the fact that no additional information is required for calculations except that if we can give the requisite properties of the control rod, provided the conditions for the diffusion theory to hold, do not break down seriously. The method treats the control rods as additional sinks of neutrons with no source term.

With this point in mind, some measurements for control rod effectiveness were carried out. The control element used was mild steel. In one set of experiments one control rod was increased per eight fuel elements, in the vacancy created by removing the 9th fuel rod as shown (a) below, (refer FIG.A-1-1).

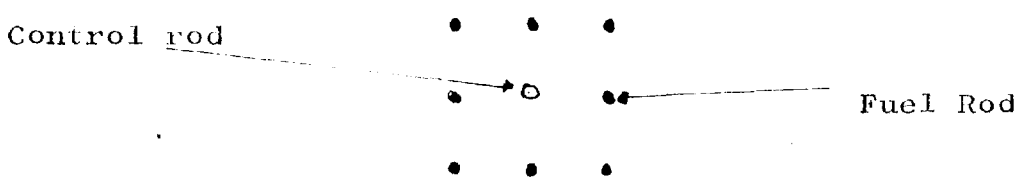

(a) FIG.7.1.1

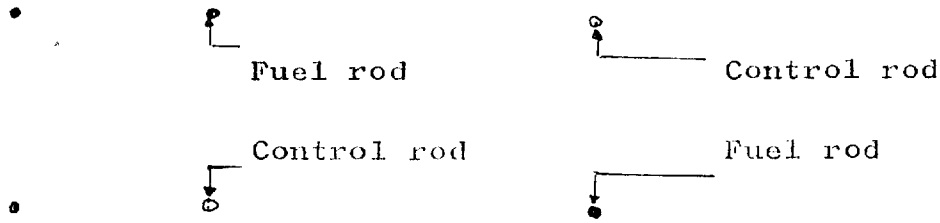

(b) (c)

FIG.7.1.1

In the 2nd and 3rd set one control rod was inserted per three fuel elements, in the vacancy created by removing the 4th and 2nd fuel rod position as in (b) and (c) of FIG.7.1.1.

The relaxation length measurements were carried out with and without the control rods in the sub-critical assembly.

The relevant results of measurements are tabulated in section 2.5.2 of Chapter 2 bearing the name of "vacancy" or "steel" with the name of the lattice. To be more explicit they are:

1) PSCF VACANCY and STEEL for full stack and 36 fuel rod configuration.
2) PSF VACANCY and STEEL for full stack, 81-fuel rods and 9 fuel rod cases.
3) SF VACANCY and STEEL for full assembly, 36-fuel rod cases.
4) PSCF VACANCY and STEEL (1/4), i.e. denoted in the

tables as PSCF 108 VAC or Steel 36. 6 pairs of cases from 4 to 144 fuel rods, and

5) as 4) above but in this half fuel and half vacancy was assumed to be the case of full assembly.

The measurements for 4) and 5) are plotted in FIGS. 2.5.2 (B) of the same chapter; the rest have not been plotted because they are only one or two points on the curve and it's correlation on the graph will be rather obscure.

The basis of analysis for the control rod effectiveness was based on the "two-group super-cell" calculation and the heterogeneous method outlined in Chapter 6. Consideration of the two methods will be given in sections 7.2.2 and 7.3 and the experimental, along with the theoretical, results are given in 7.2.3 and 7.3, respectively. Their critical assessment is given in section 7.5.

7.2.1 THERMAL EXTRAPOLATION LENGTH FOR MILD STEEL

The most important parameters in the control rod effectiveness calculation are the extrapolation distances λ_1 and λ_2 defined by the boundary conditions of the neutron diffusion equations. The accuracy of any computation depends mainly on the true estimate of the extrapolation lengths into the control rod.

In the present study it will be assumed that the control rod is transparent to the fast neutrons and therefore the boundary condition that the fast flux gradient at the channel wall of the control rod is zero, i.e.

$$\left[\frac{\partial \varphi(r)}{\partial r}\right]_{r=r_o} = 0 \qquad 7.2.1$$

and therefore

$$\left\{\frac{\varphi(r)}{\frac{\partial \varphi(r)}{\partial r}}\right\}_{r=r_o} = \lambda_1 = \infty \qquad 7.2.2$$

where r_o is the radius of the control rod.

The problem of thermal extrapolation length has been studied extensively by Kushneruik, Kusneruik and, McKay, and Davison and Kushneruik (37). Ghafoor (38) has calculated the thermal extrapolation length on the basis of the method proposed by Kushneruik and McKay and a correction recommended by Kushneruik. The extrapolation length for thermal neutrons is a function of the geometry and nuclear properties of the control rod. Kushneruik and McKay have solved the integral transport equation by a variational approach for a circular cylinder in a purely scattering medium assuming sources at infinity and obtained the expression for the thermal extrapolation length as

$$\frac{\lambda_2}{\ell} = \frac{4}{3\beta} - g(r_o/\ell) \qquad 7.2.3$$

where λ_2 is defined as

$$\left\{\frac{\varphi(r)}{\frac{\partial\varphi(r)}{\partial r}}\right\}_{r=r_o} = \lambda_2 \qquad 7.2.4$$

Here r_o = radius of the control rod

λ_2 = thermal extrapolation length for mild steel

ℓ = mean free path in the surrounding medium (graphite)

β = blackness, i.e. fraction of neutrons incident on the channel wall which are absorbed in the rod,

and $g(r_o/\ell)$ is a function depending only on the relative size of the cylinder, i.e. r_o/ℓ and such that $g(r_o/\ell)$ is zero when r_o/ℓ is zero and $g(r_o/\ell)$ increases monotonically to 0.623 as r_o/ℓ increases to infinity.

It is relevant to remark that a similar expression obtained by Carter (39) by the application of multiple collision methods developed by Stuart (26), :

$$\frac{\lambda_2}{\ell} = \frac{4}{3\beta} - \frac{2}{3} \qquad 7.2.5$$

is in error since the function $f(r_o/\ell)$ is simply replaced by a constant (2/3) and neglects the consideration of the size of the control rod element.

Instead of getting involved in a separate field, of various methods for the calculation of extrapolation lengths, etc. from the present study, the values of extrapolation lengths for mild steel were directly taken from Ghafoor (38) who has investigated the interaction of control rods in a nuclear reactor lattice and carried out the experimental measurements at the College sub-critical assembly. His values for thermal extrapolation lengths are

	Kusheruik-McKay	Experimental Value
λ_2 =	17.467 cm	22.10

The estimate of the scattering mean free path required for the purpose was made according to the recommendations of Grant (24).

7.2.2 CONTROL ROD EFFECTIVENESS ON THE BASIS OF SUPER-CELL CALCULATIONS

The theoretical estimate of the reactivity controlled were made using the so-called Super-cell method (45). Briefly described it considers any zone of a reactor where there is an array of control rods on a "square super-lattice". It is assumed that the zone is infinite in all directions, so by symmetry, each control rod lies on the central axis of an infinitely long square super-lattice. The neutron-current across the face boundaries

of the lattice is everywhere zero. The square lattice is replaced by a circular cylinder of equal cross-sectional area, as is normally done in the case of lattice calculations. The two-group diffusion equations are solved inside the super-lattice cylinder for the geometrical buckling β_c^2 knowing the thermal extrapolation length at the control rod channel wall under the additional boundary condition of zero flux gradients at the outer boundary of the super-lattice. The super lattice under investigation is shown in FIG.7.1.

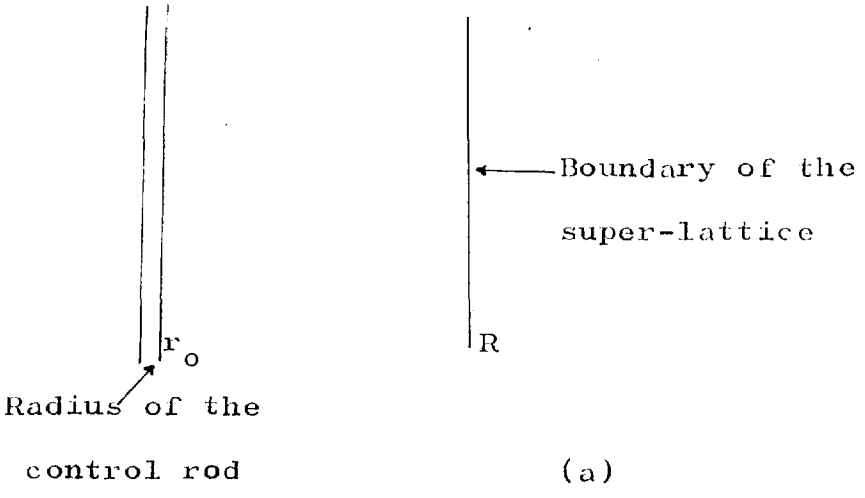

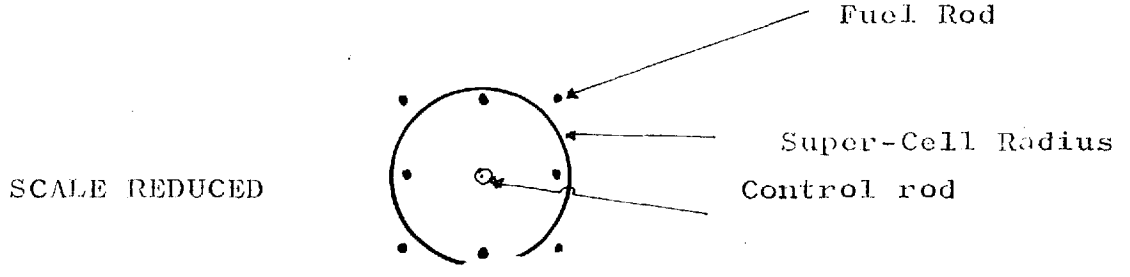

Let N be the number of fuel channels per one control rod, the equivalent super-cell radius is

$$\pi R^2 = Np^2 \qquad 7.2.6$$

p is the pitch of the lattice.

Assuming that the equivalent radius R is less than the core radius and the space between the control rod (radius r_o) and the super-cell boundary is filled with a homogenised material having the same nuclear properties as the reactor lattice, the two-group steady-state equation can be written

$$D_f \nabla^2 \varphi_f(r) - \Sigma_f \varphi_f + K_\infty \Sigma_{am} \varphi_m = 0 \qquad 7.2.7$$

$$D_m \nabla^2 \varphi_m(r) - \Sigma_m \varphi_m + \Sigma_f \varphi_f = 0 \qquad 7.2.8$$

Their general solution in the radial direction is

$$\varphi_m = AJ_o(\beta_c r) + BY_o(\beta_c r) + CI_o(\gamma_c r) + DK_o(\gamma_c r) \quad (a)$$

$$\varphi_f = S_1(AJ_o(\beta_c r) + BY_o(\beta_c r)) + S_2(CI_o(\gamma_c r) + DK_o(\gamma_c r)) \qquad 7.2.9 \quad (b)$$

The values of S_1 and S_2 are the reciprocals of the ones defined in Chapter 5, section 5.2 while

$$\gamma_c^2 = \beta_c^2 + \left(\frac{1}{L_R^2} + \frac{1}{L_{SR}^2}\right) \qquad 7.2.10$$

β_c^2 characterises the leakage of neutrons from the

super-cell while the overall flux-shape in the reactor remains the same. The equations 7.2.9 (a,b) are solved under the boundary conditions

$$\left.\frac{\varphi_m}{\frac{\partial \varphi_m}{\partial r}}\right|_{r=r_o} = \lambda \qquad (a)$$

λ = thermal neutron extrapolation distance into the control rod.

$$\left(\frac{\partial \varphi_m}{\partial r}\right)_{r = R} = 0 \qquad (b)$$

$$\left(\frac{\partial \varphi_f}{\partial r}\right)_{r = r_o} = 0 \qquad (c) \qquad 7.2.11$$

that the control rod is transparent to fast neutrons.

$$\left(\frac{\partial \varphi_f}{\partial r}\right)_{r = R} = 0 \qquad (d)$$

Eliminating A, B, C and D from equations 7.2.9 we would obtain

$$\frac{1}{S_1} \cdot \frac{1}{\beta_c} \cdot \left[\frac{J_o(\beta_c r_o)Y_1(\beta_c R) - Y_o(\beta_c r_o)J_1(\beta_c R)}{J_1(\beta_c r_o)Y_1(\beta_c R) - Y_1(\beta_c r_o)J_1(\beta_c R)}\right] +$$

$$\frac{1}{S_2} \cdot \frac{1}{\gamma_c} \cdot \left[\frac{I_o(\gamma_c r_o)K_1(\gamma_c R) + K_o(\gamma_c r_o)I_1(\gamma_c R)}{I_1(\gamma_c r_o)K_1(\gamma_c R) - K_1(\gamma_c r_o)I_1(\gamma_c R)}\right]$$

$$+ \lambda \left[\frac{1}{S_1} - \frac{1}{S_2}\right] = 0 \qquad 7.2.12$$

Equation 7.2.12 is solved for β_c by trial and error. The neutron absorption in the control rod is, therefore, represented by an equivalent leakage given by β_c^2, from

the super-cell.

7.2.3 THEORETICAL AND EXPERIMENTAL RESULTS

In this section the experimental and theoretical results obtained on the concept developed in section 7.2.2 will be given.

The calculations for the purpose were carried out by a programme practically identical to the one described in A-2.5, except for minor changes because of the relations concerned.

The basis of control rod effectiveness study in an experiment with the sub-critical assembly is the fact that the equation

$$K_\infty = (1+B_r^2 L_R^2 - \gamma_{11}^2 L_Z^2)(1+B_r^2 L_{SR}^2 - \gamma_{11}^2 L_{SZ}) \qquad 7.2.13$$

must be satisfied in the vertical direction,

where

B_r^2 is the radial geometric buckling appropriate to the external boundary condition

$-\gamma_{11}^2$ is the axial buckling which satisfies the above condition.

In modified one-group theory the material buckling is -

$$B_m^2 = B^2 - \frac{M_Z^2}{M_R^2}\gamma_{11}^2 \qquad 7.2.14$$

When a control rod is inserted the overall flux shape remains the same but it has to satisfy additional

boundary conditions at the surface of control rods in each super-lattice. This results in additional radial leakage characterised by β_c^2 defined by equation 7.2.12.

Since the materials buckling of the reactor system is unchanged before and after the introduction of the control rod the γ_{11}^2 (square of inverse relaxation length) takes up a value which satisfies the equations 7.2.13 and 7.2.14. The measured change in the relaxation length is, therefore, taken as the additional radial leakage; symbolically we can write

$$\Delta (B_r^2) = \frac{M_z^2}{M_R^2}\left((\gamma_{11})^2_{steel} - (\gamma_{11}^2)_{vac} \right)$$

$$\Delta B_r^2 = \frac{M_z^2}{M_R^2} \cdot \Delta \gamma_{11}^2 \qquad 7.2.15$$

The dimensions of the assembly are assumed to be the same in both cases, therefore,

$$\Delta B^2 = \beta_c^2$$

and for comparison of experiment with theory

$$\beta_c^2 = \frac{M_z^2}{M_R^2} \cdot \Delta\gamma_{11}^2 \qquad 7.2.15$$

The results of computation and experiment are given in Table 7.2.1 (a). The results reported are only for the experimental value of extrapolation length (22.10 cm)

given in section 7.2.1, for the extrapolation length (17.467 cm) they do not change so much as to warrant reporting. The errors quoted for $\frac{M_z^2}{M_R^2} \Delta\gamma_{11}^2$ are entirely experimental errors corresponding to the fitting error in b_{11} in the corresponding cases, for reasons given in section 7.2.4.

To find the reactivity controlled we need the original K_∞ of the system so that when the control rods are inserted, the reactivity controlled may be calculated.

To calculate the K_∞ of the system when there are vacancies, the method of calculating reflector savings given in full detail in Chapters 4 and 5 was used and the results of computation are given in Table 7.2.1(B). Only the material bucklings and K_∞ for the system are quoted, other terms being understood with reference to previous interpretation of the cases. The errors in the material bucklings and K_∞ for two-group theory are not quoted because of repetition (Chapter 2).

The reflector savings used to calculate K_∞ for the system were used corresponding to the A case of Chapter 4, i.e. given by

$$\delta = \frac{D_c}{D_r} L_r \tanh (\varkappa_r T)$$

The reason for this choice was the behaviour of a partially filled sub-critical assembly on two-group theory as shown in the last section of Chapter 5,

LATTICE	CASE	THEORETICAL β_c^2 x 10^{-6} cm^{-2}	$M_z^2/M_R^2\ \gamma_{11}^2$ x10^{-6} cm^{-2}
PSCF 128	(1/9)	156.33	106.01 ± 1.690
PSCF 32	"	130.76	85.54 ± 1.32
PSF 128	"	135.44	103.71 ± 1.64
PSFD 72	"	116.86	104.72 ± 1.64
PSFD 8	"	126.12	43.43 ± 0.65
SF 128	"	234.66	81.95 ± 1.48
SF 32	"	136.92	62.97 ± 1.01
144		PSCF (1/4) SET x10^{-4}	x10^{-4}
144	1/2	20.0848	$2.4778 \pm .0394$
100	"	19.9887	$2.4683 \pm .0385$
64	"	19.7439	$2.2960 \pm .0355$
36	"	19.4812	$2.8149 \pm .0423$
16	"	18.8810	$1.0960 \pm .0164$
4	"	18.1690	$0.3550 \pm .0052$
		PSCF (1/2) SET	
144	1/2	14.2678	$5.4484 \pm .0817$
100	"	14.2053	$5.4344 \pm .0812$
64	"	14.5245	$4.9650 \pm .0743$
36	"	15.3576	$3.8821 \pm .0575$
16	"	16.5398	$2.2714 \pm .0336$
4	"	17.6050	$0.7111 \pm .0965$

TABLE 7.2.1 (A)

PSCF 108 VAC 36

NO. OF FUEL RODS	ONE-GROUP B_m^2 $\times 10^{-4} cm^{-2}$	ONE-GROUP K_∞	TWO-GROUP B_m^2 $\times 10^{-4} cm^{-2}$	TWO-GROUP K_∞	K_∞ (Theory)
144	0.664147	1.04846±.00089	0.664147	1.04904	1.05554
100	0.681314	1.04971±.00092	0.750792	1.05552	"
64	0.754987	1.05508±.00103	0.791958	1.05861	"
36	0.999886	1.07295±.00140	1.137870	1.08472	"
16	1.712970	1.12498±.00250	2.371560	1.18044	"
4	4.222246	1.30805±.00654	7.359260	1.60834	"
PSCF 72 VAC 72					
144	-.063232	0.99424±.00011	-.062232	0.99425	0.99483
100	-.064784	0.99410±.00039	0.05258	1.0048	"
64	0.271887	1.00248±.00047	0.180335	1.01649	"
36	0.337618	1.03076±.00060	0.693017	1.06406	"
16	1.180308	1.10753±.00216	2.246730	1.21438	"
4	3.780434	1.34440±.00611	7.887190	1.83814	"
1/9 VACANCY CASES					
PSCF 128 VAC 16	0.959279	1.06405±.00118	0.959279	1.06508	1.07042
PSCF 32 VAC 4	1.28893	1.08607±.00165	1.416670	1.09683	"
PSF 128 VAC 16	0.899628	1.06316±.00116	0.899628	1.06415	1.07190
PSF 72 VAC 9	0.893868	1.06224±.00117	0.996806	1.07061	1.07294
PSF 8 VAC 1	2.52939	1.17612±.00364	4.077650	1.30408	"
SF 128 VAC 16	0.923550	1.08124±.00166	0.923550	1.08292	1.08350
SF 32 VAC 4	1.34579	1.11845±.00248	1.408130	1.12773	"

TABLE 7.2.1 (B)

specifically the curve between reflector thickness vs. reflector saving which shows the break-down of the concept of reflector saving at a certain stage (36 fuel rods).

7.3 HETEROGENEOUS METHOD FOR THE CONTROL ROD EFFECTIVENESS AND THE COMPUTED RESULTS

The study of control rod effectiveness on the basis of heterogeneous reactor analysis is not very different from that of the actual lattice with fuel elements embedded in the moderator. The only thing which has to be taken into consideration is the fact that:

1) the control rods are additional absorbers of thermal neutrons and
2) the resonance escape probability is equal to unity.

The absorption property of the control rod is characterised by the thermal constant for the control rod defined

$$\gamma_h = \frac{2\pi r_o D_m}{\lambda} \qquad 7.3.1$$

where

λ = thermal neutron extrapolation length into the control rod

D_m = the diffusion coefficient for the moderator; in the present case it is the radial diffusion coefficient.

Thus for the control rod we define

$$\gamma_h = \frac{2\pi a_o D_{MR}}{\lambda}$$

$$\eta = 0$$

$$p = 1$$

and the rest of the two-group heterogeneous theory of Chapter 6 is directly applicable to the present section in full with the above-mentioned modifications. The results of the present calculations are given in Tables 7.2.2. while the definition of moderator constants is given below:-

A correspond to the graphite density homogenised up to the surface of can; volume of the solid includes volume of the fuel and can and the streaming factors are taken for the core given in Tables 3.

B These are completely reflector constants defined in the context as "A".

The case B (by using pure reflector constants "A") was necessitated for the sake of comparison with the super-cell calculations given in the previous section.

ρ_{EXPH} = % reactivity calculated by λ_2 = 22.10 (experimental value) and

ρ_{KMKY} = % reactivity controlled by λ_2 = 17.467 (Kusheriuk-McKay 38).

CASE	β'_u	η_5	η_{nat}	p	$\eta(\varepsilon\eta_{nat})$
PSCF 128 VAC 1 16	0.090,51	2.021,67	1.291,287	0.927,72	1.328,292
PSFD 128 VAC 11 16	0.092,74	2.021,40	1.291,127	0.925,87	1.327,988
SF 128 VAC 111 16	0.105,08	2.019,90	1.290,234	0.915,58	1.327,780
PSCF 108 VAC 1V 36	0.077,30	2.023,33	1.292,276	0.938,66	1.328,292

CASE	V RATIO	L_R^2	L_{SR}^2	D_{MR}	D_{FR}	γ_h (Thermal Co.) $\bar{\gamma}_{KMK}$	$\bar{\gamma}_{EXPH}$
1 A	0.957,60	2685.50	328.46	0.912,813	12.503,208	0.417,011	0.329,589
1 B	0.942,86	2764.38	336.55	0.929,585	12.703,116	0.424,613	0.335,645
11 A	0.933,768	2863.14	352.66	0.930,071	12.758,237	0.424,895	0.335,821
11 B	0.919,026	2940.54	358.71	0.949,164	12.927,469	0.433,617	0.342,715
111 A	0.813,736	4842.44	632.99	1.222,341	17.187,627	0.558,416	0.441,351
111 B	0.798,994	4312.37	513.73	1.185,927	15.684,936	0.541,780	0.428,203
1V A	0.955,292	2694.93	329.75	0.911,851	12.490,142	0.416,571	0.329,242
1V B	0.942,853	2764.14	337.01	0.925,174	12.649,236	0.422,658	0.334,052

TABLE 7.3.1 (A)

(P) (B)

K_{EFF}

CASE	VAC	STEEL EXPH	STEEL KMKY	ρ_{EXPH}	ρ_{KMKY}
PSCF 32 VAC 4	1.007,518	1.047,323	1.039,667	3.9508	3.1909
PSFD 8 VAC 1	0.984,785	1.033,331	1.025,883	4.9296	4.1733
SF 32 VAC 4	0.998,863	1.032,058	1.023,078	3.2164	2.4243

(A)

PSFD 8 VAC 1	0.974,750	1.020,599	1.013,368	4.7037	3.9618
SF 32 VAC 4	1.006,669	1.049,111	1.039,676	4.2161	3.2788

TABLE 7.3.1 (B)

PSCF 108 VAC or STEEL 36

(A) FUEL

100	1.014,328	1.119,632	1.099,240	10.3817	8.3712
64	1.013,813	1.120,682	1.100,647	10.5413	8.5651
36	1.007,156	1.100,744	1.081,834	9.1923	7.4147
16	0.986,832	1.059,913	1.042,644	7.4056	5.6557
4	0.864,943	0.907,379	0.894,774	4.9062	3.4489

(B) PSCF 108 VAC or STEEL 36

100	1.015,872	1.123,650	1.102,914	10.6094	8.5692
64	1.015,859	1.125,322	1.104,930	10.7811	8.7680
36	1.010,476	1.106,811	1.087,515	9.5336	7.6240
16	0.993,742	1.070,249	1.052,486	7.6988	5.9114
4	0.885,494	0.932,617	0.919,167	5.3217	3.8027

TABLE 7.3.1 (C)

7.4 COMPARISON OF RESULTS FROM "SUPER-CELL" "HETEROGENEOUS" TYPE OF CALCULATIONS AND EXPERIMENT

For comparison purpose of the controlled effectiveness on the basis of two theories outlined in the last two sections, the percentage reactivity controlled in each case was calculated.

(a) In case of super-cell calculations, we know the theoretical leakage characterised by β_c^2 due to the introduction of the control rod and the experimental leakage $\frac{M_z^2}{M_R^2} \Delta\gamma_{11}^2$ as a consequence of the two exponential experiments performed before and after the introduction of the control rod. This is the change in leakage on the assumptions laid down in section 7.2.2. The reactivity controlled is given by

Reactivity = (leakage x migration area) 7.4.1

This is then expressed as a percentage of the total reactivity of the system before the introduction of control rod. These results are given under column 1 of Tables 7.4.1.

(b) In case of heterogeneous method, to predict the reactivity controlled, use is made of the fact that, for a clean core of a given size, the critical parameter K_{EFF} (A-III) is determined for the system. On the insertion of control rods, the new critical parameter K'_{EFF}

LATTICE	CASE	SUPER-CELL THEORETICAL ρ% 1	11	EXPERIMENT ρ% 1	11	HETEROGENEOUS B	A
PSCF 128	1/9	9.82	5.06	6.65±1.60	3.42	*	*
PSCF 32	"	8.04	4.14	5.28±1.53	2.72	3.95	*
PSF 128	"	8.98	5.00	6.88±1.58	3.45	4.93	*
PSFD 72	"	7.71	3.84	6.91±1.57	3.44	*	*
PSFD 8	"	0.75	0.38	2.59±1.49	1.29	*	4.70
SF 128	"	19.10	8.49	8.56±1.81	3.81	*	*
SF 32	"	10.78	4.79	4.96±1.61	2.20	3.22	4.22
		PSFC 108 VAC and STEEL 36					
144	1/4	139.76	76.50	17.24±1.59	9.44	*	*
100	"	138.93	76.05	17.16±1.56	9.39	10.61	10.38
64	"	136.53	74.73	15.96±1.55	8.74	10.78	10.54
36	"	132.47	72.51	12.34±1.52	6.75	9.53	9.29
16	"	122.45	67.02	7.11±1.49	3.89	7.70	7.41
4	"	101.31	55.45	1.98±1.47	1.08	5.32	4.91
		PSCF 72 VAC and STEEL 72					
144	1/2	130.73	83.04	49.92±1.50	31.71	*	*
100	"	130.18	82.69	49.80±1.49	31.63	*	*
64	"	131.99	83.84	45.12±1.50	28.66	*	*
36	"	135.73	86.22	34.31±1.48	21.79	*	*
16	"	136.05	86.42	18.68±1.48	11.87	*	*
4	"	119.30	75.78	4.82±1.46	3.06	*	*

TABLE 7.4.1

"so that the reactor is critical" is calculated. Therefore the control rod effectiveness in terms of percentage reactivity controlled will be given by

$$\rho = \frac{K'_{EFF} - K_{EFF}}{K_{EFF}} \times 100 \qquad 7.4.$$

The results are given in Table 7.4.1 under columns (A,B) for each set of data in each case. The errors in the reactivity calculated in the experimental predictions correspond to the sum of % errors in axial bucklings in experimental determination of the relaxation lengths.

The significance of the results given under Column 11 in Table 7.4.1 will be discussed in the following lines.

7.5 DISCUSSION

Let us consider the results of super-cell calculations first.

(a) These results can be sub-divided into two categories: (i) 1/9 cases and (ii) 1/4 and 1/2 cases. In the case of the first category (1/9) case, the reactivity controlled given under column 1 of the tables in section 7.4, the measure of agreement with the experimental predictions, is within reasonable limits (45), these calculations can predict. Considering each case separately PSCF (128, 32), PSF 128 and PSFD (72,8) is quite satisfactory.

While in the case of SF 128 and 32 fuel cases (16 and 4 steel rods respectively) the deviations are quite large.

The category (ii) in both the sets just do not bear any resemblance to the experimental results. The leakage (β_c^2) or the reactivity being relative terms only, the scale of difference is too large. There are many sources of error in the theoretical predictions which could be briefly summarized as below:

1) Error in thermal extrapolation length used.
2) Neglect of fast neutron absorption.
3) The extent of assumptions previously described in Section 7.2 do not hold exactly.
4) There are intense spectrum changes over a small core region.
5) The basis of the super-cell calculations, that the zone is infinite in all directions and that the control rod lies on the axis of an infinitely long square, is not true. In the present case a control rod is put at the corner of the square in case of 1/4 and in line in case of 1/2 as shown in section 7.1 except in case of 1/9. Quite a few more defects can be related in this context.

Since all these aforementioned assumptions in most of the cases under study do not hold, so one could expect these large variations in respect of the predictions of

experimental results. The experimental results cannot be contested because there is sufficient experimental as well as theoretical evidence to support the basis of experimental procedure (Chapters 2 and 3). It is believed that there is another basic reason for this discrepancy which will be discusssed in the next part of the present section.

(b) The predictions of heterogeneous theory for reactivity are consistent IF considered independently; but in comparison to experiment there are large differences.

Since the heterogeneous theoretical predictions are based on the experimental results(measured axial bucklings) and if we believe that the heterogeneous theory is right, then we should have expected agreement between the two. All through this analysis and others (16, 17) absolute agreement between theory and experiment on this concept has always been obtained. Therefore it is felt that "to derive the reactivity controlled from experiment" is suspect. In this respect it should be mentioned that in deriving a figure for reactivity the following additional information has been made use of:

i) M_z^2/M_R^2 (asymmetry factor),

ii) Original reactivity in terms of K_∞,

and iii) the migration area M_R^2 .

The asymmetry factor is fairly accurately calculated

and for that matter in the present case of PSCF 128 VAC or steel 16 it is of the order of unity anway. Therefore this cannot affect the results.

Secondly, the original reactivity (K_∞) is very close to the theoretical value as tabulated in section 7.2.3. Even the use of the theoretical value does not make any difference. Thus the error cannot certainly be attributed to these two factors. However, when the number of fuel elements concerned is very small then serious deviation due to this (K_∞) reason could be expected. It was precisely for this reason that the one-group reflector saving concept for the corresponding vacancy cases was used to predict K_∞ of the system. Though the correctness in K_∞ (Chapters 4 and 5) is for different reasons. Therefore the use of migration area (M_R^2) to calculate reactivity may be in error.

It is felt that to calculate the reactivity controlled as the product of leakage and migration area is in error if we assume that the control rod does not absorb fast neutrons. Because such a control rod is transparent to any fast neutrons and therefore in a super-cell leakage (β_c^2) it is only the thermal neutrons which are affected by the presence of the control rod. Consequently the leakage properties of the fast neutrons are not affected at all by the introduction of a control rod.

This is further substantiated by the fact that if we use the one-group super-cell formulation to calculate β_c^2 and neglect the fast neutron absorption as has been done in the present analysis, the resultant value of β_c^2 is not affected to any appreciable extent. Thus with these considerations in mind the reactivity is redefined as the product of diffusion area (core) and leakage characterised by β_c^2 or $(M_z^2/M_R^2\ \Delta\gamma_{11}^2)$ and retabulated under the column 11. The error in experimental value is not quoted but is given in the left-hand column.

Now if we compare the columns 11 of super-cell, experiment and heterogeneous reactivity results, they show excellent agreement, in case of 1/9 cases. In the case of 1/4 cases the agreement between heterogeneous theory and experiment remains good, while in the case of super-cell vs. experiment it is not changed at all except for magnitudes. In 1/2 cases of the heterogeneous theory the results could not be compared for the same reasons as given at the end of section 6.7.1. The 1/4 cases are plotted in FIG.7.5 for the purpose of comparison. The experimental error is rather large because we are interested in the differences of very small quantities and the percentage errors are added on successively (axial buckling). The sudden fall of reactivity predicted

by experiment becomes apparent because of excessive increase of K_∞ in the corresponding vacancy case, since it tends to be inaccurate after 36 fuel elements downwards.

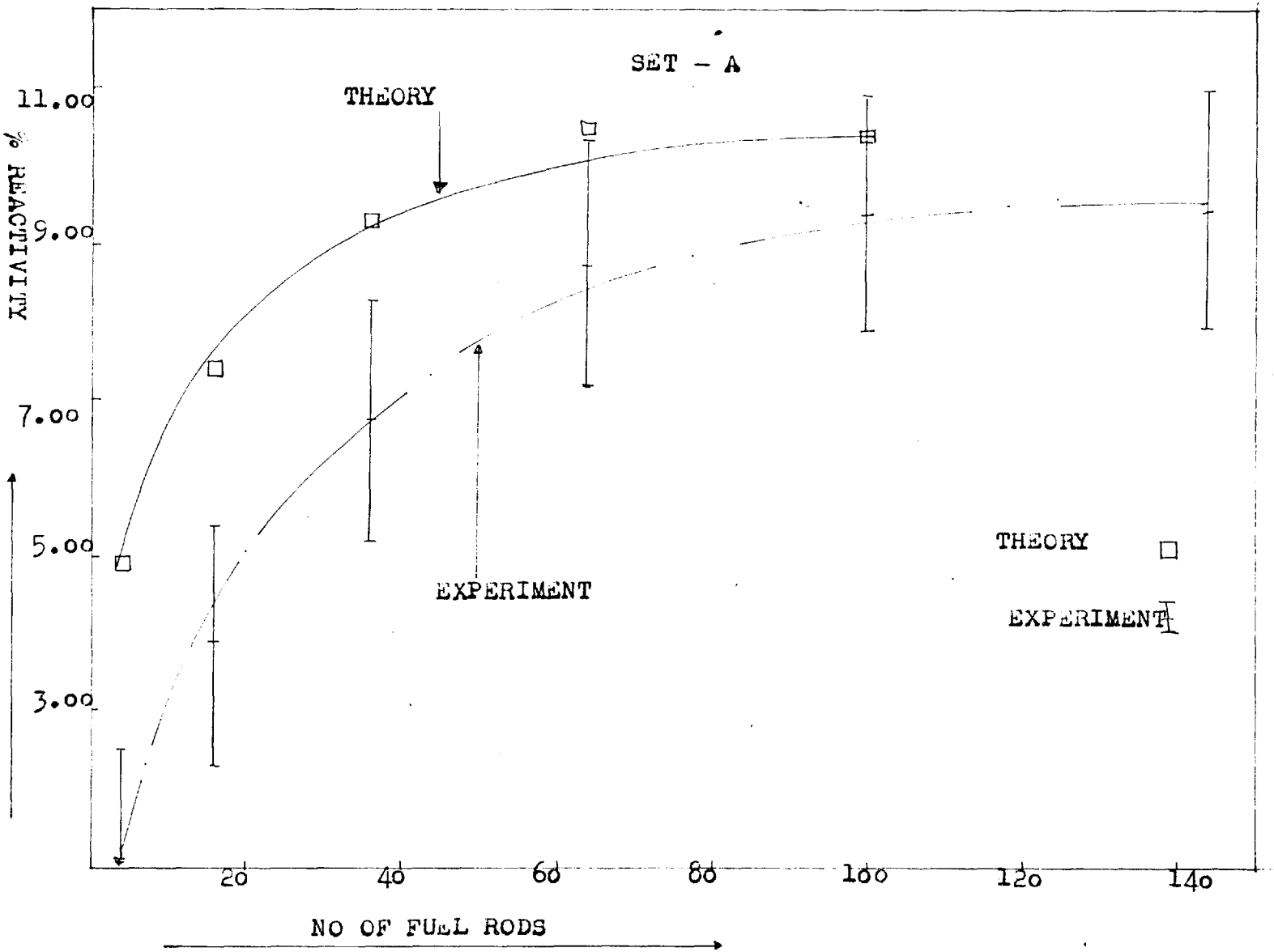

FIG. 7.5 % REACTIVITY CONTROLLED PREDICTED BY EXPERIMENT VS REACTIVITY% ON HETROGENOUS THEORY

CHAPTER 8

RESULTS FROM NUMERICAL METHODS AND COMPARISON WITH ONE- AND TWO-GROUP HOMOGENISED THEORY AND HETEROGENEOUS THEORY

8.1 INTRODUCTION

The details of the fueled assembly (fully or partially filled) cases/analysis have already been given in Chapters 3, 4, 5 and 6. The basis of analysis have been:

1) the concept of reflector savings based on one-and two-group theories of neutrons in a reactor system; and

2) two-group heterogeneous theory for finite systems based on the explicit consideration of fuel as sources of fast neutrons and sinks for thermal neutrons.

In this case it had not been possible to analyse the full fueled assembly cases because of geometrical conditions. However, the criticality predictions showed that for the heterogeneous system 16 or more fuel elements is practically infinite and there is no practical advantage in using more fuel for the purpose. Thus it (full assembly cases) does suffice to say that for the purpose of comparison with other theories 100 fuel element case is equivalent to the corresponding full assembly case.

All these twenty-nine "clean core" cases have also been analysed on

the basis of numerical methods based on the "finite difference methods" as detailed in Appendix A-2.3. (CRAM). This has been variously referred to in the text and it is thought advisable to present all results, specifically, the criticality parameter and the flux distribution for the system in each case.

8.2 INPUT DATA FOR CRAM

The programme CRAM (44) briefly described in Appendix A-2.3 is fairly commonly used (22) programme for the solution of multigroup diffusion equations by finite difference methods for reactor analysis. The reactor is divided into a number of homogeneous regions and the programme computes the critical value of K.

All fueled cases of the sub-critical assembly have been solved in two dimensions X and Y by indicating "GEOMETRY XY" in the GC (General Constants) card. The measured axial buckling (Chapter 2) has been used to take account of the 3rd direction (Z) in the form of net-flow of neutrons into the system because of the presence of neutron sources at the bottom. The sign of the axial buckling being negative, since the term [(axial buckling)(Diffusion Coefficient)] will be added to the absorption in each group. Because of streaming corrections in the radial and axial directions, the anisotropic

diffusion coefficients were used.

The problem has been treated as symmetrical about the Y-axis and the boundary conditions under which the two-group diffusion equations

$$D_1\nabla^2\varphi_1 - A_1\varphi_1 + \frac{F_2}{K}\varphi_2 = 0 \qquad 8.2.1$$

$$D_2\nabla^2\varphi_2 - A_2\varphi_2 + C_{12}\varphi_1 = 0 \qquad 8.2.2$$

are solved, are

1)zero current at the internal boundary and

2)zero fluxes at the external boundary of the assembly.

12-mesh points of 10.16 cms were used in all cases. The core constants are taken from Tables 3.4.1 in Chapter 3 and the reflector constants given in Appendix A-1.2. Both the sets marked A and B were used. However for the purpose of valid comparison only the constants set-A should be considered. The size (width) of the assembly corresponded to the extrapolated lengths in combination with the physical width of the assembly. The measured extrapolation lengths and axial bucklings are given in Tables 2.5.1 and 2.5.2 of the second chapter respectively.

8.3 RESULTS AND DISCUSSION

All the theories referred to in section 8.1 have two experimentally measured parameters common, specifically

1) Relaxation lengths and

2) Extrapolation lengths.

Other core and reflector constants are also common with the exception of heterogeneous theory moderator constants. Because it is in the nature of the heterogeneous theory that "the homogenised parameters of a lattice cannot be used", therefore, the nearest equivalent case for valid comparisons is the set-3 of section 6.7 which are the constants set-A defined in Appendix A-1.2. The case SF is corresponding to set-6 since in the case of set-3 the programme did not work properly for all cases.

The figures given in the tables are the criticality parameters K on the basis of one-, two-group theory, heterogeneous theory and the critical constants K as predicted by the programme of A-2.3. Since all the constants in the theories are the same (specifically size and axial buckling), in theory they should predict the same critical constant. As it can be seen from Appendix A-2.3 the critical constant K is the ratio of the theoretical infinite multiplication constant to the experimental value which will be predicted in combination with

the measured material buckling of the reactor system. So all K_∞'s of the Chapters 4 and 5 for Set-A have been normalised with the theoretical value of K_∞ as reference for criticality. The measured axial bucklings are quoted alongside in the first column and no error is given because they have been already given and discussed in detail in the 2nd Chapter. Only the values for the purpose of representation have been given here. As usual, first column denotes the number of fuel elements in the assembly and the other symbols are the familiar ones. The resultant critical constants are given in Table 8.3.

Before considering the critical evaluation of each theory in comparison to the other, let us consider the criticality constant as predicted by the numerical methods given in Table 8.3 under CRAM A and B. The figures under the heading A and B correspond to reflector constants set-A and set-B (A-1.2) in combination with core constants given in Table 3.4.1. Obviously the set-A reflector constants give better results as compared to the set-B.

In the first three sets, PSCF, PSF and PSFD, the critical constant K predicted, is a very good fit down to 36 (PSCF), 16 (PSF) and 25(PSFD) cases of fuel elements in the assembly. Therefore, it seems to imply that the

PSCF

CASE	AXIAL $\times 10^{-4}$ cm^{-2}	ONE GROUP	TWO-GROUP	HETERO. THEORY	CRAM A	CRAM B
144	2.040	1.004492	1.003275	*	1.005617	1.005017
100	2.122	1.003276	1.003762	1.012380	1.005629	1.003002
64	2.415	0.997519	0.997848	1.011620	1.002886	0.998132
36	3.100	0.984611	0.977568	1.007061	0.996469	0.989227
16	4.235	0.947099	0.911023	0.990602	0.978885	0.968420
4	5.572	0.833981	0.701739	0.903273	0.893273	0.879563

PSF

144	2.119	1.007411	1.006266	*	1.005588	1.005588
100	2.186	1.007164	1.007766	1.017642	1.007193	1.002472
64	2.469	1.003006	1.002925	1.017337	1.006373	0.997486
36	3.155	0.994110	0.985167	1.016266	1.005656	0.991320
16	4.285	0.962730	0.920852	1.008966	1.001517	0.977521
4	5.617	0.857766	0.711412	0.962668	0.973142	0.921704

PSFD

121	2.152	1.009302	1.009322	1.017752	1.009379	1.007583
81	2.300	1.005973	1.007144	1.017930	1.008142	1.002427
49	2.599	0.988884	0.986915	1.004955	0.993324	0.984270
25	3.669	0.980303	0.961566	*	1.000002	0.986543
9	4.955	0.918094	0.842383	0.995420	0.978595	0.960322

SF

144	2.178	1.002322	1.000812	*	0.981730	0.981730
100	2.273	0.996839	1.000521	*	0.977498	0.970782
64	2.476	0.985293	0.990118	1.009211	0.967620	0.955725
36	2.908	0.962425	0.959555	1.010112	0.947434	0.930180
16	4.433	0.799181	0.672152	0.952894	0.739229	0.712866

cont..

TABLES 8.3.1

OCF

144	2.317	1.004996	1.003613	*	0.960947	0.960947
100	2.387	0.988626	0.994163	1.006430	0.945138	0.941942
64	2.559	0.968867	0.976610	1.007850	0.926626	0.920751
36	2.896	0.934340	0.935207	0.998858	0.893691	0.885563
16	3.488	0.873665	0.845085	0.976588	0.833142	0.823037
4	4.124	0.748775	0.633308	0.852930	0.636187	0.627152

TABLES 8.3.1

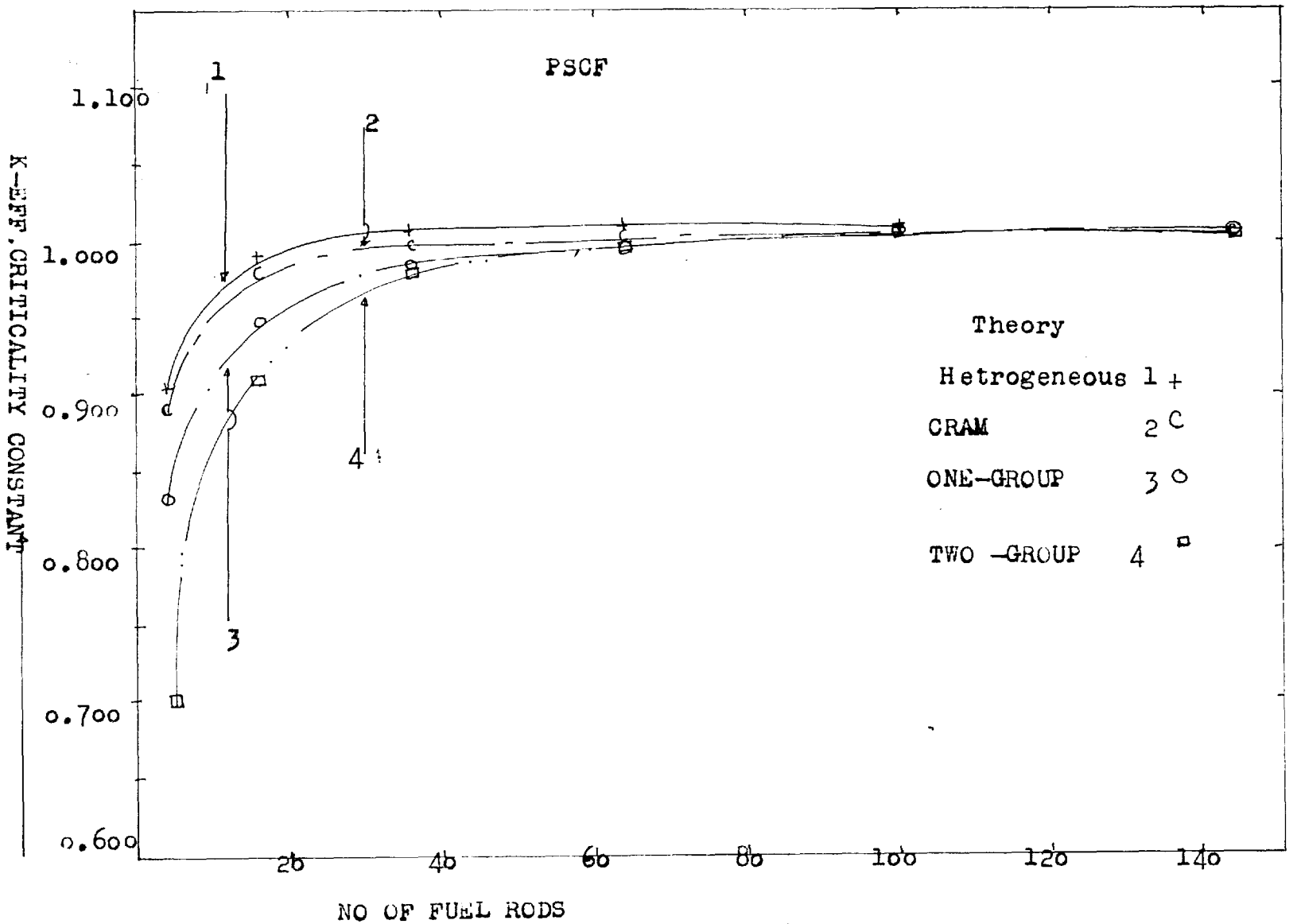

FIG. 6.3 K-EFF. VS NO OF FUEL RODS IN ASSEMBLY (ALL THEORIES)

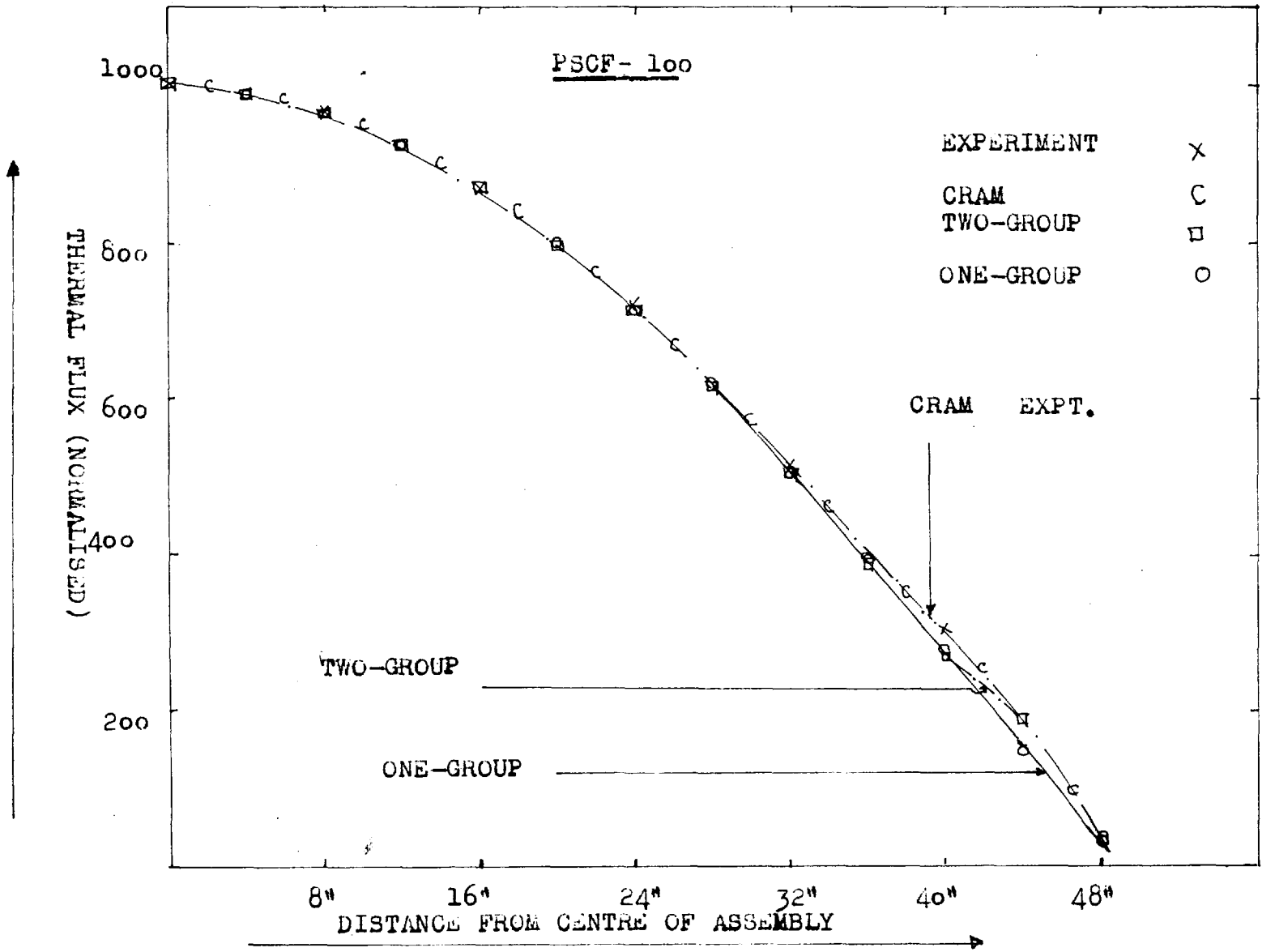

FIG. 8.3 COMPARISON OF THEORETICAL FLUX FROM ONE-, TWO-group THEORY AND NUMERICAL METHODS WITH EXPERIMENT.

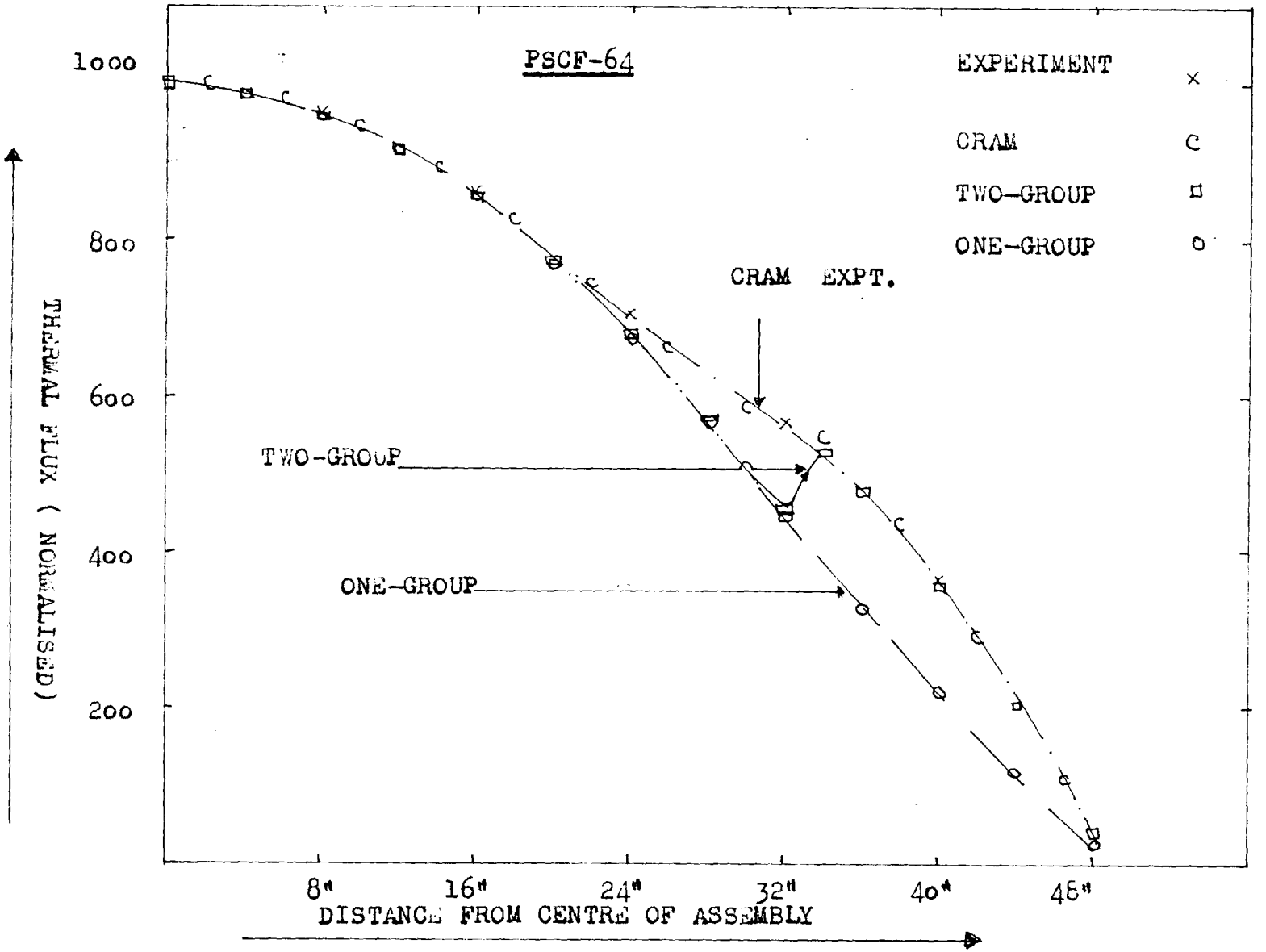

FIG. 8.3 COMPARISON OF THEORETICAL FLUX FROM ONE-, TWO-GROUP THEORY AND NUMERICAL METHODS WITH EXPERIMENT.

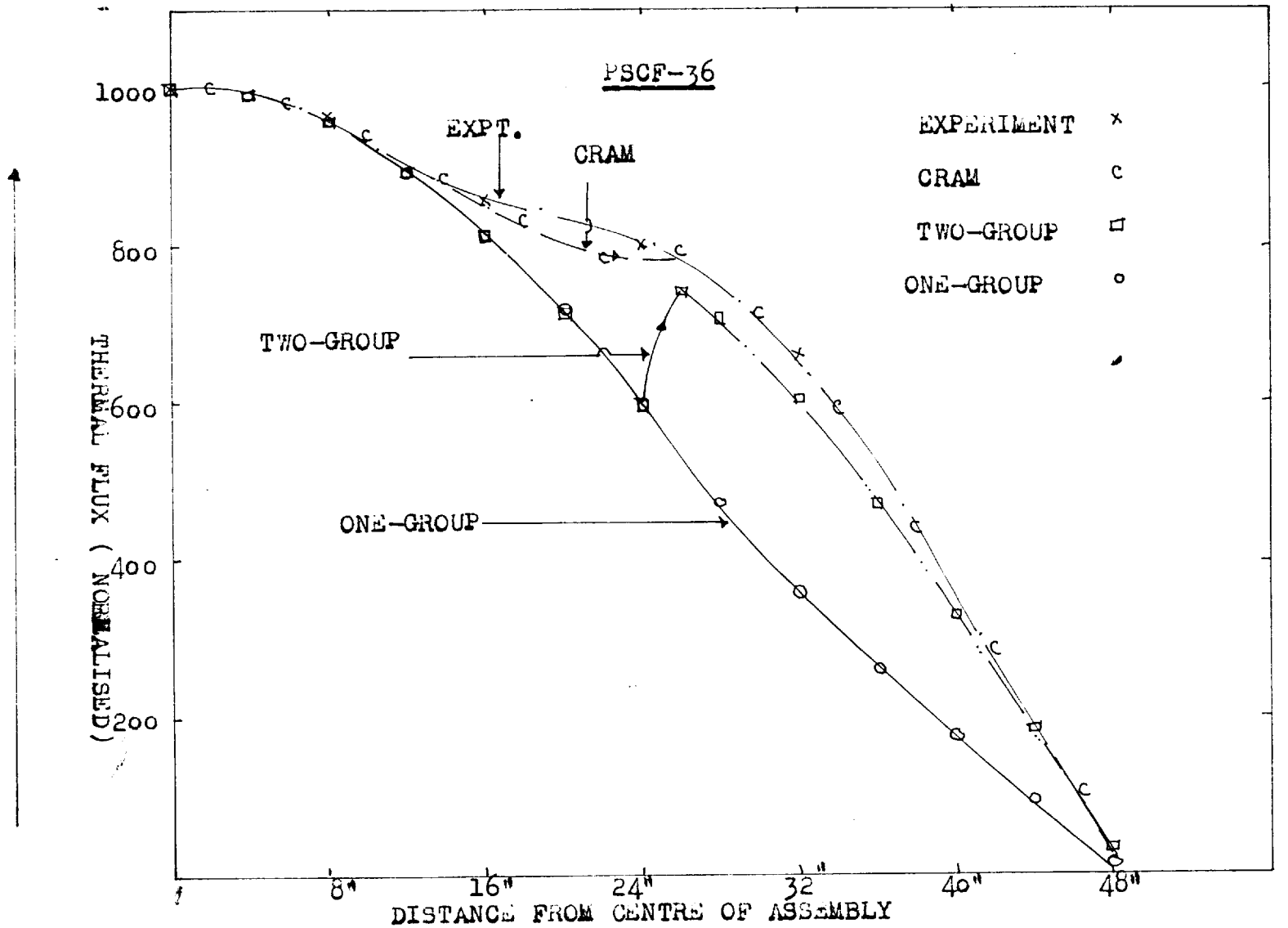

FIG. 8.3 COMPARISON OF THEORETICAL FLUX FROM ONE-, TWO-GROUP THEORY AND NUMERICAL METHODS WITH EXPERIMENT.

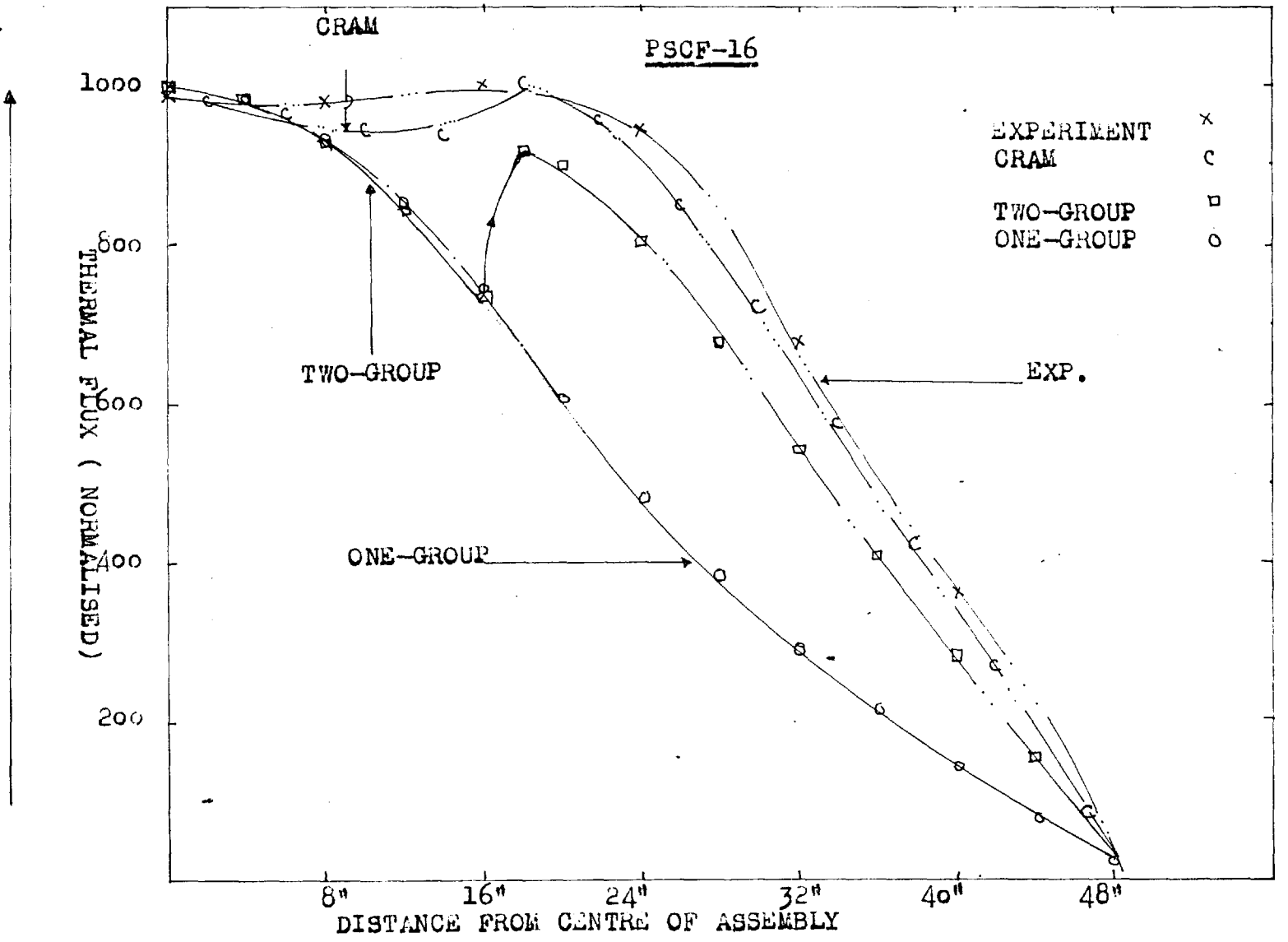

FIG. 8.3 COMPARISON OF THEORETICAL FLUX FROM ONE-?TWO-GROUP THEORY AND NUMERICAL METHODS WITH EXPERIMENT.

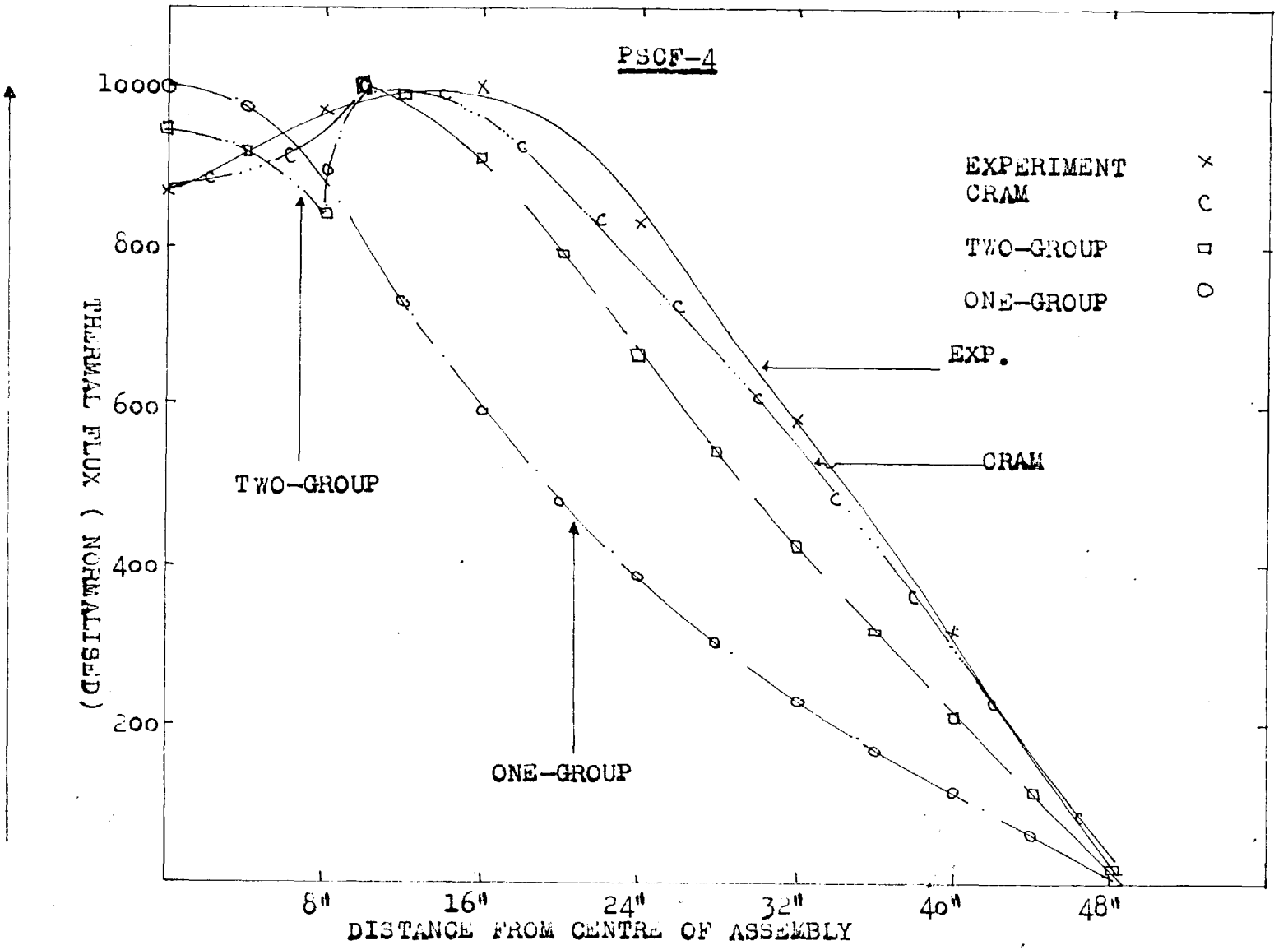

FIG. 8.3 COMPARISON OF THEORETICAL FLUX FROM ONE-, TWO-GROUP THEORY AND NUMERICAL METHODS WITH EXPERIMENT.

consideration of an average flux over the mesh point for a small core is approximation only. This is in accord with the physical reasoning, because, for a very small core, there are intense flux variations over a small region and it is bound to over-estimate the leakage from the reactor core. However, it is to be pointed out that the void ratio in these three cases is $\approx$ 6% and 8% respectively.

In the case of SF and OCF results these imply that the lattice parameters are not correct even for the full assembly. Because even for full assembly the numerical methods fail to predict criticality which obviously is due to incorrect streaming corrections, and hence inaccurate characteristic areas.

The under estimation is less in case of SF and quite substantial in case of OCF.

Since in the present analysis the mesh-point spacing and other characteristic constants were kept identical to the solid graphite cases, perhaps change of mesh spacing might help to improve the results. Obviously this is due to over-estimation of the neutron leakage from the reactor system, because the flux distribution is assumed to be constant over a mesh-region as detailed in A-2.3. But from physical point of view there is flux variation (macroscopic) in addition to local flux variation

(Chapter 3) due to the presence of fuel in the region.

Now let us consider all the theoretical results in comparison to each other. First of all it would be right to say that the heterogeneous theory over-estimates the criticality to some extent. It is very difficult to estimate exactly because of the boundary (cylindrical-isation of the sub-critical assembly) effects and for this precise reason the critical constant was normalised (Table 6.7.3) to the maximum to give a fair idea of the point where serious deviation starts to become apparent.

The numerical method (CRAM) predicts the criti-cality of the system much better than its counterpart in the homogenised field of reactor analysis, where the numerical method (SF and OCF cases) fails to predict the criticality parameter in combination with the measured axial buckling. The two theories, namely one- and two-group theory, are very good in comparison to numerical method for large channels. The one-group theory con-tinues to predict a comparatively correct answer with regard to two-group theory at a cost of the neglect of various other physical reasons. Two-group theory is equally instructive in that it shows the physical break-down of various assumptions (FIG.5.3.1 last).

Finally, the heterogeneous theory seems to predict the best parameter down to 16 fuel elements in almost all

cases and in case of PSFD even 9 fuel elements, it is 0.9954 only 0.46% less than the criticality constant (unity) for a critical system.

For the purpose of comparison, the critical constants of all theories are plotted in FIG.8.3(A) and since the variation of all the rest is identical except for magnitudes they have not been considered.

The flux distribution predictions of heterogeneous theory can not be compared with those of the rest since this predicts the flux over the fuel region while the others (homogenised) represent the macroscopic picture of the flux shape. Therefore, heterogeneous theory is not considered in this context. The flux predictions of CRAM, two- and one-group theory are tabulated in Appendix A-2.6 and only representative five flux plots for PSCF 100, 64, 36, 16 and 4 fuel elements are shown.

The relationship of theoretical one- and two-group flux distributions has already been discussed in the appropriate places. Here they are plotted to show the limitations of each. The thermal flux distribution predicted by the numerical methods is by far the best in comparison to experiment. The deviations become apparent only when the number of fuel elements is 36 and less. This can be improved upon by selecting appropriate mesh-spacing. In this regard it is reasonable

to say that the numerical methods are comparable to those of the heterogeneous theory.

CHAPTER 9

CONCLUSIONS

The purpose of the present project has been to investigate the behaviour of a sub-critical assembly as a function of fuel loading. The theoretical and experimental results have been discussed in each chapter separately. The broad outline of the conclusions reached can be summed up briefly as below.

1) The experimental measurements of relaxation lengths and extrapolation lengths carried out over the vast spread of lattice arrangements leads to the conclusion that a sub-critical assembly is and will remain a powerful tool for reactor analysis unless a reactor facility is available for the purpose.

2) The computed parameters, namely relaxation lengths and extrapolated length from flux measurements, verify the fact that the size of the assembly is quite large for measurements of the relaxation length in an asymptotic region so that the accuracy in the fitting process is much less than the maximum experimental error due to other causes.

3) Neglect of harmonics and restricting the measurements to a region away from boundary effects give satisfactory agreement with previous measurements (4) wherein all harmonics have been considered.

4) In full assembly cases (in some cases only in an implied way) the agreement between theory and experiment is very good.

5) The process of homogenization has been extended to the limit (half fuel taken out but implying assembly is full); even then the unit-cell concept retains its integrity and is in marked agreement with the experimental predictions.

6) The experimentally measured axial and material bucklings are within the limits of accuracy, an exponential experiment can predict.

7) The measurements of criticality constants for four clean core cases with varying size of coolant channels are in accord with already established methods (7) of calculation.

8) The calculated parameters (7) have been used to predict the behaviour of a partially fueled assembly, which in turn have been used to predict the critical parameters of a large reactor.

9) A simple approach to the case of a partially fueled assembly on the basis of one-group theory does give satisfactory results within its limitations.

10) A rigorous treatment (two-group theory) of the reflected core assembly shows improvement over the simple approach. However the approach is very instructive and

revealing in that one can see the physical breakdown of the basic assumptions.

11) The measured thermal flux distributions are in good agreement if the number of fuel elements is at least 64. With anything less than this number of fuel element cases a process of degeneration sets in.

12) The numerical methods predict the behaviour of the reactor system under investigation fairly well if the void ratio in the lattice does not exceed 8%.

13) The experimentally measured and theoretically calculated flux distributions (two-group and numerical methods), though strictly not in agreement (in extreme cases), do emphasize the excessive leakage from a small core, reflected system, which indirectly shows the importance of a reflector outside the core through the increase of cross-hatched area under the integral curve.

14) Analysis of the cases under study on the basis of two-group heterogeneous (source-sink) theory for finite systems has been much more satisfactory than its counterpart method of analysis.

15) The radial diffusion coefficient (thermal and fast) have therefore been defined for a reflector (7) in a more realistic way. These diffusion coefficients in conjunction with heterogeneous theory predict the Eigen-value much more satisfactorily than all the sets tried. However, for

nearly full assembly cases this definition improves the agreement between theory and experiment in most of the cases (set-B).

16) In going over the heterogeneous methods, the flux distribution for less number of fuel elements is much more satisfactory than in the case of homogenised concept and is in very good agreement with experimental measurements.

17) The chief advantage in heterogeneous analysis is the control rod effectiveness study. The homogenised concept of a reactor super-lattice is suitable for very large reactors when the amount of absorber present is comparatively small. Even then, the predictions have a wide range of variation. But in case of heterogeneous theory the smaller size (not excessively small) does not affect the results significantly.

It may be added as a final remark that heterogeneous method of reactor analysis is best if the number of fuel elements involved is small and/or if it concerns the control rod effectiveness investigations. But for very large reactors there is no practical advantage in doing these sophisticated calculations; the homogenised concept of a lattice does present the basic characteristics fairly accurately and there is no difference between the two theories.

The present theoretical analysis is not absolutely complete in all respects. The possible improvements may be briefly listed below.

1) The partial fuel loadings of the assembly cases, and the analysis on the basis of one-and two-group theorygo seriously wrong in all respects when the number of fuel elements is less than 36. The results should, therefore, be analysed by considering the core as a "cylinder" rather than a "slab" for 36 or a lesser number of fuel elements.

2) In case of heterogeneous analysis some account should be taken of the boundary effects.

3) The increase in resonance escape probability for a small core surrounded by a reflector should be considered. At least this fact alone will account for serious deviations in the results for 4 and in some cases for 16 fuel elements.

4) Finally, it is to be said that in the present analysis the thermal constant in heterogeneous calculations has been kept constant. It may well be instructive to keep η constant and thermal constant γ_h is treated (46) as Eigen-value. This would certainly help to check the accuracy in the value of the thermal constant.

N O T A T I O N

Indices

F of f	Fast
g	graphite or geometrical
c	core
M or m	thermal
n	can or number
o	diffusion area, or uranium
u	uranium
R	radial
S	slowing down
z	axial
r	reflector or radial

List of Symbols

A,B,C,	Arbitrary constant
D	diffusion coefficient
E	neutron energy
F	arbitrary constant
G,H	constants
I_o, I_1	modified Bessel functions of the first kind
K_o, K_1	modified Bessel functions of the second kind
J_o, J_1	Bessel functions of the first kind
Y_o, Y_1	Bessel functions of the second kind
L^2	length squared
M^2	migration area
S_i	effective density of element 'i' to reference density
N	thermal
b_{11}	Fundamental mode of relaxation length in the vertical direction
W	Westcott flux n/cm²-sec.
P	resonance escape or collision probability
Q	source term or constant
K_∞	infinite multiplication constant
K	Eigen value
σ	microscopic cross-section
Σ	macroscopic cross-section
Φ	neutron flux n/cm^2-sec or $\frac{\text{Void}}{\text{V(solid)}}$ ratio
δ	reflector saving (cm)
T	relfector thickness (cm)
a'	width of fuel region in the partially filled assembly case (cm)
a	extrapolated width of the assembly (cm)
B^2	buckling (cm^{-2})
γ_{11}^2	fundamental mode axial buckling
$\mathcal{f}$	migration area asymmetry (M_z^2/M_R^2)
λ	linear extrapolation length (cm)
ξ	average logarithmic energy decrement
μ^2	fundamental mode radial buckling (cm^{-2})
ν^2	higher mode radial buckling.

Other notation is explained in the text.

REFERENCES

1) Glasstone, S. and Edlund, M.S. "The Elements of Nuclear Reactor Theory", New York, D. Van Norstrand Co. (1960).

2) Meghreblian, R.V. and Holmes, D.K. "Reactor Analysis" 1960.

3) Galanin, A.D. "Thermal Reactor Theory", Pergamon Press (1960).

4) Macdonald, D.A.N., Ph.D. Thesis, University of London, 1965.

5) Till, C.E. Studies on a Graphite Natural Uranium Exponential Assembly". University of London Ph.D. Thesis, 1961.

6) Pershagen, B. and Varvik, I. AEF-71, Atomenergi, Sweden.

7) Syrett, J.J. AEEW-R.94.

8) Brown, G. AERE R/R 2697.

9) Smythe, W.D. M.Sc. Thesis, University of London, 1962.

10) Campbell, C.G. and Freemantle, R.G. AERE RP/R 2031.

11) Horning, W.A. "Small Source Theory of Thermal Reactors", HW-24282.

12) Feinberg, S.M. Proc. Int. Conf. on the Peaceful Uses of Atomic Energy. PP484-500, Vol.5, Geneva, 1956.

13) Galanin, A.D. Proc. Int. Cof. Geneva, P.477-83, Vol.5, 1956.

14) Leslie, D.C. AEEW-M 18, 1959.

15) Leslie, D.C. AEEW-R 272.

16) Jonsson, A. et al. Proc. Int. Conf. Geneva P/683 1964.

17) Jonsson, A. RFR-181, 1962.

18) Sneddon, I.N. "Finite Fourier Transforms", McGraw-Hill Book Co. (1951).

19) Watson, G.N. "A treatise on the theory of Bessel functions". Cambridge University Press, 1922.

20) Klahr, C.N. et al. NYO-2680, 1961.

21) Näslund, G. TPM-RFN-176, 1964.

22) King, D.C. et al. AEEW-R 428.

23) British Industries Collaborative Exponential Programme. ("BICEP") Vols. I, II and III. AEEW-R 235.

24) Grant, I.S. AERE R/R 2568.

25) Zink, J.W. NAA-SR-3222, 1959.

26) Stuart, G.W. Proc. A. Conf. Geneva, Vol.16, P/624, 1958.

27) Nemarch, D.A. AERE RP/R 1957.

28) Cohen, E.R. Nucl. Sci. Eng., Vol.1, 1956.

29) Brown, C. et al. AERE R/R 2697, 1959.

30) Meetz, K. Naturforschung, Z.F. Band 12a, 1957.

31) Reactor Handbook. Sodak, H. (Editor). Vol.3, Part A. John Wiley & Sons, New York, 1962.

32) Auerbach, T. et al. A. Conf. P/690, 1964.

33) Carter, C. Reactor Science and Technology, J. Nucl. Energy, Vol.15, p.76-80, 1961.

34) Galanin, A.D. et al. I.A.E.A. Symposium on Heavy Water Lattices, PL-73/30, 1963.

35) Buckler, A. et al. TRG Report 227 (R).

36) Gibson, M. et al. AEEW-R. 211.

37) Kusneriuk, S.A., McKay, C. and Davison, B. Reports CRT-666 (1956), CRT-712 (1956), TPI-45 (1956).

38) Gahfoor, M.A., M.Sc. Thesis, University of London 1964.

39) C rter, C. et al. Reactor Science and Tech. J. Nuclear Energy, Vol.15, Oct. 1961.

40) Johnson, P.W. "PARFIT" Imperial College Report 1965.

41) Benoist, P. Translated by Grant, I.S. AERE Trans. 842.

42) Topping, J. Errors of observations and their treatment. 1955.

43) Campbell, C.G. et al. AERE M 1020, 1962.

44) Hassit, A. "CRAM" TRG. Report 229 (R).

45) Grant, P.J. Private Communication.

46) Albertoni, S. et al. EUR 1839.C, 1964.

APPENDIX-I

A-1.1 NOMENCLATURE OF THE LATTICES

To facilite the understanding of the various terms used in the text to denote various lattices and to avoid verbosity of writing the same expression again and again, certain notation has been used. The following letters in this context have special importance:

N = No Fuel

P = Plug

S = Sleeve

C = Corner or channel depending upon its relationship

O = Open

F = Fuel

D = ODD (not very often used)

B = Block.

It may be noted specially B, C, P and S are the initials of the graphite components used to build-up the lattices under study. Since B (block) is the basic unit with which a lattice is constructed and is present in all cases, therefore it is omitted from the name of the lattice. The letters P, S and F denote the presence of the respective components in the cell. The letter N is often used to imply the negation of fuel. Even if F is written and N is there

it would mean that there is NO fuel in the sub-critical assembly.

In one case of fueled lattices the lattices of squares of odd numbers were also possible, so the word Odd is sometimes attached to the name of a lattice since the corresponding K_∞ etc. change from its counterpart. Now it remains to make clear the significance of C. C may denote "Corner hole filled with graphite" or it may mean "channel" in conjunction with "Open". With this notation following lattices will be frequently mentioned in the text.

A lattice name below would imply the presence of

PSCF = plug-sleeve-corner-fuel (meaning that these components of the lattice are present, the block being understood to be there).

PSF = plug-sleeve-fuel are present while the corner holes are empty.

SF = sleeve-fuel (no plug and no corner filling).

OCF = open-channel-fuel (means plug and sleeve have been taken out of the lattice and no corner filling).

These are the four main lattices and placing N before F will negate the presence of fuel; at the same time it would retain its identity, e.g. OCNF means open channel No Fuel lattice; to put it briefly, only blocks constitute the lattice. It seems difficult, but was found

to be most useful in the present study. Sometimes numbers with notation will tell the "number of fuel elements" in the stack.

In this sense the notation PSCF-64 means the lattice is PSCF and only 64 fuel elements are present.

It may be mentioned that why it has been necessary sometimes in the text to distinguish between PSF-100 and PSF-81 as PSF-100 and PSF (ODD) -81 or more precisely PSFD-81, is that in the case of PSF, the fuel rods are placed at the centre of the fuel lattice while in the case of PSF(ODD) or PSF 81 the fuel position is not at the centre of the lattice but in the corner hole position which is normally used for flux measuring purposes.

In the control rod effectiveness studies, a variety of vacancy cases was investigated. For that the notation adopted was to put VAC instead of vacancy and write how many vacancies there are. For example, in the case of full sub-critical case PSCF let us suppose we create one vacancy per nine fuel lattices, then it is understandable to say PSCF 128 VAC 16; meaning that in the case of PSCF case there were 16 vacancies created in a matrix of 128 fuel elements in the sub-critical assembly. And if the vacancies have been filled with steel it is as easy to write PSCF 128 Steel 16, and so on. This notation has been made clear diagrammatically in

FIGS. A-1.1.

The dimensions of the graphite and fuel components are given below.

Dimensions:

Lattice pitch = 8'.0

Equivalent radius = 4.515"

1) Block 8' square with 4.25" diameter hole with 0.625" corner squares.

Density = 1.751 gm/c.c.

2) Sleeve. Outer radius = 3.875"

Inner radius = 3.375"

Density = 1.696 gm/c.c.

3) Plug. Outer radius = 3.357"
Inner radius = 1.220"

Density = 1.748 gm/c.c.

4) Corner square hole side = 1.25"
Density = 1.748 gm/c.c.

5) Can. The inner radius of the inner aluminium can was assumed equal to the outer radius of uranium fuel and the aluminium was homogenised up to the outer diameter of can = 1.0625".

Density = 99.99% pure

Reference density = 2.73 gm/c.c.

6) Fuel. 1" diameter slugs of 18.59 gm/c.c. density. Length of one slug is 11.56" and there are 8 slugs in one fuel element.

A-1.2 THE PROCESS OF HOMOGENISATION AND REFLECTOR CONSTANTS

The basis of the unit cell model is the study of homogenised cell in a reactor system. In the case of graphite moderated reactors there are always holes and gas spaces for one reason or another. To represent the parameters of such a cell a graphite of reduced density is supposed to exist so that the reaction rates remain constant while the gas spaces do not show up as defects in the system. It is therefore very important to understand the extent to which the process of homogenisation has been applied and the limit to which this process works out. In the next few lines in each lattice the formula for homogenisation has been written.

1) In case of PSCF

$$\rho_{PSCF} = \frac{(\text{Block area})(\rho_B)+(\text{sleeve area})(\rho_{Sl})+(\text{plug area})(\rho_{Pg}) + (\text{sq.hole area})(\rho_{Sq})}{\text{Total lattice area-area of inner circle of plug}}$$

$S_{G_{PSCF}}$ = 1.013,568.

ρ = density of graphite while the subscript is the component referred.

2) PSF

$$\rho_{PSF} = \frac{(\text{Block area})(\rho_B)+(\text{Sleeve area})(\rho_{S1})+(\text{plug area})(\rho_{Pg})}{\text{Total lat. area - (plug inner circle area)}}$$

$$S_{G_{PSF}} = 0.987,841$$

3) PSF (ODD)

$$\rho_{PSFD} = \frac{(\text{Block area})(\rho_B)+(\text{Sleeve area})(\rho_{S1})+(\text{plug area})(\rho_{Pg})}{\text{Total lat. area - (sq. hole area)}}$$

$$S_{G_{PSFD}} = 0.993,474$$

Note $\rho_{PSF} \neq \rho_{PSFD}$ because the sq. hole area $\neq$ plug inner circle area.

4) SF

$$\rho_{SF} = \frac{(\text{Block area})(\rho_B)+(\text{Sleeve area})(\rho_{S1})}{\text{Total lat. area- (inner sleeve area)}}$$

$$S_{G_{SF}} = 0.983,961.$$

5) OCF

$$\rho_{OCF} = \frac{(\text{Block area})(\rho_B)}{\text{Total lat. area - (inner block area)}}$$

$$S_{G_{OCF}} = 1.028,719.$$

6) One VACANCY per nine lattices. Only for one lattice the process is written;for others it would be similar

$$\rho_{PSCF128VAC16} = \frac{(\text{Bl.area})(\rho_B)+(\text{Sl.area})(\rho_{Sl})+(\text{Pl.area})(\rho_{Pg})}{\text{Total lat.area}-(\text{plug inner area})+\frac{\text{plug inner area}}{9}}$$

7) In case of one vacancy per four and two lattices, 9 in the above relationship will be replaced by 4 and 2 respectively.

The core constants are given in Chapter 3 and reflector constants (7) are tabulated in this section for reference.

REFLECTOR CONSTANTS

A-CASES

	D_{MR}	D_{MZ}	D_{FR}	D_{FZ}	$\frac{V(SOLID)}{V(REF)}$
PSCNF	0.933,148	0.959,450	12.746,478	13.105,757	0.942,858
PSNF	0.948,931	1.001,730	12.913,717	13.632,229	0.919,026
PSNF(ODD)	0.955,239	1.008,372	12.999,588	13.722,657	0.919,026
SNF	1.240,674	1.609,367	16.330,041	21.182,857	0.798,994
OCNF	1.519,298	2.240,942	19.501,269	28,764,091	0.754,508

B-CASES

PSCNF	0.971,625	0.999,012	13.272,056	13.646,149	0.981,735
PSNF	1.013,680	1.070,081	13.794,866	14.562,406	0.981,735
PSF(ODD)	1.014,079	1.070,485	13.800,327	14.567,935	0.975,636
SNF	1.335,740	1.732,683	17.581,317	22.805,975	0.860,216
OCNF	1.567,285	2.311,724	20.117,227	29.672,620	0.778,340

TABLES A.1.2

REFLECTOR CONSTANTS (STREAMING FACTORS)

A-CASES / B-CASES	S_{MR}	S'_{MZ}/S_{MZ}	S_{FR}/S_{FZ}	S'_{FZ}	M_Z^2/M_R^2
PSCNF	1.054,806	1.084,537	1.050,779	1.080,397	1.028,187
		1.072,422		1.064,369	
PSNF	1.072,540	1.132,215	1.064,460	1.123,686	1.055,640
		1.107,890		1.091,730	
PSNF (ODD)	1.085,826	1.146,222	1.077,648	1.137,590	1.055.622
		1.121,601		1.105,247	
SNF	1.606,615	2.084,055	1.542,200	2.000,498	1.297,171
		1.888,430		1.759,601	
OCNF	2.178,187	3.212,794	2.038,987	3.007,477	1.474,986
		2.787,183		2.508,785	

DIFFUSION AND SLOWING DOWN AREAS

A-CASES / B-CASES	L_R^2 cm^2	L_Z^2 cm^2	L_{SR}^2 cm^2	L_{SZ}^2 cm^2	L_o^2/L_{So}^2 cm^2
PSCNF	2777.43	2855.72	337.00	346.50	2633.12
					320.71
PSNF	2949.24	3113.34	359.39	379.39	2749.77
					337.63
PSNF (ODD)	2955.66	3120.06	359.73	379.74	2722.04
					333.81
SNF	4448.92	5771.01	524.81	680.76	2769.12
					340.30
OCNF	5571.19	8217.43	634.80	936.32	2557.72
					311.33

TABLES A-1.2

A-CASES REFLECTOR CONSTANTS

CASE	D_{MR}	D_{MZ}	D_{FR}	D_{FZ}	$\frac{V(SOLID)}{V(REF)}$
PSCNF 128 VAC 16	0.929,585	0.952,927	12.703,116	13.022,090	0.942,858
PSNF128 VAC 16	0.943,603	0.990,459	12.851,683	13.489,846	0.919,026
PSF(ODD) 128 VAC 16	0.949,164	0.990,269	12.927,469	13.569,033	0.919,026
SNF 128 VAC 16	1.185,927	1.497,362	15.684,936	19.803,936	0.798,994
PSCNF 108 VAC 36	0.925,174	0.944,958	12.649,236	12.919,722	0.942,853
PSCNF72 VAC 72	0.916,953	0.929,979	12.549,056	12.727,327	0.942,858

B-CASES REFLECTOR CONSTANTS

PSCNF 128 VAC 16	0.969,916	0.994,270	13.254,248	13.587,061	0.983,764
PSNF 128 VAC 16	1.010,073	1.060,229	13.756,981	14.440,097	0.983,764
PSF(ODD) 128 VAC 16	1.010,380	1.060,523	13.761,222	14.444,163	0.978,299
SNF 128VAC 16	1.208,981	1.526,469	15.989,836	20.188,905	0.814,525
PSCNF 108 VAC 16	0.967,806	0.988,501	13.232,107	13.515,057	0.986,299
PSCNF 72 VAC 72	0.963,644	0.977,333	13.188,044	13.375,392	0.990,867

TABLES A-1.2

REFLECTOR CONSTANTS (STREAMING FACTORS)

A-CASES
B-CASES

CASE	S_{MR}	S'_{MR}	S_{FR}	S'_{FZ}	M_z^2/M_R^2
PSCNF 128VAC 16	1.048,611	1.074,941 1.064,213	1.045,044	1.071,285 1.057,080	1.025,110
PSNF 128VAC 16	1.064,317	1.117,167 1.095,627	1.057,161	1.109,655 1.081,314	1.049,656
PSF (ODD)128 VAC 16	1.076,001	1.129,401 1.107,636	1.068,770	1.121,811 1.093,174	1.049,628
SNF128 VAC 16	1.508,485	1.904,626 1.742,450	1.455,007	1.837,105 1.635,495	1.262,609
PSCNF 108VAC 36	1.040,955	1.063,214 1.054,146	1.037,940	1.060,135 1.048,116	1.021,384
PSCNF 72 VAC 72	1.027,072	1.041,662 1.035,719	1.025,095	1.039,657 1.031,766	1.014,206

REFLECTOR CONSTANTS
DIFFUSION AND SLOWING DOWN AREAS

A-CASES
B-CASES

CASE	L_R^2 cm^2	L_Z^2 cm^2	L_{SR}^2 cm^2	L_{SZ}^2 cm^2	$2L_o^2/L_{So}^2$ cm^2
PSCNF 128VAC16	2764.38	2833.79	336.55	345.00	2636.23 322.04
PSNF128 VAC16	2937.42	3083.28	358.41	376.20	2759.91 339.03
PSF(ODD) 128VAC16	2940.54	3086.47	358.71	376.51	2732.84 335.62
SNF128 VAC16	4312.37	5444.83	513.17	647.94	2858.74 352.70
PSCNF108 VAC36	2755.94	2814.87	335.98	343.17	2647.51 323.70
PSCNF72 VAC72	2742.00	2780.95	334.82	339.58	2669.73 326.63

TABLES A-1.2

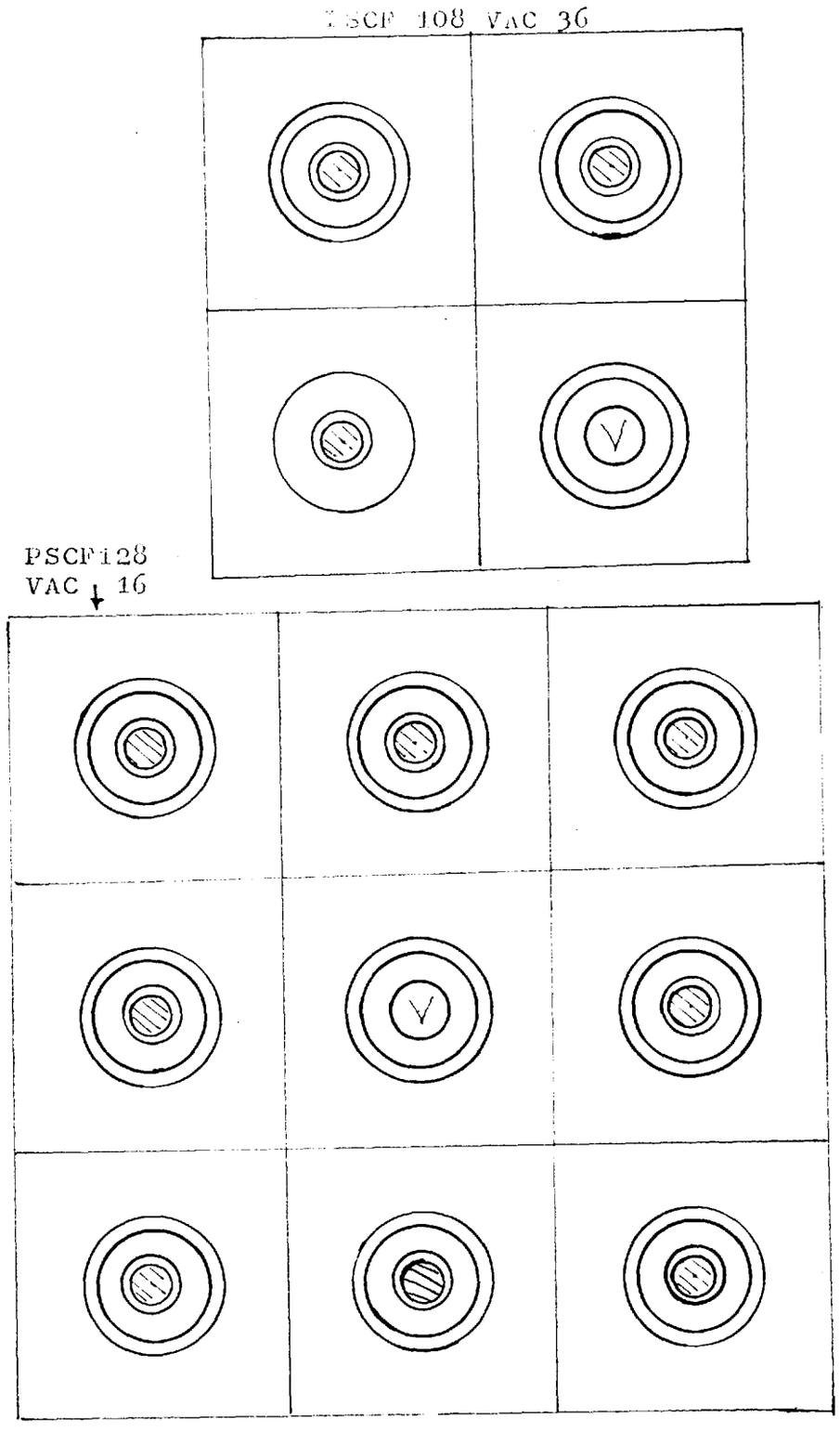

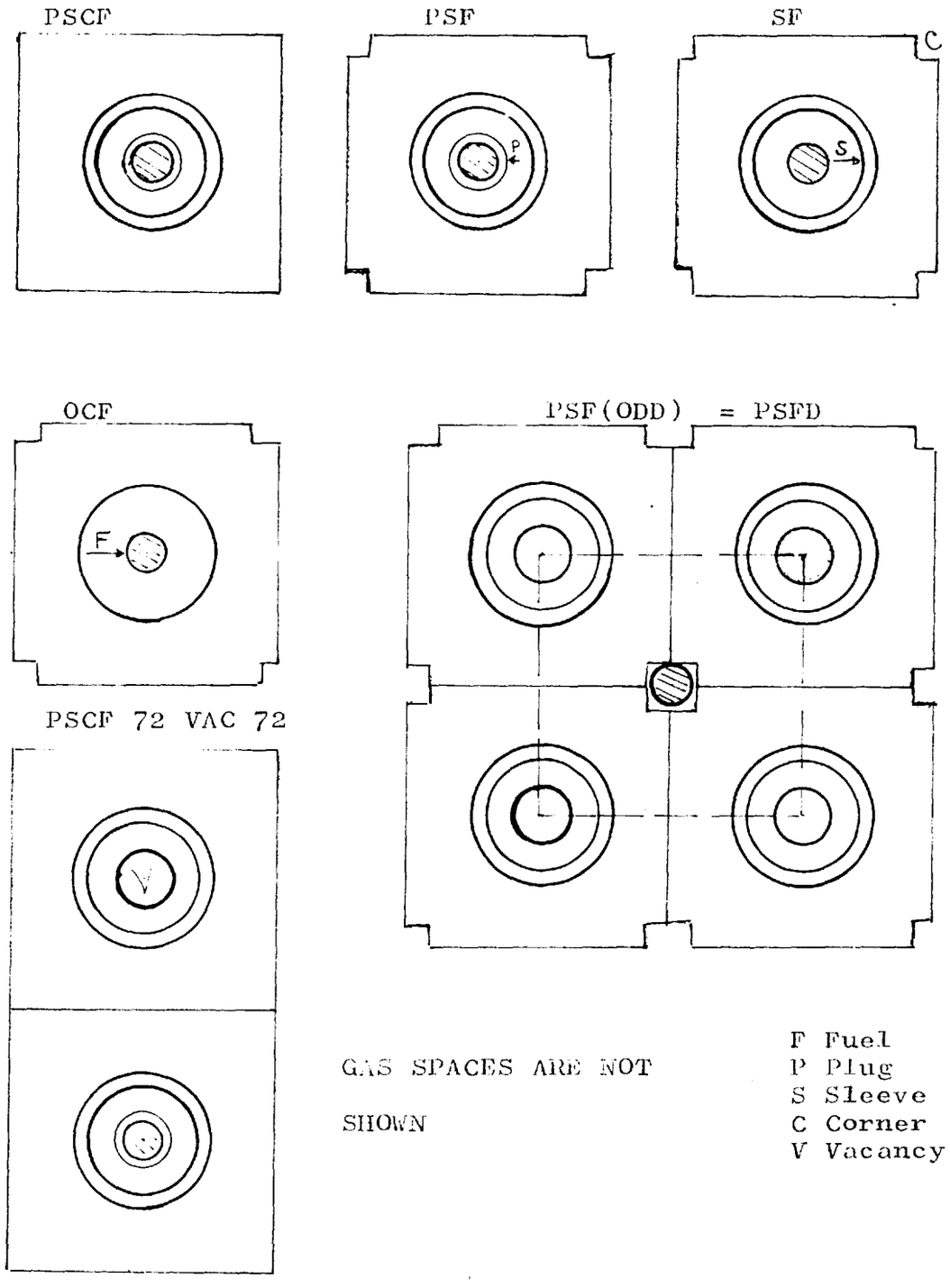

FIG. A-1.1 NOMENCLATURE OF LATTICES

APPENDIX II

A-2.1 SINH AND COSINE FITTING

Practically all the calculations reported have been done, some on the Mercury and Atlas Computers of University of London (mostly sinh and cosine fitting and some preliminary calculations on heterogeneous reactors) and the rest of the calculations on IBM-7090 computer at the College. The programmes (mostly) used for the purpose are described in this Appendix and the next one.

Programmes[4] have been written to fit experimental flux measurements to the following functions by least squares fitting.

1) Sinh Fitting.

$$\varphi_i(z_i) = A \frac{\sinh((c-z_i)\gamma)}{\sinh(\gamma c)} \qquad \text{A-2.1.1}$$

for γ, A and c.

This is the function expressing the theoretical variations of neutron flux perpendicular to the source plane in an exponential assembly. The constants A, γ, and c are to be estimated from a series of measurements of flux φ_i at various heights z_i. The expression A-2.1.1 is made linear by expanding the function as a Taylor series and considering only the first derivatives.

$$\varphi_i(A,\alpha,\gamma) = \varphi_o(A_o,\alpha_o,\gamma_o) + \left(\frac{\partial \varphi_i}{\partial A}\right)_o \delta A + \left(\frac{\partial \varphi_i}{\partial \alpha}\right)_o \delta\alpha + \left(\frac{\partial \varphi_i}{\partial \gamma}\right)_o \delta\gamma \qquad \text{A-2.1.2}$$

where $\alpha = c\gamma$

and o refers to the first guess values. Rewriting the equation and changing the notation

$$m_i = a_i \delta A + b_i \delta\alpha + c_i \delta\gamma \qquad \text{A-2.1.3}$$

The equation for the sum of squares of residuals is formed and differentiated w.r.t. each variable to give the normal equations. These are solved for δA, $\delta\alpha$ and $\delta\gamma$.

It was always found that fixing the height does reduce the fitting error approximately by a factor of 2 so the fitted values of b_{11} corresponding to the best fitted value of c was always taken.

The standard deviations of c and b_{11} are estimated on the basis of the following assumptions.

1) The function is linear within the range of the standard deviations.

2) The variables are independent. However it was found that b_{11} and c are very strongly interdependent and for this reason c was fixed and had previously been fitted to cosine distributions by Macdonald and average of c corresponding to a large number of results was taken.

3) The net influence of combinations of positive or

negative deviations of points from the best fit line does not affect since their effect will be balanced by other positive deviation. The details of the calculations of errors may be found in Macdonald's work (4).

The initial guesses of γ_o $(1/b_{11})$ and c_o are fed into the computer as data, together with flux values, and the programme uses these to calculate an initial estimate of A_o. Then the analysis for δA, $\delta\alpha$ and $\delta\gamma$ follows for improvements over the guessed values and the process is repeated until the correction factor $\delta\gamma$ is $<0.01\%$ of γ. Usually 2 to 3 interations are sufficient for the convergence to be reached and if the conditions detailed are not reached then the whole process is repeated again with the last values of the constants.

The out-put consists of the related parameters during each cycle with the residual sum and on reaching convergence the standard deviations of the fitted parameters and the standard deviation of the flux from the theoretical values.

2) Cosine Fitting.

$$\varphi_i(x) = A \cos(\beta x_i) \qquad \text{A-2.1.4}$$

for A and β.

The fitting procedure is basically the same as detailed in (1) of the present section. The cosine-function is non-linear and an initial value of β is

obtained from the stack width and an estimate of the extrapolation distance. The value of A_o in the present case was simply taken as the largest flux value read into the computer.

Again in this case, the computer output consists of the values of the fitted parameters in each cycle and when convergence is reached, the standard deviations of the fitted parameters. There are additional refinements; the flux could be read in for (1) and (2) either as a flux with given variance, or as a "time" for a given number of counts. The relevant calculations are carried out by the computer.

These two programmes were written for the Atlas and/or Mercury Computer and they have been superseded by a sub-routine "PARFIT" (40), which is a Fortran IV sub-routine designed to fit a set of up to 50 experimental observations by the method of least squares fitting procedure to a theoretical expression which may contain 2, 3 or 4 parameters, the values of which are to be optimised to give the closest fit to the experimental points. The chief advantage in this sub-routine is that the expression to be fitted is supplied by the user in the form of a sub-routine and therefore is very useful in this respect. Consequently there is no distinction between a SINH FIT and a COSINE FIT: it is just a matter

of giving the proper function.

A-2.2 CALCULATION OF LATTICE PARAMETERS

All the basic lattice parameters calculated on the basis of the theory outlined in Chapter 3 have been carried out by a programme written in the Nuclear Power Group, Imperial College, for the computation of the lattice parameters of graphite moderated, gas cooled reactors for the Atlas Computer. The programme can be used for the calculation of the lattice parameters of reactors with enriched uranium fuel, with or without canning material, the material being aluminium, iron or magnax. The fuel elements can be hollow with or without inner case.

The input data are the lattice cell dimensions, density of the materials, operating temperature, data for streaming and any other data required for calculations.

The out-put from the programme has been given in Chapter 3 section 3. Specifically, the constants are K_∞, f_5, η_5, ε, p, flux-fine structure ratios, diffusion and slowing down areas, without or with streaming corrections applied in radial and axial directions according to the asymmetry factor A = 1.73 in the relation

$$\left[\left(\frac{M_z^2}{M_R^2}\right)_{\text{expt.}} - 1\right] = 1.73 \left[\left(\frac{M_z^2}{M_R^2}\right)_{\text{theory}} - 1\right] \qquad \text{A}\pi 2.2.1$$

The streaming factors S_{MR}, S_{MZ}, S_{FR} and S_{FR} are calculated according to the recommendations of Syrett, namely that the sheathing material geometrical constants should be calculated for volumes including any part of the end-cap which protrudes into the streaming channel. The effect of gaps between graphite blocks and control rod holes on modifying L^2 and L_s^2 is partly compensated by defining S_g as an effective graphite density detailed in Appendix A-1.1. Thus in the streaming factors defined by the equations 3.3.24 (a,b) and 3.3.25 (a,b) the contribution 2ϕ should be omitted for control rod holes and Wigner gaps, but the term $(Q_r\varphi/I)$ should be included for the holes and gaps associated with one lattice cell. Values of Q for holes of varying μ are given in Bernoist's report (41). The running time for the computer is approximately 10 seconds per set of data.

A-2.3 CRAM (44)

The programme CRAM solves the multi-group diffusion equations

$$D_g \nabla^2 \varphi_g - A_g \varphi_g + Q_g = 0 \qquad \text{A-2.3.1}$$

The source term Q_g is made up from scattered and fission neutrons as

$$Q_g = \Sigma'_g \left(C'_{gg} + \frac{1}{k} X_g F'_g\right)\varphi'_g \qquad \text{A-2.3.2}$$

The multi-group equations are solved by finite difference methods. The reactor is divided into a number of homogeneous regions, and an approximation to equation A-2.3.1 is made in each region. The programme computes the critical value of K and can handle many other calculations of complex nature.

The terms in equations A-2.3.1-2 are defined as

A_g - Absorption cross-section in group g, including removal by scattering.

D_g - Diffusion coefficient in group g.

C'_{gg} - Cross-section for scattering from group g' to group g.

F_g - Fission source in group g.

K - Effective multiplication of system defined as

$$K = \frac{K_\infty \text{ (theory)}}{K_\infty \text{ (experiment)}} ,$$

The value of K_∞ (exp) which would be expected if measured where K_∞ (theory) is presumed to be known.

X_g - Fission spectrum

φ_g - Neutron flux in group g, not normalised.

The input constants were taken from the two-group model due to Syrett (7) so it would be advisable to identify the various constants in equations A-2.3.1. If we write the equation A-2.3.1 for the two energy groups of neutrons

$$D_1\nabla^2\varphi_1 - A_1\varphi_1 + \frac{F_2}{K}\varphi_2 = 0 \qquad - (C_1)$$

$$D_2\nabla^2\varphi_2 - A_2\varphi_2 + C_{12}\varphi_1 = 0 \qquad - (C_2)$$

where $X_1 = 1$ for fast neutron fission spectrum and $X_2 = 0$ for thermal neutron fission spectrum.

$$F_1 = 0$$

$$C_{11} = C_{21} = C_{22} = 0.$$

Writing the two-group equations according to Syrett's model we have

$$D_F\nabla^2 W_F - \Sigma_F W_F + K_\infty \Sigma_M W_M = 0 \qquad - (R_1)$$

$$D_M\nabla^2 W_M - \Sigma_M W_M + \Sigma_F W_F = 0 \qquad - (R_2)$$

Identifying C_1 as R_1 and C_2 as R_2 we find that

$$A_1 = \Sigma_F = \frac{D_{FR}}{L_{SR}^2} \qquad (a) \qquad \text{A-2.3.3}$$

$$A_2 = \Sigma_M = \frac{D_{MR}}{L_R^2} \qquad (b) \qquad \text{A-2.3.3}$$

$$\Sigma_F = C_{12} \qquad (c) \qquad \text{A-2.3.3}$$

$$F_2 = K_\infty(\text{theory}) \times \Sigma_M \qquad (d) \qquad \text{A-2.3.3}$$

so that $$K = \frac{K_\infty(\text{theory})}{K_\infty(\text{expt})} \qquad \text{A-2.3.4}$$

Normally the programme expects the input cross-

sections in microscopic form isotope by isotope but in the present use macroscopic cross-sections were fed directly. However in this case the mix routines built in the programme become degenerate.

The finite difference method may be briefly summarized as below.

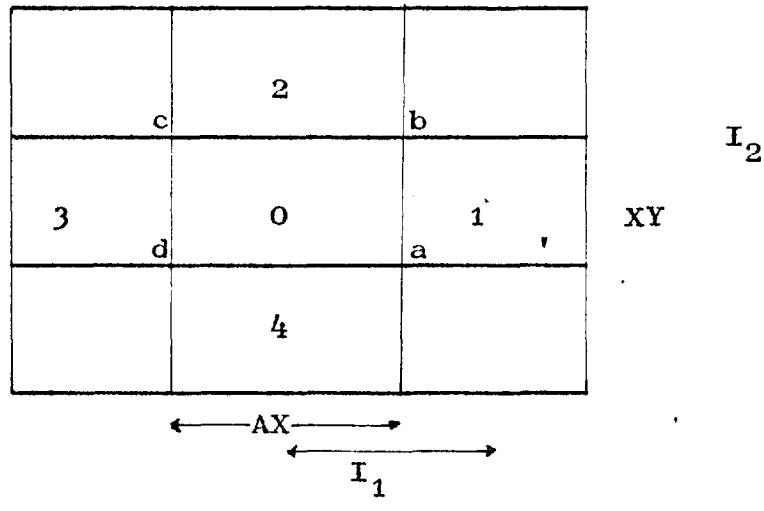

FIG.A-2.5.1 THE X-Y MESH

The reactor is divided into a number of regions and the macroscopic cross-sections in each region are assumed to be constant. This implies that the core-reflector interfaces have to be at the end of a mesh point. The boundary of each region must be lines of constant X and constant Y as shown in Fig.A-2.5.1. The

programme computes the average flux in each region which is supposed to be the same as the flux at the mesh-point. Point 0 in the Figure has neighbours 1, 2, 3, 4 and equation A-2.3.1 is integrated over the volume ($x = \frac{1}{2} X$; $y = \frac{1}{2} Y$). The result of various approximations for the terms $D\nabla^2\varphi$, $A\varphi$ etc. leads to an expression for the multi-group equation A-2.3.1 as

$$\frac{\overline{D}_1(\varphi_1-\varphi_o)S_1}{I_1} + \frac{\overline{D}_2(\varphi_2-\varphi_o)\ S_2}{I_2} + \frac{\overline{D}_3(\varphi_3-\varphi_o)S_3}{I_3}$$

$$+ \frac{\overline{D}_4(\varphi_4-\varphi_o)S_4}{I_4} - A\varphi_o V + Q_o V = 0 \qquad \text{A-2.3.5}$$

and the source term

$$Q_o = \sum_{g'} \left(C'_{gg} + \frac{X_g F'_g}{K}\right) \varphi'_{go} \qquad \text{A-2.3.6}$$

where $S_4 = S_2 = \Delta X$

$S_3 = S_1 = \Delta Y$

and $V = \Delta X \Delta Y$.

The programme allows the boundary condition of zero-current and zero-flux by defining a number $\lambda=0$ or a very high number (10^9 say). A typical input data set consists of defining the number of energy group, control type, geometry, anisotropy, buckling (axial, since the programme solves the multi-group diffusion equations,

in two dimensions

this could be omitted if so required), definition of mesh points and boundary condition, isotropic data, definition of core region and reflector (if present) and the last card should define the spectrum in two energy groups SP 1.0 0. This should be followed by the cards for out-put required. If there is another set of data to follow, there should be a card with NEXT.

In the present analysis it was found necessary to use the ACCURACY card which defines the accuracy

$$A_1 \quad A_2 \quad A_3 \quad A_4 \quad A_5$$

In control type 1 problem the steady state will be reached if (MAX^n etc. defined on next page)

$$Max^n - Min^n < A_2$$

$$Max^n - 1.0 < A_3$$

$$\lambda^n - \lambda^{n+1} < A_1$$

and for iterations other than those in an acceleration cycle, the current estimate of K is multiplied by

$$(I+1)(\lambda-1)\ 20\ A_5 + 1$$

I = number of points in X direction divided by 10. This will gradually adjust K to its correct value and in the present case A_5 was reduced from its built-in value of 0.05 to 0.01. The bullt-in values of the accuracy

constants are

A_1	A_2	A_3	A_4	A_5
.0005	.0005	.0005	.0001	0.05

In control type 1 A_4 is not used. Any of them can be over-written, e.g. ACCURACY .001 .002 will over-write A_1 and A_2 but not A_3, A_4 and A_5. In the present study the value of A_5 had been reduced to 0.01 for strict convergence.

The card can be omitted if not required and should be placed after the General Constants card.

The values of Max^n and λ^n are defined as

$$I(n) = \sum_{i,j,g} [\varphi^2(i,j,g,n)]$$

$$\lambda^n = (I^n/I^{n-1})^{\frac{1}{2}}$$

and

$$Max^n = \max_{i,j,g} [\frac{\varphi(i,j,g,n)}{\varphi(i,j,g,n-1)}].$$

Similarly Min^n.

The out-put consists of a print of the input, a figure of K when steady state has reached, defines mesh-points, and the flux distributions for both fast and thermal fluxes are given.

The programme uses the following tape units.

IBM-7090 Programme. Logical Tape Units

Programme Tape	4
Coefficient Tape	7
FLUX ONE	9
FLUX TWO	10
OFF LINE Output	3
DUMP	6
INPUT	2
Chain Intermediate	5

Tho programme runs under Fortran Monitor Control system.Tape 6 is required unless a dump is called for.

At the moment the programme has been in almost constant use during the last one year and there have been practically no difficulties in its use. A set of 6 PSCF cases normally takes 21.5 minutes of the computer, while in case of SF or OCF with large channels and large streaming corrections the time increases to 27.1 and 31.4 minutes respectively which increases particularly due to the cases with small (4, 16) number of fuel elements. The computed results have been quite satisfactory.

A-2.4 ONE GROUP THEORY CRITICALITY CALCULATIONS

The programme has been written for the IBM-7090 computer. The programme consists of 4 sub-routines and a fairly big programme. The function of two sub-routines is to write the name of the programme and the title card. The third one calculates the function defined by the equation A-2.4.5 below and the fourth calculates and writes the flux distribution in the core and the reflector on the basis of modified one-group theory.

The basis of the programme is the criticality condition obtained in Chapter 4, specifically

$$\tan(\alpha\delta) = \frac{D_c}{D_r \kappa_r} \alpha \tanh(\kappa_r T), \qquad \text{A-2.4.1}$$

and the approximation defined as

$$\delta = \frac{D_c}{D_r \kappa_r} \tanh(\kappa_r T) \qquad \text{A-2.4.2}$$

where δ is the reflector saving corresponding to a particular thickness of reflector surrounding a core of given size.

First the reflector savings are calculated according to the expression A-2.4.2 and then all the related parameters, namely material buckling for a given axial buckling, equivalent core size of the bare homogeneous reactor, K_∞ on the basis of modified one-group theory, two-group theory, etc. and the corresponding errors are calculated

and written. The thermal flux distributions according to the expression

$$\varphi_c = \cos(\alpha x) \qquad \text{A-2.4.3}$$

$$\varphi_r = C/A \sinh\left(\frac{a'}{2} + T - x\right) \qquad \text{A-2.4.4}$$

$$C/A = \cos\left(\frac{a'}{2}\alpha\right)/\sinh(\kappa_r T)$$

are calculated and written.

Then the programme goes into a very big loop for iteration, then all the above said calculations are repeated if the number of cases is more than one. After each iteration the flux distribution for that configuration will be written with number of the fuel elements being written at the top of the next page.

The iteration is based on the principle that we give two guess values to the independent parameter, say to reflector saving or the corresponding radial buckling in one direction. In the programme reflector saving has been taken as independent parameter. It is assumed that they should have given the function defined as

$$f(y) = \tan(\alpha\delta) - \left(\frac{D_c}{D_r} \cdot \frac{1}{\kappa_r} \tanh(\kappa_r T)\right)\alpha \qquad \text{A-2.4.5}$$
$$= 0$$

If it is not , then let L be the iteration number, the correction to the last value will be

$$CN = \frac{f_L(y)\ ((f_L(x) - f_{L-1}(x))}{f_{L-1}(y) - f_L(y)} \qquad \text{A-2.4.5}$$

The process is continued till the desired built-in accuracy of 10^{-6} cm in reflector saving is reached. Often 4 to 5 iterations have been enough. This process is repeated till the number of given cases is finished.

At the end of this cycle it would expect one card with one number (D_r) and repeat the calculations up to the calculation of reflector saving etc. by the expression A-2.3.2 and will expect a new set of data (no flux distribution for this change is given); this corresponds to the set-B defined in the text.

The input to the programme are the core and the reflector characteristic constants namely diffusion coefficients, diffusion and slowing down areas, number of cases, number of the fuel elements, corresponding reflector thicknesses and axial bucklings. The out-put consists of, the input exactly written on the output tape and then already mentioned calculations done and are written on the out-put tape.

The time for one set of 6 cases is usually $\approx$1.0 minute on IBM-7090 computer.

A-2.5 TWO-GROUP THEORY CRITICALITY CALCULATIONS

This programme is also written for the IBM-7090 computer. It consists of ten sub-routines and one controlling programme. All the computed results reported in Chapter 5 have been calculated with the help of this programme. Since the two-group theory reflected core system calculations are quite complicated, so the programme has been designed to calculate everything so that it should never fail to give an answer. The experience with other programmes showed that it is advisable to have all the practical locations available. The input data are the familiar core and reflector constants, core size, reflector thickness, axial buckling and so on.

The programme will:

1) Write all the input on the out-put tape.
2) Do calculations to see the form of the function (discussed in the latter part of the section) and plot it on the out-put tape.
3) Iterate for the criticality condition equation (5.2.17) to hold.
4) Calculate the constants and give the two fluxes and fluxes plotted on the out-put tape.
5) Then wait for the next problem or finish up.

The basis of the criticality condition is the solution of the four differential equations for the two fluxes in the core and the reflector regions for plane slab in one dimension. The conditions of equal currents and fluxes at the core-reflector interface gives the criticality condition in the form of determinant defined by equation 5.2.15. This being a complicated function of various quantities, it is solved by iteration procedure as given in section A-2.4. So that the determinant is equal to zero, ($\approx 10^{-8}$) and the corresponding accuracy in μ is usually $\approx 10^{-6}$ cm^{-1} (μ^2 being the radial buckling in x or y direction), the flux is calculated by the equations

$$\varphi_{fc}(x) = \cos(\mu x) + C/A \cosh(\nu x) \qquad \text{A-2.5.1}$$

$$\varphi_{mc}(x) = S_1 \cos(\mu x) + C/A\ S_2 \cosh(\nu x) \qquad \text{A-2.5.2}$$

$$\varphi_{fr}(x) = F/A \sinh\left(\kappa_{fr}\left(\frac{a'}{2} + T - x\right)\right) \qquad \text{A-2.5.3}$$

$$\varphi_{mr}(x) = G/A \sinh\left(\kappa_{mr}\left(\frac{a'}{2} + T - x\right)\right) + F/A\ S_3 \sinh\left(\kappa_{fr}\left(\frac{a'}{2} + T - x\right)\right) \qquad \text{A-2.5.4}$$

The flux plots as well as flux values of the fluxes at an interval of 5.08 cms are also given.

To detail the function of each sub-routine is a lengthy process; however the most important ones are:

1) POINTS (DIN, NR) Given number of points and

location of the variables. This routine will plot the graph.

2) DETRME (CMEW). If the value of $\mu = \frac{\pi}{a}$ is given, it will give the corresponding value of the determinant.

3) ROTATE (MAX). It does the main function of iteration, and would see that the number of iterations does not exceed the given number MAX.

4) FLUXPT. It will calculate, plot and write the two fluxes corresponding to distances, normalise them to Maximum as 1000 and find the flux ratios etc.

Much of the out-put can be avoided if not required by giving certain numbers as negative.

One set of 5-cases normally takes 1 to 2 minutes however depending upon the type of problem and constants involved. During its use the iteration process has never failed to converge to the required accuracy.

A.2.6 TABLES OF FLUXES FROM ONE-GROUP, TWO-GROUP THEORY AND CRAM (FINITE DIFFERENCE METHODS)

The thermal flux distributions calculated on the basis of one-group and two-group theory have been shown alongside experimental values in graphs in Chapters 4 and 5. Here are tabulated the flux distributions at representative points from CRAM (finite difference methods) as well, and they have been shown in graphs in Chapter 8 (for 5 representative cases of PSCF (100, 64, 36, 16, 4)) for the sake of comparison with experimentally measured thermal flux distributions. The calculated fast fluxes from CRAM and two-group theory are also quoted.

The flux values quoted correspond to values at points where measurements cannot be done. Since the mesh points in CRAM are so designed that the flux distribution is given at these points.

COMPARISON OF ONE-GROUP, TWO-GROUP, CRAM FLUXES

PSCF

CASE	TWO-GROUP		ONE GROUP	CRAM	
Distance cms	FAST	THERMAL	THERMAL	THERMAL	FAST
5.08	79.83	997.94	997.94	1000.00	78.90
25.40	75.92	949.04	949.04	950.99	75.03
45.72	67.04	838.04	838.04	839.74	66.25
66.04	53.78	672.20	672.20	673.54	53.14
86.36	36.99	462.38	462.38	463.26	36.55
106.68	17.78	222.31	222.31	222.67	17.57

PSCF 100

5.08	78.78	997.90	997.86	1000.00	78.87
25.40	74.83	947.87	947.41	949.83	74.90
45.72	65.87	834.38	832.97	836.21	65.89
66.04	52.50	665.05	662.27	667.97	52.37
86.36	35.62	451.19	446.85	460.71	34.88
106.68	13.21	253.08	203.25	255.00	12.90

PSCF 64

5.08	78.95	997.65	997.63	1000.00	78.86
25.40	74.52	941.72	941.22	945.53	74.42
45.72	64.50	815.30	813.74	825.11	64.18
66.04	49.65	627.86	624.81	662.80	47.77
86.36	21.47	528.86	388.74	545.60	21.04
106.68	6.17	280.46	169.61	289.16	6.25

PSCF 36

5.08	79.37	997.00	997.04	1000.00	78.30
25.40	73.66	925.86	926.87	940.08	72.47
45.72	60.86	766.53	769.54	827.53	57.71
66.04	27.16	743.17	536.07	792.76	26.48
86.36	8.85	542.24	312.72	588.52	8.94
106.68	2.54	257.07	136.44	283.42	2.65

TABLES A-2.6

PSCF 16

CASE	TWO-GROUP		ONE GROUP	CRAM	
Distance cms	FAST	THERMAL	THERMAL	THERMAL	FAST
5.08	80.01	995.61	995.87	982.26	72.49
25.40	71.22	892.39	898.33	943.35	62.43
45.72	32.89	921.76	671.80	1000.00	29.13
66.04	10.86	745.66	428.67	851.01	9.77
86.36	3.54	478.43	250.07	573.61	3.25
106.68	1.02	216.93	109.10	268.91	0.95

PSCF 4

5.08	72.67	936.94	993.43	884.13	45.34
25.40	37.40	1000.00	810.75	1000.00	20.90
45.72	21.50	955.20	536.06	925.57	6.45
66.04	4.08	603.77	342.06	725.15	2.09
86.36	1.33	368.54	199.54	484.28	0.69
106.68	0.38	163.87	87.06	228.28	0.20

PSF

5.08	82.24	997.95	997.95	1000.00	81.11
25.40	78.22	949.27	949.27	951.20	77.15
45.72	69.12	838.74	838.74	840.44	68.17
66.04	55.51	673.59	673.59	674.91	54.74
86.36	38.28	464.55	464.55	465.42	37.75
106.68	18.56	225.26	225.26	225.60	18.30

PSF-100

5.08	80.86	997.93	997.89	1000.00	81.04
25.40	76.86	948.56	947.12	950.54	77.02
45.72	67.79	836.53	835.18	838.53	67.88
66.04	54.23	669.25	666.60	672.45	54.16
86.36	37.09	457.77	458.62	468.24	36.38
106.68	14.17	261.15	210.69	263.24	13.96

PSF-64

5.08	80.98	997.70	997.68	1000.00	80.93
25.40	76.53	942.94	942.60	947.18	76.49
45.72	66.46	819.07	818.02	830.01	66.21
66.04	51.52	635.19	633.12	674.22	49.69
86.36	22.91	540.32	399.64	561.14	22.74
106.68	6.79	289.90	176.38	301.82	7.04

TABLES A-2.6

PSF-36

CASE Distance cms	TWO-GROUP FAST	TWO-GROUP THERMAL	ONE-GROUP THERMAL	CRAM THERMAL	CRAM FAST
5.08	81.27	977.09	977.15	1000.00	79.99
25.40	75.59	928.02	929.48	944.13	74.23
45.72	62.83	773.13	777.54	841.97	59.58
66.04	28.84	756.16	549.08	816.97	28.43
86.36	9.72	557.18	322.93	616.27	10.05
106.68	2.88	267.73	140.53	302.08	3.10

PSF-16

5.08	81.63	995.79	996.08	955.67	70.91
25.40	72.96	896.53	903.42	927.53	61.40
45.72	34.64	933.66	684.50	1000.00	29.80
66.04	11.84	763.07	440.62	868.66	10.50
86.36	3.99	494.84	259.14	596.10	3.66
106.68	1.18	227.35	114.37	284.36	1.12

PSF-4

5.08	73.30	933.40	933.89	867.07	41.42
25.40	38.71	1000.00	819.28	897.21	19.84
45.72	13.25	862.70	546.94	947.71	6.45
66.04	4.53	617.32	352.07	758.94	2.20
86.36	1.53	380.68	207.06	515.49	0.76
106.68	0.45	171.44	91.39	247.02	0.1309

PSF-121

5.08	81.37	997.95	997.93	1000.00	81.52
25.40	77.39	949.14	948.77	951.01	77.53
45.72	68.35	838.34	837.21	839.83	68.46
66.04	54.86	672.79	670.57	673.84	54.90
86.36	37.77	463.30	459.83	464.40	37.70
106.68	18.23	223.56	218.85	227.50	17.83

PSF-81

5.08	81.43	997.83	997.81	1000.00	81.53
25.40	77.22	946.27	945.67	948.63	77.29
45.72	67.68	829.43	827.55	833.11	67.62
66.04	53.47	655.37	651.69	666.06	52.85
86.36	35.57	436.10	430.37	480.80	32.41
106.68	10.02	281.84	191.88	284.57	10.04

TABLES A-2.6

PSF-49

CASE Distance cms	TWO-GROUP FAST	TWO-GROUP THERMAL	ONE GROUP THERMAL	CRAM THERMAL	CRAM FAST
5.08	82.04	997.44	997.23	1000.00	81.74
25.40	77.02	936.58	936.48	943.33	76.64
45.72	65.69	799.41	799.10	823.82	64.51
66.04	48.99	597.15	596.49	695.12	43.06
86.36	15.14	564.34	356.72	587.24	15.23
106.68	4.49	283.06	157.46	296.83	4.70

PSF-25

5.08	82.11	996.52	996.65	1000.00	79.09
25.40	75.15	914.20	927.35	946.99	71.68
45.72	59.68	731.19	740.50	886.56	50.72
66.04	18.54	780.18	488.69	867.94	18.16
86.36	6.25	531.04	287.48	612.98	6.38
106.68	1.85	248.43	127.90	294.31	3.21

PSF-9

5.08	80.83	983.54	995.09	890.24	59.19
25.40	68.98	860.38	879.64	911.82	45.25
45.72	22.05	948.95	610.61	983.56	15.46
66.04	7.54	714.20	393.16	802.21	5.34
86.36	2.54	449.47	231.28	542.17	1.85
106.68	0.75	204.10	102.09	258.01	0.57

SF

5.08	100.05	999.97	997.97	1000.00	99.04
25.40	95.20	949.59	949.59	951.51	94.24
45.72	84.19	839.74	839.74	841.42	83.33
66.04	67.73	675.55	675.55	676.86	67.04
86.36	46.88	467.63	467.63	468.48	46.40
106.68	23.00	229.44	229.44	229.77	22.76

SF-100

5.08	98.05	997.90	997.86	1000.00	99.20
25.40	93.15	948.02	946.95	948.88	94.11
45.72	82.03	834.87	831.54	833.20	82.56
66.04	65.43	665.99	659.48	661.75	65.27
86.36	44.47	452.67	442.50	449.47	43.19
106.68	17.97	251.96	201.52	232.78	17.54

TABLES A-2.6

SF-64

CASE Distance cms	TWO-GROUP FAST	TWO-GROUP THERMAL	ONE-GROUP THERMAL	CRAM THERMAL	CRAM FAST
5.08	98.36	997.69	997.63	1000.00	99.32
25.40	92.94	942.82	941.34	945.73	93.64
45.72	80.67	818.73	814.12	826.17	80.55
66.04	62.47	634.54	625.56	663.91	60.03
86.36	30.12	543.11	393.79	527.08	30.60
106.68	10.27	299.04	179.47	287.20	11.46

SF-36

5.08	98.93	997.18	997.15	1000.00	98.25
25.40	92.19	930.38	929.63	946.36	90.96
45.72	77.06	780.43	778.00	847.53	72.91
66.04	38.62	789.54	555.75	806.67	39.41
86.36	15.46	603.30	339.33	621.82	17.76
106.68	5.27	301.39	154.65	315.55	6.63

SF-16

5.08	98.76	996.18	996.23	963.24	87.25
25.40	88.96	906.15	907.17	941.59	75.52
45.72	46.22	987.55	701.71	1000.00	41.47
66.04	18.95	848.32	473.19	885.32	18.92
86.36	7.58	577.45	288.92	626.50	8.38
106.68	2.59	276.14	131.67	307.76	3.10

SF-4

5.08	82.01	903.52	994.41	902.17	55.83
25.40	47.29	998.32	1838.63	1000.00	30.16
45.72	19.46	910.24	590.92	940.10	12.79
66.04	7.98	690.60	398.48	755.07	5.64
86.36	3.19	446.7	243.30	515.99	2.47
106.68	1.09	209.05	110.88	250.30	0.79

OCF

5.08	107.20	997.99	997.99	1000.00	106.25
25.40	102.05	950.06	950.06	952.97	101.15
45.72	90.36	841.23	841.23	842.89	89.56
66.04	72.88	678.46	678.46	679.75	72.22
86.36	50.72	472.20	472.20	473.03	50.26
106.68	25.31	235.66	235.66	235.96	25.07

TABLES A-2.6

OCF-100

CASE Distance cms	TWO-GROUP FAST	TWO-GROUP THERMAL	ONE GROUP THERMAL	CRAM THERMAL	CRAM FAST
5.08	104.58	997.88	997.82	1000.00	106.94
25.40	99.29	947.37	946.07	948.19	101.37
45.72	87.28	832.85	828.80	830.97	88.74
66.04	69.38	662.05	654.13	657.24	69.88
86.36	46.78	446.52	434.16	441.44	45.89
106.68	19.14	243.54	194.91	221.05	18.92

OCF-64

5.08	105.16	997.65	997.57	1000.00	107.30
25.40	99.25	941.71	939.72	945.03	101.00
45.72	85.87	815.28	809.09	823.92	86.52
66.04	66.05	627.86	615.81	657.89	64.06
86.36	32.45	530.33	383.63	507.48	33.63
106.68	11.81	196.17	179.18	648.23	13.52

OCF-36

5.08	106.01	997.16	997.08	1000.00	105.95
25.40	98.68	929.72	927.73	947.64	97.86
45.72	82.24	778.43	772.19	849.68	78.09
66.04	42.17	786.48	549.71	793.41	43.82
86.36	18.16	606.23	341.96	613.27	21.46
106.68	6.61	310.26	159.71	317.89	8.59

OCF-16

5.08	105.42	996.26	996.16	973.69	93.44
25.40	94.94	908.00	905.53	955.17	80.68
45.72	50.60	994.12	702.01	1000.00	46.09
66.04	22.43	864.15	483.31	887.25	23.06
86.36	9.66	599.80	300.66	636.32	11.10
106.68	3.51	194.56	140.42	319.91	4.40

COF-4

5.08	85.57	901.04	994.39	920.49	60.18
25.40	50.73	996.86	843.67	1000.00	33.83
45.72	22.62	921.76	608.66	936.72	15.81
66.04	10.02	714.93	419.08	757.94	7.63
86.36	4.32	472.55	260.68	522.56	3.62
106.68	1.57	227.16	121.45	258.49	1.43

TABLES A-2.6

APPENDIX III

HETERO-PROGRAMMME

BASIC THEORY OF THE PROGRAMME

A.3.1

The programme is essentially the same as described by Näslund (21) with the exception of a few minor changes to make it suitable for use on the computer IBM-7090 at the College. The programme had not been used for the cases involving measurements on the sub-critical assembly (exponential cases). However it had been used extensively by Jonsson (16) for quite complicated calculations involving power-distribution in heavy-water moderated reactor, burn-up calculations, etc. Therefore it was thought to use the programme with its sub-routines involving Matrix calculations as such so that much trouble involving the testing of Matrices, numerical method and Iteration process could be avoided.

The mathematical details have been given in Chapter 6 section 6.3 ; only the relevant equations are quoted here.

The diffusion equation solved in the programme both for two or three dimensions are

$$\nabla^2 \varphi_1(\bar{r},z) - \frac{1}{\tau}\varphi_1(\bar{r},z) - \frac{1}{D_{mf}} \sum_{n=1}^{N} (A_n)^f \, \delta(\bar{r}-\bar{r}_n) = 0$$

A.3.1.1

$$\nabla^2 \varphi_2(\bar{r},z) - \frac{1}{L^2}\varphi(\bar{r},z) + \frac{D_{mf}}{\tau_m D_{ms}} \varphi_1(\bar{r},z) -$$

$$\frac{1}{D_{ms}} \sum_{n=1}^{N} (A_n)^s \delta(\bar{r}-\bar{r}_n) = 0 \qquad \text{A-3.1.2}$$

The boundary conditions are

$$\varphi_1(R,z) = \varphi_2(R,z) = 0 \qquad \text{(a)}$$

$$\varphi_1(\bar{r},H) = \varphi_2(\bar{r},H) = 0 \qquad \text{(b)}$$

A-3.1.3

$$(A_n)^f = \gamma_{11}^{n} \varphi_{1n} - \gamma_{12}^{n} \varphi_{2n} \qquad \text{(c)}$$

$$(A_n)^s = -\gamma_{21}^{n} \varphi_{1n} + \gamma_{22}^{n} \varphi_{2n} \qquad \text{(d)}$$

where

$$\gamma_{12} = \frac{\eta\, \gamma_{22}}{K_{eff}} \qquad \text{(e)}$$

The general solution of the equations A-3.1.1 - 2 applicable to the present situation can be written (17)

$$2\pi D_{mf} \varphi_{1K} = \sum_{\mu} \sum_{n} f_{nK}(\tau) \{-\gamma_{11}^{n\mu} \varphi_{1n\mu} + \gamma_{12}^{n\mu} \varphi_{n\mu}\} \qquad \text{A-3.1.4}$$

$$2\pi D_{ms}\, 2K = \sum_{\mu} \sum_{n} F_{nK} \{-\gamma_{11}^{n\mu} \varphi_{1n\mu} + \gamma_{12}^{n\mu} \varphi_{n\mu}\}$$

$$+ \sum_{\mu} \sum_{n} f_{nK}(L^2) \{\gamma_{21}^{n\mu} \varphi_{n\mu} - \gamma_{22}^{n\mu} \varphi_{n\mu}\}$$

A-3.1.5

where

$$f_{nK}(L^2) = K_o\left(\frac{|\bar{r}_n - r_K|}{L}\right) - \sum_m I_m\left(\frac{r_n}{L}\right) I_m\left(\frac{r_K}{L}\right)$$

$$\frac{K_m\left(\frac{R}{L}\right)}{I_m\left(\frac{R}{L}\right)} \cdot \cos m(\varphi_n - \varphi_K) \qquad \text{A-3.1.6}$$

$$F_{nK} = \frac{1}{1-\tau/L^2}\{f_{nK}(L^2) - f_{nK}(\tau)\} \qquad \text{A-3.1.7}$$

$$(\tau)^{-1} = (\tau_m)^{-1} - \frac{M_z^2}{M_R^2}\left(\frac{1}{b_{11}}\right)^2 \qquad (a)$$

A-3.1.8

$$(L^2)^{-1} = (L_m^2)^{-1} - \frac{M_z^2}{M_R^2}\left(\frac{1}{b_{11}}\right)^2 \qquad (b)$$

φ_{1K} = fast flux at element K

φ_{2K} = thermal flux at element K.

The solution to the homogeneous equations defined by equations 6.3.14 and 6.3.15 or their equivalents A-3.1.4-5 is calculated in the programme for the greatest inherent value K_{eff} (Eigen-value).

If $\gamma_{11} = 0$ and $\gamma_{12} = 0$ i.e. absorption of fast neutrons in the element and the slowing down of neutrons inside the fuel is zero, which in case of natural uranium is practically the case, the fast flux can be eliminated from the set of homogeneous equations and that simplifies the calculations to a large extent. However, to take into consideration the fast fission factor the η-value was

multiplied by the fast fission factor as calculated in Chapter 3 section 3.2.3 and the theoretically calculated values of ε are tabulated in section 3.4.1 of the same chapter.

A.3.2 NUMERICAL METHOD FOR K (EIGEN-VALUE) AND EIGEN-VECTOR (THERMAL FLUX)

The matrix equation A-3.1.5 to be solved in the programme can be written as

$$(F\Lambda - K(f\lambda + 1))\,\varphi = 0 \qquad \text{A-3.2.1}$$

or

$$(A - K(B + 1))\,\varphi = 0 \qquad \text{A-3.2.2}$$

The method of straightforwardly inverting the matrix $(B+1)$ is not very useful here because the dimension of B is often very high. Instead the power iteration method is used by putting

$$\varphi_{n+1} = (A - KB)\,\varphi_n \qquad \text{A-3.2.3}$$

2 - for thermal flux is omitted to avoid confusion. Using an approximate value for $K_n = K + \Delta K_n$ in equation A-3.2.3 a term of the form $(\Delta K_n\, B\, \varphi_n)$ is involved, and, to compensate that, a term $\alpha\varphi_n$ is added to compensate for that disturbance where α will be the criterion for convergence, and we get

$$\varphi_{n+1} = (A-KB)\varphi_n - \Delta\, KB\varphi_n + \alpha\varphi_n \qquad \text{A-3.2.4}$$

putting

$$\varphi_n = \sum_j A_j \varphi_j^c = B_j \varphi_j^e \qquad \text{(a)}$$

A-3.2.5

$$\varphi_j^e = \sum_i b_{ij} \varphi_i^e \rightarrow A_i = \sum_j B_j b_{ij} \qquad \text{(b)}$$

where

φ_j^e = Eigen-vector for the matrix (A-KB)

φ_j^e = Eigen-vector for the matrix B and

K_j^c, K_j^e are the corresponding Eigen-values.

From equations (A-3.2.4 and A-3.2.5)

$$\varphi_{n+1} = \sum_j \sum_i B_i b_{ji} \varphi_i^c (K_j^c + \alpha - \Delta K_n K_1^e) \qquad \text{A-3.2.6}$$

As condition for absolute convergence

$$\left| \frac{\sum B_i b_{ji} (K_j^c + \alpha - \Delta K_n K_i^e)}{\sum B_i b_{1i} (K_1^c + \alpha - \Delta K_n K_i^e)} \right| < \left| \frac{A_j}{A_1} \right| =$$

$$\frac{\sum_i B_i b_{ji}}{\sum_i B_i b_{1i}} \qquad \text{where} \quad j \neq 1$$

K_1^e is the desired eigen-value. Therefore convergence will be reached if

$$\frac{K_j^c + \alpha - \Delta K_n K_1^e}{K_1^c + \alpha - \Delta K_n K_1^e} < 1 \qquad j \neq 1$$

This will hold if

$$\alpha > \Delta K_n K_1^e - K_j^c$$

or $$\alpha \geq \frac{\Delta K_n}{K_n} K_n K_1^e + K_1^c \qquad \text{A-3.2.7}$$

Now choosing α quite large, one gets a series of approximation for the flux φ_n, φ_{n+1}, φ_{n+2} which should converge to the desired eigen-value.

By the use of δ^2 process according to Näslund (41) the best approximation is

$$K_{n+1} = K_1^e + \frac{\Delta K_{n+1}}{1 + s} \qquad \text{A-3.2.8}$$

In the programme, equation A.3.2.8 is used to calculate the eigen-value; following choices have been made:

(i) Equation A-3.2.5 namely

$$K_{n+1} = K_1 + \frac{\Delta K_{n+1}}{1 + s}$$

is used to calculate the eigen-value.

(ii) $\alpha = 0.5 K_n s$

where s is an approximation for K_1^e according to

$$K_{n+1} = K_1^c + \Delta K_{n+1} + ((A - K_n B)\varphi_n)\varphi'_n$$

$$\therefore \quad K_{n+1} = r - (K_1 + \Delta K_n)s$$

if $\varphi_n \varphi_n' = 1$ is taken.

The factor $\frac{\Delta K_n}{K_n} = 0.5$ has been taken which is relatively large and is kept constant to make Sure that the largest eigen-value will always be positive in equation A-3.2.4.

(iii) $0.5 \leq a \leq 2$, where 'a' the relaxation parameter is defined as below. By choosing α large enough, one gets a sequence of approximations for the eigen-vector φ_n, φ_{n+1}, φ_{n+2} which converges to the desired eigen-vector. By using Aithen's δ^2 process, one defines a Relaxation parameter "a"

$$a = \frac{\varphi_{n+1} - \varphi_n}{\varphi_{n+1} - \varphi_n - (\varphi_{n+2} - \varphi_{n+1})}$$

(iv) In the computation the vector η_n is used, which according to Naslund leads to gain in computing time; the eigen-value is the K(effective) of the system.

A-3.3 DESCRIPTION OF THE PROGRAMME

The total number of sub-routines and the links including the parent programme is 85. There is one parent link which controls 5 links.

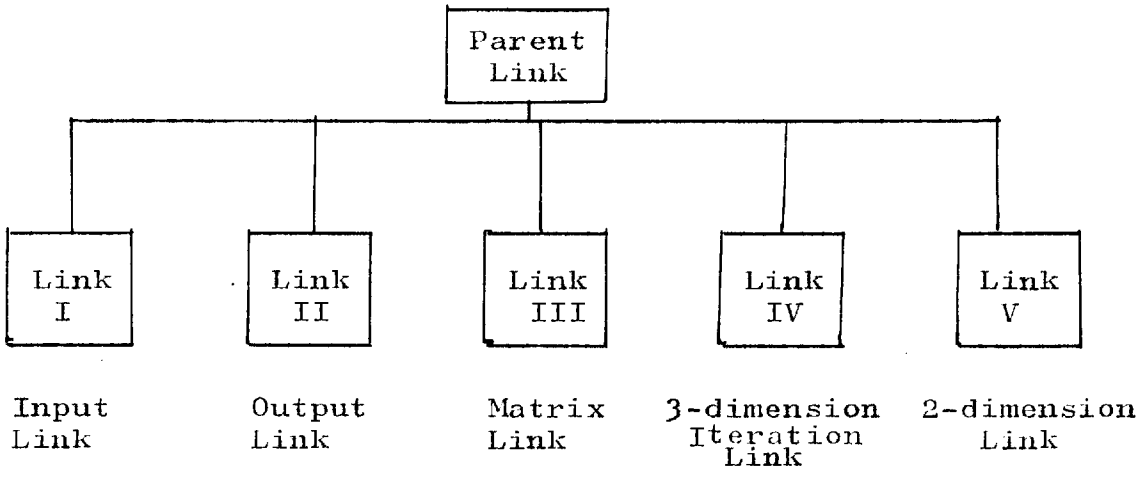

FIG.A-3.3.1

Briefly the description of the various links is :

LINK I. INPUT LINK.

It consists of one sub-routine which controls the input of the programme with 32 subsidiary routines. To facilitate the read-in of the input-data they are grouped and the first "three letters" of the headings (punched in columns 1-3) of the sub-routines are in the memory and therefore only the first three letters of the heading are important;in the rest of the card columns one could write anything. Each data group is preceded by a card with heading.

Each of the data constants takes up 10 positions and is punched as adjusted on the right. Blanks are taken as zeros and each name below makes one card if nothing else is stated. The names with all the three letters

in capitals must be given without fail otherwise the programme will fault. The names of the input-data sub-routines are

TIT, PRO, MOD, COO, Res, ELE, Cor, Ope, Pow, Bur, Rar, Acc, Out, Inc, Axr, Lra, Cra, Fou, STA, END, Sto, Tem, Dum, Rel.

The following group remains in the computer memory after the finish of the calculations until they are read-in afresh.

PRO, MOD, COO, Res, Cor, Ope, Pow, Bur, Acc, Out, Lra, Cra and Tem.

LINK II. OUT-PUT LINK.

It contains ten sub-routines with one sub-routine controlling the rest. This link gives the out-put as requested in the sub-routine OUT (see description) or as required in various input sub-routines. Details of the out-put that can be requested is given in the description of the input for the sub-routine OUT.

Out-put from t .e programme consists of the basic input data as well as the conditions which the input data implies. For example it will print out number of groups, co-ordinates of the fuel and or control rods, accuracy etc. The word out-put link implies the calculation of

(i) resonance escape probability defined by the

expression

$$-\ln \rho_n = \sum_{i=1}^{N} \frac{V_m N_m RI_m}{(\xi \Sigma_s)_m} \cdot \sum_{i=1}^{N} \alpha_i \frac{e^{-\frac{\bar{r}_n - \bar{r}_m}{4\tau_{im}}}}{4\pi\tau_{im}}$$

(ii) Thermal neutron flux, power distribution, etc.

(iii) Burn out, axial form factors for flux and power. Radial form factors for flux and power besides a huge number of variations of other requisites.

LINK III. MATRIX LINK consists of 15 sub-routines.

LINK IV. 3-DIMENSION ITERATION LINK consists of 12 sub-routines.

LINK V. 2-DIMENSION ITERATION LINK consists of 12 sub-routines.

These three links are the main body of the programme and, as their name implies, Links carry out the formation of the elements as required, whether the case is two-, or three, dimensional and or an exponential case. An exponential case cannot be 3-dimensional for obvious reasons. In addition there are two more sub-routines with the parent link. No link can intercommunicate directly except through the parent link. The parent link along with its two sub-routines is accessible to all the links and the common numbers are also available

through the common statement, otherwise the links are independent from one another.

The following input sub-routines have been used all along and brief description of each is given here.

i) TITle is used for identification of the input data group and the card after TIT can have any alpha-numerical text which is copied direct on to the out-put tape.

ii) PROblem is used to specify which type of problem is to be treated.

1-card.

N	μ	s	fas	exp	d	dim
1-10	11-20	21-30	31-40	41-50	51-60	61-70

N = number of fuel groups

μ = maximum number of Fourier components.

s = axial symmetry or not.

fas= fast absorption and slowing down in the fuel elements or not.

exp= case exponential or otherwise.

d = no significance at present.

dim= case 2-dimensional or 3-dimensional.

Letter One - implies yes and 0 means no and the data ≠0 need to be given only. Limits on the problem are

(a) $N \leq 150$

(b) $\mu \leq 64\ (1+s) - s.$

(c) $N(\mu+s) \leq 1500\ (s+1)$

(d) dim $\geq$ exp.

(iii) MODerator.

1-Card

D_{ms}	D_{mf}	τ_m	L_m^2	h	R
1-10	11-20	21-30	31-40	41-50	51-60

The symbols are self-explanatory, except that

$$h = \begin{cases} \text{(Height of reactor if exp} = 0 \\ \\ \left(\frac{M_z}{M_R}\right)^2 \gamma_{11}^2 \quad \text{if exp} = 1 \end{cases}$$

No negative sign is to be attached with the axial buckling since in the programme it is assumed that it is negative, otherwise the programme will just make a mess of the whole situation. The first four constants correspond to the radial direction.

(iv) COOrdinates.

This sub-routine gives information about the lattice geometry and composition of the fuel, control rods, etc.

1-Card g S_x S_y

2-Card $(g_n)_i$ $(g_a)_i$ $(g_t)_i$ x/S_x y/S_y

1-10 11-20 21-30 31-40 41-50

where

i = 1, N therefore N cards.

The significance of the symbols is

g = lattice type

g_t = type of the element in the group

g_n = number of the group

g_a = number of elements in the group

S_x = pitch in the x-direction

S_y = pitch in the y-direction

x,y = co-ordinates of one element in the group.

The following combinations of g and g_a are possible:-

	Type	Axes of Symmetry	Type	Permitted number of
g=	0	0	$g_a=1$	
	1	1	$g_a=1$	or $g_a=2$
	2	2	rect. $g_a=1$,	$g_a=2$ or $g_a=4$
	3	3	hex. $g_a=1$,	$g_a=3$ or $g_a=6$
	4	4	rect. $g_a=1$,	$g_a=4$ or $g_a=8$
	6	6	hex. $g_a=1$	$g_a=6$ or $g_a=12$

A typical lattice arrangement for g=1 and 4 is shown in FIG. A-3.3.1.

(v) RESonanace Escape Probability.

This sub-routine was not used to help calculate p which could be done, but was only used to feed the values of p.

1 Card	g_t	nK		
2a Card	$(g_n)_i$	p_i	i=1, N	N cards
2b Card	-1			

The cards 2(a,b) are given if pt = 1 and nK = 0 as explained.

pt = (0 p is given as a function of burn out only if dim = 0
(1 p is calculated or read-in

nK = (0 p is read-in. For element groups not read-in p is set = 1
(n>0 p is calculated with n cores.

The card 2b is only required if the resonance escape probability is not to be given for one or more number of element groups. For example in the case of control rods p is one. In this case when p for the number of fuel elements is finished, a card with negative sign will tell that p for the rest is equal to 1.

(vi) ELEment Group.

This sub-routine gives input data for each type of element which has been given in coordinates. Only the relevant cards will be explained.

In the present study it was assumed that there is no absorption of fast neutrons in the fuel and there is no slowing down inside the fuel, which simplifies the input considerably.

1-Card

g_t eK

2a a v n ω_o A

2b γ_{11} γ_{21}

only if fas = 1 and dim = 1

2c R1 N V_{cell} .

only if pt = 1 and nK > 0. (Res).

2d η γ_h Σ F

only if dim = 1 if eK = 3 Σ and F are discretionary

2e N_i i i i F_i p_i γ_{11}^i γ_{21}^i

i = 1, K, K $\leq$ 50; K $\geq$ 3

This concerns burn-up calculations

2f -1

(2e-f) only if dim = 0

if pt = 1 p is discretionary

if fas= 0 γ_{11} and γ_{12} are not needed.

2a to 2f are given if eK $\neq$ 1

3a a γ

3b γ_{11} γ_{21}

only if fas = 1

3a and 3b only if eK = 1.

g = type of element (COO)

		0	Fuel element
		1	Control rod
eK	=	2	Fuel element with given $\eta(K_{eff})$
		3	Dummy fuel element.

1-3 cards are repeated for each fuel element. The last is given

4 - 1

Maximum of 10 fuel types (including control rods and so on) can be read in.

On closer examination of these cards we will find that if we do not calculate p with the programme we need to give only

a = radius of the fuel rod in card (2a)

or radius of the control rod in card 3a.

γ = thermal constant

η = multiplication constant for the fuel under study.

The other numbers in the cards could be left blank implying zeros but it is safe to put 1 in each column.

(vii) CORrection.

This shows if the correction has to be applied for the finite size of the fuel rod or the correction is to be omitted.

1 1c

2a gt ac)
) only if 1c = 2
2b -1)

0 Linear sources

1c = 1 Cylindrical sources with radius as in ELE

2 Cylindrical sources with radius which is read in.

gt = type of element

ac = radius

(viii) ACCuracy

1	ε_{fou}	ε_{flux}	i_{max}	i_c
	1-10	11-20	21-30	31-40

ε_{fou} = $K_{eff}(\mu) - K_{eff}(\mu + \mu)$

ε_{flux} if the mean value of the absolute deviation between the Eigen-vector in two successive interations is less than ε_{flux}, the iterations are terrupted. This happens only when convergence has reached

i_{max} the maximum number of iterations to the eigenvalue.

i_c = 0 if i_{max} has been reached. Then the calculations are interrupted and the calculations continue with the last K-value as if convergence had been reached.

The built-in accuracies are

ε_{fou} = 0

ε_{flux} = 0.01

i_{max} = 200

i_c = 0

If data is omitted these values hold.

(ix) OUT-put.

This is used to indicate what additional output is required other than the K-effective value and the flux distributions. Since the interest was in these two parameters this was not used at all.

(x) STArt.

To initiate the final calculations the sub-routine STA is read-in. When this is read-in a calculation is made as to whether this has not happened before .
in the calculations

1) p
2) The F MATRIX.
3) The A MATRIX provided FOU (increase of Fourier component) has been read before and dim = 0.
4) The Eigen-value and flux distribution.
5) If anything more has been requested in OUT.

(xi) END

The reading of END means that calculations of the previous set has been finished and the control sets everything at zero, after which a new TITle card is looked for.

FIG. A-3.3.1 LATTICE TYPES

LATTICE SYMMETRY

g = 4

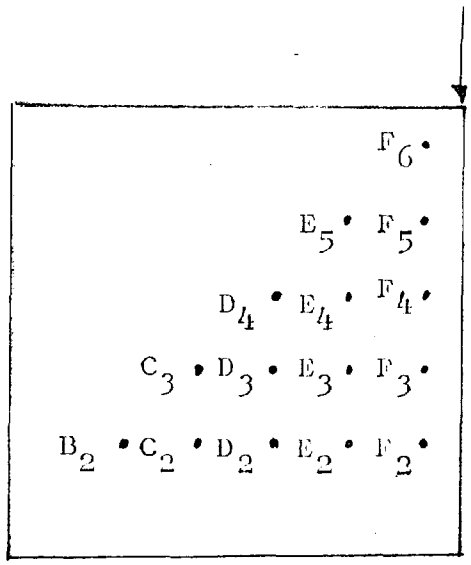

ONLY THE OCTAT IS SHOWN

LATTICE SYMMETRY

g = 1

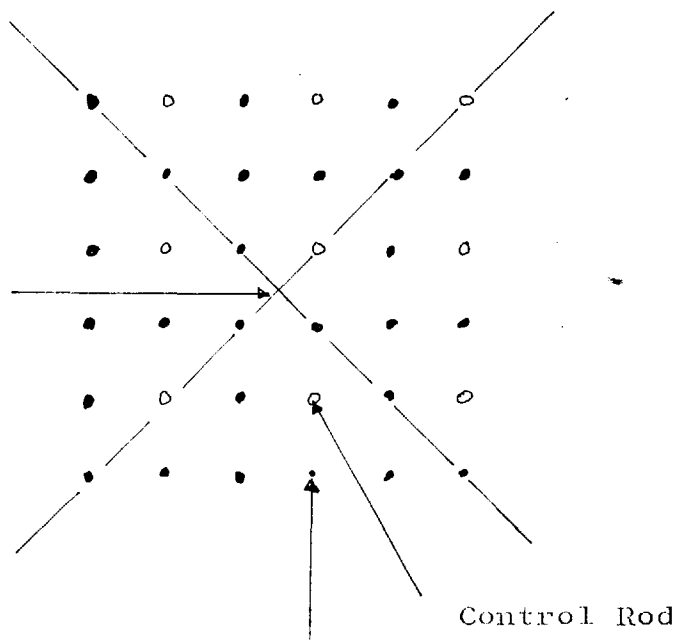

A TYPICAL CASE OF PSCF 27 STEEL 9

A-3.4 OPERATIONAL INSTRUCTIONS

Tape units 1-10 are used; and individual tapes carry out the following operations.

1 Used as working area for different results.

2 Store Matrix F.

3 Store Burn-up Data.

4 Store Matrix Lambda.

5 For Input (DEC).

5 For Out-put (DEC)

7 Store DUW (REL) DATA. In the programme this tape is called 8.

11 Store Eigen-vector (FLUX).

If the programme is already loaded on tape then the tape is loaded on B6. Loading time by $IEDIT has been found to be of the order of 1.4 to 1.6 minutes, and ordinarily simple 5 sets of data, wherein the number of fuel elements involved is 100, 64, 36, 16 and 4 takes 3.6 to 3.8 minutes. There is no simple correlation of time since it is very strongly a function of N the number of element groups and the conditioning of the matrices involved.